Molecular regulation of p53-dependent tumour suppressor responses by the p53 binding protein 1

Thesis submitted in partial fulfilment of the requirements for the degree of

Doctor of Philosophy in Clinical Medicine



Raquel Cuella Martin

Chromatin and Genome Integrity Group

Nuffield Department of Medicine

and

St Hugh's College

University of Oxford

Trinity 2018

Molecular regulation of p53-dependent tumour suppressor responses by the p53 binding protein 1

Raquel Cuella Martin

Nuffield Department of Medicine and St Hugh's College, University of Oxford.
Thesis submitted in partial fulfilment of the requirements for the degree of Doctor of Philosophy in Clinical Medicine, Trinity 2018.

Abstract

The tumour suppressor p53 binding protein 1 (53BP1), a fundamental node in DNA double strand break (DSB) repair, was identified as a p53-interacting protein over two decades ago. However, its contribution to p53-dependent responses has remained largely enigmatic. Here, using a combination of detailed structure-function approaches and *in vivo* analyses I aim to unravel this aspect of 53BP1 functionality. I showed 53BP1 to enhance genome-wide p53-dependent transactivation events in response to multiple stress stimuli. Oligomerised 53BP1 relies on the tandem BRCT domain, dispensable for 53BP1-driven DSB repair, to bridge dual interactions with p53 and the ubiquitin specific protease 28 (USP28). These interactions are both essential for 53BP1-dependent modulation of p53 functionality. Indeed, the cooperation between 53BP1 and USP28 is required for proficient p53-dependent G1/S checkpoint and senescence responses. Mechanistically, the action of the USP28-53BP1 complex involves differential ubiquitination events that ultimately stimulate p53's ability to bind the responsive elements (RE) in its target genes. Furthermore, I demonstrated 53BP1-driven p53 modulation to function independently of 53BP1's well-described DSB repair roles, and be separable by specific point mutations within 53BP1 architecture. Translation to *in vivo* mouse models revealed 53BP1-driven DSB repair to be responsible for 53BP1's role in the physiology of the immune system, while functional 53BP1-p53 connections result in effective quality control of chromosomal dosage upon defective mitotic division. Collectively, my findings define 53BP1 as an integral node in genome stability control, driving efficient DSB repair and mitotic surveillance mechanisms.

Acknowledgments

First, I would like to thank my supervisor, Prof J. Ross Chapman for his guidance, patience and endless support. You are an impressive scientist and your enthusiasm and love for science is contagious. After such a ride, I can only be proud and extremely thankful for what we have achieved together. It has been an honour to be your first DPhil student and grow scientifically under your mentorship, and I do hope to have set the bar high!

To my people in the Chapman lab, a big fat THANK YOU. You have put up with my annoying self, quirks, craziness, and constant ramblings (and music!). You have taught me so much, inspired me so much, and loved me so much; you are just my Oxonian family. You, and all the moments shared during this journey will always hold a special place in my heart.

To my entire family, always loving and caring. Thanks for constantly motivating me to be a strong, independent woman, and reminding me I could truly accomplish anything. Special thanks to my mother, who has lovingly taken care of a 26-year old 'pollito' that could not see beyond the 'thesis, thesis, thesis' horizon. You, dad and 'mirre' are simply my home, no matter how alone I get or how far I go. To my grandparents, aunts, uncles and cousins: I love you. I am thankful for every little part you played to make me grow into the woman I am now, academic achievements and all (I am almost a Dr!).

I am lucky, and extremely grateful to have a little bunch of great friends. Thank you to my precious miscellanea of friends, from high school to Uni, from Spain to all over the world; you came to stay, and damn well you have stayed through thick and thin. Special thanks to my 'cuartafileros', you are such a light,

constantly present in my heart. And finally, to my people in Oxford, all so different and all so special. Many relationships built in times of hardships, where you have shared my struggle, and put the smile back on my face. Thank you.

Now, I am both lost for words and despising the space constraints, so I do hope my actions did, do, and will, always make you feel special.

My DPhil studies were funded by a Nuffield Department of Medicine Prize studentship and undertaken under a Cancer Research UK (CRUK) grant (C5255/A18085).

Declaration

I confirm that this thesis has been composed by myself and has not been submitted for any degree in this University or elsewhere. The results here presented were obtained by myself, unless otherwise acknowledged in the text. The content of this thesis has been partially published in a peer-reviewed journal as an article that I first-authored (see [1]).

List of Abbreviations

53BP1	tumour suppressor p53 Binding Protein 1
AID	Activation-Induced cytidine Deaminase
APC	Allophycocyanin
APC/C	Anaphase-Promoting Complex/Cyclosome
Arf-BP1	Alternative-Reading Frame Binding Protein 1
ASPP2	Apoptosis-Stimulating of p53 Protein 2
ATM	Ataxia Telangiectasia Mutated
ATR	Ataxia Telangiectasia and Rad3-related protein
BARD1	BRCA1-Associated RING Domain protein 1
BAX	BCL-2 Associated X
BBC3	BCL-2 Binding Component 3
BCL-2	B-Cell Lymphoma 2
BER	Base Excision Repair
BrdU	Bromodeoxyuridine
BRCA1	Breast Cancer-Associated protein 1
BRCA2	Breast Cancer-Associated protein 2
BRCT	BRCA-1 C-terminus
BSA	Bovine Serum Albumin
Cas9	CRISPR associated protein 9
CBP	CREB-binding protein
CDC25A	Cell Division Cycle 25A
Cdh1	CDC20 homolog 1
CDK1	Cyclin-Dependent Kinase 1

CDKN1A	Cyclin-Dependent Kinase inhibitor 1A
C_H	Heavy Chain Constant region
Ch	Chimera
ChIP	Chromatin IP
Chk1	Checkpoint kinase 1
Chk2	Checkpoint kinase 2
CHX	Cycloheximide
COP1	Constitutive Photomorphogenesis Protein 1
CRISPR	Clustered Regularly Interspaced Short Palindromic Repeats
CSR	Class-Switch Recombination
CTD	C-Terminal Domain
CtIP	CTBP-Interacting Protein
DBD	DNA Binding Domain
DDR	DNA Damage Response
DMEM	Dulbecco's Modified Eagle's Medium
DN	Double negative
DNA-PK	DNA-dependent Protein Kinase
DP	Double positive
DR5	Death Receptor 5
DSB	Double-Strand Break
DUB	Deubiquitinating enzyme
DYNLL1	Dynein Light Chain LC8 type 1
ES	Embryonic Stem cells
FBS	Foetal Bovine Serum
Fbw7	F-Box/WD repeat-containing protein 7

FITC	Fluorescein isothiocyanate
GADD45A	Growth Arrest and DNA-Damage-inducible 45 Alpha
GAR	Glycine-Arginine Rich
GFP	Green Fluorescent Protein
GOF	Gain-Of-Function
gRNA	Guide RNA
GST	Glutathione S-Transferase
H2AX	Histone 2A variant X
HEK	Human Embryonic Kidney
HPRT1	Hypoxantine-guanine phosphoribosyl-transferase 1
HR	Homologous Recombination
HSC	Hematopoietic Stem Cell
iASPP	inhibitor of ASPP
IARC	International Agency for Research on Cancer
IF	Immunofluorescence
Ig	Immunoglobulin
IP	Immunoprecipitation
IR	Ionising radiation
LC8	8 KDa dynein Light Chain
Lig4	Ligase 4
LOH	Loss Of Heterozygosity
LPS	Lipopolysaccharide
MAD2L2	Mitotic Arrest Deficient 2 Like 2
MAR	Matrix Attachment Region
Mb	Megabase

MDC1	Mediator of DNA damage checkpoint protein 1 (MDC1)
MDM2	Mouse Double Minute 2
MDM4	Mouse Double Minute 4
MEF	Mouse Embryonic Fibroblast
MMR	Mismatch Repair
MPF	M-phase promoting factor
MRN	MRE11-RAD51-NBS1
mTOR	mammalian Target Of Rapamycin
N3	Nutlin-3
NEM	N-Ethylmaleimide
NES	Nuclear Export Signal
NHEJ	Non-Homologous End Joining
NLS	Nuclear Localisation Signal
OD	Oligomerisation Domain
OIS	Oncogene-Induced Senescence
Opti-MEM	Optimised low serum Minimal Essential Medium
ORF	Open Reading Frame
PARP	Poly (ADP-Ribose) Polymerase
PAXX	Paralog of XRCC4 and XLF
PCR	Polymerase Chain Reaction
PE	Phycoerythrin
PEI	Polyethylenimine
PI	Propidium Iodide
Pirh2	p53-Induced RING-H2
PLK1	Polo-Like Kinase 1

PLK4	Polo-Like Kinase 4
pRB	Retinoblastoma protein
PTIP	Paxx Transactivation domain Interacting Protein
PTM	Post-Translational Modification
RAG1	Recombination-Activating Gene 1
RAG2	Recombination-Activating Gene 2
RAP80	Receptor-Associated Protein 80
RE	Responsive Element
RIF1	Rap-1 Interacting Factor homolog
RNF8	RING Finger 8
RNF168	RING Finger 168
RPE-1	Retinal Pigmental Epithelial 1
RPMI	Roswell Park Memorial Institute
RS	Recombination Sequence
RT-qPCR	Real Time- quantitative PCR
S	Switching
SAC	Spindle Assembly Checkpoint
SDS-PAGE	Sodium Dodecyl Sulfate-Polyacrylamide Gel Electrophoresis
SETD7	SET Domain containing protein 7
SETD8	SET Domain containing protein 8
SOC	Super Optimal broth with Catabolite repression
ssDNA	single stranded DNA
ssODN	single stranded Oligonucleotide
TAD	Transactivation Domain
TCR/BCR	T/B- cell receptor

TD	Tetramerisation Domain
Th	T helper
TIDE	Tracking Indels by DEcomposition
TIRR	Tudor Interacting Repair Regulator
TopBP1	Topoisomerase (DNA) II Binding Protein 1
TP53	Tumour Protein p53
TSS	Transcription Start Site
UBA	Ubiquitin-Associated domain
UBC13	Ubiquitin-Conjugating enzyme E2 13
UBR	Ubiquitin-Binding Region
UDR	Ubiquitination-dependent recruitment
UIM	Ubiquitin-Interacting Motif
USP7	Ubiquitin Specific Protease 7
USP10	Ubiquitin Specific Protease 10
USP25	Ubiquitin Specific Protease 25
USP28	Ubiquitin Specific Protease 28
V(D)J	Variable, Diversity, Joining
VDR	Vitamin D nuclear Receptor
WB	Western Blot
WT	Wild Type
XLF	XRCC4-Like Factor
XRCC4	X-ray Repair Complementing 4

Table of contents

Chapter 1. Introduction **1**

1.1 The DNA double-strand break response **1**

1.1.1 DSB signalling: from ATM downward 1

1.1.2 DSB repair: NHEJ *vs* HR 3

1.1.3 The transcriptional response to DSB 5

1.2 53BP1: a key element in the NHEJ pathway **6**

1.2.1 53BP1 domains and their functions 7

1.2.1.1 The N-terminal region 7

1.2.1.2 The oligomerisation domain 10

1.2.1.3 The tandem Tudor domain 11

1.2.1.4 The UDR motif 13

1.2.1.5 The tandem BRCT domain 13

1.2.2 Physiological and pathological functions of 53BP1 17

1.2.2.1 V(D)J recombination in lymphocyte maturation 17

1.2.2.2 Class switch recombination 19

1.2.2.3 Oncogenic function in BRCA1-deficient tumours 20

1.3 p53: the guardian of the genome **22**

1.3.1 The p53 protein 22

1.3.1.1 The N-terminal region: the transactivation domain 23

1.3.1.2 The DNA binding domain 24

1.3.1.3 The tetramerisation domain 27

1.3.1.4 The C-terminal regulatory region 28

1.3.2 Layers of p53 regulation 28

1.3.2.1 Layer 1: p53 stability 29

1.3.2.2 Layer 2: antirepression 30

1.3.2.3 Layer 3: target-specific activation 31

1.3.3 Functional diversity of the p53 protein 32

1.3.3.1 Cell cycle control: the checkpoints 33

1.3.3.2 Senescence 35

1.3.3.3 Apoptosis 36

1.3.4 p53 and tumourigenesis 37

1.4 53BP1 and p53: the connection 40

1.4.1 53BP1 discovery and early studies 40

1.4.2 Structural insights 41

1.4.3 Cooperation *vs* synergy 43

1.5 Aims 45

Chapter 2. Materials and Methods 47

2.1 Cell methods 47

2.1.1 Cell lines and cell culture 47

2.1.2 Generation of stable knockout cell lines by CRISPR/Cas9 48

2.2 Mice and primary mouse cell isolation methods 50

2.2.1 Mouse strains 50

2.2.2 Mouse strain generation using the CRISPR/Cas9 technology 50

2.2.3 Mouse genotyping 52

2.2.4 Mouse embryonic fibroblast isolation 53

2.2.5 Splenocyte preparation and B-cell isolation 54

2.3 Virus methods 54

2.3.1 Generation of lentiviral constructs 54

2.3.1.1 Cloning of open reading frames (ORFs) of interest 55

2.3.1.2 Generation of point and domain specific mutants 56

2.3.1.3 Generation of USP28-USP25 chimeric gene products 56

2.3.1.4 Cloning into expression vectors 59

2.3.2 Lentivirus generation and lentiviral transduction 59

2.4 Protein methods 60

2.4.1 SDS/PAGE-Western Blot 60

2.4.2 Immunoprecipitation 62

2.4.3 p53 tetramerisation analysis 63

2.4.4 Immunofluorescence (IF) assays 64

2.4.5 Chromatin immunoprecipitation (ChIP) 64

2.5 Transcriptome analysis 66

2.5.1 Target-specific analysis: real time quantitative PCR (RT-qPCR) 66

2.5.2 Whole transcriptome analysis: RNA-seq 67

2.6 p53-dependent cell cycle arrest and apoptosis assays 68

2.6.1 Drug sensitivity assays 68

2.6.2 Clonogenic IR survival assay 69

2.6.3 Apoptosis evaluation: AnnexinV/Propidium iodide (PI) staining 69

2.6.4 G1/S checkpoint analysis 70

2.7 Immune system analysis 71

2.7.1 B-cell development: Hardy fractions 71

2.7.2 T-cell development 72

2.7.3 Class-switch recombination assay 73

2.8 Cytogenetics-based assays 74

2.8.1 Metaphase spread preparation 74

2.9 Statistical methods 75

Chapter 3. Contribution of 53BP1 to p53-dependent responses 76

3.1 Introduction 76

3.2 Results 77

3.2.1 53BP1 enhances p53 transcriptional activity 77

3.2.2 Oligomerisation and tandem BRCT domains are required for p53 modulation 84

3.2.3 53BP1 regulates G1/S transition *via* p53 89

3.2.4 53BP1's tandem BRCT fosters dual p53-USP28 interactions required for modulation of p53 responses 93

3.3 Concluding remarks 97

Chapter 4. Defining a role for USP28 in p53-dependent responses 100

4.1 Introduction 100

4.1.1 The USP28 protein 100

4.1.2 USP28 functions 103

4.1.3 Why USP28? 104

4.2 Results 105

4.2.1 USP28 modulates p53-dependent responses alongside 53BP1 105

4.2.2 USP28 catalytic activity is required for p53 modulation 110

4.2.3 Sequences in USP28's catalytic domain and C-terminal are essential for its function in p53 responses 111

4.3 Concluding remarks 115

Chapter 5. Mechanism of USP28-53BP1-dependent p53 modulation 118

5.1 Introduction 118

5.2 Results 119

5.2.1 53BP1 and USP28 do not regulate p53 stability and localisation 119

5.2.2 Regulation of p53's DNA binding activity by 53BP1 and USP28 124

5.2.3 The role of 53BP1's Tudor in modulation of p53 responses is methylp53-interaction independent 136

5.3 Concluding remarks 139

Chapter 6. 53BP1 integrates NHEJ and p53 modulation activities 142

6.1 Introduction 142

6.2 Results 145

6.2.1 *In vitro* separation of function: UDR *vs* BRCT mutant in IR responses 145

6.2.2 *In vivo* separation of function: NHEJ-driven repair *vs* mitotic surveillance 147

6.3 Concluding remarks 159

Chapter 7. Discussion 162

7.1 53BP1 in p53 responses: the tandem BRCT and the structural implications 162

7.2 USP28 and the ubiquitin-dependent regulation of p53 responses 166

7.3 The 'separation of function' and the physiological relevance of the USP28-53BP1-p53 axis 170

7.4 Conclusions and proposed model **173**

Chapter 8. References **176**

List of Figures

Figure 1.1. DNA-double strand break repair signalling. 2

Figure 1.2. NHEJ and HR are the major pathways in DSB repair. 4

Figure 1.3. Schematic representation of 53BP1's domain organisation. 7

Figure 1.4. 53BP1 N-terminal domain. 9

Figure 1.5. 53BP1's tandem BRCT shares the topology and binding properties of other well-characterised DDR proteins, but it is not required for bulk NHEJ activities. 15

Figure 1.6. V(D)J recombination requires NHEJ and is intrinsically linked to B and T cell development. 18

Figure 1.7. Schematic representation of p53's domain organisation. 23

Figure 1.8. Tetrameric p53 binds to the DNA through key residues in the DBD region. 26

Figure 1.9. Overview of p53's cellular functions. 32

Figure 1.10. Mechanisms of action of mutant p53 proteins. 38

Figure 1.11. Structural insights on 53BP1-p53 interactions. 43

Figure 1.12. Nutlin-3a is a potent MDM2 antagonist. 45

Figure 2.1. CRISPR/Cas9-mediated generation of protein- and domain-knockout cell lines. 49

Figure 2.2. Genotyping strategy for *L1616A* and *NDRR* mice. 53

Figure 3.1. Characterisation of 53BP1 and p53 knockout cell lines. 78

Figure 3.2. 53BP1-deficient cells display intermediate resistance to N3. 79

Figure 3.3. 53BP1 absence results in suboptimal induction of p53 target genes in response to N3 and IR. 80

Figure 3.4. 53BP1 is a co-activator of p53-dependent transcriptional programmes. 83

Figure 3.5. Reconstitution of 53BP1 point- and domain- mutant protein expression in *53BP1Δ* cells. 85

Figure 3.6. 53BP1 relies on oligomerisation and BRCT domains to modulate p53 responses. 87

Figure 3.7. Functional oligomerisation and BRCT domains are essential for 53BP1-p53 interactions. 88

Figure 3.8. Endogenous deletion of 53BP1's tandem BRCT mimics complete 53BP1 absence in p53-dependent responses. 90

Figure 3.9. 53BP1 regulates IR-induced p53-dependent G1/S checkpoint arrest. 92

Figure 3.10. $53BP1^{R1811A}$ and p53-binding mutants fail to support efficient N3-mediated cellular arrest. 94

Figure 3.11. 53BP1's BRCT mediates p53 and USP28 interaction *via* different surfaces. 96

Figure 4.1. Schematic representation of USP28 isoforms. 101

Figure 4.2. USP28 structural predictions. 102

Figure 4.3. USP28 depletion confers resistance to Nutlin-3. 106

Figure 4.4. USP28-deficiency largely mimics 53BP1 deficiency in p53-dependent responses. 108

Figure 4.5. 53BP1 and USP28 act together in p53 modulation. 109

Figure 4.6. USP28 relies on the catalytic activity, but not the ubiquitin binding motifs, to regulate p53-dependent responses. 110

Figure 4.7. USP28 C-terminal region is required for USP28 functionality

in p53 regulation. 112

Figure 4.8. USP28 catalytic environment and C-terminal module are required for modulation of p53-dependent N3 toxicity. 114

Figure 5.1. 53BP1 and USP28 do not regulate the turnover of basal and N3-induced p53 protein. 121

Figure 5.2. p53 localises to the nucleus independently of 53BP1 and USP28 status. 123

Figure 5.3. 53BP1 and USP28 stimulate p53 binding to the *CDKN1A* REs. 126

Figure 5.4. 53BP1 and USP28 enhance p53-RE interactions. 127

Figure 5.5. Reconstitution of p53 expression in *p53Δ* MCF-7 cells restores N3 sensitivity. 130

Figure 5.6. USP28 does not interfere with the functionality of p53's DBD. 133

Figure 5.7. Absence of 53BP1 or USP28 affects p53 ability to sustain tetramerisation. 135

Figure 5.8. The role of 53BP1's Tandem Tudor domain in regulating p53 responses does not involve interactions with dimethylated p53 C-terminal residues. 137

Figure 5.9. Mutation in residue D1521 within 53BP1's tandem Tudor domain blocks the interaction with USP28. 139

Figure 6.1. 53BP1 and USP28 deficiency does not confer N3 resistance to RPE-1 cells. 143

Figure 6.2. RPE-1 cells lacking 53BP1 or USP28 override centrinone-induced cell cycle arrest. 144

Figure 6.3. 53BP1 independently regulates NHEJ-driven repair and p53-driven cell death in response to IR. 146

Figure 6.4. 53BP1 simultaneously mutated in N1845 and D1861 fails to bind p53 and promote N3-induced cellular arrest. 148

Figure 6.5. B-cell development requires intact 53BP1-driven NHEJ activities. 150

Figure 6.6. 53BP1 action in T cell maturation depends exclusively on its ability to support NHEJ. 153

Figure 6.7. 53BP1 requires its NHEJ activity but not p53 regulatory functions to promote efficient CSR and survival to IR. 155

Figure 6.8. Cellular response to centrosome loss depends on 53BP1-p53 physical interactions. 157

Figure 6.9. Loss of 53BP1-dependent p53 modulation results in enhanced chromosomal gains in splenocytes. 159

Figure 7.1. 53BP1's tandem BRCT fosters non-canonical interactions with USP28 using residue R1811 within the phosphobinding pocket. 164

Figure 7.2. Proposed model of 53BP1 functionality as a hub of genome stability control. 175

List of Tables

Table 2.1. gRNA sequences used for knock-in genome editing. 51

Table 2.2. ssODN sequences to insert the desired mutations *via* homology-directed repair. 51

Table 2.3. Primer pairs used for ORF amplification and cloning. 55

Table 2.4. Primer pairs used for gene fragment amplification and chimera generation. 59

Table 2.5. List of primary antibodies used throughout this study. 61

Table 2.6. Locus-specific ChIP primers used throughout this study. 65

Table 2.7. Primer pairs sequences for RT-qPCR amplification. 67

Table 2.8. List of antibodies used for Hardy fraction analysis. 72

Table 2.9. List of antibodies used for T-cell maturation analysis. 73

Table 2.10. Cytokine cocktails used to induce class switching to the Ig isotypes indicated. 74

Table 2.11. Primary antibodies used for immunoglobulin staining in CSR analysis. 74

Table 3.1. Number of activated and repressed genes in RNA-seq analysis. 82

Chapter 1

INTRODUCTION

The genome is a storage unit that contains all the instructions needed by an organism to function. Nonetheless, the genome is intrinsically fragile, and its exposure to endogenous and exogenous damage endangers its integrity. The preservation of genomic stability is thus the cellular top priority, and accordingly organisms have evolved specific mechanisms to repair the array of lesions that constantly compromise the information contained in their DNA.

1.1 The DNA double-strand break response

DNA double-strand breaks (DSBs) are extremely toxic lesions that arise when both DNA strands are broken. Indeed, deleterious DSBs can lead to genomic rearrangements and ultimate cell death. Accordingly, defective DSB repair has been linked to a plethora of malignancies including impaired development, neurological and immunological disorders, and tumourigenesis [2-4]. In order to efficiently perform the repair of DSBs, cells rely on a tightly controlled signalling network and two major effector pathways, classical non-homologous end joining (NHEJ) and homologous recombination (HR) [5,6].

1.1.1 DSB signalling: from ATM downward

When a DSB occurs, the MRE11-RAD51-NBS1 (MRN) complex rapidly senses the available DNA ends and fosters the recruitment of the ataxia-telangiectasia mutated (ATM) kinase and its activation by auto-phosphorylation

(pATM^{S1918}) (Fig. 1A) [7,8]. ATM targets an array of proteins involved in the DNA damage response (DDR), including the checkpoint kinase 2 (Chk2), and the tumour suppressor p53 amongst others, thereby triggering the activation of cell cycle checkpoints and the transcriptional response to genotoxic stress [9]. At damaged chromatin, ATM phosphorylates the histone 2A variant X (H2AX) at Ser139 (γH2AX) (Fig. 1.1A) [10]. This signalling event ensues within minutes after the DSB occurs, and rapidly spreads throughout a large genomic region surrounding the damaged chromatin [11]. The signal amplification is achieved thanks to a positive feedback loop starting with the recognition of γH2AX by the scaffolding protein mediator of DNA damage checkpoint protein 1 (MDC1) which subsequently recruits more MRN complexes and phosphorylated ATM to break sites (Fig. 1.1A) [12-14].

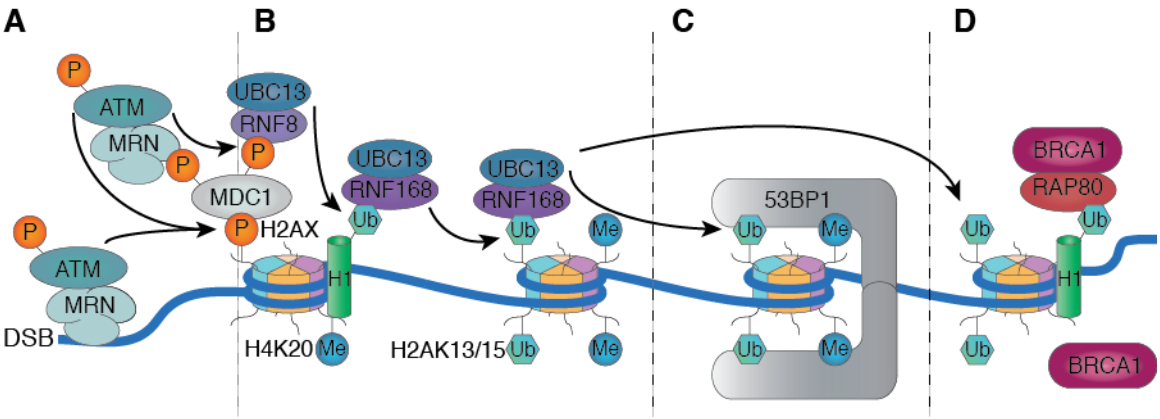


Figure 1.1 DNA-double strand break repair signalling. (A) Initiation. (B) Ubiquitin-dependent events. (C) 53BP1 recruitment for NHEJ-driven repair. (D) BRCA1 recruitment for HR-driven repair. Adapted from [15].

In addition, ATM phosphorylates MDC1, creating a docking site for the E3 ubiquitin ligase RING finger 8 (RNF8) [16-18]. RNF8 then cooperates with the ubiquitin-conjugating enzyme E2 13 (UBC13) to ligate K63-linked ubiquitin chains to linker histone H1 variants (Fig. 1.1B) [19]. A second E3 ubiquitin ligase, RNF168, physically binds H1-Ub-K63 and deposits a monoubiquitination mark on

core histone H2A at lysines 13 and/or 15 (H2AK13/15Ub) (Fig. 1.1B) [19,20]. RNF168's ability to interact with its own signature mark drives the amplification of the ubiquitin signal by a positive feedback loop that extends the ubiquitination to adjacent nucleosomes (Fig. 1.1B-D) [21,22]. This ubiquitination signalling provides an interaction platform for both NHEJ and HR factors. p53 binding protein 1 (53BP1) displays a dual interaction with the widespread dimethylated Lys20 in histone H4 (H4K20me2) and the highly specific H2AK15Ub that ensures the anchorage to chromatin where generates a unique scaffolding hub for downstream NHEJ effectors (Fig. 1.1C) [23,24]. The K63-linked ubiquitin chains have been reported to recruit receptor-associated protein 80 (RAP80) which by direct interaction brings the HR factor breast cancer-associated protein 1 (BRCA1) to damaged chromatin (Fig. 1.1D) [25-27]. However, absence of RAP80 does not impede BRCA1 association to chromatin and subsequent HR-driven repair, suggesting an alternative RAP80-independent recruitment mechanism for BRCA1 still to be discovered [28].

1.1.2 DSB repair: NHEJ *vs* HR

The initial, common signalling response to DSBs converges with specific cell cycle-driven modulation to determine the ultimate pathway that accomplishes the repair of broken DNA. 53BP1 gets recruited to the repair factories (microscopically visible units named foci, singular focus) throughout the cell cycle, but ultimately the error-prone NHEJ pathway preserves DNA integrity primarily in G0/G1. Conversely, in S/G2, when a homologous sister chromatid is available to act as a template, BRCA1-mediated 53BP1 eviction from the focus core directs the repair to error-free HR [29]. Although the mechanistic details

defining 53BP1 and BRCA1's competition at damage sites are still subject to study, it remains clear that a tightly regulated balance between NHEJ and HR safeguards the genome from deleterious DSBs [30].

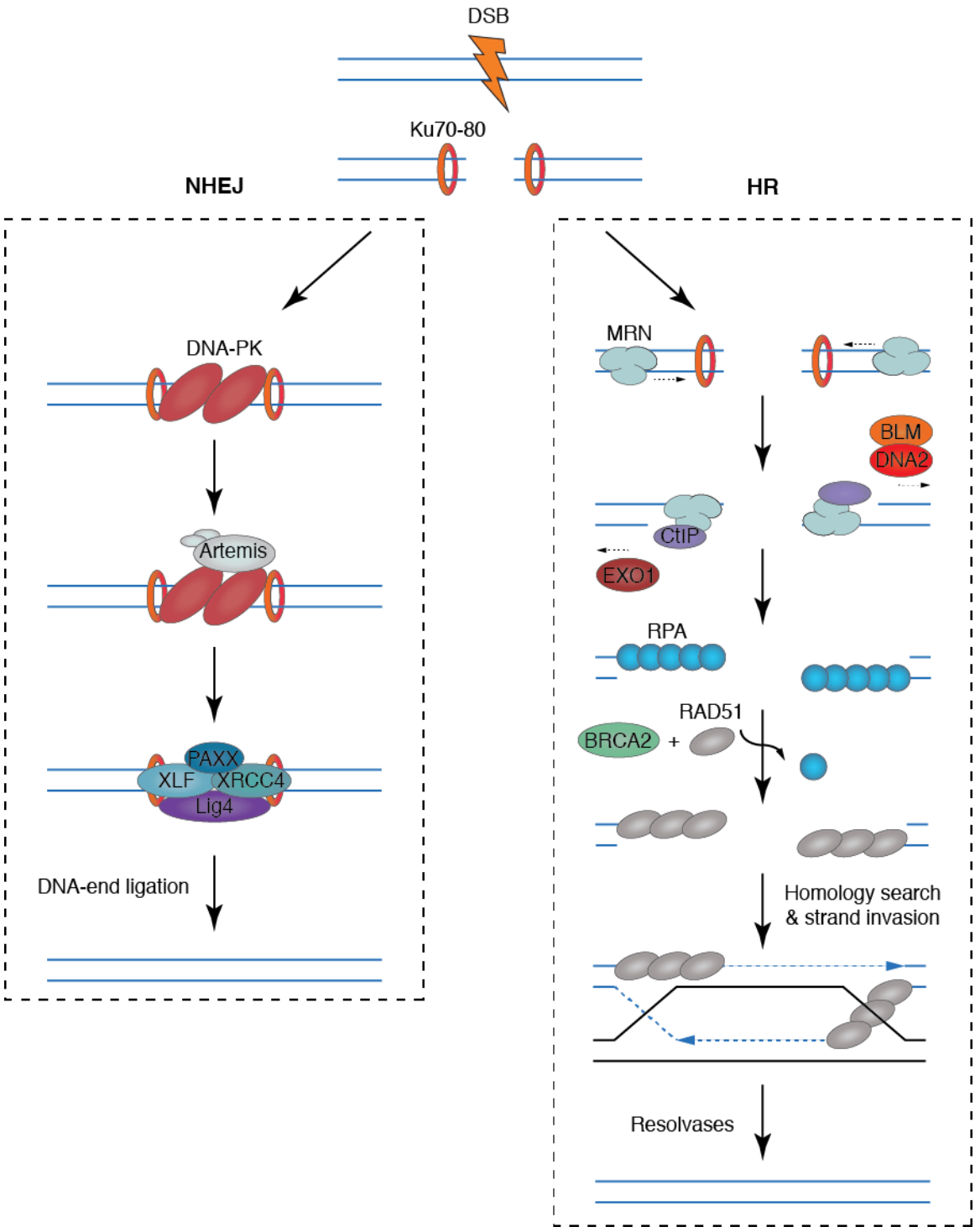


Figure 1.2. NHEJ and HR are the major pathways in DSB repair. (Left panel) Main events in the 53BP1-driven NHEJ cascade are depicted. (Right panel) Main steps in BRCA1-dependent HR.

Briefly, when the break occurs, the Ku70-80 (Ku) heterodimer binds the DNA ends with high affinity (Fig. 1.2). In G0/G1, Ku anchors DNA-dependent protein kinase (DNA-PK) which recruits end-processing factors, such as Artemis, and the ligation complex (Ligase 4 (Lig4), X-ray repair complementing 4 (XRCC4), XRCC4-like factor (XLF) and paralog of XRCC4 and XLF (PAXX)) (Fig. 1.2, left panel) [5]. The combined action of these proteins results in a ligation product that may contain small errors due to the nature of the Artemis-dependent end trimming. In post-replicative chromatin, the CTBP-interacting protein (CtIP)-MRN complex promotes clipping next to the break site to overcome the Ku block and thereby generates a mildly-processed end for extensive resection mediated by the EXO1 and Bloom syndrome protein helicase (BLM)-DNA2 nuclease complex (Fig. 1.2, right panel) [31]. The single stranded DNA (ssDNA) generated is coated by replication protein A (RPA), which is subsequently exchanged by RAD51 in a BRCA2-dependent manner. The RAD51-coated ssDNA filament searches for homology and allows the synthesis of the resected strand. Finally, the DNA structure formed is processed by resolvases, successfully completing the repair of the lesion in an error-free fashion (Fig. 1.2, right panel) [6].

1.1.3 The transcriptional response to DSB

Upon DSB occurrence, the activation of the DDR is immediate and the cascade of post-translational modifications (PTMs) drives the quick recruitment of DNA repair factors to the damage sites. As part of the cascade, activating phosphorylation of the transcription factor p53 initiates the transcriptional branch of the response. p53 binds to specific sequences at gene promoters and transactivates genes primarily involved in cell cycle arrest (*CDKN1A* (p21)),

apoptosis (*BAX*, *BBC3* (PUMA), *FAS*) and senescence (*GADD45A*). Through p21, the action of p53 inhibits cell cycle progression and slows down the replication machinery to avoid the deleterious fork-break encounters [32-35]. While this mechanism initially grants the cell time to repair the damage, permanent cell cycle arrest and the induction of cell death programmes lead to irreversible outcomes. The choice between temporary cell cycle arrest and ultimate senescence and apoptosis is, however, far more complex, and depends on intrinsic p53-DNA binding properties, the intensity of the stress stimulus, and the cell type amongst other factors [36-38]. Altogether, p53-driven transcription and the consequent cellular processes elicited are a crucial component of the DNA damage response. Accordingly, loss of p53, and thus loss of the transcriptional response to DSBs, allows cells to progress throughout the cell cycle and divide harbouring high levels of genomic instability, a hallmark of tumourigenesis [39,40].

1.2 53BP1: a key element in the NHEJ pathway

In 1994, a yeast two-hybrid screen identified 53BP1 for its ability to bind the DNA binding domain of the tumour suppressor p53 [41]. However, it quickly gained the attention of the DNA DSB repair field, which has since extensively characterised 53BP1, its functional partners and physiological relevance [15,42]. In the NHEJ pathway, 53BP1 is a core scaffolding element whose unique structure allows tight nucleosome contacts while providing a platform for multiple DDR protein complexes. 53BP1 is then able to inhibit the nucleolytic processing of the free DNA ends, known as resection, thereby counteracting HR and promoting NHEJ.

53BP1-driven NHEJ can be a double-edged sword. Physiologically, it is essential for the generation of the antibody repertoire in the immune system, where it coordinates the critical recombination steps, V(D)J and class-switch recombination (CSR). Nevertheless, 53BP1 is also the driver of tumourigenesis in BRCA1-deficient cancers where it triggers chromosomal rearrangements and genomic instability [15].

1.2.1 53BP1 domains and their functions

The multidomain architecture of 53BP1 is crucial for its functionality in the NHEJ signalling cascade. Showing no enzymatic activity, 53BP1's 1972 amino acids encompass an unstructured N-terminal tail, an oligomerisation domain (OD), a tandem Tudor domain, an ubiquitination-dependent recruitment (UDR) motif and a tandem BRCA-1 C-terminus (BRCT) domain (Fig. 1.3) [43].

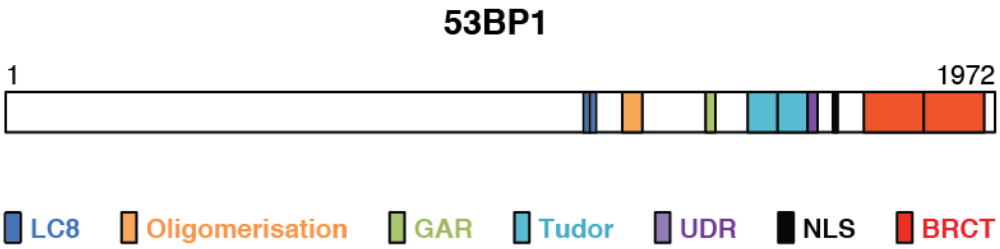


Figure 1.3. Schematic representation of 53BP1's domain organisation. Aside from the main functional domains, 53BP1 owns two 8 kDa dynein light chain (LC8) binding motifs in the N-terminal region, a glycine-arginine rich region (GAR) of unknown function and a nuclear localisation signal (NLS). Schematic representations are conveniently scaled and the positions of all features depicted accordingly.

1.2.1.1 The N-terminal region

53BP1 possesses an unstructured N-terminal region that extends over the first 1200 amino acids of the protein. 53BP1's N-terminal tail has remarkably increased in length throughout evolution, in parallel to the need to accommodate

downstream protein complexes for its newly acquired functional properties (Fig. 1.4A). 53BP1's yeast orthologues, Rad9 in *Saccharomyces cerevisiae* and Crb2 in *Schizosaccharomyces pombe*, act as checkpoint activators, while 53BP1 has become primarily a DSB repair factor with reduced contribution to checkpoint responses [44].

The most prominent feature of 53BP1's N-terminal region is the presence of 28 Ser/Thr-Gln (S/T-Q) motifs, which are consensus target sequences for the ATM kinase (Fig. 1.4B). Although many have been found to be phosphorylated in proteomics-based approaches, little is still known about the relevance of site-specific ATM-dependent phosphorylation events in 53BP1-driven NHEJ [45,46]. Upon DNA damage, ATM-driven phosphorylation of 53BP1 at S25 creates a surface for the recruitment of the Pax2 transactivation domain-interacting protein (PTIP) (Fig. 1.4B) [47]. 53BP1-PTIP complexes function in pathological NHEJ, driving fusion of deprotected telomeres and aberrations in BRCA1-deficient cells [48]. A distinct N-terminal region of hyperphosphorylated 53BP1 binds Rap-1 interacting factor homolog 1 (RIF1) (Fig. 1.4B) [48]. RIF1 is an essential factor in NHEJ signalling and acts together with 53BP1 to prevent DNA-end resection and inhibit HR [49-51]. Recent studies suggest that RIF1 is involved in the recruitment of the downstream factor mitotic arrest deficient 2 like 2 (MAD2L2, also and here referred as REV7) although the precise mechanism remains to be elucidated [52,53].

In mitosis, 53BP1 is phosphorylated in its N-terminal domain in a DNA-damage-independent manner [54,55]. Phosphorylation on 53BP1's Ser380 by Polo-like kinase 1 (PLK1) has been related to efficient G2/M checkpoint activation, which could be analogous to the function of its yeast orthologues (Fig.

1.4B) [56]. In addition, cyclin-dependent kinase 1 (CDK1) and PLK1 target 53BP1 on Ser1618, in an event that restricts 53BP1-driven NHEJ in mitosis by

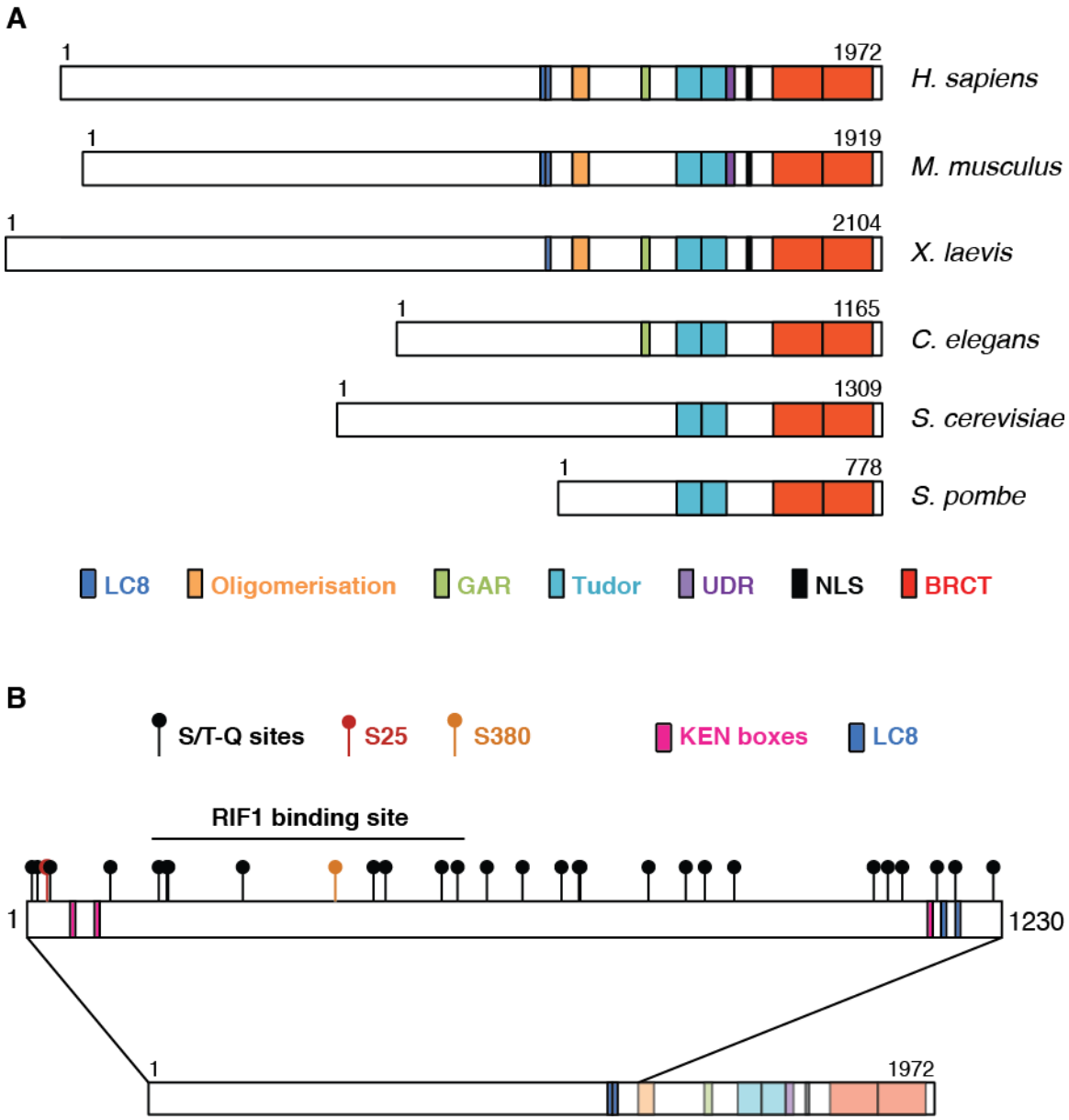


Figure 1.4. 53BP1 N-terminal domain. (A) Schematic representation of 53BP1 in different species, including 53BP1's orthologues Rad9 in *S. cerevisiae* and Crb2 in *S. pombe*. Higher organisms present a substantially larger N-terminal region and an increasing degree of functional domain complexity. (B) The N-terminal region contains 28 S/T-Q canonical ATM phosphorylation sites. The third N-terminal SQ (S25) site is responsible for PTIP recruitment. Additionally, amongst the potential CDK phosphorylation sites, S380 is outlined for its functional interest. The RIF1 binding site and the positions of three putative KEN boxes and two LC8 motifs are also represented. Schematic representations are conveniently scaled and the positions of all features depicted accordingly.

preventing its H2AK15Ub-dependent recruitment [57]. Recently, a novel role has been suggested for 53BP1 in mitosis mediated by the three putative KEN boxes present in the N-terminal region (Fig. 1.4B) [58]. 53BP1's KEN boxes foster interactions with the anaphase-promoting complex/cyclosome (APC/C) to regulate its E3 ubiquitin ligase activity, consequently influencing mitotic protein degradation and cell cycle progression [58].

Closely placed to the oligomerisation domain, 53BP1 owns two 8 kDa dynein light chain (LC8) binding motifs (Fig. 1.4B). 53BP1 establishes a phosphorylation independent interaction with dynein light chain LC8 type 1 (DYNLL1) which is equally robust when only the second motif is available [51]. Accordingly, mutation of the first LC8 motif shows no alterations in 53BP1-driven NHEJ at deprotected telomeres [59]. Interestingly, interaction of 53BP1 with DYNLL1 is required for 53BP1-driven responses [60]. The LC8 motifs are specific to 53BP1 vertebrate orthologues, and coincide with the presence of longer N-terminal regions (Fig. 1.4A). Considering the role of DYNLL1 in protein dimerisation and structural organisation, binding of DYNLL1 to 53BP1 is likely to act as a molecular velcro assisting the oligomerisation and three-dimensional organisation of this large, unstructured N-terminal tail.

1.2.1.2 The oligomerisation domain

To form the scaffold where the NHEJ complexes are built, various molecules of 53BP1 associate together. The ability of 53BP1 to self-interact was first described using co-immunoprecipitation assays using distinctly tagged 53BP1 molecules, and the interaction motif was mapped upstream the tandem Tudor domain to the region comprising residues 1052 to 1475 [61]. Interestingly,

this interaction was independent of DNA damage [61]. Later, a thorough study to define the minimum sequence requirements for 53BP1 focus formation on 53BP1 fine-mapped the oligomerisation domain to residues 1230 to 1270 [62]. The oligomerisation domain contains highly conserved residues; indeed, this region is interchangeable with the corresponding one in *S. pombe*'s Crb2 and still accomplish efficient foci formation in the context of the minimal focus forming region fragment [24,62].

Despite keeping some residual foci formation activity, mutants harbouring a deletion of the oligomerisation domain are not proficient for 53BP1-driven NHEJ in the context of class-switch recombination, and do not present genomic instability in a BRCA1-deficient background [63]. Conversely, 53BP1 cells lacking this domain display only a minimal deficiency in fusion of deprotected telomeres, where its residual recruitment ability may suffice to promote successful NHEJ [59].

1.2.1.3 The tandem Tudor domain

Tudor domains are methyl-lysine and methyl-arginine binding modules present in adaptor proteins responsible for the assembly of macromolecular complexes. 53BP1 possesses two Tudor domains (hereinafter referred to as Tudor) that are organised in tandem, each individual domain acquiring a β-barrel structure [64]. This structure, comprising amino acids 1484 to 1603, shows high plasticity and is capable of accommodating a variety of lysine-methylated substrates without a defined consensus sequence [23,65-69].

Although 53BP1's Tudor was initially associated to the recognition of dimethylated histone H3 in Lys79 (H3K79me2) at damage sites, subsequent

evidence proved that H4K20me2 was effectively the mark directing 53BP1 Tudor-dependent recruitment to damaged chromatin [23,65]. H4K20me2 is highly abundant within the genome in an asynchronous cell population, and thus its contribution to the specific recruitment of 53BP1 to damaged chromatin remains controversial. Notably, H4K20me2 is regulated throughout the cell cycle; cells in S-phase display lower levels of the mark coinciding with the incorporation of new, unmethylated H4. In G2/M, the combined action of SET domain containing protein 8 (SETD8) and Suv4-20h1/h2 methyltransferases deposits sequentially the two methyl moieties in H4K20 to restore the dimethyl form [70,71]. New insights point to the relevance of H4K20me2 as a mark of pre-replicative chromatin as opposed to post replicative chromatin, where H4K20me2 nucleosomes will be diluted with the naked, H4K20me0. Although not sufficient on its own to direct 53BP1 specifically to the damage sites, enrichment in H4K20me2 marks single-copy DNA for 53BP1-driven NHEJ [72]. Furthermore, a novel 53BP1 interacting protein, Tudor interacting repair regulator (TIRR), contributes to the regulation of 53BP1's Tudor-dependent binding to chromatin by competing with H4K20me2 for the interaction surface [69]. Upon damage, phosphorylation of 53BP1 and RIF1 recruitment will prompt TIRR eviction and favour the chromatin interaction essential for 53BP1's NHEJ activities.

Two pivotal tumour suppressors are also recognised by 53BP1's Tudor. The retinoblastoma protein (pRb) is methylated in Lys810 by SETD7, inhibiting CDK-dependent phosphorylation and affecting the positive regulation of pRb over the transcription factor E2F [73]. pRbK810me2 is read by 53BP1's Tudor suggesting a link between the DNA damage response and pRb-driven tumour suppression [67]. The tumour suppressor p53 is also targeted for methylation in

lysines located in the C-terminal regulatory region. Recognition of these methylation events by 53BP1's Tudor will be discussed later in this chapter (Section 1.4.2).

1.2.1.4 The UDR motif

Functional oligomerisation and Tudor domains are required but insufficient for the recruitment of 53BP1 to damaged chromatin. The region C-terminal to the Tudor domain comprises a nuclear localisation signal (NLS) and a small peptide segment conserved in higher eukaryotes, which displays a weak homology with the ubiquitin interacting motifs (UIM) in NBS1 and RAP80 [62]. Elegant work showed that this region contained a motif unique to 53BP1, not present in its yeast counterpart Crb2, that specifically recognises damage-induced, RNF168-dependent H2AK15Ub [24]. Named UDR motif, it comprises from amino acids 1604 to 1631, and collaborates with the Tudor domain to establish contacts with the histone octamer at damage sites [74]. Accordingly, mutation of central residues (I1617A, L1619A) is sufficient to completely abolish 53BP1 recruitment to damage sites and disrupt NHEJ-dependent activities [24].

1.2.1.5 The tandem BRCT domain

Phospho-dependent interactions are key in the DNA damage response. Hence, protein modules that specifically foster interactions with phosphoserine/threonine residues are a requisite for the assembly of many DDR multiprotein complexes. BRCT domains, initially identified in the BRCA1 protein, are highly specific binding modules with a preference for pS-containing peptides [75]. Besides the classical interaction mode, BRCT domains, which are usually

organised as single units or tandems, have also been associated to DNA and PAR binding, and phospho-independent interactions [76].

53BP1 contains two BRCT domains disposed in tandem (hereinafter referred as tandem BRCT) in its extreme C-terminal region (amino acids 1711-1972). Structurally, the individual BRCT repeats (BRCT1 and BRCT2) resemble the single XRCC1 BRCT domain, and the overall topology of the tandem is similar to the tandem BRCT domain in other DDR proteins including BRCA1, BRCA1-associated RING domain protein 1 (BARD1), and MDC1 (Fig. 1.5A) [77-79]. Different tandem BRCTs display small structural divergences that define target specificity and thus, functional uniqueness. In fact, contrary to the case of the strikingly similar Crb2's tandem BRCT, 53BP1's tandem BRCT does not dimerise and has no role in the recruitment of 53BP1 to damaged chromatin [80]. Furthermore, and perhaps surprisingly, 53BP1's tandem BRCT domain is dispensable for bulk NHEJ activities [59,63].

Then, what is the role of such conserved domain module in 53BP1? Several interaction partners have been identified over the years but their functions have remained unclear.

In budding and fission yeast, γH2A (analogous to γH2AX in higher organisms) directly recruits Crb2 and Rad9 respectively, to DSBs *via* interaction through the tandem BRCT domain [81,82]. Although 53BP1 has evolved other mechanisms for the recruitment to chromatin, the tandem BRCT of 53BP1 has been co-crystallised with the γH2AX peptide. The interaction presents the characteristic BRCT-pS binding pattern, where a lysine residue (K1814) establishes a hydrogen bond with the phosphorylated serine and an arginine (R1811) contacts with the amino moiety of the aromatic residue in position +3

(Fig. 1.5B). Furthermore, this interaction showed *in vitro* binding properties less robust than the MDC1-γH2AX module, albeit still within the range of a potentially relevant interaction, posing a conundrum for 53BP1's BRCT functionality [83,84].

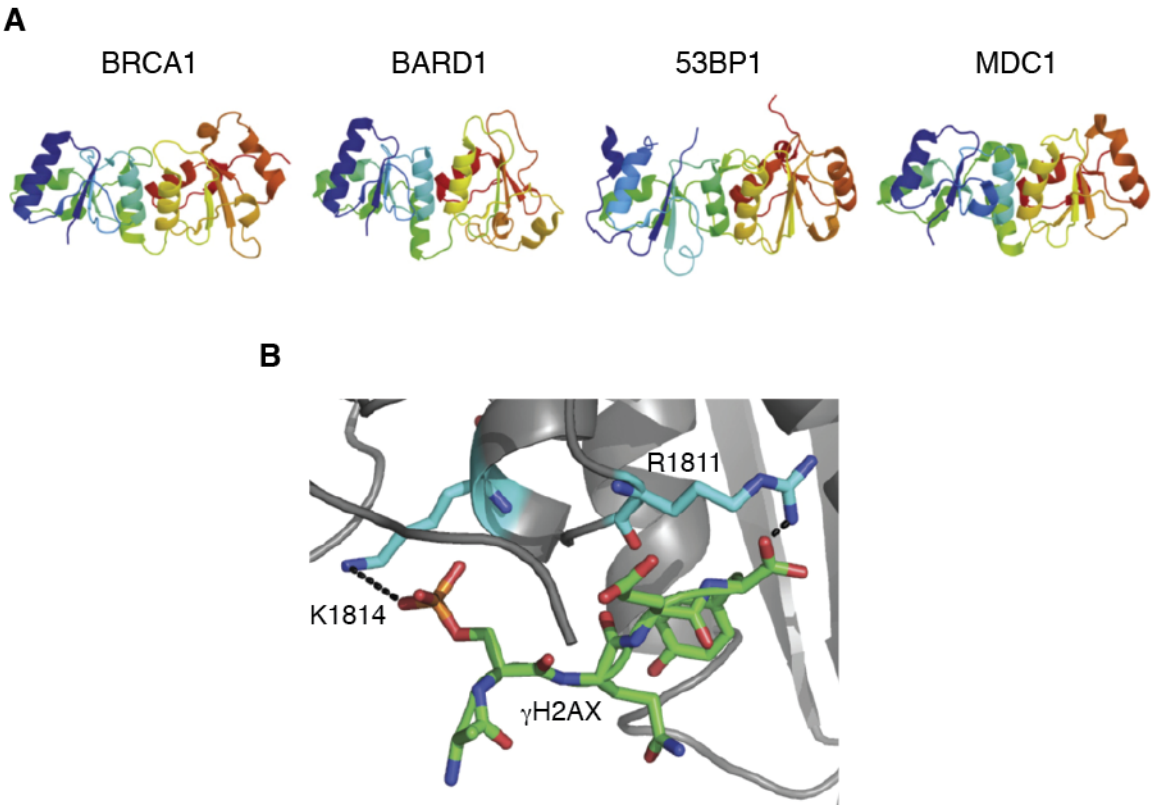


Figure 1.5. 53BP1's tandem BRCT shares the topology and binding properties of other well-characterised DDR proteins, but it is not required for bulk NHEJ activities. (A) Structure of the tandem BRCT of different DDR proteins [79]. (B) γH2AX peptide (green) bound to 53BP1's BRCT (grey, with key residues in blue) from [84]. γH2AX is the only phospho-dependent interactor described to date for 53BP1's BRCT module.

The chromatin-remodelling factor EXPAND1 has also been reported to bind 53BP1's tandem BRCT [85]. The extreme N-terminal region of EXPAND1 interacts constitutively with the tandem BRCT in a phospho-independent manner and is sufficient to recruit EXPAND1 to damaged chromatin [85]. The subsequent role of EXPAND1 in chromatin remodelling and its potential impact on DNA repair is still to be defined.

As previously mentioned, 53BP1 uses the KEN boxes placed in its N-terminal region to bridge interactions with APC/C in mitosis (see Section 1.2.1.1). While the KEN boxes specifically interact with the cell division cycle 20 (Cdc20) subunit, the tandem BRCT establishes physical contacts with the CDC20 homolog 1 (Cdh1) subunit [58]. Cdh1 knockout results in a reduction in 53BP1 protein levels, suggesting that the BRCT-mediated contacts are specifically required for the stability of the 53BP1 protein [58]. Accordingly, 53BP1's tandem BRCT, whose involvement in the DDR remains controversial, could potentially play a role in the regulation of 53BP1 protein turnover.

About a decade ago, the ubiquitin specific protease 28 (USP28) was identified as a DDR factor and 53BP1 binding partner [86]. As a deubiquitinating enzyme (DUB), USP28 was proposed to regulate the turnover of many DDR proteins, including MDC1, NBS1, Chk2, and 53BP1 itself, and be involved, through Chk2, in the preservation of p53's apoptotic function [86]. More recently, USP28 has been reported to interact with 53BP1's tandem BRCT in a DNA damage independent manner [87]. In agreement with the dispensability of 53BP1's tandem BRCT for bulk NHEJ, this study failed to show any alterations in DDR response proteins and 53BP1-driven NHEJ upon USP28 knockout in both cells and mouse models [87]. Resolution of the controversy surrounding USP28's contribution to DNA damage will potentially shed light on other functions of 53BP1's tandem BRCT.

It is remarkable the absence of the best-characterised 53BP1's tandem BRCT binding protein in this section. As the main focus of this study, p53, and the details of 53BP1-p53 interactions will be extensively discussed later in this chapter (Section 1.4).

1.2.2 Physiological and pathological functions of 53BP1

The NHEJ pathway for DSB repair not only safeguards genome integrity in non-dividing cells but also presents crucial functions in specific physiological and pathological scenarios.

Physiologically, 53BP1-driven NHEJ acquires a pivotal role in the repair of programmed DSBs in the immune system to complete the rearrangement of the gene segments that confer antigen receptor diversity and encode the different antibody isotypes. In a pathological context, loss of HR turns the NHEJ cascade into a driver of genomic instability by promoting aberrant ligation of free DNA ends to generate genomic rearrangements of tumorigenic potential.

1.2.2.1 V(D)J recombination in lymphocyte maturation

Variable, diversity and joining (V(D)J) recombination is a lymphocyte-specific recombination process that functions to assemble complete antigen receptor genes. This process, which is intrinsically associated to the development of B and T lymphocytes, is crucial for the generation of diversity at the immunoglobulin (Ig) and T-cell receptor (TCR) gene loci (Fig. 1.6A) [88]. Successful gene rearrangements require physical organisation of gene sequence in loops, the insertion of programmed site-specific DSBs and efficient repair by the NHEJ machinery (Fig. 1.6B).

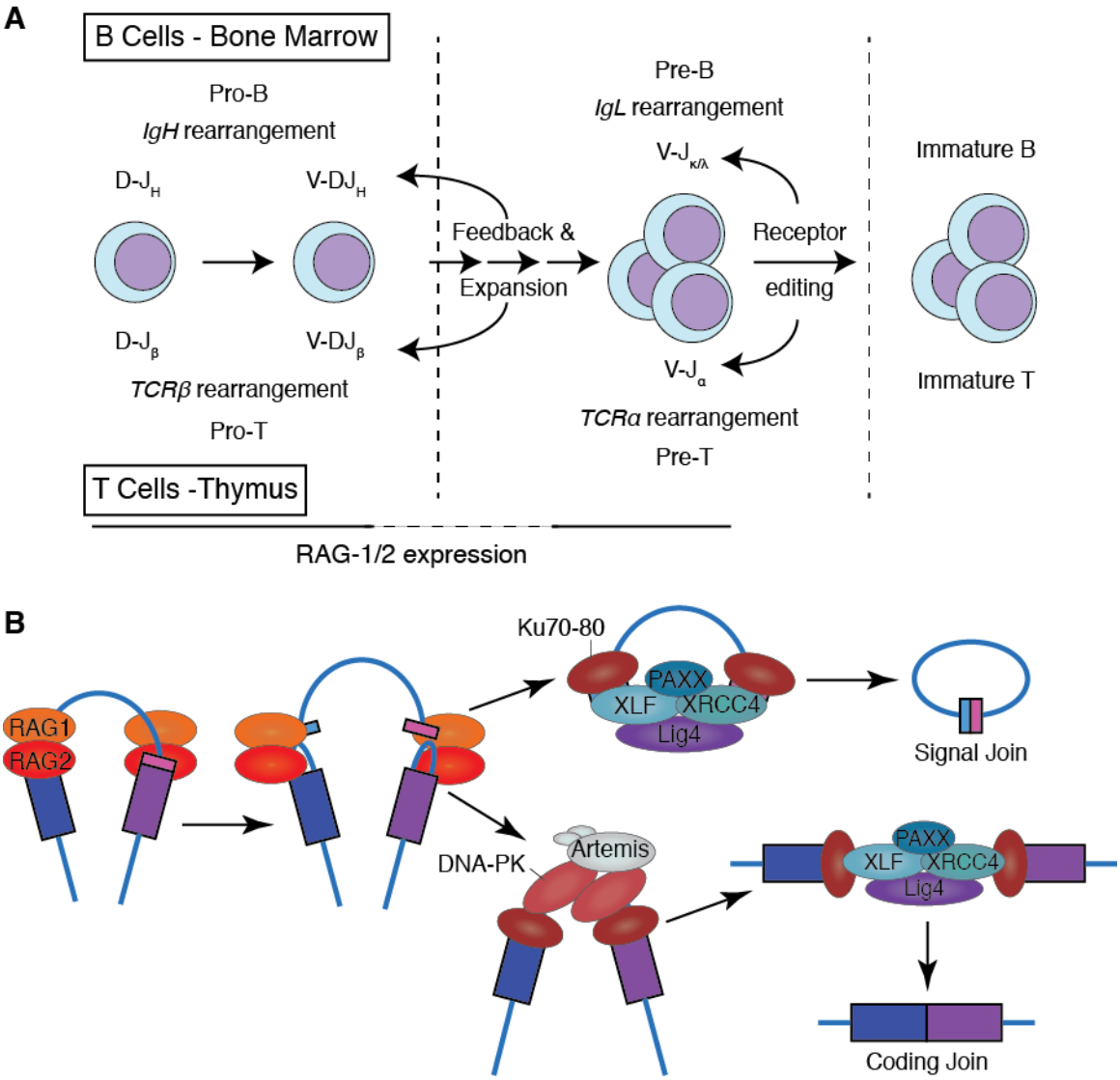


Figure 1.6. V(D)J recombination requires NHEJ and is intrinsically linked to B and T cell development. (A) Schematic representation of B- and T-cell maturation processes. At the early stage of lymphocyte development in the bone marrow (pro-B), recombination-activating gene 1 (RAG1) and 2 (RAG2) protein expression activates the rearrangement at the *IgH* locus (TCRβ and δ genes in pro-T cells in the thymus) [89]. Similarly, when productive V(D)J occurs and pro-B cells successfully continue the maturation process to a pre-B cells stage, V and D fragments of the κ and λ light immunoglobulin chains are rearranged to generate functional IgM (TCRα and ɣ chains in pre-T cells) [90]. Two critical checkpoints (dashed lines) control productive rearrangement and induce apoptosis of cells with absent or aberrant receptors [91,92]. Adapted from [88]. (B) RAG1 and 2 recognise the recombination sequences (RSs), cut, and generate a hairpin-like structure at the flanking regions of V, D, and J segments [93]. The programmed DSBs trigger the DNA damage response and the recruitment of the NHEJ factors. On one side, the NHEJ machinery performs the self-ligation of the loop carrying the undesired gene fragments. On the other side, the Artemis/DNA-PK complex opens the hairpin ends, and the V, D, and J fragments are further ligated together in a process that may result in the generation of sequence variability by insertions and deletions [88,94].

Due to the particular structure of the loci encoding the antigen receptors, the distance between different V, D, and J segments ranges from hundreds of base pairs to megabases (Mb). In the context of the TCR, 53BP1 has been specially involved in the rearrangement of distant gene segments while not being an essential requirement in short-range V(D)J [95]. Accordingly, 53BP1-deficient mice have problems in lymphocyte development that manifest in lymphopenia [95-97]. Interestingly, the same holds true for *Atm*$^{-/-}$ mice but no such effect has been observed in *Rif1*$^{-/-}$ and B-cell-specific *Rev7*$^{-/-}$ mice [49,95,97]. Collectively, these observations suggest a more structural contribution of 53BP1 in the context of V(D)J recombination, possibly related to its ability to facilitate chromatin mobility, and highlight the requirement for specific interaction partners in distinct physiological contexts [98,99].

1.2.2.2 Class switch recombination

Class switch recombination (CSR) and V(D)J recombination are joined processes that enable an efficient adaptative immune response. Upon V(D)J arrangement of a proficient B-cell receptor or IgM, mature B cells rely on NHEJ to switch the heavy chain constant (C_H) region of the immunoglobulin and produce the spectrum of function-specific antibodies that are required to efficiently fight infections [100]. Despite having different DSB generation and regulatory mechanisms, CSR and VDJ recombination rely on 53BP1-driven NHEJ [101].

In order to initiate CSR, activation-induced cytidine deaminase (AID) deaminates cytidines to uracils at the corresponding switching (S) regions [102]. The mismatch is subsequently processed by the base excision repair (BER) and

the mismatch repair (MMR) pathways, generating DSB substrates for NHEJ-mediated repair [103].

B cells from 53BP1-deficient mice show a profound defect in CSR to a panel of isotypes in *in vitro* stimulation studies [104,105]. Accordingly, basal serum Ig levels in *53bp1*$^{-/-}$ mice are depleted except in the case of IgM, where no CSR is required [105]. Remarkably, in the absence of classical NHEJ proteins, such as XRCC4, Lig4 or Ku70, the alternative NHEJ machinery catalyses a substantial amount of CSR events leaving a characteristic microhomology signature [106-108]. Despite displaying comparable CSR deficiency, 53BP1-deficient cells show little microhomology at the productive junctions, indicating that 53BP1 does not interfere with the classical NHEJ ligation step but rather has upstream roles that are of crucial relevance for the process [109]. Outlining a clear mechanistic difference with V(D)J recombination, 53BP1 has been reported to act alongside RIF1 and REV7 in the inhibition of DNA-end resection at the switch regions [49,53,97]. Hence, both *Rif1*$^{-/-}$ and B-cell-specific *Rev7*$^{-/-}$ mice present immunodeficiency comparable to *53bp1*$^{-/-}$ mice, result of unproductive CSR [49,97]. Recent studies have brought us closer to an understanding of 53BP1-dependent NHEJ in CSR by identifying a novel REV7-related complex, Shieldin, that prevents DNA end-resection at switch regions likely acting as a physical impediment *via* the direct binding to ssDNA [97,110].

1.2.2.3 Oncogenic function in BRCA1-deficient tumours

The repair of DSBs is crucial to keep genome integrity and cellular homeostasis. Homologous recombination protein BRCA1 is a *bona fide* tumour

suppressor whose loss-of-function is associated not only with breast cancer, but also ovarian, pancreas and prostate tumours [111,112].

In the absence of BRCA1, the HR pathway is abrogated with the consequent disruption of the cell cycle-regulated equilibrium between NHEJ and HR. Under these conditions, 53BP1-driven NHEJ directs the repair of replication-associated lesions generating chromatid and chromosome fusions, genomic instability and rearrangements of oncogenic potential [113]. Therefore, 53BP1-dependent NHEJ becomes dangerously oncogenic, but 53BP1 elimination suffices to restore the HR pathway and genomic stability [113,114]. The same holds true for 53BP1's functional partners RIF1 and REV7 but not Lig4, reflecting the relevance of the choice between NHEJ and HR over the ligation step *per se* in this context [49,53,113].

Mechanistic knowledge of the equilibrium between NHEJ and HR is of crucial importance in clinic. Tumours harbouring BRCA1 loss-of-function are extremely sensitive to selective inhibition of poly (ADP-ribose) polymerase (PARP) [115]. PARP inhibition results in an inability to repair DNA nicks whose conversion to DSBs during replication generates a substrate for the HR pathway. Consequently, in *BRCA1*$^{-/-}$ tumours, failure to repair those lesions triggers massive 53BP1-driven genomic instability that ultimately kills tumour cells. Drug resistance is, nonetheless, a constant threat to patients suffering from these tumours, and it is heavily linked to the restoration of the HR pathway. Genome-wide knockout screens in BRCA1-deficient tumour cells have identified loss of 53BP1, and associated NHEJ proteins such as REV7, as a major mechanism of PARP inhibitor resistance [53]. With the recent irruption of PARP inhibitors in the clinic, these mechanistic studies constitute a potent tool to dissect the 53BP1-

driven NHEJ pathway and consequently identify caveats and alternatives in treatment of BRCA1-deficient tumours.

1.3 p53: the guardian of the genome

The maintenance of genomic integrity is orchestrated by a plethora of specific pathways that respond to endogenous and exogenous genotoxic insults. Differing in signalling molecules and effectors, they all rely on p53 to take the ultimate life-death cell fate decision. Since its discovery in the late 70s, p53 has been the subject of more studies than any other protein [116-118]. Named 'the guardian of the genome', p53 is a transcription factor with major functions in activation of cellular checkpoints, and induction of the apoptotic and senescent programmes [119]. Thanks to this pivotal role in cell cycle control and genome stability, p53 exerts a potent tumour suppressor action.

1.3.1 The p53 protein

The tumour suppressor p53 is a small protein consisting of 393 amino acids structured in 4 functional domains [120]. p53 owns a transactivation domain in its N-terminal region, followed by a central, globular, and highly-structured DNA binding domain. A downstream tetramerisation domain allows the association of four p53 monomers to constitute a functional transcription factor unit. At the extreme C-terminal, an unstructured, lysine-rich region acts as platform for PTMs directed to modulate p53's activity (Fig. 1.7).

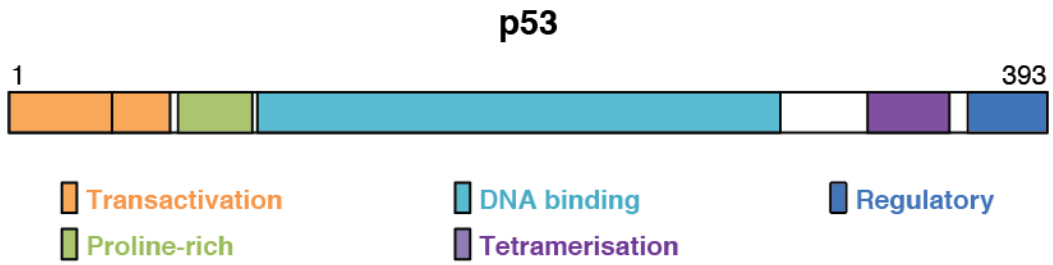


Figure 1.7. Schematic representation of p53's domain organisation. The transactivation domain (1-60) is divided into two distinct sub-activation domains (1-39, 40-61) [121]. The structural, proline-rich region spans amino acids 64 to 92. The core, sequence-specific DNA binding domain (94-292) is connected to the tetramerisation (325-356) domain by a large, unstructured loop. The extreme C-terminal (363-393) constitutes a heavily modified, lysine-rich regulatory region. Schematic representations are conveniently scaled and the positions of all features depicted accordingly.

1.3.1.1 The N-terminal region: the transactivation domain

The N-terminal region of p53 encompasses an unstructured transactivation domain (TAD) and a proline-rich peptide. Whereas the proline-rich region is likely to have a structural role in domain connection, the TAD integrates several aspects of p53 regulation and functionality [122].

The TAD is divided in two sub-domains (TAD1, TAD2) that independently induce transactivation events. Functionally, the TAD acts as a platform for protein-protein interactions with negative regulators of p53 (MDM2, MDM4), transcriptional co-activators (p300/CBP, KAT2A (also GCN5)), and the transcriptional machinery itself (TFHII) [121,123-126]. Binding to the E3 ubiquitin ligases mouse double minute 2 (MDM2) and 4 (MDM4, also MDMX) occurs *via* a small peptide comprising residues 15 to 29 and regulates p53 turnover by proteasomal degradation [127-129]. Additionally, MDM2/4 compete for binding to the TAD1 with positive regulators of p53, further inhibiting p53 activity. This competition is unbalanced upon stress stimuli; exposure to ionising radiation triggers the phosphorylation of p53's TAD1 in Ser15 and Ser20. These

phosphorylation events result in the release of p53 from the negative regulation partners while simultaneously increase the affinity for transcriptional co-activators like p300/CREB-binding protein (CBP) [130-134]. p53 interaction with the acetyltransferases p300/CBP requires multiple contacts with both TAD1 and TAD2 spanning a larger region than the MDM2 binding site [135,136]. p300/CBP can acetylate p53 itself in the C-terminal region, but it is also known to deposit the H3K18ac and H3K27ac marks that are related with chromatin relaxation and transcriptional activation [137].

The N-terminal region therefore has a dual regulatory role by i) restricting p53 activity in stress-free conditions and ii) fostering the recruitment of co-activators that promote chromatin opening and deposit C-terminal modifications required for complete p53 transactivation events.

1.3.1.2 The DNA binding domain

The central region of p53 is occupied by the core DNA binding domain (DBD), a highly structured module that binds the DNA at specific sequences. The crystal structure of the DBD, that spans residues 94 to 292, bound to DNA revealed key contact residues and a set of structurally crucial arginines surrounding the double helix [138]. Indeed, five arginines within this region (R175, R248, R249, R273, R282) concentrate more than 20% of all p53 mutations in human cancers and are thus named ‘hot spots’ (Fig. 1.8A). Mutation of these residues can directly affect p53-DNA binding, namely contact mutants (R273, R248), but can also impact p53’s structure leading to an aberrant folding configuration (conformational/structural mutants, R175, R249, R282) [139].

The structure of the p53's DBD also determines the specificity for a DNA consensus sequence [140]. The motif 5'-RRRCWWGYYY-3' is positioned in tandem at the promoters of p53's target genes, constituting the p53 responsive element (p53-RE). These palindromic tandem motifs form the perfect platform for a tetrameric p53 to tightly bind the DNA helix (Fig. 1.8B) [141]. The variability included in p53's consensus sequence determines distinct interaction dynamics and binding affinities at different p53-RE influencing subsequent transactivation events [141].

p53 binding to the RE of its target genes is also regulated by the presence of PTMs in the DBD. Although many PTMs in the DBD have been detected in high-throughput proteomics studies, the attribution of physiologically relevant functions to specific modifications still remains challenging. An exception to the rule is the Tip60 and hMOF-dependent acetylation of K120. Upon DNA damage, this modification is deposited in p53's K120, increasing p53's affinity for the RE of apoptotic genes such as BCL-2 associated X *(BAX)* and BCL-2 binding component 3 (*BBC3*, *PUMA*) but not the negative regulator *MDM2* [142,143]. Accordingly, $p53^{K120R}$ mutants have impaired apoptotic responses but trigger proficient growth arrest, reflecting how p53-dependent cell fate responses can be regulated at the level of p53's DNA binding properties. Interestingly, mice harbouring mutations in the acetylation sites analogous to human K120 and K164 (K117, K161, K162) lack proficient cell cycle arrest, apoptosis and senescence responses but still accomplish efficient tumour suppression *via* p53-depedent metabolic control and the cell death mechanism ferroptosis [144-146].

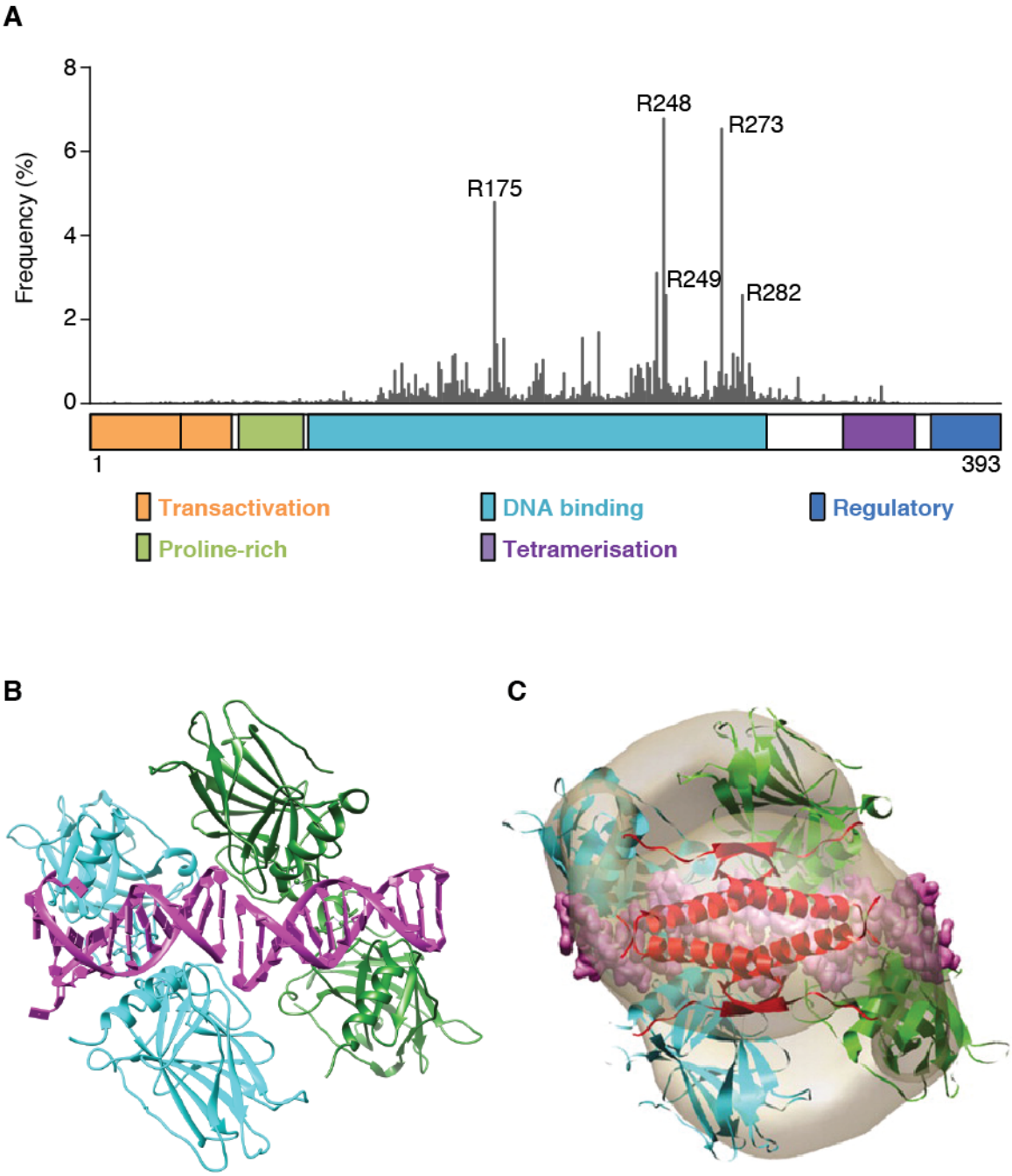


Figure 1.8. Tetrameric p53 binds to the DNA through key residues in the DBD region. (A) Localisation and frequency of p53 mutations in human cancers. Data were obtained from the International Agency for Research on Cancer (IARC) p53 Database (http://p53/iarc.fr), R18, April 2016 for N=27,852 patients [147]. (B) Structural representation of the quaternary structure of human p53 DBD bound to DNA (PDB ID: 2AC0). Model whereby a dimer of dimers (blue and green) binds cooperatively to DNA (magenta) [141]. (C) 3D-EM map for human tetrameric p53 bound to a single DNA molecule. The tetramerisation domain (red) is substantially separated from the DBD-DNA complexes and provides a rigid stable structure. Image from [148].

In addition to DNA, this central region has been reported to foster protein-protein interactions. The SV40 large T antigen undertakes the inactivation of p53 activities *via* direct binding to the DBD and disruption of p53 transactivation. The cofactor proteins 53BP1 and 53BP2 also interact with p53's DBD and enhance p53 transcription [41]. While the extent of p53 modulation by 53BP1 is still unknown, 53BP2, better known as apoptosis-stimulating of p53 protein 2 (ASPP2), has been extensively characterised as a specific activator of p53's apoptotic function [149].

1.3.1.3 The tetramerisation domain

Early findings reported p53's ability to form high order structures both in absence and presence of DNA [150-152]. These structures were only formed in presence of an intact C-terminal region, where a 30-amino acid region was eventually identified as the ultimate tetramerisation domain (TD) [153,154]. The crystal structure revealed a β-sheet connected to an α-helix by a one-amino acid sharp turn forming a V-shape structure [154]. Two monomers aggregate by interconnecting their TD with the β-sheets in an antiparallel conformation creating a helix structure with a hydrophobic surface that connects with another p53 dimer, forming the final tetramer as a dimer of dimers (Fig. 1.8C) [154]. A long, unstructured loop connects the DBD to the TD, initially conferring flexibility to the whole structure and eventually allowing the tetramer to bind the DNA [141]. Remarkably, although the DBD of p53 is able to bind DNA in isolation, tetramerisation increases the binding affinity and the overall stability of the protein-DNA complex [155].

1.3.1.4 The C-terminal regulatory region

The C-terminal tail of p53 is a lysine-rich peptide segment with non-specific DNA binding properties [156]. This C-terminal domain (CTD), so called, the regulatory region, is subject to a plethora of PTMs, including methylation, acetylation, ubiquitination, phosphorylation, neddylation and sumoylation [157]. In this specific case, small-scale, targeted approaches have led to an extremely sensitive detection of CTD modifications; however, the biological implications remain enigmatic. In humans, two 3K clusters (K370, K372, K373; K380, K382, K386) concentrate almost exclusively the CTD PTMs, with a small representation of phosphorylation in S/T residues in that region. Interestingly, mice harbouring mutations in the equivalent lysines ($p53^{7KR}$) and acetylation-deficient mice ($p53^{6KR}$) display no dramatic phenotypic features, showing cell cycle arrest and apoptotic responses comparable to the wild-type (wt) counterparts [158,159]. However, $p53^{7KR}$ mice present a slight hyperactivity in response to DNA damage which manifests in general hypersensitivity to IR by alterations of the hematopoietic stem cell (HSC) homeostasis [158,160]. Collectively, these observations suggest very specific context-dependent roles for the PTMs in p53's CTD region.

1.3.2 Layers of p53 regulation

Proficient p53 function is crucial for cellular homeostasis and tumour suppression. In order to achieve a timely-regulated, accurate p53-dependent response in a given context, cells rely on a multi-layered regulatory system. As per Kruse and Gu classification, p53 regulation occurs mainly at three levels: i) stability, ii) antirepression and iii) target-specific activation [161].

1.3.2.1 Layer 1: p53 stability

Keeping p53 protein levels at bay is critical for unstressed cells to allow cell cycle progression. This regulation is undertaken at a post-translational level with the engagement of ubiquitin ligases and the subsequent proteasomal degradation. MDM2 is the primary E3 ubiquitin ligase for p53; MDM2 homodimers, or alternatively MDM2-MDM4 heterodimers, bind to p53's TAD and reportedly conjugate ubiquitin in the highly modified CTD but also DBD and TD which suffice to target p53 for proteasomal degradation [127,128,162-164]. In addition, stress stimuli activate a feedback regulatory loop. Initially, the MDM2-p53 complex is disrupted with the consequent abrogation of the degradation mechanism and increase in p53 protein levels. Active p53 induces transcription of the *MDM2* gene, leading to an accumulation of MDM2 protein and a restoration of the degradation-based regulation [165,166]. This classical model has, nonetheless, some caveats. While the degradation dogma remains true, its ultimate relevance to p53 regulation still remains to be determined. Loss of MDM2 in mice causes early embryonic lethality, rescued by simultaneous loss of p53 [167,168]. Interestingly, mice harbouring specific mutation on the RING domain of MDM2, that efficiently disrupts the E3 ubiquitin ligase activity but keeps intact p53 binding and dimerisation properties, show normal embryonic development [169]. Additionally, human cells with analogous MDM2 mutations have limited p53 activity despite presenting increased levels of p53 protein [170]. The response to DNA damage is, however, exacerbated in that specific cellular background and leads to lethality, outlining the relevance for MDM2-mediated p53 degradation in stress responses [169].

Other E3 ubiquitin ligases have been reported to contribute to p53 turnover in an MDM2-independent manner. *In vivo* and *in vitro* approaches have identified p53-induced RING-H2 (Pirh2), constitutive photomorphogenesis protein 1 (COP1), and alternative-reading frame binding protein 1 (Arf-BP1) as effective regulators of p53 degradation [171-173]. How these proteins contribute to the overall extent of p53-dependent responses is still an outstanding question that may open new research avenues in the ubiquitin-dependent modulation of the p53 network.

1.3.2.2. Layer 2: antirepression

The missing part of the MDM2-p53 puzzle may come from a degradation-independent regulatory mechanism, called antirepression. Another MDM family member, MDM4, forms heterodimers with MDM2 that bind p53. MDM4 has been reported to impact on p53 stability by modulating MDM2 E3-ubiquitin ligase activity over p53 [129,166,170]. However, unlike MDM2, MDM4 alone is unable to promote p53 degradation but eventually impedes p53-dependent transactivation [124]. Accordingly, MDM4-deficient mice die in early embryonic stages in an MDM2-independent manner, and the lethality can be overcome by p53 loss [174-176]. This suggests both cooperation between MDM2 and MDM4 and a non-concomitant mechanism of MDM4-mediated p53 repression.

Both MDM2- and MDM4-p53 complexes have been detected in association with the RE of p53's target genes, correlating with an inhibition of p53's transactivation events [144,177-179]. *In vitro*, CBP/Tip60-mediated acetylation of p53 promotes the release of MDM2 and MDM4 from the DNA complexes [144]. Similarly occurs *in vivo*, where DNA damage frees the p53-RE complex from

MDM2 and MDM4 eliminating the *in situ* repression barrier to transcription [144,180]. A p53 acetylation dead mutant ($p53^{8KR}$) is inactive by constitutively binding MDM2 and MDM4 at the promoters, and it can become active by artificially removing those factors, suggesting that it may not be the acetylation *per se*, but the release of its negative regulators what triggers p53 activity [144].

1.3.2.3 Layer 3: target-specific activation

p53 responds to cellular stresses of diverse origin and nature by inducing different transcription programmes. How a specific physiological scenario dictates p53 *in vivo* selectivity is still unclear, although some hints have been left over the years.

The REs on the promoters of p53 target genes vary in their nucleotide composition [140,141]. This alone determines the binding dynamics with the p53 tetramer and results in differential binding affinities [141,181]. Genes involved in cell cycle arrest and the negative regulator *MDM2* are under the control of high-affinity p53-RE. Conversely, a general trend towards low affinity p53-REs is present in the promoters of the apoptotic gene panel [181]. The *in vitro* affinity studies correlate significantly with the *in vivo* timeline for p53-dependent gene transactivation. Genes involved in cell cycle arrest are activated early, while apoptotic genes reach their transcriptional peak later in the response [182]. Moreover, activation of the transcriptional apoptotic programme requires several circumstances to concur, including release from specific inhibitors (iASPP), cofactor recruitment (ASSP1/2) and specific p53 acetylation, adding a tighter control to an irreversible cellular scenario [161].

1.3.3 Functional diversity of the p53 protein

Classically, p53 has been closely linked to the DNA damage response and protection against oncogenic stimuli. Decades of study have extended the array

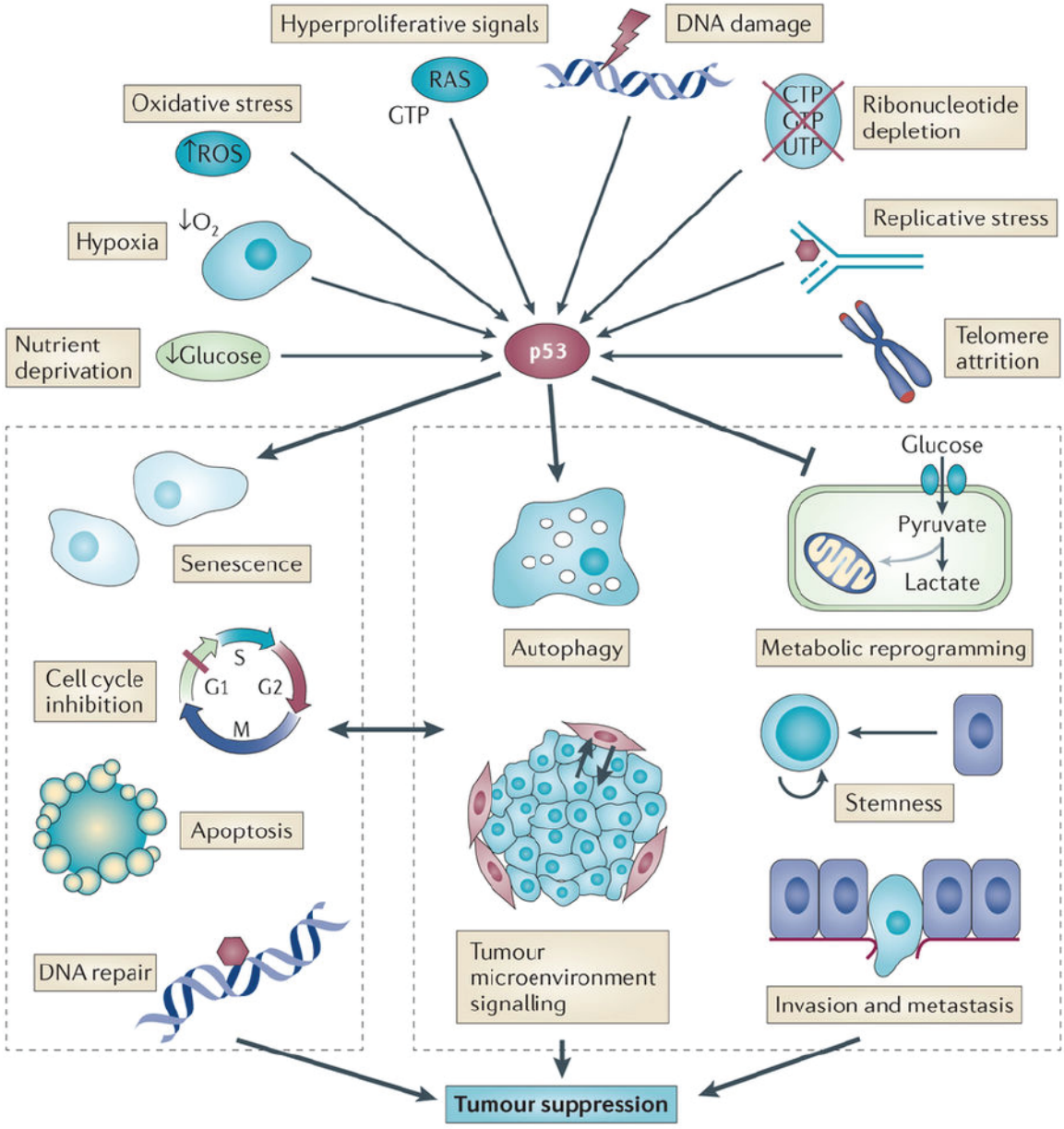


Figure 1.9. Overview of p53's cellular functions. p53 responds to an array of cellular stresses that ultimately endanger genome integrity and cellular metabolism. p53 action is exerted at two major levels (left) i) activation of cell cycle checkpoints to allow the evaluation and repair of DNA lesions and ii) induction of cell death in irreversibly damaged cells. However, p53's vast transcriptional programme extends to other relevant processes in cellular physiology and microenvironment control (right). Altogether, p53 activities are directed to safeguard cellular homeostasis and consequently, are a major force against tumourigenesis. Image from [183].

of stresses that endanger our genome, as well as reported metabolic stimuli that elicit p53-dependent responses. Additionally, deep study of the p53-dependent transcriptome has provided glimpses of p53's contribution to metabolic control, differentiation, cell migration and cell to cell communication [183]. These processes connect with the three major axes of p53-dependent life-death cell fate decisions, i) checkpoint control, ii) senescence, and iii) apoptosis to provide control of cellular homeostasis and complete anti-tumorigenic responses (Fig. 1.9).

1.3.3.1 Cell cycle control: the checkpoints

As per Hartwell and Weinert's definition, cell cycle checkpoints are the controls that ensure the order of cell cycle events [184]. The presence of an intact pre-replicative chromatin, the accurate replication and a correct chromosomal segregation in mitosis are key features evaluated at the G1/S, G2/M and the spindle assembly checkpoints (SAC), respectively, and ensure an intact genome to be transmitted to the next cell generation.

DNA lesions elicit reversible, p53-dependent cell cycle arrest at the G1/S transition in order to allow DNA repair to occur and prevent deleterious replication of damaged DNA. Mechanistically, transactivation of the cyclin-dependent kinase inhibitor 1A (*CDKN1A*) gene leads to a prompt accumulation of its protein product, p21 (CIP1, WAF). p21 binds and inactivates the G1 cyclin-CDK complexes preventing S-phase entry [32]. Mice lacking p21 are defective in blocking progression to S-phase after ionising radiation albeit to a lesser extent than the complete deficiency of their *p53*$^{-/-}$ counterparts, suggesting an involvement for additional p53 targets [185-187].

The involvement of p53 in the G2/M transition is less prominent and shows a cell-specific component [188]. Initial G2 arrest after ionising and UV radiation occurs in a p53-independent manner and is mediated by the rapid degradation of the cell division cycle 25A (CDC25A) protein induced by the ataxia telangiectasia and Rad3-related protein (ATR)-Chk1 pathway [189]. p53 activity is nonetheless involved in the later checkpoint maintenance *via* activation of its target genes growth arrest and DNA-damage-inducible 45 alpha (*GADD45A*) and *14-3-3*. Both GADD45A and 14-3-3 proteins inhibit the activation of the M-phase promoting factor (MPF) complex thereby impeding G2/M transition [190-192]. Prolonged, transcriptionally-controlled, p53-dependent G2/M arrest eventually leads to a loss of reversibility and definitive cell fate decisions such as senescence [193,194].

Early studies also linked p53 and the control of cellular ploidy by the SAC. The first phenotypic manifestation observed was the increase of polyploid cells in a *p53*$^{-/-}$ mouse embryonic fibroblast (MEF) population after exposure to microtubule poisons [195]. Later studies outlined a step-wise surveillance mechanism; misegregations result of aberrant SAC activity were subject to specific p53-dependent evaluation in the succeeding G1 phase [196]. The similarities with the classical DNA-damage induced G1/S checkpoint are notorious, showing a heavy reliance on p21-dependent arrest [197]. Nonetheless, it seems likely that specific traits apply to the sensing of this particular form of DNA aberration and the subsequent activation of the p53 surveillance mechanism.

1.3.3.2 Senescence

Senescence could be defined as a state of permanent growth arrest. Senescent cells display a characteristic flat and enlarged morphology, a loss of replicative capacity and a constant repression of cell cycle progression *via* p53 and p16-pRB activities [198]. DNA damage, oncogenic activation, telomere shortening or increased levels of oxidative stress can initiate a p53-dependent senescence programme [199]. p53-induced p21 expression is crucial for both temporary and permanent cell cycle arrest. Interestingly, the boundaries between short-term arrest and senescence are poorly understood and the step that dictates the eventual withdrawal of the cell cycle may be context-specific. For instance, in G2 arrested cells, nuclear retention of cyclin B1 mediated by the p53-p21 axis marks the switch to a senescent state [193].

Similarly to p53-deficiency, human fibroblasts lacking p21 failed to arrest in culture, completely bypassing the senescence response [200]. Additionally, inactivation of p53 or p21 in senescent cells promotes cell cycle re-entering [201]. Remarkably, the capability of p53 inactivation in reversing the senescent state correlates with a simultaneous deficiency in the second branch of the senescent response, p16-pRB [201]. Furthermore, either loss-of-function p53 or p16 are sufficient to override oncogene-induced senescence (OIS) in murine but not human cells [202]. Altogether, both independent and cooperative actions of those two pathways are essential for the maintenance of the irreversible senescent state induced by diverse stimuli.

1.3.3.3 Apoptosis

When the cellular homeostasis is irrevocably perturbed, cells can initiate a cascade of events leading to controlled and programmed cell death: the apoptotic cascade [203].

Apoptosis encompasses two different p53-controlled, high-complexity pathways, named intrinsic and extrinsic. Endogenous stress stimuli target the intrinsic apoptotic pathway, coordinated by the tight balance between the pro- and the anti-apoptotic B-cell lymphoma 2 (Bcl-2) family members. Specifically, induction of p53 by the DDR results in the transactivation of three major pro-apoptotic targets, *BAX*, *BBC3* (PUMA), and *NOXA*, eliciting the onset of the apoptotic response [204,205]. Initially, pro-apoptotic proteins cause the loss of permeability in the mitochondria followed by the activation of the apoptotic effector Caspase cascade. External, receptor-mediated death stimuli signal through the extrinsic apoptotic pathway ultimately converging in the Caspase cascade. For instance, the accumulation of the p53 targets death receptor 5 (DR5) and the pair receptor-ligand, FAS-FASLG sensitise the cells to apoptosis by generating a cellular scenario more receptive to death signals [36].

Aside from its classical transcription-related roles, p53 is involved in apoptosis in a non-transcriptional manner [206,207]. Cytoplasmic p53 can directly interact with several Bcl-2 family members and promote mitochondria permeability [208]. Additionally, cytoplasmic p53 inhibits the autophagy process directed to eliminate altered mitochondria thus allowing apoptotic progression [209]. Together, the different levels of apoptotic control *via* p53 ensure the activation of a robust cell death mechanism upon endogenous and/or exogenous stress signals.

1.3.4 p53 and tumourigenesis

The role of p53 in safeguarding genome integrity and cellular homeostasis is crucial for the prevention of tumourigenesis. Somatic mutations in the *TP53* gene are present in more than 50% of all cancers and genetic inherited monoallelic mutations cause a cancer predisposition disorder, the Li-Fraumeni syndrome [210]. Furthermore, *p53*$^{-/-}$ mice are tumour prone and p53 mutation is often associated with both loss of tumour suppression and acquisition of oncogenic properties [211].

Initially, evidence of p53 accumulation in tumour cells coupled with overexpression studies hinting to p53's oncogenic potential promptly classified p53 as a proto-oncogene. Some years and several contradictory reports later, it became apparent that such studies were characterising mutant p53, and not its wt form [212]. The term 'mutant p53' includes a myriad of p53 proteins with different structural and functional properties. Tumorigenic mutations concentrate in hot-spot regions, corresponding to the DNA binding domain, and select for complete loss of normal p53 transcriptional activity (Fig. 1.8A). Interestingly, specific monoallelic mutations on p53 suffice to annihilate tumour suppression. Mutant, highly stable p53 forms act as dominant negative over its wt counterpart; a single aberrant subunit holds the capacity to disrupt the tetrameric structure of transcriptionally active p53 forms [213]. In addition to the loss of tumour suppression, p53 mutation may result in pro-oncogenic gain-of-function (GOF) [210]. Aberrant p53 presents unique characteristics and exerts is oncogenic action *via* new interaction partners (Fig. 1.10).

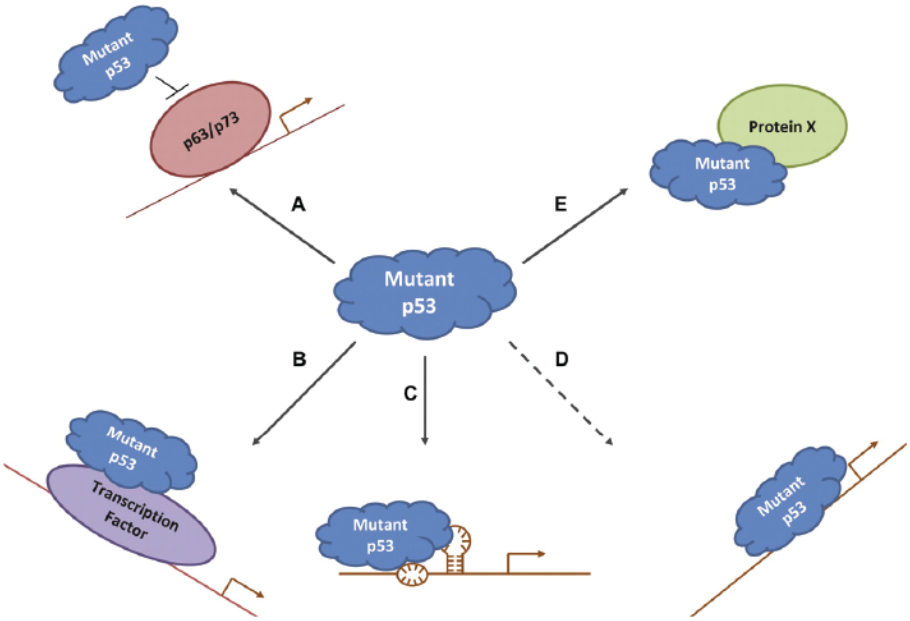


Figure 1.10. Mechanisms of action of mutant p53 proteins. (A) Mutant p53 (R175H, Y220C, R248W) interacts with the p63/p73 transcription factors and inhibits the activity. (B) Mutant p53 can also enhance transcription factor activity; for instance, $p53^{R157H}$ binds the vitamin D nuclear receptor (VDR) and stimulates the activation of cell survival genes. (C, D) Structure and sequence-specific DNA binding by mutant p53 regulates a new transcriptional programme. While sequence-specific binding is still unclear, reflected by the dashed arrow, binding to AT-rich, non-canonical DNA structures at matrix attachment regions (MARs) has been recurrently reported [214]. (E) A novel interactome has been defined for mutant p53, including MRE11, TopBP1, and PML proteins. Image from [210].

Although missense mutations constitute the most frequent form of p53 alteration in human cancers, frameshift and nonsense mutations account for 9.06% and 8.17% of all cases, respectively (IARC p53 Database, R18, April 2016 for N=28,869 patients [147]). Moreover, monoallelic dominant-negative mutations are often accompanied by loss of heterozygosity (LOH), pinpointing the relevance of the loss of the *WT* allele in tumour progression [215]. Notably, $p53^{-/-}$ mice develop tumours at an early age with a high incidence of T-cell lymphomas with recurrent aneuploidy while $p53^{+/-}$ mice tumours have a later onset, usually upon LOH, closely mimicking human Li-Fraumeni syndrome [211,216,217]. The well-characterised loss-of-function phenotype has been extensively used as a

reference to study the contribution of distinct p53 functions to tumour suppression. Separation of function mutants that retain the ability to induce cell cycle arrest but show deficient apoptotic responses ($p53^{R172P}$ and $p53^{E177R}$, equivalent to human $p53^{R175P}$ and $p53^{E180R}$, respectively) suppress early onset T-cell lymphomas in biallelically-mutated mice strains [217,218]. Nonetheless, the protection is not complete, as mice from both genotypic backgrounds suffer from lymphoma at later stages. Notably, late lymphomas do not display aneuploidy, highlighting the relevance of chromosomal stability in tumour suppression [217]. Simultaneous loss of p21 in $p53^{R172P/R172P}$ mice is still insufficient to recapitulate the phenotype of their $p53^{-/-}$ counterparts [219]. Cell cycle arrest and apoptosis are thus required but not sufficient for complete p53 anti-tumorigenic activities, with other p53-dependent processes significantly contributing to the overall response.

p53 loss is also relevant in the context of oncogene-driven cancers. In the *Eμ-Myc* model for high incidence spontaneous B-cell lymphoma, loss of *p53* itself, and to a lesser extent, individual loss of the apoptotic genes *PUMA* and *BAX* result in accelerated lymphomagenesis [220-223]. Similarly, apoptotic defective $p53^{R172P}$ and $p53^{E177R}$ mice present early onset B-cell lymphoma in this context [218,224]. Similar to p53-driven apoptosis, p53-dependent OIS represents a strong barrier to tumour development and accordingly, p53 loss is a key enabling factor for oncogenic transformation. Studies in both murine and human cells with oncogene expression link tumour suppression to a mechanism whereby chronically active DNA damage checkpoint responses is at the source of senescence [225,226]. In addition, p53 induces senescence in RAS-transformed murine liver carcinomas promoting tumour shrinking in coordination

with the innate immune system [227]. Oncogenic transformation by high expression of RAS is also counteracted by p53-dependent senescence in the mammary glands, where p53 inactivation is required for tumour progression [228].

Altogether, p53 is considered the central player in the control of life *vs* death cell fate decisions upon stress stimuli, and accordingly, p53-driven responses constitute the major cellular barrier against tumourigenesis.

1.4 53BP1 and p53: the connection

As its name implies, 53BP1 was discovered as a p53 binding protein more than two decades ago. Despite the extensive and thorough research that has since surrounded both proteins only scarce studies have attempted to draw a functional relationship between them. Structural approaches revealed that p53 interacts with 53BP1 tandem BRCT and tandem Tudor domains and *in vivo* and *in vitro* studies hinted to 53BP1 as a positive regulator of p53 activity and a collaborator in tumour suppression. However, the 'Hows', 'Wheres' and 'Whens' of this protein duo remain enigmatic.

1.4.1 53BP1 discovery and early studies

In the 90s, the understanding of p53 physiological functions and the identification of interaction partners experienced significant advances, starting to build up the complex p53 network. In 1994, a yeast-two hybrid screen identified two novel, unrelated proteins that interact with the DNA binding domain of p53 and named them 53BP1 and 53BP2 (also known as the aforementioned ASPP2) [41]. This initial study reported a robust interaction between the last 270 amino

acids of 53BP1 and the core of p53, generating an impediment to p53's DNA binding activity [41,229]. Despite the impossibility of a 53BP1-p53-DNA complex, 53BP1 was soon reported to activate p53-mediated transcription in a reporter-based assay and p21 expression *in vivo* [230].

In parallel, protein sequence alignments of the region in 53BP1 fostering the interaction with p53 revealed a striking similarity with the BRCT domain in BRCA1 [231]. BRCT domains had been previously identified in other DNA repair and checkpoint proteins, including 53BP1's yeast orthologues Crb2 and Rad9, and a potential functional association with 53BP1 was immediately suggested [231,232]. This idea was further supported by the nuclear distribution of 53BP1, a characteristic dotted pattern resembling the organisation of DNA damage-induced BRCA1 and RAD51 [230]. A potential DNA damage-related role for 53BP1 opened new research avenues, and initial efforts tying 53BP1's tandem BRCT into p53-dependent transcription were soon neglected.

1.4.2 Structural insights

Despite the rarity of functional approaches, some structural studies provided valuable insight into 53BP1-p53 interaction. The crystal structure of 53BP1's tandem BRCT bound to p53's DBD depicted an interaction surface requiring the inter-BRCT linker in 53BP1 (Fig. 1.11A) [78]. The multiple hydrogen bonds connecting 53BP1 and p53 emerge mainly from R248 and R249 in p53. R248 bridges with D1861 at the inter-BRCT linker and also L1847 while R249 hydrogen bonds with N1845 and N1844 placed at the C-terminal end of the first BRCT domain [78,233]. Accordingly, individual mutation of the hot spots R248 and R249 is sufficient to completely abolish 53BP1-p53 interaction [229]. The

interaction dynamics between 53BP1 and p53 further supported the idea of BRCT domains as more than phosphobinding modules in agreement with the pioneer inter-BRCT linker structure of the XRCC4-Lig4 complex [234]. In fact, 53BP1's BRCT-p53 interaction does not interfere with the phospho-ligand binding pocket, thereby potentially permitting the simultaneous presence of other BRCT interactors in the complex (Fig. 1.11A).

In addition to 53BP1's BRCT, several reports have also described the ability of 53BP1's tandem Tudor domain to foster interactions with p53 by reading lysine methylation marks in the C-terminal regulatory region. The environment surrounding K382 in p53 closely resembles the H4K20 peptide, hence dimethylation in this residue creates a perfect substrate for 53BP1's Tudor domain recognition (Fig. 1.11B) [235]. Actually, the peptide containing the dimethylated form of K382 (p53K382me2) displayed an even stronger affinity for 53BP1's Tudor than the H4K20me2 in *in vitro* binding assays [68]. Both peptides use a hydrophobic cage within the first Tudor unit where the methylated lysine is encased by the side chains of four aromatic amino acids W1495, Y1502, F1519 and Y1523. Additionally a fifth residue, D1521, forms a hydrogen bond with the methylated lysine [68]. 53BP1's Tudor is a dynamic module whose plasticity allows the accommodation of methylpeptides with remarkable sequence divergence (Fig. 1.11B) [236]. Despite its divergence in sequence with H4K20me2 and p53K382me2 peptides, p53K370me2 is able to robustly interact with 53BP1's Tudor *in vitro* albeit with lesser affinity [236]. The same holds true for p53K372me2 evidencing the multiple binding alternatives of p53's C-terminal tail as a 53BP1 docking site (Fig. 1.11C).

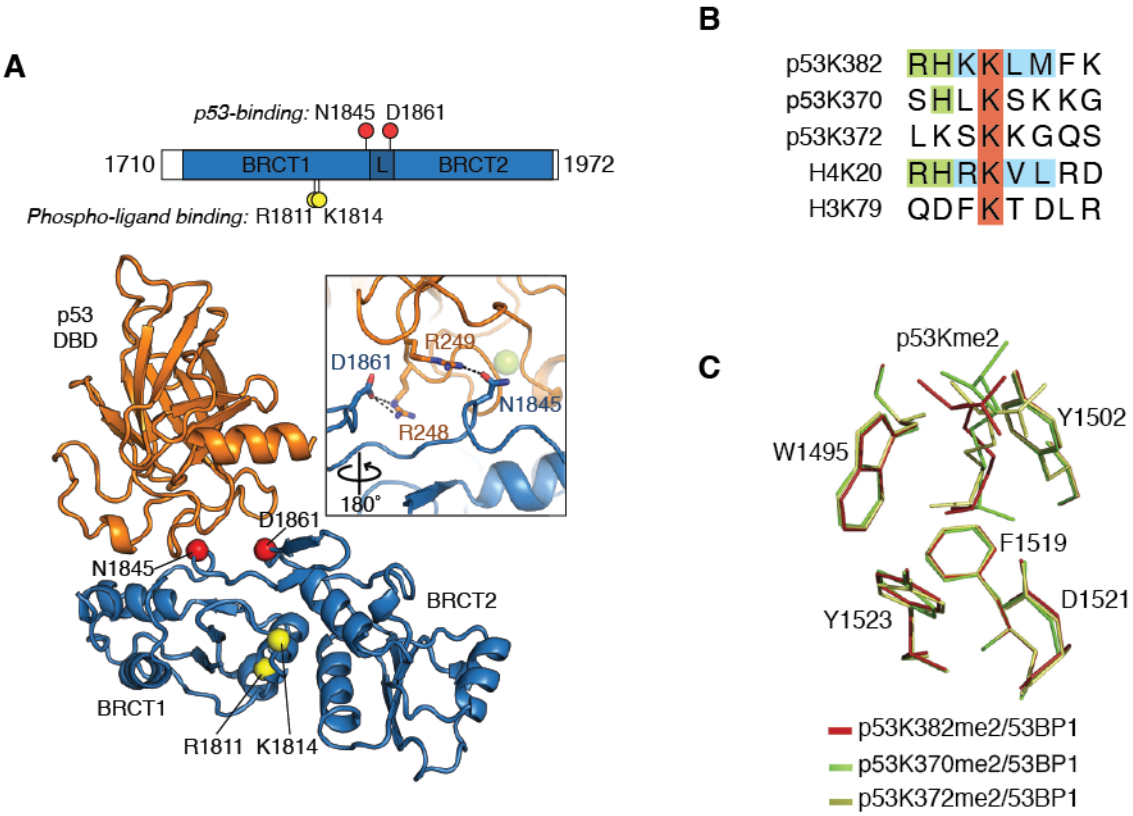


Figure 1.11. Structural insights on 53BP1-p53 interactions. (A) Structure of p53 DBD bound to the tandem BRCT of 53BP1 (PDB ID: 1KZY). Key residues for p53 binding (red) and phospho-ligand binding (yellow) are highlighted in the structure. Structure depiction generated by Prof C. Siebold and Prof J. R. Chapman. (B) Sequence alignment of p53, H4 and H3 peptides that bind to 53BP1's Tudor domain. Lysines targeted for dimethylation are depicted in orange and moderately and weakly conserved residues in green and blue. (C) Superimposed 53BP1's Tudor hydrophobic cage bound to the three p53Kme2 residues. Image adapted from [236].

1.4.3 Cooperation *vs* synergy

In addition to the initial characterisation and the structural insights above described, a few studies provided evidence of a functional interaction between those two proteins.

Consistent with 53BP1's role in the immune system, *53bp1*$^{-/-}$ mice suffer from unresolved DSBs at the recombination regions that are prone to translocation. Efficient checkpoint activities accomplish the elimination of aberrant B and T cells, and therefore *53bp1*$^{-/-}$ mice display immunodeficiency but

have minor tumour predisposition [96,237,238]. However, simultaneous loss of 53BP1 and p53 results mainly in thymic lymphomas whose appearance occurs even earlier than in a *p53*$^{-/-}$ genetic background [238]. Cytogenetically, those early-onset malignancies fall into two separate categories, lymphomas with clonal translocations, and a subset harbouring aneuploidy [237,238]. While aneuploidy is a characteristic trait of *p53*$^{-/-}$ tumours, the presence of clonal translocations suggests an abnormal progression of T cells with defective 53BP1-dependent NHEJ. In this context, 53BP1 and p53 present a synergistic relation in tumour suppression by exerting the regulation of two independent but functionally-connected pathways [239]. Nonetheless, this regulatory scenario whereby loss of p53 allows progression of *53BP1*$^{-/-}$ cells with acquired pre-malignant translocations fails to explain the purpose of the physical interaction between 53BP1 and p53.

Separately, the p53 field was invested in the discovery of MDM2 inhibitors and their prospective application in cancer therapy. The small-molecule MDM2 antagonist Nutlin-3a (N3a) strongly interacts with MDM2 (IC_{50}= 90 nM) *via* the same surface required for p53 binding (Fig. 1.12A) [239]. This potent competitor allows the release and stabilisation of p53, transactivation of target genes and subsequent cell death (Fig. 1.12B) [240].

A shRNA screen aiming to identify genes that mediated cellular toxicity to (±)-Nutlin-3 (N3) in the MCF-7 breast cancer cell line reported a correlation between resistance to this MDM2 antagonist and 53BP1 downregulation [240].

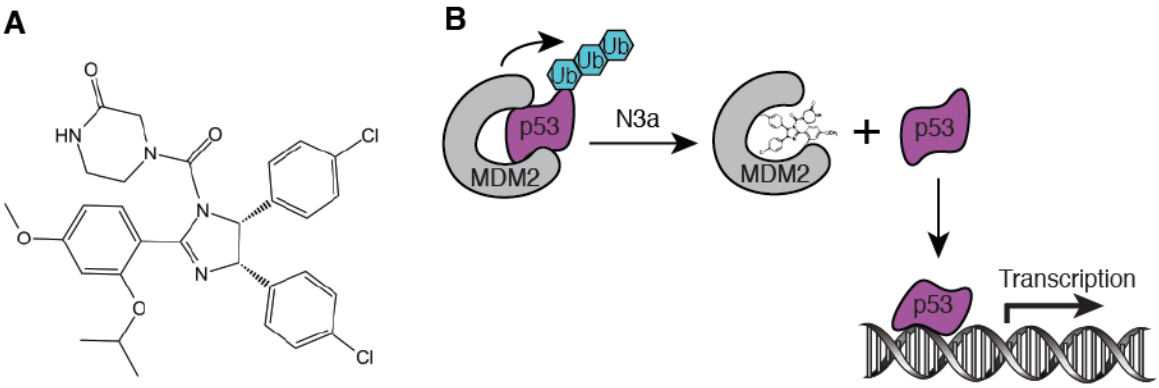


Figure 1.12. Nutlin-3a is a potent MDM2 antagonist. (A) Chemical structure of Nutlin-3a. Despite being commercialised as a racemic (±)-Nutlin-3 (N3), the second enantiomer, Nutlin-3b has very low inhibitory activity (IC_{50}= 13.6 μM) (B) Schematic representation of Nutlin-3a mechanism of action.

Besides p53 itself, 53BP1 was the screen's top hit, hinting at a cooperative relationship between 53BP1 and p53 in this specific cellular response. Cells with depleted 53BP1 proliferated in the presence of N3 and displayed suboptimal p21 and MDM2 induction [240,241]. Similar incomplete p53-dependent transactivation events were observed in response to the DNA intercalating agent doxorubicin [241]. Although both observations strongly suggest a cofactor role for 53BP1 in p53-mediated stress responses, the mechanism whereby 53BP1 modulates p53-dependent transactivation events is, nonetheless, ill-defined.

1.5 Aims

The present study aims to conclusively shed light into the 53BP1-p53 interplay by establishing the functional relevance of 53BP1 in p53-dependent responses and defining the associated mechanisms underpinning 53BP1-p53 connections. To this end, four major outstanding questions will be specifically examined:

1. The function of 53BP1 in p53-mediated responses. Initially, the effect of 53BP1 on the regulation of p53-dependent responses will be defined using both phenotypical and molecular readouts. The 53BP1 protein will be subsequently dissected in detailed structure-function analyses to determine the individual domain contribution to p53 responses.
2. The characterisation of USP28's function in p53 responses. As a scaffolding protein, 53BP1 recruits effector partners to ultimately achieve the functional effect. 53BP1's tandem BRCT interacts with the deubiquitinase USP28, whose involvement in p53 responses has been previously suggested [86,240]. Thus, the impact of USP28 in 53BP1-dependent p53 regulation will be evaluated. Additional structure-function analyses will be performed to tackle the architecture of the USP28 protein and determine the minimum sequence requirements for the modulation of p53-dependent responses.
3. The mechanistic implications for p53 functionality. Regulation of p53 responses can be undertaken at different levels (Section 1.3). The influence of 53BP1 and USP28 in the different layers of p53 regulation will be examined, with special emphasis on the potential relevance of ubiquitin-dependent modulatory events in p53.
4. The *in vivo* significance of the connection between 53BP1 and p53. The concept of 53BP1 as an integrating node of NHEJ-driven repair and p53 modulation will be tested *in vivo*. The well-described 53BP1 functionality in the immune system will be revisited, alongside specific p53-dependent responses, in order to contextualise the physiological relevance of 53BP1-dependent p53 regulation.

Chapter 2

MATERIALS AND METHODS

2.1 Cell methods

2.1.1 Cell lines and cell culture

MCF-7 human breast adenocarcinoma, hTERT RPE-1 retinal pigmental epithelial and human embryonic kidney (HEK) 293T cell lines were cultured in Dulbecco's Modified Eagle's Medium (DMEM) (Sigma-Aldrich, St Louis, MO, USA) supplemented with 10% (v/v) foetal bovine serum (FBS) (Firstlink, Woelhampton, UK), 50 units/ml penicillin, 50 mg/ml streptomycin (Sigma-Aldrich) and 2 mM L-glutamine (Sigma-Aldrich) in a humidified atmosphere at 37 ^{o}C and 5% CO_2.

Primary mouse embryonic fibroblasts were cultured following the aforementioned conditions in an oxygen-controlled environment at 3% O_2.

Primary splenocytes and purified B lymphocytes were cultured in Roswell Park Memorial Institute (RPMI) medium (Sigma-Aldrich) supplemented with 10% (v/v) FBS (Life Technologies, Carlsbad, CA, USA), 50 units/ml penicillin, 50 mg/ml streptomycin (Sigma-Aldrich), 2 mM L-glutamine (Sigma-Aldrich), 5% (v/v) non-essential amino acids (Life Technologies), 5% (v/v) sodium pyruvate (Sigma-Aldrich) and 50 μM β-mercaptoethanol (Sigma-Aldrich) in a humidified atmosphere at 37 ^{o}C and 5% CO_2.

2.1.2 Generation of stable knockout cell lines by CRISPR/Cas9

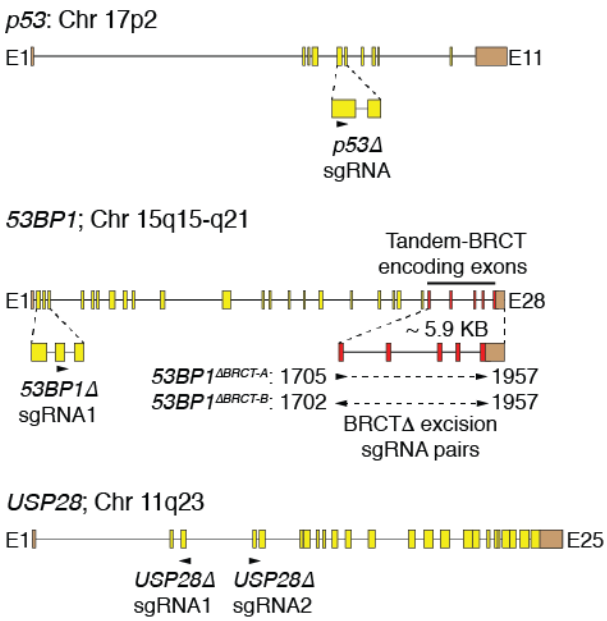
Tumour suppressor p53 (*TP53*, *p53*), p53 binding protein 1 (*TP53BP1, 53BP1*) and ubiquitin specific protease 28 (*USP28*) genes were targeted using the clustered regularly interspaced short palindromic repeats (CRISPR)/associated protein 9 nuclease (Cas9) system. Guide RNAs (gRNAs) targeting different exons (Fig. 2.1A-B) were designed using a CRISPR design online tool (http://crispr.mit.edu) and cloned into the pX330 vector (Addgene 42230) modified to include a puromycin resistance gene (hereinafter pX330-PURO, a gift from Dr B. Davies).

Briefly, oligonucleotide pairs for each individual gRNA were incubated at 95 ^{o}C in annealing buffer [10 mM Tris (pH 7.5), 0.1 M NaCl, 1 mM EDTA] for 5 minutes and subsequently gradually cooled to room temperature (RT) to allow gRNA annealing. gRNAs were ligated to BbsI-linearised (New England Biolabs, Ipswich, MA, USA) pX330-PURO using the Quick-Stick ligase (Bioline, London, UK) as per manufacturer's indications. For plasmid amplification, 2 µl of ligation reaction were mixed with 10 µl of KCM buffer (500 mM KCl, 150 mM $CaCl_2$, 250 mM $MgCl_2$) in a 50 µl reaction and incubated with 50 µl chemically competent DH5-α *E. coli* cells for 20 min on ice followed by 10 min at RT. Bacteria were then cultured in 900 µl of super optimal broth with catabolite repression (SOC) medium at 37 ^{o}C for 1 h and plated in the corresponding antibiotic-enriched LB-agar plates for overnight incubation at 37 ^{o}C. Single colonies were grown overnight in LB medium and plasmid extracted using the Qiaprep Spin Miniprep Kit (Qiagen, Hilden, Germany). Depending on purity and quantity requirements, larger LB cultures were used and plasmids purified using the Qiaprep Spin

Midiprep Kit (Qiagen). Correct gRNA integration was assessed by restriction digestion and Sanger sequencing.

MCF-7 cells were plated at a density of $2x10^5$ cells/well in a 6-well plate and transfected with the 2 µg of the individual plasmids using Fugene HD (Promega, Madison, WI, USA) transfection reagent according to manufacturer's instructions. After a 16 h-transfection, MCF-7 cells were treated with puromycin (Invivogen, San Diego, CA, USA) at 2 µg/ml for 48 h to select transfected cells. Recovered cell populations were seeded at low density and isogenic clones isolated. Ablation of protein expression or specific domain deletions were evaluated by SDS-PAGE/WB and immunofluorescence, and gene-editing events assessed by Sanger sequencing.

A



B

Target gene		Sequence (5'-3')
p53		gtgcagctgtgggttgattc
53BP1	1	gaacgaggagacggtaatagt
	BRCT N1	ctgtgagagtggagacaaca
	BRCT N2	tttgtgagcccctgtgagag
	BRCT C	ctcattgttggggagagaat
USP28	1	tgtagcaacagtgtcttgac
	2	tgccattgctttgagtctac

Figure 2.1. CRISPR/Cas9-mediated generation of protein- and domain- knockout cell lines. (A) *p53*, *53BP1* and *USP28* loci illustrating the hybridisation sites of the gRNAs that yielded the knockout cell lines used throughout this study. (B) Corresponding gRNA sequences. For the generation of $53BP1^{\Delta BRCT}$ cells, two different gRNAs targeting the N-terminal region, BRCT N1 for $53BP1^{\Delta BRCT-A}$ and BRCT N2 for $53BP1^{\Delta BRCT-B}$ were combined with a common gRNA targeting the C-terminal region, BRCT C.

2.2 Mice and primary mouse cell isolation methods

2.2.1 Mouse strains

Mice used throughout this study were generated on a C57BL/6 background. All experiments involved 8-16 week old and sex-matched littermate control animals on an inbred C57BL/6 background. *53bp1*^{L1616A} and *53bp1*^{NDRR} mice were custom generated by Dr B. Davies' group and provided alongside the protocol detailed in Section 2.2.2. *53bp1*$^{-/-}$ mice (MGI: 2654201; also C57BL/6) were generated and described elsewhere [96]. All experiments were approved by the University of Oxford Ethical Review Committee and performed under a UK Home Office Licence.

2.2.2 Mouse strain generation using the CRISPR/Cas9 technology

Mice harbouring mutations in leucine 1616 (analogous to L1619 in human) and asparagine 1845/aspartate 1861 (N1845, D1861) were provided by Dr Ben Davies' group and generated as subsequently described. Mutations were introduced by homology-directed repair using the CRISPR/Cas9 technology. Briefly, gRNAs targeting the exons containing the corresponding residues of interest in the *trp53bp1* gene (Table 2.1) were designed using the CRISPOR online tool (www.crispor.tefor.net) and cloned into pX330-PURO as in Section 2.1.2. Single stranded oligonucleotides (ssODN) harbouring mutations, altering the target amino-acid sequence to Alanine (L1616A) or Arginine (N1845R/D1861R) were designed to use as template for homology-directed repair (Table 2.2). Additionally, a silent mutation was included to introduce a PstI restriction site for downstream diagnostic analysis.

Target exon (mutation)		Sequence (5'-3')
exon 22 (L1616A)		AAGGCAGCAGATATCAGCTT
exon 26 (NDRR)	1	CCCTGAAGAGCAACGAATTC
	2	AATTACGATAGTTTTGAAGT

Table 2.1. gRNA sequences used for knock-in genome editing.

Target exon (mutation)	Sequence (5'-3')
exon 22 (L1616A)	AGAGAGCAATATGGGCTTGGCCCATATGAAGCTGTCACA CCGCTCACGAAGGCAGCAGATATCTCTGCAGGTAAGACT TTCCTGAACAACTGCCTGTGGATCCAGGCTTCGCTTAAAG GGAGGAATGGTTCCCAGGATA
exon 26 (NDRR)	CCAGTGGCATTCCTTGTGTGTCTCATGTCTGGGTCCATGA CAGTTGCCATGCCAATCAACTTCAAAACTATCGTCGGTAT CTGCTGCCTGCAGGCTATAGCCTTGAAGAGCAACGAATT CTGCGGTGGTGAGTGTTTGGAAGCCCATTTAGAGCTGAG ACAACAGGAAGAATGGCATT

Table 2.2. ssODN sequences to insert the desired mutations *via* homology-directed repair.

In the specific case of L1616A mutation, 20 ng/µl in-vitro transcribed (MEGAshortscriptTM T7 Kit, Thermo Fisher Scientific, Waltham, MA, USA) and purified (Megaclear Transcription Clean-up Kit, Thermo Fisher Scientific) gRNA, 10 ng/µl protein Cas9, along with the ssODN as a homology template at 10 ng/µl were microinjected into one of the pronuclei of one-cell stage C57BL/6J embryos and injected embryos were cultivated overnight to the two-cell stage. Two-cell embryos were then implanted into the oviduct of pseudo-pregnant CD1 foster mothers at 0.5 days post-coitum. Two monoallelically-edited C57BL/6J females were obtained and crossed to wt C57BL/6J males. Heterozygous crosses were subsequently established to obtain the biallelically-edited mice (referred to as *53bp1*^{L1616A} or *L1616A)* for experimental purposes.

Double mutation in N1845 and D1861 residues was achieved by blastocyst injection of successfully edited embryonic stem (ES) cells. Specifically, 10^6 JM8F6 ES cells were electroporated with 2.5 µg of each pX330-puro cloned gRNA alongside 8 µg of the ssODN using the Neon transfection system (Life Technologies) (3x1400V, 10 ms). Twenty-four h post-electroporation cells were selected with a 48-h puromycin pulse (600 ng/ml) and individual clones isolated and assessed for correct editing events by PstI digestion and Sanger sequencing. Twelve to sixteen ES cells from the selected clone harbouring the knock-in mutation in one allele were injected into the cystic cavity of individual blastocysts obtained from an albino C57BL/6J cross. Blastocysts were kept in culture to recover and further implanted into the uteri of 2.5-day pseudo-pregnant foster CD1 mice. Born chimeric male mice were visually evaluated and the ones showing higher percentage of ES-cell incorporation were crossed to albino C57BL/6J females. Heterozygous crosses were established to obtain the biallelically-edited mice (*53bp1*^{NDRR} or *NDRR)* for experimental purposes.

2.2.3 Mouse genotyping

Mice used in this study were genotyped *via* polymerase chain reaction (PCR) amplification of the target genomic region and subsequent PstI restriction digestion of the PCR products. DNA was extracted from mouse ear clips using a hotshot protocol. Briefly, ear clips were incubated in 75 µl of alkaline lysis reagent (pH 12) [25 mM NaOH, 0.2 mM disodium EDTA] for 30 min at 95 ^{o}C. DNA samples were then cooled to 4 ^{o}C and neutralised using 75 µl a 40 mM Tris-HCl (pH 5) solution. PCR amplification was typically carried out in 20 µl reactions using specific primer pairs (Fig. 2.2A) and the OneTaq® Quick-Load® 2X Master

Mix (New England Biolabs) as per manufacturer's instructions. 5 µl of PCR reaction were subject to digestion with 0.5 µl PstI (FastDigest, Thermo Fisher Scientific) in a 20-µl reaction. Digested and undigested PCR products were run on a 2% (w/v) agarose gel at 120 V for 35 min (Fig. 2.2B).

A

Genotype	Primer sequence		Ann T (°C)
L1616A	Fwd	agggacagccaagttcagccca	63
	Rev	ccgataggaggagaaaggccag	
NDRR	Fwd	agcagtttgggcttttcagtga	57
	Rev	tgaggctctggcaataaagtac	

B

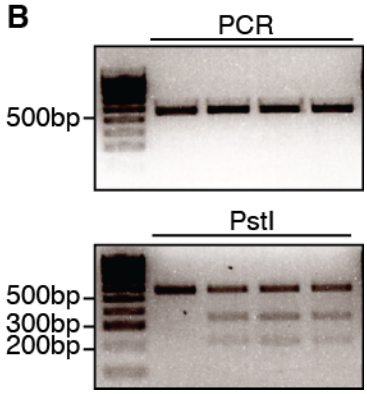


Figure 2.2. Genotyping strategy for *L1616A* and *NDRR* mice. (A) Primer sequences used for locus-specific amplification. Optimised annealing temperatures (Ann T) are depicted. (B) Representative image of an agarose gel for characterisation of F1 *NDRR* mice. 532 and 556 bp amplicons were obtained for *L1616A* and *NDRR* alleles (top panel), respectively and subsequently digested with PstI (bottom panel). *Wt* allele remained undigested, and edited alleles resulted in the formation of a doublet (*L1616A*: 311, 211 bp; *NDRR*: 335, 221 bp). *Wt*: ~500 bp band (lane 1, bottom panel); heterozygous: ~500 bp, ~300 bp and ~200 bp bands (lane 2-4, bottom panel); homozygous: ~300 bp and ~200 bp bands (not depicted).

2.2.4 Mouse embryonic fibroblast isolation

Uteri containing 12.5 to 14.5 days post-coital embryos were extracted from euthanised females and extensively washed in PBS in 50 ml falcon tubes. Individual uteri were transferred to 10 cm dishes and the uterine wall was carefully cut to allow embryo extraction. Using two pairs of watchmaker's forceps, brain, heart and liver were removed and the remaining embryo washed in PBS prior transferring to a 15 ml falcon tube containing 2.5 ml of ice-cold trypsin-EDTA (Sigma-Aldrich). Simultaneously, the yolk sac was separated to perform genotyping as in Section 2.2.3. Embryos were incubated in trypsin for 5 min at 37

^{o}C, trypsin inactivated by medium addition and embryos further dissected with a 1000-µl pipette tip until achieving a homogenous cell suspension. Cell suspensions were transferred to 10 cm dishes and cultured overnight. Biallelically mutated and *wt* MEFs were selected for downstream analysis.

2.2.5 Splenocyte preparation and B-cell isolation

Spleens were extracted from culled mice and placed in 15 ml falcon tubes containing 10 ml of ice-cold R2 medium [RPMI supplemented with 5% (v/v) FBS (Life Technologies), 50 mg/ml streptomycin (Sigma-Aldrich), 2 mM L-glutamine (Sigma-Aldrich), and 10 mM HEPES (Life Technologies)]. The content was then poured through a 70-µm strainer placed in a 10 cm dish and spleen mashed using the plunger end of a 2.5 ml syringe. Cells suspensions were recovered and centrifuged at 300g for 8 min at 4 ^{o}C. Cell pellets were disgregated in 1 ml of cold ACK buffer (pH 7.4) [8.3 g/l NH_4Cl, 10 mM $KHCO_3$, 0.1 mM EDTA (pH 8)] and incubated at RT for 5 min to achieve complete lysis of red blood cells. Upon addition of 9 ml of cold R2, cells were pelleted and primary splenocytes resuspended in culture medium for further applications. B cells were purified by magnetic negative selection using a B Cell Isolation Kit (Miltenyi Biotec, 130-090-862, Bergisch Gladbach, Germany) as per manufacturer's guidelines.

2.3 Virus methods

2.3.1 Generation of lentiviral constructs

All constructs used throughout this study were generated using the recombination-based Gateway cloning technology.

2.3.1.1 Cloning of open reading frames (ORFs) of interest

Cloned full-length 53BP1 in the donor vector pDONR221 was already established in the laboratory, and full length USP25 in pDONR223 was purchased from the Target Discovery Unit (TDI, NDM building, University of Oxford) in-house library. USP28 and p53 ORFs were amplified from MCF-7 complementary DNA (cDNA). Briefly, 10^6 MCF-7 cells were plated and 24 h after total RNA was trizol/chloroform-extracted and further purified with the RNeasy Mini Kit (Qiagen) incorporating a DNaseI step (Qiagen) to remove DNA contamination. cDNA was generated from 1 µg of total RNA using the SuperScript™ II reverse transcriptase (Thermo Fisher Scientific) as per manufacturer's instructions. ORFs were amplified using specific primers (Table 2.3) carrying attB recombination sites for downstream cloning processes and the Q5 high-fidelity DNA polymerase (New England Biolabs).

Target gene		**Sequence (5'-3')**
USP28	Fwd	ggggacaagtttgtacaaaaaagcaggcttc GCCATGACTGCGGAGC
	Rev	ggggaccactttgtacaagaaagctgggt TTATTTCACTGTCACAGTTGAAACTCC
p53	Fwd	ggggacaagtttgtacaaaaaagcaggcttc ATGGAGGAGCCGCA
	Rev	ggggaccactttgtacaagaaagctgggt TCAGTCTGAGTCAGGCCCTTCTGTCT

Table 2.3. Primer pairs used for ORF amplification and cloning. Common attB overhangs are presented in lowercase followed by the gene specific primer in uppercase.

Products were purified and cloned into pDONR221 *via* the site-specific recombination BP reaction using the Gateway® BP Clonase® Enzyme Mix (Invitrogen, Carlsbad, CA, USA) and transformed into chemically competent

DH5-α *E. coli* cells for amplification as in Section 2.1.2. Final products were verified by restriction digestion and Sanger sequencing.

2.3.1.2 Generation of point and domain specific mutants

Site-directed mutagenesis was used to generate the point and domain mutant constructs used throughout this study. Donor vectors including the ORFs of interest were mutated using the Q5® Site-Directed Mutagenesis Kit (New England Biolabs) and specific primer pairs designed with the NEBaseChanger™ software according to manufacturer's indications. Products were purified as in Section 2.1.2, analysed by restriction digestion, fully sequenced by Sanger sequencing, and conveniently stored at -20 ^{o}C.

2.3.1.3 Generation of USP28-USP25 chimeric gene products

Chimeric USP28-USP25 constructs were generated by overlap-extension PCR. Desired gene fragments were amplified from the pDONR221-cloned full-length ORFs using primers with 30nt homology overhangs (Table 2.4) and the Q5 high-fidelity DNA polymerase (New England Biolabs) in 50 µl PCR reactions. Individual fragments were gel purified (QIAquick gel extraction kit, Qiagen) and mixed in equal quantities to use as template for overlap-extension PCR. Typically, 30 ng of each individual gene fragment were used for final 50-µl PCR reactions. Duplicate PCR reactions were performed with the outermost primer pairs containing attB recombination sites and Q5 high-fidelity DNA polymerase (New England Biolabs) at fixed 55 and 60 ^{o}C annealing temperatures. Final products were cloned into pDONR221 and amplified as in Section 2.1.2 and subsequently restriction digested, fully sequenced and stored at -20 ^{o}C. Chimera

10 was generated by site-directed mutagenesis as in Section 2.3.1.2 with the primer pairs specified (Table 2.4).

Ch	Gene fragment	Sequence (5'-3')	
1	5'	Fwd	ggggacaagtttgtacaaaaaagcaggcttcATGACCGTGGAGCAGAACGT
		Rev	tttagtttctgcagaggttgcttcatgcatTCTGCTAATGGCTTGTTCCT
	3'	Fwd	ataactgatgaggaacaagccattagcagaATGCATGAAGCAACCTCTGC
		Rev	ggggaccactttgtacaagaaagctgggtTTATTTCACTGTCACAGTTGAAACTCC
2	5'	Fwd	ggggacaagtttgtacaaaaaagcaggcttcGCCATGACTGCGGAGC
		Rev	tttattctctgctatgctggcttcaagaacCCTGTTAAGATCTCTTCCATCAG
	Central	Fwd	attcaagctgatggaagagatcttaacaggGTTCTTGAAGCCAGCATAGC
		Rev	cattggattttcagatttgttcctgggactCTCCTCTTCAGCTTTCATTTG
	3'	Fwd	gatgccttccaaatgaaagctgaagaggagAGTCCCAGGAACAAATCTGA
		Rev	Ch1 3' Rev
3	5'	Fwd	Ch2 5' Fwd
		Rev	catggggttctttggcttctcttcatccgtGTTAACATTAACAGCTAGCTGG
	Central	Fwd	gacgcattccagctagctgttaatgttaacACGGATGAAGAGAAGCCAAA
		Rev	gtcactttcaggtggacagctttctgaggcAGGTTTACTTGAGGCAAATTCCA
	3'	Fwd	tatgcattggaatttgcctcaagtaaacctGCCTCAGAAAGCTGTCCAC
		Rev	Ch1 3' Rev
4	5'	Fwd	Ch2 5' Fwd
		Rev	gtcaatatcgtcaacaggagaagtgcaaacAGGTTTTGTACTAGCAAATTCA
	Central	Fwd	tatgttattgaatttgctagtacaaaacctGTTTGCACTTCTCCTGTTGAC
		Rev	cttgagccagctctgtcggggttgattataAATATATGCCCAGTAGTGCC

	3’	Fwd	gctaatgctgggcactactgggcatatattTATAATCAACCCCG ACAGAG
		Rev	Ch1 3’ Rev
5	5’	Fwd	Ch2 5’ Fwd
		Rev	cttcatccatctgctttcacgatgatcaaaGATATAGGCCCAATA GTGTC
	Central	Fwd	gcaaatgctggacactattgggcctatatcTTTGATCATCGTGA AAGCAG
		Rev	catttgagggattttgcaagactgctcttcATCCCATTCTTCTAGT TCTT
	3’	Fwd	cgatttgaaaaagaactagaagaatgggatGAAGAGCAGTCTT GCAAAA
		Rev	Ch1 3’ Rev
6	5’	Fwd	Ch2 5’ Fwd
		Rev	ttcctgcaaagctttctgggcaagttgtgcTTCCCACTCCTCTAC TTCCT
	Central	Fwd	cggtttgagcaggaagtagaggagtgggaaGCACAACTTGCC CAGAAA
		Rev	gacaaggacatgctgaagtcgaggatcactTTCTGGTGGGGT GTCTT
	3’	Fwd	aagttggcccaagaagacaccccaccagaaAGTGATCCTCGA CTTCAGC
		Rev	Ch1 3’ Rev
7	5’	Fwd	Ch2 5’ Fwd
		Rev	gaccactacatgatgtaaacgataatcggtGTGAGAGGTGGGG GTCTC
	Central	Fwd	cagcttgccaaagagacccccacctctcacACCGATTATCGTT TACATCAT
		Rev	gaacaaactataatcttcatgccacttcttATATTCCTCCAAGTT TACTTCT
	3’	Fwd	ggtccagatgacatgaatatggaagagtacGAGGAGTGGCAT CAGGAT
		Rev	Ch1 3’ Rev
8	5’	Fwd	Ch2 5’ Fwd
		Rev	acagatgaggaacagcaaggaatctatataCTTTCCTTTTTGA TAGAGTT
	Central	Fwd	acaggcctagaactctatcaaaaaggaaagTATATAGATTCCT TGCTGTTC
		Rev	cccaaggtaagagcaccaatggtttctcatATCTTCTACAGCTA GTATATCC

	3’	Fwd	gaagaaaaggatatactagctgtagaagatATGAGAAACCATTGGTGCTC
		Rev	Ch1 3’ Rev
9	5’	Fwd	Ch2 5’ Fwd
		Rev	accaaggtaggaacaccatcgatttctcatGACCTCAATGGCATCCAG
	3’	Fwd	tccaaggatgatctggatgccattgaggtcATGAGAAATCGATGGTGTT
		Rev	ggggaccactttgtacaagaaagctgggtaTTATCTTCCATCAGCAGGAGTTCG
10		Fwd	agccgacggccggTAAACCCAGCTTTCTTGTAC
		Rev	ggggtccggctcagTGACTCCATGACAGCTGC

Table 2.4. Primer pairs used for gene fragment amplification and chimera generation. Homology overhangs are presented in lowercase followed by the gene specific sequence in uppercase.

2.3.1.4 Cloning into expression vectors

Products were cloned in the corresponding destination vectors pLenti-PGK-PURO-DEST (w529-2) (Addgene 19068) and pHAGE-N-FLAG-HA *via* a LR reaction using the Gateway® LR Clonase® II Enzyme Mix (Invitrogen) according to manufacturer’s indications. Reactions were transformed into chemically competent STBL3 *E. coli* and plasmid purification undertaken as in Section 2.1.2. Correct recombination events were evaluated by restriction digestion. Final expression vectors were stored at -20 ^{o}C.

2.3.2 Lentivirus generation and lentiviral transduction

In order to generate cell lines stably expressing different 53BP1, USP28 and p53 gene products or the corresponding green fluorescent (GFP) and glutathione S-transferase (GST) controls, lentiviral transduction was carried out.

Typically, $2x10^6$ HEK293T cells were seeded in 6 cm dishes in antibiotic-free supplemented DMEM. Sixteen h later, cells were cotransfected with 3.2 µg of the lentiviral expression construct of interest and the vectors encoding the lentiviral packaging components gag-pol, VSV-G, rev, and tat (0.16 µg pHDM-Hgpm2, 0.32 µg pHDM-VSG-G, 0.16 µg pRC/CMV-rev1b and 0.16 µg pHDM-tat1b, respectively). Vectors were mixed in 200 µl optimised low serum minimal essential medium, Opti-MEM (Life Technologies) and an equivalent volume of a solution of the transfection reagent polyethylenimine (PEI) in Opti-MEM added at a ratio 1:1.29 (w/w) total DNA/PEI. Following 15 sec of thorough vortexing, solutions were incubated for 15-20 min to allow formation of DNA-PEI complexes. Upon incubation, dilution of the complexes was performed until reaching a final volume of 4 ml and directly added to the HEK293T cultures. Forty-eight and 72 h post-transfection, viral supernatants were collected, cell remnants eliminated by filtration through a 0.45 µm filter and directly applied over the cell line of interest growing at a 50% confluency with 4 µg/ml polybrene for 12 h. After transduction, cells were treated with puromycin at 2 µg/ml for 48 h and further maintained in culture in complete DMEM with 1 µg/ml puromycin. Viral titers and transduction rounds were optimised to achieve the desired transduction efficiency by serial dilution of viral supernatants and immunoblotting of the puromycin-selected cell populations.

2.4 Protein methods

2.4.1 SDS/PAGE-Western Blot

Whole cell protein extracts were isolated using Benzonase buffer [25 mM Tris (pH 8.0), 40 mM NaCl, 0.05% SDS, 2 mM $MgCl_2$, 10 U/ml Benzonase

(Merck Millipore, Burlington, MA, USA), 2 mM N-Ethylmaleimide (NEM), 0.05% (v/v) phosphatase inhibitors (P0044 and P5726; Sigma-Aldrich) and protease inhibitors (Complete™, Roche, Basel, Switzerland)], with a minimum incubation time of 30 min on ice to allow complete DNA digestion. Protein concentrations were quantified using the Bio-Rad Protein Assay Dye Reagent Concentrate (Bio-Rad, Hercules, CA, USA) and a bovine serum albumin (BSA) standard curve as a reference. Samples were diluted in 3X Laemmli buffer and boiled at 95 ^{o}C for 5 min. Sodium dodecyl sulfate-polyacrylamide gel electrophoresis (SDS-PAGE) was performed using NuPAGE® Novex® (Life Technologies) or Criterion® (Bio-Rad) 4-12% gradient acrylamide gels before transfer onto 0.45 µM nitrocellulose membranes (Life Technologies) using the Bio-Rad wet transfer system for 75 min at 100 V. Primary antibodies (Table 2.5) were diluted in 3% BSA in PBS- 0.05% (v/v) Tween20 and membranes incubated overnight at 4 ^{o}C. Proteins were detected using the corresponding HRP-conjugated secondary antibodies (Dako, Santa Clara, CA, USA, 1:10000 dilution) and enhanced chemiluminescence (Clarity, Bio-Rad). Signals were acquired digitally on a Gel Doc™ XR system (Bio-Rad).

Target	Manufacturer (clone)	Application (Dilution)
53BP1	Novus Biological (NB100-304)	WB (1:2500), IF (1:250)
	Novus Biological (NB100-305)	WB (1:2500)
	Millipore (clone B13)	IF (1:250)
MDM2	Santa Cruz Biotechnology (clone SMP14)	WB (1:500)
p53	Dako (clone DO-7)	WB (1:1000), IF (1:100)
	Santa Cruz Biotechnology (clone DO-1)	IF (1:100)

p21	BD Transduction Laboratories	WB (1:1000)
CHK2	Millipore (clone 7)	WB (1:1000)
$pCHK2^{T68}$	Cell signalling (clone C13C1)	WB (1:1000)
USP28	Abcam (clone EPR4249)	WB (1:1000)
USP25	Abcam (clone EPR15019)	WB (1:1000)
HA-11	Covance Research (clone 16B12)	WB (1:2000)
RPA-34	Thermo Fisher Scientific (clone 9H8)	WB (1:1000)
β-actin	Sigma-Aldrich	WB (1:2000)
α-Tubulin	Sigma-Aldrich (Tat-1)	WB (1:10000)
ɣ-H2AX	Millipore	IF (1:500)
Cyclin A	Clone E23.1, a gift from Julian Gannon, The Francis Crick Institute	IF (1:250)

Table 2.5. List of primary antibodies used throughout this study.

2.4.2 Immunoprecipitation (IP)

Cells initially lysed in Benzonase IP Buffer [20 mM HEPES (pH 7.9), 40 mM KCl, 2 mM $MgCl_2$, 12% glycerol, 0.5% CHAPS, 50 U/ml Benzonase, 0.05% (v/v) phosphatase inhibitors (P0044 and P5726; Sigma-Aldrich) and protease inhibitors (Complete™)] for a minimum of 30 min, were supplemented with KCl to a 450 mM final concentration and gently mixed for 30 min at 4 ^{o}C in a rotating wheel. Following clarification by centrifugation (13,000g for 15 min), lysates were then cassette-dialysed (Slide-A-Lyzer™ MINI, Thermo Fisher Scientific) into dialysis buffer [20 mM HEPES (pH 7.9), 100 mM KCl, 0.2 mM EDTA, 10% (v/v) Glycerol, 0.5 mM DTT, 0.5 mM PMSF, 5 mM NaF, 10 mM β-glycerolphosphate]

for an initial overnight step followed by addition of fresh buffer and further dialysis for 4 h. Retrieved protein lysates were quantified as in Section 2.4.1 and Flag-HA-53BP1 or endogenous p53 complexes were purified from 2 mg total protein using anti-FLAG® M2 magnetic resin (Sigma-Aldrich) or p53 DO-1 antibody (Santa Cruz Biotechnology, Dallas, TX, USA) previously coupled to protein G Dynabeads (Thermo Fisher Scientific). Magnetically purified protein-bead complexes washed extensively in detergent-free wash buffer [20 mM HEPES (pH 7.9), 100 mM KCl, 10% (v/v) Glycerol, 0.5 mM DTT, and protease inhibitors (Complete™)] were either directly boiled in Laemmli buffer or eluted in 3X Flag peptide (Sigma-Aldrich) according to manufacturer's instructions prior boiling in Laemmli buffer at 95 ^{o}C for 5 min. Subsequent SDS-PAGE/WB analysis was performed as in Section 2.4.1.

2.4.3 p53 tetramerisation analysis

p53 oligomerisation status was assessed by glutaraldehyde-based protein-protein crosslink coupled to SDS-PAGE/WB. 4x10^5 cells were seeded in 6-well plates and treated with N3 for the indicated times. Cells were lysed in NP40-based Benzonase lysis buffer [20 mM Tris (pH 7.5), 40 mM NaCl, 2 mM $MgCl_2$, 0.5% NP40, 50 U/ml Benzonase, 2 mM NEM, and protease inhibitors (Complete™)] for 30 min on ice. Protein-protein crosslink was achieved by adding 0.01% (v/v) glutaraldehyde (Sigma-Aldrich) to the protein solution and subsequent incubation for 20 min on ice. Crosslinking reactions were stopped by direct addition of 3X Laemlli buffer and boiling for 5 min. Samples without crosslinking agent were used as input controls for successive immunoblotting.

2.4.4 Immunofluorescence (IF) assays

Cells were seeded in coverslips in 6-well plates at a cell density of $4x10^5$ cells/well. After treatments, cells were fixed in a 2% (w/v) *p*-formaldehyde solution for 15 min. *p*-Formaldehyde was removed completely by repeated washes with PBS and cells were subsequently permeabilised with 0.2% (v/v) Triton-X100 in PBS for 5 min. Coverslips were blocked for 15 min in 3% (w/v) BSA/0.1% (v/v) Triton-X100 in PBS prior incubation with primary antibodies (Table 2.5) for 1 h at RT. Excess of antibody was eliminated by 3 consecutive 5-min washes with 0.1% (v/v) Triton-X100 in PBS. Incubation with corresponding secondary antibodies, anti-mouse and anti-rabbit Alexa Fluor 488, 594 and 647 (1:500 dilution, Molecular Probes, Eugene, OR, USA) was carried out for 1 h at RT in the dark. Upon removal of antibody excess, coverslips were mounted using DAPI (Prolong™, Thermo Fisher Scientific) for DNA staining. Images were captured in a Zeiss LSM 510 Meta confocal scanning microscope (Zeiss, Oberkochen, Germany) or a Leica SP8 confocal microscope (Leica, Wetzlar, Germany) with a 63X magnification objective.

2.4.5 Chromatin immunoprecipitation (ChIP)

ChIP experiments were performed from 30-50 µg MCF-7 chromatin essentially as previously described [49]. Briefly, chromatin was immunoprecipitated using 3 µg anti-p53 (DO-1, Santa Cruz Biotechnology), 1.5 µg anti-RNAP2 $pCTD^{S5}$ (clone 4H8), 2.5 µg anti-histone H3K9ac (ab4441, Abcam, Cambridge, UK), or 2.5 µg anti-histone H4ac (06-598, Merck Millipore) antibody coupled to 25 µl Protein-A/G Dynabeads. DNA quantities recovered in control IgG (Santa Cruz Biotechnology) ChIP experiments were consistently

below the detectable range. Relative quantities of ChIP-enriched DNA were calculated relative to total input chromatin by qPCR in triplicate on a CFX96 Real Time analyser (Bio-Rad) using QuantiFast SYBR Green Master Mix (Qiagen) and locus-specific primer pairs (Table 2.6).

Target gene/locus	**Sequence (5'-3')**	
CDKN1A (*p21*) -2965	Fwd	CCGGCCAGTATATATTTTTAATTGAGA
	Rev	AGTGGTTAGTAATTTTCAGTTTGCTCAT
CDKN1A (*p21*) -2283	Fwd	AGCAGGCTGTGGCTCTGATT
	Rev	CAAAATAGCCACCAGCCTCTTCT
CDKN1A (*p21*) -1391	Fwd	CTGTCCTCCCCGAGGTCA
	Rev	ACATCTCAGGCTGCTCAGAGTCT
CDKN1A (*p21*) -20	Fwd	TATATCAGGGCCGCGCTG
	Rev	GGCTCCACAAGGAACTGACTTC
CDKN1A (*p21*) +507	Fwd	CCAGGAAGGGCGAGGAAA
	Rev	GGGACCGATCCTAGACGAACTT
CDKN1A (*p21*) +4001	Fwd	AGTCACTCAGCCCTGGAGTCAA
	Rev	GGAGAGTGAGTTTGCCCATGA
CDKN1A (*p21*) +8566	Fwd	CCTCCCACAATGCTGAATATACAG
	Rev	AGTCACTAAGAATCATTTATTGAGCACC
CDKN1A (*p21*) +11443	Fwd	TCTGTCTCGGCAGCTGACAT
	Rev	ACCACAAAAGATCAAGGTGAGTGA
MDM2 5'	Fwd	GGGCTATTTAAACCATGCATTTTC
	Rev	GTCCGTGCCCACAGGTCTA

MDM2 3'	Fwd	CTTTCTCGAGGAGGCAGGTTT
	Rev	GCTCAACCCTAGGCGCTATTC
GADD45A p53-RE	Fwd	GCCTTTGTCCGACTAGAGTGT
	Rev	GGATCTCTTCCGCTGCTG
FAS p53-RE	Fwd	GCACCGAAGCAGTGGTTAAG
	Rev	GCCTCCAGAAGCTCATTCAG

Table 2.6. Locus-specific ChIP primers used throughout this study. Primer sequences were obtained from [242].

2.5 Transcriptome analysis

2.5.1 Target-specific analysis: real time quantitative PCR (RT-qPCR)

Cells were seeded at a density of $5x10^5$ cells per well in 6-well plates and subsequently treated with 4 μM N3 or 5 Gy ionising radiation for the indicated durations. Trizol/chloroform-extracted total RNA was purified with the RNeasy Mini Kit including an additional DNaseI step to remove DNA contamination. cDNA was generated from 1 μg of total RNA using the iScript® cDNA Synthesis Kit (Bio-Rad). qPCR was carried out using QuantiFast SYBR Green Master Mix and transcript-specific primer pairs (Table 2.7). PCR reactions were analysed on a CFX96® Real Time analyser with the following conditions: enzyme activation-5 min 95 ^oC; 40 cycles denaturation-10 s 95 ^oC annealing/extension-30 s 60 ^oC; final melting curve-15 s 65 ^oC, 15 s 95 ^oC. Cycle threshold values (C_T) were used to perform quantification and analysis using CFX Manager software (Bio-Rad). Hypoxanthine-guanine phosphoribosyl-transferase 1 (*HPRT1*) was used as housekeeping gene for normalisation. All values were presented as fold-changes compared to the appropriate control.

Target gene	Sequence (5'-3')		RTPrimerDB ID
CDKN1A (*p21*)	Fwd	CCTCATCCCGTGTTCTCCTTT	631
	Rev	GTACCACCCAGCGGACAAGT	
BAX	Fwd	CCTTTTCTACTTTGCCAGCAAAC	1539
	Rev	GAGGCCGTCCCAACCAC	
BBC3 (*PUMA*)	Fwd	CCTGGAGGGTCCTGTACAATCT	3500
	Rev	GCACCTAATTGGGCTCCATCT	
TP53I3	Fwd	AGGGTGAAGTCCTCCTGAAGGT	3501
	Rev	GTGGGTCATACTGGCCTTGTCT	
MDM2	Fwd	GGCCTGCTTTACATGTGCAA	3499
	Rev	GCACAATCATTTGAATTGGTTGTC	
HPRT1	Fwd	TGACACTGGCAAAACAATGCA	5
	Rev	GGTCCTTTTCACCAGCAAGCT	

Table 2.7. Primer pairs sequences for RT-qPCR amplification. Sequences were obtained from the RTPrimerDB and the corresponding identifiers are depicted [243].

2.5.2 Whole transcriptome analysis: RNA-seq

Cells were plated, treated and total RNA extracted as in Section 2.5.1. Libraries prepared from ribosomal-RNA depleted total RNA isolates using the Ribo-Zero rRNA removal kit (Illumina, San Diego, CA, USA) were subjected to RNA-seq analysis. Results presented are based on three biological experimental replicates for each condition and genotype. Briefly, sample preparation was carried out according to Illumina guidelines using in-house adapters for library preparation [244]. Library quantification and quality control were performed using

Picogreen and Tapestation measurements, and equimolar quantities of each library pooled into a 36-plex. 36-plex pools were sequenced (100 bp paired-end reads) across two lanes of a HiSeq4000 sequencer (Illumina). Following subtraction of low-quality reads and duplicate reads (Picard Tools MarkDuplicates), between 10-15 million high-quality reads per sample were analysed and aligned to the human reference genome (GRCh37), using TopHat2 [245]. Counts for Ensembl-annotated genes were summarised from the mapped reads, and filtered to exclude genes with fewer than 10 reads on average per sample. Analysis for differential expression was performed using the edgeR package [246]. RNA-sequencing datasets generated in this study are archived and publically available under the accession number NCBI GEO: GSE84986. Library preparation and high-throughput sequencing were performed by the Oxford Genomics Centre (Wellcome Centre for Human Genetics, University of Oxford). Dr H. E. Lockstone analysed all RNA-seq datasets.

2.6 p53-dependent cell cycle arrest and apoptosis assays

2.6.1 Drug sensitivity assays

(±)-Nutlin-3 (Cayman Chemicals, Ann Arbor, MI, USA) was purchased as a solid and dissolved in pure ethanol (Sigma-Aldrich) to a final concentration of 10 mM. N3 solution was distributed in 100 µl aliquots and stored at -20 ^{o}C. MCF-7 cells were seeded in triplicate at 1.25x10^{4} cells/well in 6-well plates and 16 h later, were treated with 4 µM N3 or left untreated. RPE-1 cells were seeded at a density of 3x10^{3} cells/well in 6-well plates and treated as above described. For absolute percentage calculation, all cultures were stopped 7 days after treatment.

For relative measurements, treated cultures were left for an additional four-day period. Cells were subsequently fixed and stained using crystal violet solution [0.5% (w/v) in 20% methanol]. For quantification, bound crystal violet was dissolved in 10% (v/v) acetic acid and absorbance of 1:50 dilutions measured at 595 nm.

Centrinone (Tocris Bioscience, Bristol, UK) was purchased as a solid and dissolved in DMSO (Sigma-Aldrich) to a final concentration of 12.5 mM. The final solution was distributed in 50 µl aliquots and stored at -20 ^{o}C. RPE-1 cells were seeded at a density of 500 cells/well in 6-well plates and treated with 125 nM centrinone or mock-treated for 11 days. MEFs were seeded at a density of 3x10^{3} cells/well (6x10^{3} cells/well for *53bp1*$^{-/-}$ lines) in 6-well plates and treated with 250 nM centrinone or mock-treated for 11 days. Cells were then fixed as described and absorbance of 1:10 dilutions measured at 595 nm.

2.6.2 Clonogenic IR survival assay

Cells were plated in triplicate on 10 cm dishes at densities of 4x10^{2}, 6x10^{2}, and 2x10^{3} cells/dish, and sensitivity to 1, 2, and 4 Gy, respectively (CellRad, Faxitron, Tucson, AZ, USA) was assessed relative to non-irradiated control plates. Fourteen days after treatment, plates were stained with crystal violet as described above and single colonies manually counted.

2.6.3 Apoptosis evaluation: Annexin V/Propidium iodide (PI) staining

Primary splenocytes were seeded at a density of 5x10^{5} cells/ml in 12-well plates and stimulated with 5 µg/ml lipopolysaccharide (LPS) (Sigma-Aldrich, L7770-1MG). Eighteen h post-stimulation, cells were irradiated at the indicated

doses and harvested 24 h later. Staining was performed using fluorescein isothiocyanate (FITC)-Annexin V/PI apoptosis detection kit (BioLegend, San Diego, CA, USA). Briefly, cells were washed twice in PBS with 2% BSA and 0.025% sodium azide and subsequently resuspended in 50 µl of 2.5% (v/v) FITC-Annexin V in Annexin V binding buffer. Following a 15-min incubation at RT in the dark, cell suspensions were diluted with 200 µl of Annexin V binding buffer. Five µl of 1 mg/ml PI solution were added to the cell suspension prior analysis on a FACSCanto (BD Biosciences, Franklin Lakes, NJ, USA). Data were analysed with FlowJo software (Tree Star Inc., Ashland, OR, USA).

2.6.4 G1/S checkpoint analysis

The G1/S checkpoint was assessed by bromodeoxyuridine (BrdU) incorporation. Briefly, $2x10^5$ cells were plated in 6-well plates and synchronised in G0 by serum starvation for 24 h. Cells were then released in medium containing 5% (v/v) FBS and 0.25 µg/ml nocodazole to prevent G2/M-phase cells from recycling. Four h post-release, G1-phase cells were treated with mock- or 4 Gy irradiation. Twelve and 18 h later, cells were pulsed for 30 min with 10 µM BrdU (Sigma-Aldrich), collected by tripsinisation and washed with 1% (w/v) BSA in PBS (1500 rpm, 5 min) before proceeding to overnight fixation in ice-cold 70% ethanol. Ethanol was removed by sequential washes with PBS (2000 rpm, 5 min) and DNA denaturation was performed using a solution of 0.2 mg/ml of pepsin (Sigma-Aldrich) in 2 M HCl for 20 min at RT. Cells were washed twice with PBS and resuspended in a solution containing anti-BrdU-FITC conjugated antibody (1:100, Bio-Rad) in 0.5% (v/v) Tween20, 0.5% (w/v) BSA in PBS and incubated for 1 h at RT in the dark. Finally, incubation for 15 min at 37 ^oC in a solution of

PI/RNaseA (10 µg/ml and 0.1 mg/ml respectively) in PBS provided total DNA staining. Cells were analysed in an Attune NxT flow cytometer (Life Technologies) and data processed using FlowJo software.

2.7 Immune system analysis

Unless otherwise stated, staining steps were performed in 20 µl antibody dilutions in PBS with 2% BSA and 0.025% sodium azide (flow cytometry buffer, FB) at 4 ^{o}C in the dark. Centrifugations were held at 300g for 8 min.

2.7.1 B-cell development: Hardy fractions

Bone marrow cells were extracted from one femur and one tibia. The bone edges were cut to allow insertion of a 25-gauge needle attached to a 5 ml syringe full of R2 medium. Medium was then flushed through femurs and tibias to extract the totality of the bone marrow. To avoid the presence of large cellular aggregates, the bone marrow and R2 medium were aspirated through the 25-gauge needle and placed into a 15 ml tube. Cell suspensions were centrifuged for 7 min at 1200 rpm at 4 ºC and resuspended in 5 ml fresh R2 medium. Spleen cells were dissected as in Section 2.2.5. Cells were counted on a haemocytometer prior staining with anti-mouse antibodies (Table 2.8). Mouse BD Fc Block™ (1:500, anti-mouse CD16/32, clone 2.4G2) was added to prevent non-specific antibody binding and live/dead cell discrimination was performed post-staining with Zombie Aqua viability die (1:200, BioLegend). Flow cytometric analysis was carried out using a FACSCanto and data processed using FlowJo software. Cell populations were gated according to [247]: A, B220+CD43+BP-1-CD24-; B, B220+CD43+BP-1-CD24+; C,

B220+CD43+BP-1+CD24+; C', B220+CD43+BP-1+CD24^{high}+; D, B220+CD43-IgM-IgD-; E, B220+CD43-IgM+IgD-; and F, B220+CD43-IgM+IgD+.

Target	Manufacturer (clone)	Dilution
IgD	BioLegend (clone 11-26c.2a)	1:500
IgG1	BioLegend (clone RGM1-1)	1:200
IgM	BioLegend (clone RMM-1)	1:500
B220	BioLegend (clone RA3-6B2)	1:500
BP-1	BioLegend (clone 6C3)	1:200
CD19	BioLegend (clone 6D5)	1:500
CD24	BioLegend (clone M1/69)	1:1000
CD93	BioLegend (clone AA4.1)	1:200
CD23	BD Pharmigen (clone B3B4)	1:200
CD43	BD Pharmigen (clone S7)	1:200
CD127	Thermo Fisher Scientific (clone A7R34)	1:200
CD21	BD Biosciences (clone 7G6)	1:500

Table 2.8. List of antibodies used for Hardy fraction analysis.

2.7.2 T-cell development

Thymuses were dissected following the protocol described for spleens in Section 2.2.5. Recovered cell suspensions were centrifuged for 7 min at 1200 rpm at 4 ^{o}C and resuspended in 10 ml of R2 medium. Cells were counted on a haemocytometer and subsequently stained with anti-mouse antibodies (Table 2.9). Non-specific binding was blocked with Mouse BD Fc Block™. After staining, discrimination of live/dead cells was carried out with Zombie Aqua

viability die (1:200). Data collection was performed using a FACSCanto and processed with FlowJo software. Cell populations were gated as follows: Double negative (DN), CD4-CD8-; Double positive (DP), CD4+CD8+; T helper cells, CD4+; Cytotoxic T cells, CD8+; DN1, CD4-CD8-CD44+CD25-; DN2, CD4-CD8-CD44+CD25+; DN3, CD4-CD8-CD44-CD25+; DN4, CD4-CD8-CD44-CD25-; TCRhi, CD4+CD8+CD3^{high}+.

Target	Manufacturer (clone)	Dilution
CD4	BioLegend (clone GK1.5)	1:500
CD8a	BioLegend (clone 53-6.7)	1:500
CD25	BioLegend (clone PC61)	1:500
CD44	BioLegend (clone IM7)	1:200
CD3	BioLegend (clone 17A2)	1:100

Table 2.9. List of antibodies used for T-cell maturation analysis.

2.7.3 Class-switch recombination assay

Primary B cells were plated on 12-well plates at a density of 1x10^5 cells per well. B cells were stimulated with 5 µg/ml LPS (Sigma-Aldrich, L7770-1MG), 10 ng/ml mouse recombinant IL-4 (Peprotech, 214-14-20), and 0.5 µg/ml agonist anti-CD40 antibody (Miltenyi Biotec; FGK45.5) in the combinations depicted (Table 2.10).

Cytokines	Ig isotype
LPS	IgG2b, IgG3
LPS, IL-4	IgG1, IgE

α-CD40, IL-4	IgG1

Table 2.10. Cytokine cocktails used to induce class switching to the Ig isotypes indicated.

Four days after seeding, B cells were resuspended in FB, pelleted and blocked with Mouse BD Fc Block™ for 5 min. Cells were washed in FB prior immunostaining with biotinylated IgG1, IgG2b and IgG3 antibodies for 20 min (Table 2.11). Upon washing the primary antibody excess, cells were incubated with allophycocyanin (APC)-conjugated streptavidin (1:500, Thermo Fisher Scientific). IgE expression was assessed using a phycoerythrin (PE)-conjugated antibody (Table 2.11). Live/dead cells were discriminated after staining with Zombie Aqua viability dye (1:200), and cell proliferation was assessed using Cell Trace Violet according to manufacturer's instructions (CellTrace, Life Technologies). B cells were analysed using a FACSCanto and data processed using FlowJo software.

Target	Manufacturer (clone)	Dilution
IgG1	BD Pharmingen (clone A85-1)	1:100
IgG2b	BioLegend (clone RMG2b-1)	1:100
IgG3	BD Pharmingen (clone R40-82)	1:100
IgE	BioLegend, (clone RME-1), PE conjugated	1:100

Table 2.11. Primary antibodies used for immunoglobulin staining in CSR analysis.

2.8 Cytogenetics-based assays

2.8.1 Metaphase spread preparation

Primary splenocytes were seeded and stimulated as in Section 2.6.3. At the

time of seeding, cells were treated with 1 μM centrinone or left untreated. The chromosome harvesting procedure was carefully optimised for this specific cellular type. Three days post-treatment, 30 ng/ml KaryoMAX® Colcemid™ solution in HBSS (Thermo Fisher Scientific) was added to the cell suspension and incubated for 3.5 h. Cells were collected by centrifugation at 1000g for 8 min at RT, supernatant carefully removed and cells resuspended in 10 ml of hypotonic solution (75 mM KCl) at 37 ^{o}C and incubated on ice for exactly 15 min. Cells were pelleted by centrifugation and the supernatant removed completely before resuspending in 10 ml of freshly-prepared, ice-cold Carnoy fixative solution [3:1 methanol (Thermo Fisher Scientific, BP1105-1)/acetic acid] for 30 min at RT. A second fixation step was subsequently performed with additional 10 ml of fixative solution for 10 min at RT. Fixed cells were resuspended in 200 μl of fresh fixative solution and 10 μl of suspension dropped in a clean slide immediately set to dry at 37 ^{o}C. Dried slides were stained with DAPI (Prolong™) and metaphases acquired in an Olympus BX51 microscope (Olympus, Tokyo, Japan) coupled to the CytovVision® Genus software v7.1 (Leica). Manual chromosome counting was performed using FIJI [248].

2.9 Statistical methods

Prism 6 software (GraphPad Software Inc.) was typically used for statistical analysis of datasets, with the exception of the RNAseq analyses that were performed using R (www.r-project.org). Statistical tests used for each specific experiment are described in the corresponding figure legend.

Chapter 3

CONTRIBUTION OF 53BP1 TO p53-DEPENDENT RESPONSES

3.1 Introduction

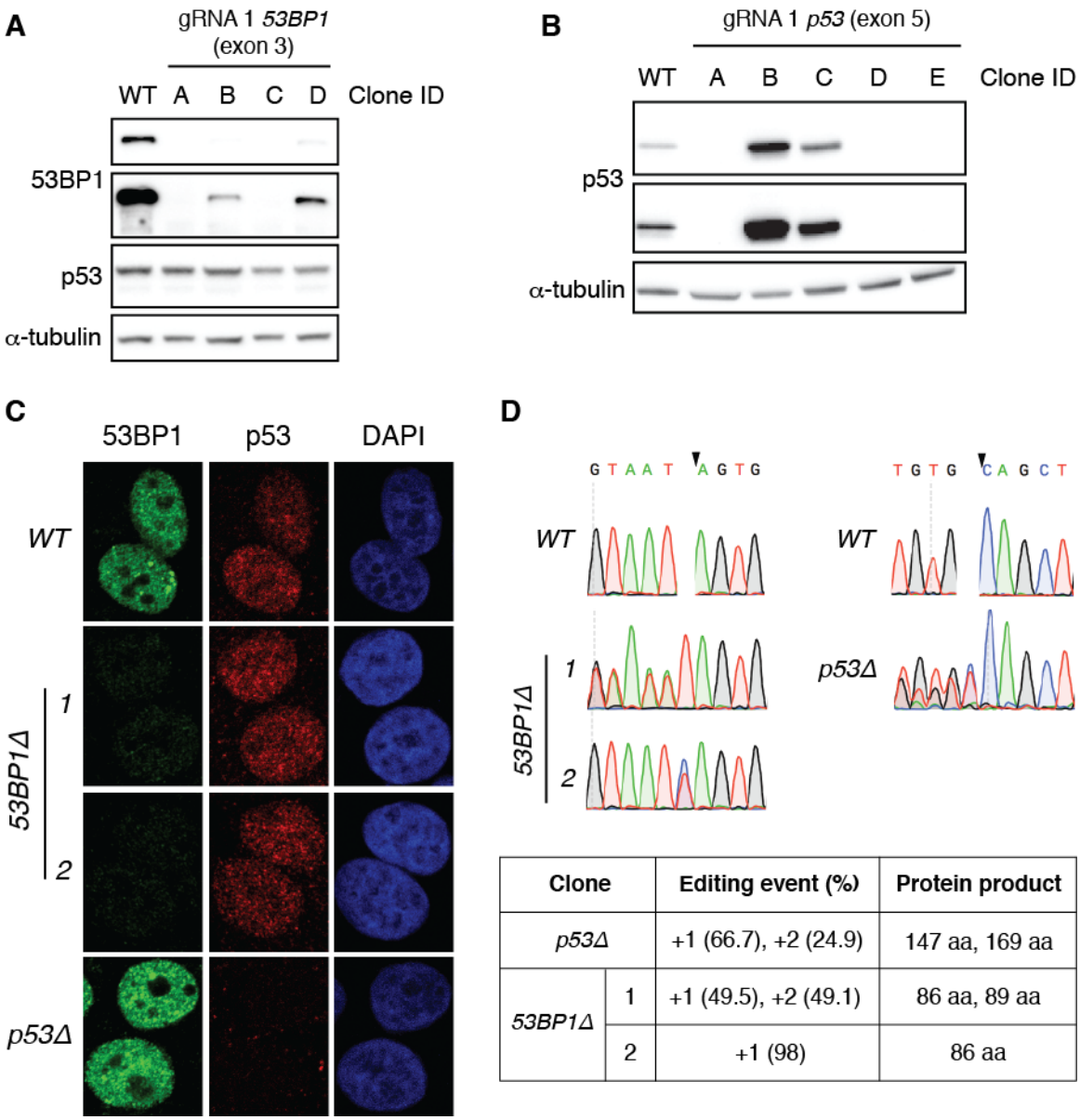
Since its discovery as a p53 interacting protein, the study of 53BP1 has been primarily focused on its contribution to the DSB NHEJ repair pathway, describing 53BP1's protein architecture, its functional partners and its physiological and pathological relevance. Here, the definition of the role of 53BP1 in p53 responses seeks to unravel a previously unappreciated aspect of 53BP1's biology, with potential implications in tumour suppression.

The barcode shRNA screen that identified 53BP1 as a mediator of the p53-dependent cellular response to N3 not only hinted to a direct functional connection between 53BP1 and p53, but also provided a model for the study of p53-dependent responses, MCF-7 breast cancer cells [240]. MCF-7 cells present robust induction of p53 and downstream target genes upon different stress stimuli. Additionally, this breast cancer cell line possesses wild-type *BRCA1* status, proficient DNA damage responses and cell cycle checkpoints. Moreover, the robust response to N3 and the clear phenotype generated by 53BP1 deficiency, alongside the amenability of MCF-7 cells to transduction and transfection represented an ideal platform for structure-function analyses. The generation of genetic knockouts in this cellular system will overcome the caveats of shRNA-mediated depletion, and provide a model to better define the impact of 53BP1 in p53-dependent responses. Finally, using a combination of traditional molecular biology and high throughput technologies I aim to tackle the 53BP1 protein and determine the cellular relevance of 53BP1-p53 connections.

3.2 Results

3.2.1 53BP1 enhances p53 transcriptional activity

In order to define the contribution of 53BP1 to p53-dependent responses, I generated isogenic knockouts in MCF-7 cells. The CRISPR/Cas9 technology was used to target the *TP53BP1* (here referred as *53BP1*) and *TP53* (here referred as *p53*) genes, and the exon-specific gRNAs that yielded productive knockout clones are depicted in Section 2.1.2 (Fig. 2.1). Clones isolated from edited MCF-7 cell populations were subject to initial SDS-PAGE/WB screening (Fig. 3.1A-B). *53BP1*-targeted clones A and C (hereinafter referred as *53BP1Δ-1* and *53BP1Δ-2*, respectively) displayed non-detectable protein in immunoblot analysis and were selected for deeper characterisation (Fig. 3.1A). In the case of p53, three independent clones showed complete absence of protein expression (Fig. 3.1B), and clone D (hereinafter *p53Δ*) was further characterised to serve as a control for p53 loss of function in downstream analyses. Knockout at the protein level was confirmed by indirect immunofluorescence (Fig. 3.1C). Additionally, successful genome editing was assessed by PCR amplification and Sanger sequencing (Fig. 3.1D). Both *53BP1Δ* clones presented biallelic frame-shift insertions at the Cas9 cutting point in exon 3 that resulted in the appearance of early stop codons in the coding sequence (Fig. 3.1D). Cas9-dependent targeting of exon 8 in the *p53* gene also generated small insertions in the genomic sequence (Fig. 3.1D). Despite the central position of the targeted region in the *p53* gene (encoding p53's DNA binding domain), nonsense-mediated mRNA decay prevented the appearance of truncated protein variants (data not shown, RNA-seq NCBI GEO: GSE84986).



Clone		Editing event (%)	Protein product
p53Δ		+1 (66.7), +2 (24.9)	147 aa, 169 aa
53BP1Δ	1	+1 (49.5), +2 (49.1)	86 aa, 89 aa
	2	+1 (98)	86 aa

Figure 3.1. Characterisation of 53BP1 and p53 knockout cell lines. (A, B) Immunoblot analysis of different 53BP1 (A) and p53 (B) clones recovered upon CRISPR/Cas9 genome-editing (Section 2.1.2). Short (top) and long (bottom) exposures are presented to ensure the absence of the protein. The p53 knockout cell lines were generated by Natalia Grolmusova and Dr J. R. Chapman. (C) Immunofluorescence staining of 53BP1 and p53 in clones selected for further analysis. (D) Sequencing traces where the Cas9 cutting point is represented with an arrow in the WT sequence panels..Deconvolution analysis of the mixed traces corresponding to different alleles was performed using the TIDE online tool [249]. Insertions and deletions are depicted with the percentage of editing provided in brackets. All editing events resulted in frame-shifts with the length of the expected protein products presented accordingly.

Previous studies reported shRNA-mediated depletion of 53BP1 in MCF-7 cells to increase resistance to the MDM2 antagonist N3 [240]. In order to assess

whether the isogenic knockout cell lines generated were able to recapitulate this phenotype, long-term N3 sensitivity assays were performed. Consistent with the presence of intact p53, *WT* MCF-7 cells robustly arrested in the presence of N3 (Fig. 3.2A).

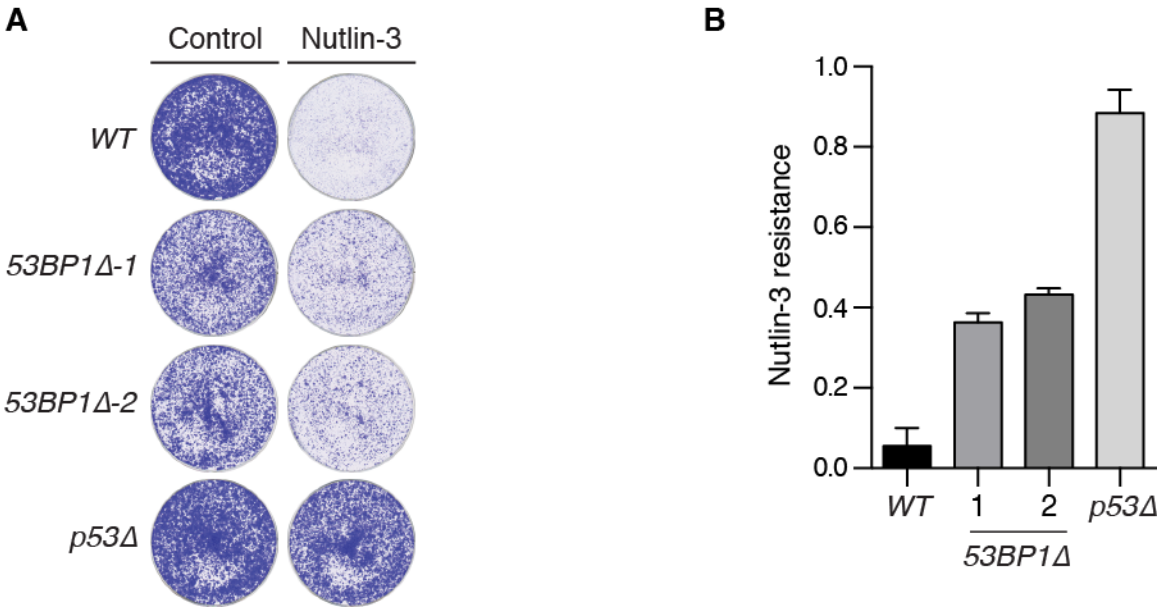


Figure 3.2. 53BP1-deficient cells display intermediate resistance to N3. (A) Cells of the indicated genotypes were treated with 4 μM N3 for 7 days or left untreated prior fixation and crystal violet staining. (B) Two independent experiments as in (A), were quantified by dissolving the cell-bound crystal violet in 10% (v/v) acetic acid and the absorbance of 1:50 dilutions subsequently measured at 595 nm. Absorbance values of N3-treated conditions were normalised against the corresponding untreated controls and the obtained ratios represented. Mean ± SD (plated in triplicate).

Conversely, N3-treated *p53Δ* cells presented growth rates similar to the untreated control, highlighting the specificity of the response. As expected, both *53BP1Δ* cell lines displayed reduced growth arrest in the presence of N3 (Fig. 3.2A). The resistance was intermediate compared to *p53Δ* cells, reaching absolute values of ~40% (Fig. 3.2B). Untreated *53BP1Δ* cells presented a growth defect compared to their *WT* or *p53Δ* counterparts (Fig. 3.2A). Remarkably, this phenotype, likely related to the loss of NHEJ-driven DSB repair activities, did not interfere with the growth advantage in N3 conferred by 53BP1 absence.

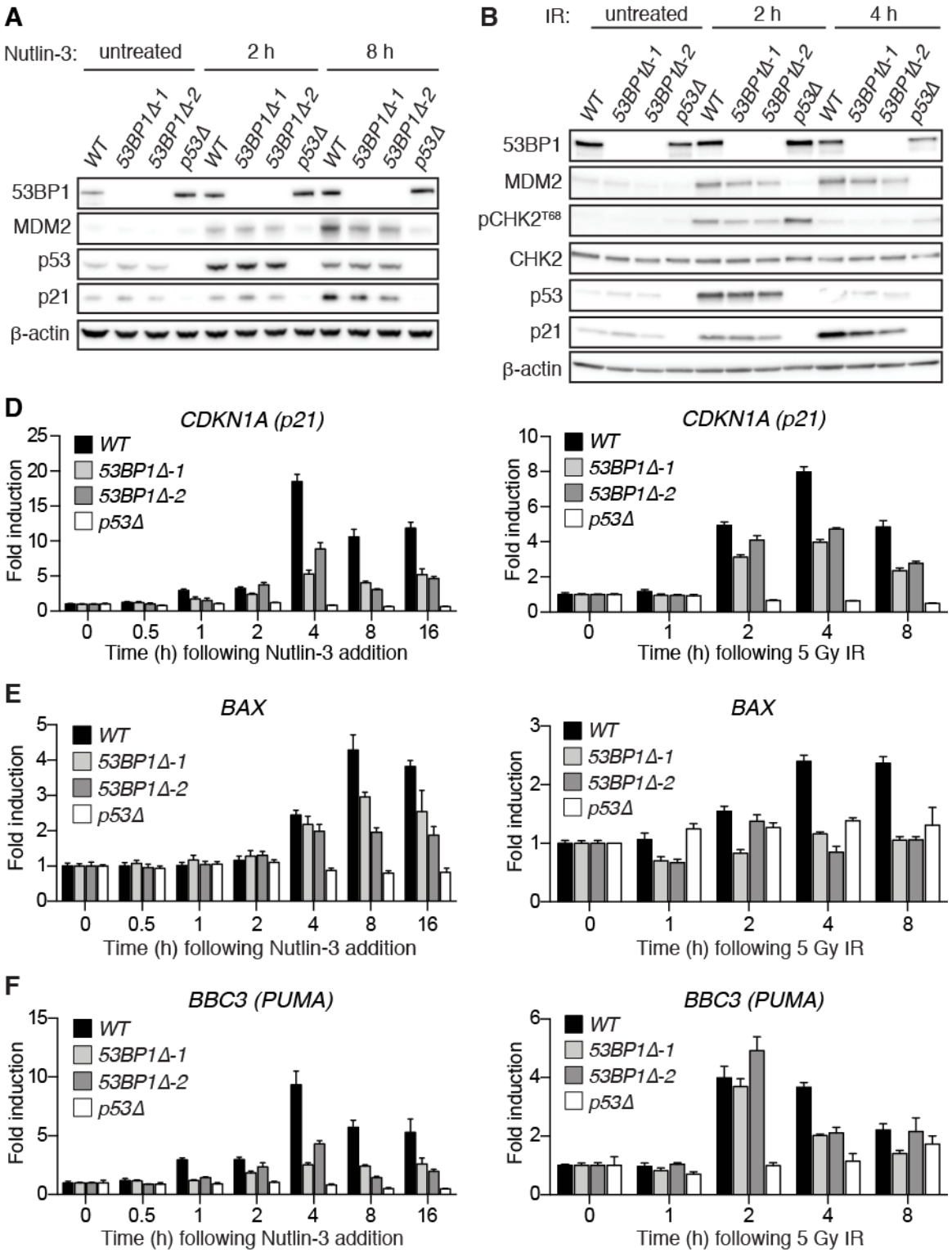


Figure 3.3. 53BP1 absence results in suboptimal induction of p53 target genes in response to N3 and IR. (A, B) Immunoblot analysis of MCF-7 lines of the indicated genotypes following exposure to 4 μM N3 (A) and 5 Gy IR (B). Time-points were selected for p53 and MDM2/p21 induction peaks. (D) *p21*, (E) *BAX*, and (F) *BBC3* (*PUMA)* transcript abundance in RNA extracts from cells treated with N3 and IR as in (A-B) quantified by RT-qPCR. *HPRT1* transcript was used for normalisation and fold-changes calculated against the corresponding untreated controls. Data are representative of two independent experiments (mean ± SD).

In agreement with a deficient p53-mediated arrest response, *53BP1Δ* lines also showed impaired induction of MDM2 and p21 protein expression upon N3 treatment (Fig. 3.3A). Furthermore, equivalent abrogation of p21 and MDM2 expression was observed upon IR-induced p53 activation (Fig. 3.3B). Interestingly, under both stimuli, p53 stabilisation was equivalent in *53BP1Δ* and *WT* cells (Fig. 3.3A-B). Altogether, these data suggested a broader impact for 53BP1 in p53-dependent responses, not solely restricted to N3-induced arrest.

Given the function of p53 as transcriptional factor, the impact of 53BP1 over the transcription of p53 target genes was then evaluated (Fig. 3.3C-E). 53BP1 deficiency resulted in a consistent ~2-fold decrease in *p21* mRNA induction at late time-points (4-16 h) under both N3 and IR stimulation (Fig. 3.3C), in close correlation with the reduction of protein expression previously reported (Fig. 3.3A-B). Analysis of the pro-apoptotic genes *BAX* and *PUMA* revealed similar trends hinting to a more extensive p53 transcriptional regulation by 53BP1 (Fig. 3.3E-F). p53-dependent transcription is regulated by cofactors that influence p53's activity and specificity (Section 1.2). In order to establish the magnitude of 53BP1's contribution to p53 transcription, genome-wide analyses were performed. *WT, p53Δ,* and the two independent *53BP1Δ* lines were treated with N3, IR or mock-treated. Three biological repeats were then subject to whole-transcriptome RNA-seq analysis. In a *WT* background, N3 and IR radiation provoked changes in 6877 and 2386 genes respectively, encompassing a similar proportion of activation and repression events (Table 3.1). Transcriptional changes were dependent on p53 almost entirely, with only 13 and 25 transcripts varying in expression in *p53Δ* cells upon N3 and IR treatments, respectively (Table 3.1).

	Gene #	Nutlin-3	IR
WT	Activated	3559	1043
	Repressed	3318	1343
53BP1Δ-1	Activated	1143	497
	Repressed	1096	686
53BP1Δ-2	Activated	1366	551
	Repressed	1624	767
p53Δ	Activated	10	6
	Repressed	3	19

Table 3.1. Number of activated and repressed genes in RNA-seq analysis of N3-(4 μM, 8 h) and IR-(5 Gy, 4 h) treated samples compared to untreated controls.

Gene numbers were significantly reduced (~50%) in the case of both *53BP1Δ* lines compared to *WT* controls, correlating with the general dampening in the transcriptional response depicted in the heatmap representation of the fold-changes of top1000 responsive genes to N3 and IR (Fig. 3.4A-B). 53BP1 absence caused suboptimal induction of N3 and IR responsive genes (Fig. 3.4A-B, in red). The attenuation of the response is reflected at the level of individual transcripts involved in different p53-dependent cellular processes. Supporting the results obtained in SDS-PAGE/WB and RT-qPCR analyses (Fig. 3.3), the cell cycle arrest *p21*, the auto-regulatory *MDM2,* and the pro-apoptotic *FAS* gene expression was significantly diminished in *53BP1Δ* cells compared to *WT* under the treatments applied (Fig. 3.4C). p53-mediated gene repression was similarly affected in *53BP1Δ* lines (Fig. 3.4A-B, in green). This effect was particularly evident in genes involved in cell cycle progression (*CHEK1*, *CDC25A*) upon N3 treatment (Fig. 3.4D), and could further explain the growth advantage displayed by *53BP1Δ* cells in long-term N3 survival assays (Fig. 3.2). Following the general

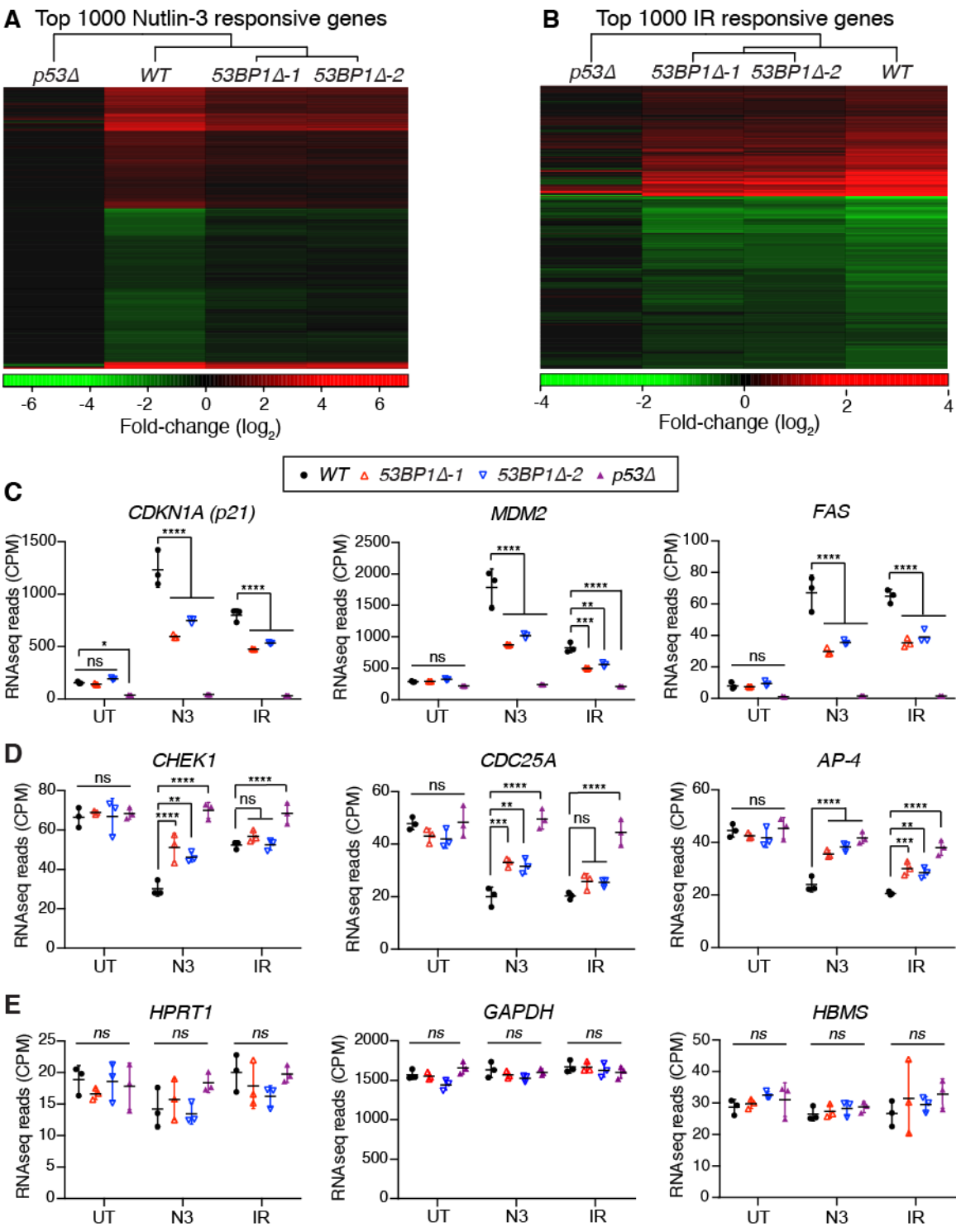


Figure 3.4. 53BP1 is a co-activator of p53-dependent transcriptional programmes. (A-B) Heatmap representation of the $\log_2$ fold changes (mean for n=3) for the top 1000 responsive genes to N3 (4 μM, 8 h) (A) and IR (5 Gy, 4 h) (B) compared to the corresponding untreated controls. (C-E) Three representative activated (C), repressed (D) and housekeeping (E) gene transcripts from three RNA-seq replicates upon the treatments in (A-B). CPM, counts per million; ns, non-significant; *p < 0.05; **p < 0.01; ***p < 0.001; ****p < 0.0001 (two-way ANOVA, mean ± SD). RNA-seq dataset analyses and heatmap representations were performed by Dr H. E. Lockstone and individual gene representations by Prof J. R. Chapman.

transcriptional trend upon IR treatment, less pronounced repression events were detected (Fig. 3.4B, D). Attenuation of p53-dependent activation and repression events was not attributed to overall defective transcription, as reflected by the equivalent expression of individual housekeeping genes across all the evaluated conditions (Fig. 3.4E).

Collectively, these data presented 53BP1 as a co-activator of p53-dependent transcription. Far from being restricted to specific genes, 53BP1's activity over p53 globally enhanced the p53's transcriptional programmes ultimately required for life-death cell fate decisions.

3.2.2 Oligomerisation and tandem BRCT domains are required for p53 modulation

53BP1 protein architecture comprises several domains whose functionality in NHEJ-driven DSB repair has been thoroughly discussed (Section 1.2.1). The coordinated action of 53BP1's domains allows the formation of chromatin-bound multiprotein complexes that ultimately promote NHEJ. In order to unravel the minimum sequence requirements in 53BP1 for modulation of p53 responses, 53BP1 gene constructs carrying point- and domain- mutations were generated (Fig. 3.5A). *53BP1Δ-2* cells (hereinafter referred as *53BP1Δ*) were subject to lentiviral transduction to achieve stable protein expression of *WT* and mutant constructs or the corresponding GFP controls (Fig. 3.5B). The ability of those mutants to promote recruitment to chromatin has been previously reported in immunofluorescence experiments (Fig. 3.5A, Foci) and their ability to promote DSB repair assessed in functional assays including CSR (Fig. 3.5A, CSR). Mutations in 53BP1's Tudor and UDR ($53BP1^{D1521R}$, $53BP1^{L1619A}$ respectively)

are reported to block interactions with modified nucleosomes and thus impede downstream NHEJ activities [24,59,63]. Despite localising to damage sites, 53BP1^{20AQ}, which harbours mutations in the first 20 ATM S/T-Q phosphorylation sites, presents a deficient recruitment of downstream effectors (RIF1, PTIP) and

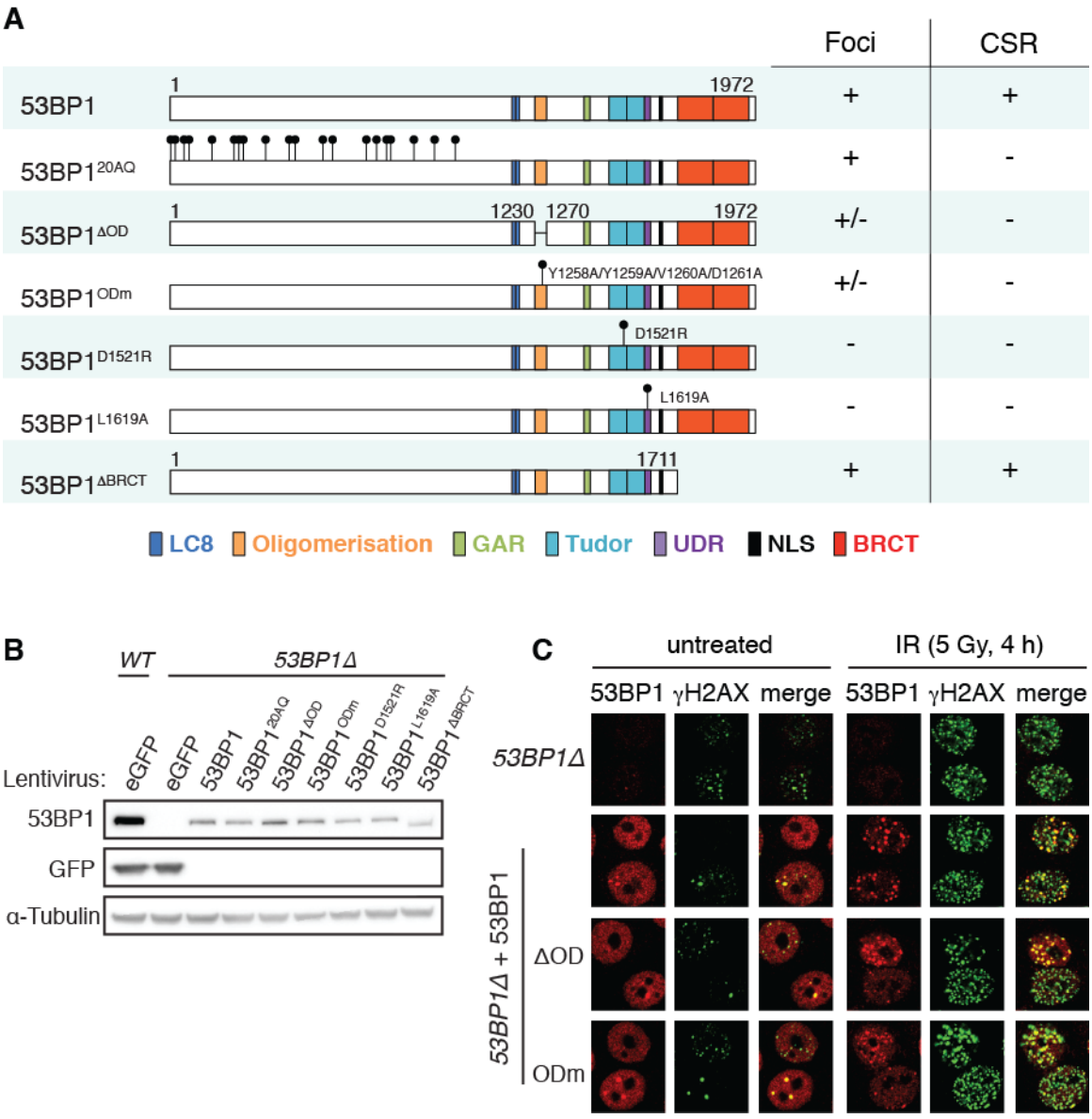


Figure 3.5. Reconstitution of 53BP1 point- and domain- mutant protein expression in *53BP1Δ* cells. (A) Schematic representation of the 53BP1 mutants analysed in this study. Proficiency to form foci and support CSR is stated: +, proficient; -, deficient; +/-, intermediate phenotype. (B) Western blot showing the protein levels of 53BP1 mutants in stably-transduced *53BP1Δ* cells using the pLenti-PGK-PURO-DEST expression vector. *WT* and *53BP1Δ* MCF-7 expressing GFP were used as experimental controls. (C) Characterisation of foci formation in 53BP1^{ODm} cells by indirect immunofluorescence upon treatment with 5 Gy IR for 4 h.

a subsequent inability to support NHEJ [49]. Alongside the well-characterised deletion of the oligomerisation domain (53BP1$^{\Delta OD}$), I evaluated the effect of a point mutation (53BP1^{ODm}) directed to disturb the domain activity while causing minimal disruption of 53BP1's overall architecture [62,63]. Accordingly, cells expressing 53BP1^{ODm} showed comparable foci formation efficiency upon IR to cells carrying 53BP1$^{\Delta OD}$ (Fig. 3.5C). In addition, recent functional assays have also shown equivalent deficiencies in supporting class-switch recombination events as the deletion itself [60]. Finally, a tandem BRCT-deletion mutant, which is fully able to support foci formation and NHEJ-driven DSB repair, was included in the analysis [49,63].

The mutants generated were then evaluated for their ability to induce N3-dependent cellular arrest. Re-expression of full-length 53BP1 was able to restore the sensitivity to the drug to levels close to *WT* MCF-7 control cells (Fig. 3.6A-B). Similarly, 53BP1^{20AQ} and 53BP1^{L1619A} mutants also sufficed to support p53-dependent arrest (Fig. 3.6A-B). Interestingly, 53BP1^{20AQ} and 53BP1^{L1619A} cells displayed a more pronounced sensitivity than cells complemented with WT 53BP1, hinting to a potential synergy between the loss of NHEJ activities and N3 action. Mutation in the Tudor domain, 53BP1^{D1521R}, conferred only partial sensitivity while individual deletion of 53BP1's tandem BRCT and deletion or mutation of the oligomerisation domain completely failed to rescue the sensitivity to N3, pinpointing to the essentiality of these regions for 53BP1-dependent p53 modulation (Fig. 3.6A-B).

The requirement for the oligomerisation domain indicated the necessity of several 53BP1 subunits potentially forming a multimeric protein complex that regulates p53. In addition, the functional involvement of the BRCT and Tudor

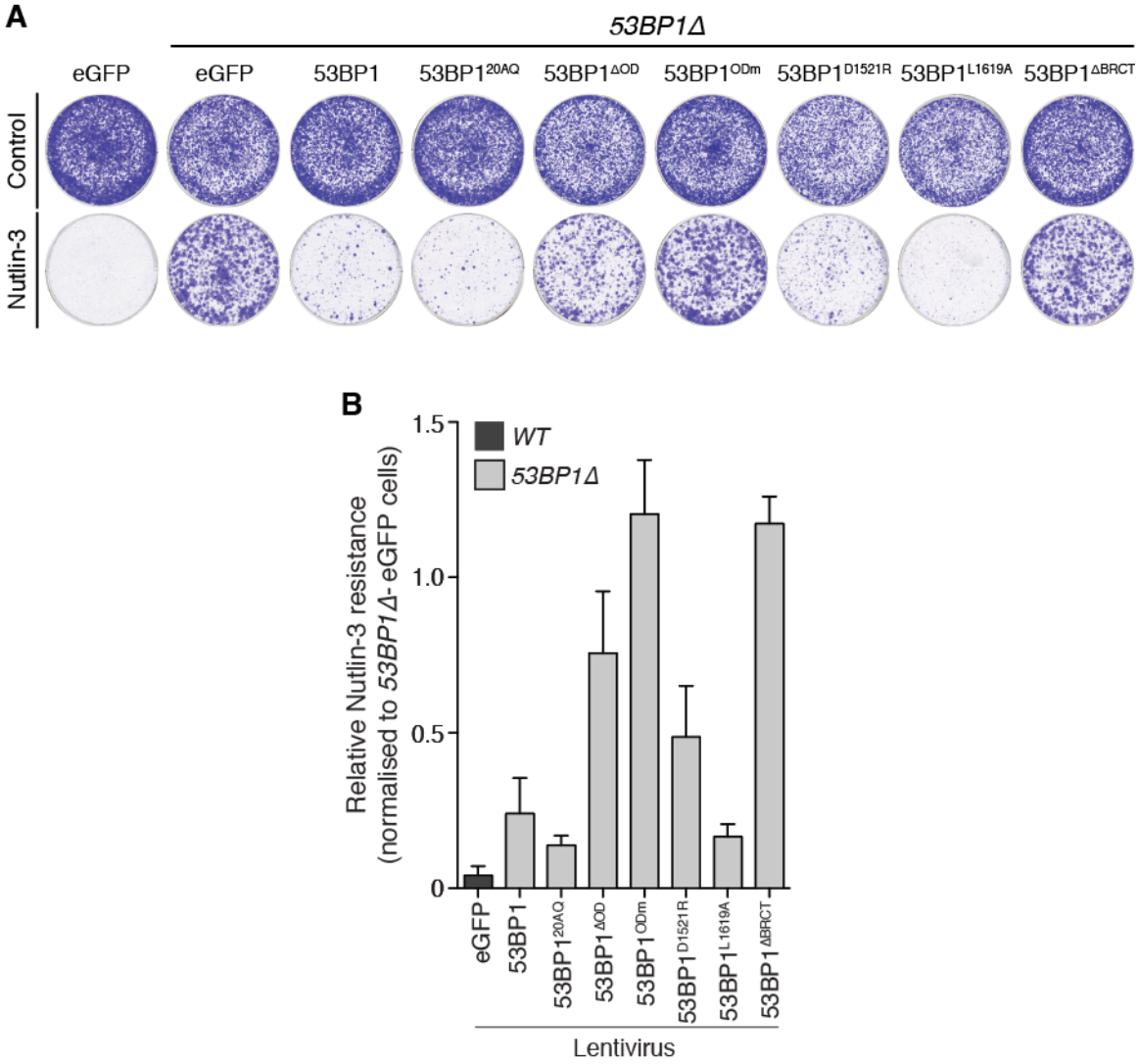


Figure 3.6. 53BP1 relies on oligomerisation and BRCT domains to modulate p53 responses. (A) Cell lines were treated with 4 μM N3 for 11 days or mock-treated for 7 days prior fixation and crystal violet staining. A representative image is shown. (B) Quantification of three biological replicates, plated in triplicate, as in (A) (mean ±SD). Absolute N3 resistance values were normalised to control eGFP-complemented *53BP1Δ* cells.

domains, coupled with prior structural data describing 53BP1-p53 interactions (Section 1.4.2), suggested that 53BP1 may modulate p53 in a way that requires physical interactions. In order to test this hypothesis, co-immunoprecipitation of 53BP1-p53 complexes was evaluated in *53BP1Δ* cells expressing 53BP1^{ODm}, 53BP1^{D1521R}, or 53BP1$^{\Delta BRCT}$ proteins. 53BP1 constitutively interacted with p53 (data not shown), and N3 treatment was used to enhance p53 protein levels and

maximise interaction visualisation. FLAG-HA-tagged 53BP1 efficiently co-immunoprecipitated p53 (Fig. 3.7A). Likewise, 53BP1-p53 complexes were precipitated using p53 specific antibodies (clone DO-1) (Fig. 3.7B). Deletion of 53BP1's tandem BRCT completely abolished p53 binding correlating with the inability of this mutant to support N3-dependent arrest (Fig. 3.7A-B). Similarly, 53BP1^{ODm} was largely unable to foster interactions with p53, outlining the relevance of 53BP1 self-interaction for the stability of 53BP1-p53 complexes (Fig. 3.7A-B). Conversely, 53BP1^{D1521R} displayed comparable efficiency in complex formation as the 53BP1 control (Fig. 3.7A-B), further demonstrating that bulk 53BP1-p53 interactions in this context were mediated by 53BP1's BRCT.

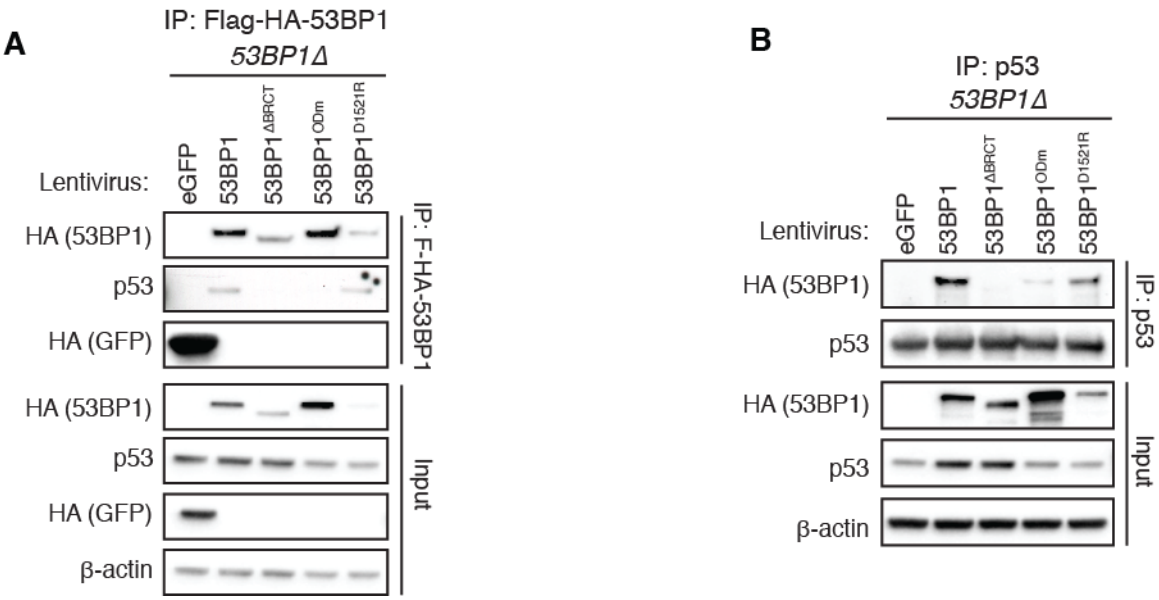


Figure 3.7. Functional oligomerisation and BRCT domains are essential for 53BP1-p53 interactions. (A) *53BP1Δ* cells were stably complemented using pHAGE-N-FLAG-HA-53BP1 constructs or the corresponding GFP control. Upon treatment with N3 (4 μM, 2 h) Flag-HA-53BP1 immunocomplexes were purified from cell lysates and interacting proteins analysed by western blot. (B) Western blot analysis of p53 immunocomplexes as in (A).

Collectively, the data showed that 53BP1 utilised structural domains for p53 modulation that were distinct from those required for NHEJ-driven repair. In fact, 53BP1^{L1619A} and 53BP1$^{\Delta BRCT}$ showed opposite phenotypes in functional NHEJ

assays and N3-induced arrest, indicating those two functions to be separable by specific mutations within the 53BP1 protein. Additionally, the data proposed a mechanistic connection between disruption of 53BP1-p53 physical contacts and resistance to N3. However, it failed to explain the intermediate N3 sensitivity of cells carrying 53BP1 mutated in the Tudor domain, hinting to a potential involvement of additional Tudor-interacting factors in 53BP1-p53 complexes.

3.2.3 53BP1 regulates G1/S transition *via* p53

The structure-function analysis of 53BP1 in p53-dependent N3-induced arrest highlighted a novel role for the tandem BRCT domain. This new evidence provided me with a unique tool to further define 53BP1's contribution to p53-dependent cellular processes without impairing NHEJ-related activities.

53BP1 has been reported to act with DNA topoisomerase 2-binding protein 1 (TopBP1) in the control of the G1/S transition [250]. However, in light of the data here presented and considering the major role of p53 in the G1/S checkpoint, it remains possible that 53BP1's action in this context occurs *via* p53.

To address this question, the gene fragment encoding the tandem BRCT domain was excised using CRISPR/Cas9 and specific gRNAs flanking the genomic region (Section 2.1.2, Fig. 2.1). Individual clones were screened using site-specific antibodies and two of them, named *53BP1$^{\Delta BRCT}$-A* and *-B*, selected for further analysis (Fig. 3.8A). Consistent with previous observations in *53bp1$^{\Delta BRCT}$* mice [63], the levels of the truncated protein were lower than their WT counterparts in both clones analysed (Fig. 3.8A). 53BP1$^{\Delta BRCT}$ efficiently formed IR-induced foci but failed to support N3-dependent growth arrest in long-term N3 viability assays, thereby mimicking 53BP1 deficiency (Fig. 3.8B, C).

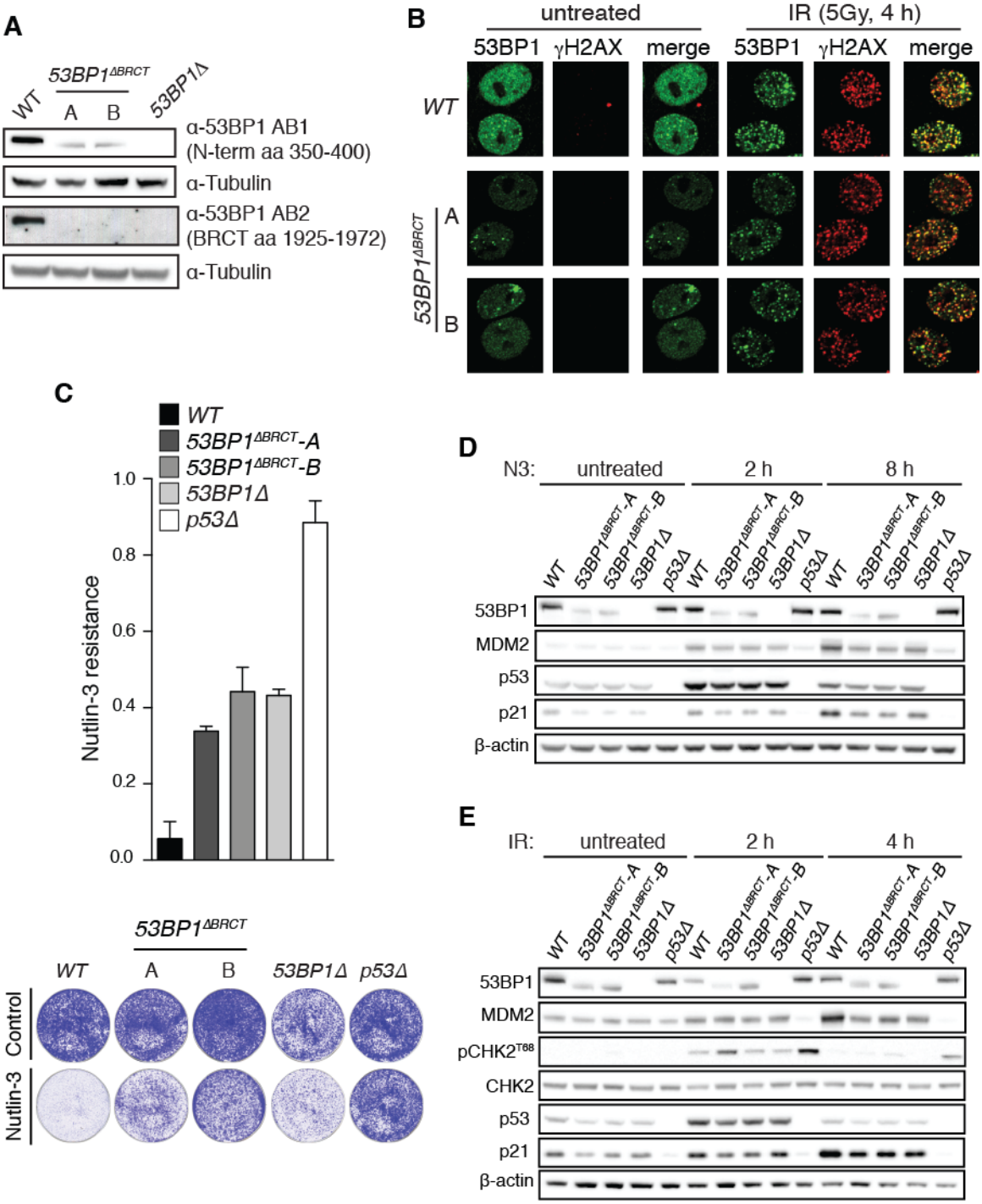


Figure 3.8. Endogenous deletion of 53BP1's tandem BRCT mimics complete 53BP1 absence in p53-dependent responses. (A) Immunoblot of *53BP1*$^{\Delta BRCT}$ lines with site-specific antibodies. (B) Immunofluorescence analysis of 53BP1 foci formation in *53BP1*$^{\Delta BRCT}$ cells upon treatment with 5 Gy IR for 4 h. (C) Long term N3 resistance assay was carried out as in (Fig. 3.2A-B). Mean ± SD (n=2, plated in triplicate). (D, E) Immunoblot analysis of MCF-7 lines of the indicated genotypes following exposure to 4 μM N3 (D) and 5 Gy IR (E). *53BP1*$^{\Delta BRCT}$ lines were generated by Dr C. Oliveira and Prof J. R. Chapman.

Remarkably, as opposed to *53BP1Δ* cells, repair-proficient *53BP1$^{\Delta BRCT}$* lines displayed no basal growth disadvantage compared to *WT* control (Fig. 3.8C, bottom panel). Additionally, immunoblot analysis upon N3 and IR treatments revealed suboptimal induction of p21 and MDM2 protein expression in *53BP1$^{\Delta BRCT}$* lines, comparable to the deficiencies observed in *53BP1Δ* cells (Fig. 3.8D, E). Collectively, characterisation of *53BP1$^{\Delta BRCT}$* lines evidenced their suitability to study 53BP1-dependent p53 functions and prominently supported the 'separation of function' hypothesis.

Using this cellular model, I proceeded to dissect 53BP1's role in regulating G1/S transition. Cells were synchronised in G1 and released into S-phase and cell cycle progression monitored after IR or mock-treatment (Fig. 3.9A). Released G1-synchronised *WT* MCF-7 cells presented a robust G1 arrest in response to IR (Fig. 3.9B). In agreement with p53's role in G1/S transition, IR-treated *p53Δ* cells overcome the G1 checkpoint control and progressed through the cell cycle following the same kinetics as the corresponding untreated controls (Fig. 3.9B). Untreated *53BP1Δ* cells displayed lower proliferation rates than the *WT* upon G1 release (Fig. 3.9C, unt. curves). Nevertheless, absence of 53BP1 resulted in less pronounced G1 arrest after treatment with IR (Fig. 3.9C, 4 Gy IR curves). Remarkably, specific endogenous deletion of 53BP1's BRCT domain did not affect the S-phase progression after G1 synchronisation. However, *53BP1$^{\Delta BRCT}$* lines presented suboptimal IR-induced G1 arrest, showing only a 50% reduction in S-phase cells at 22 h (Fig. 3.9D). Comparison of S-phase indices between 22 h and the 4-h irradiation point with additional correction for proliferation defects was performed to allow comparison amongst the different genotypes (Fig. 3.9E). This analysis revealed a significant and comparable failure in checkpoint

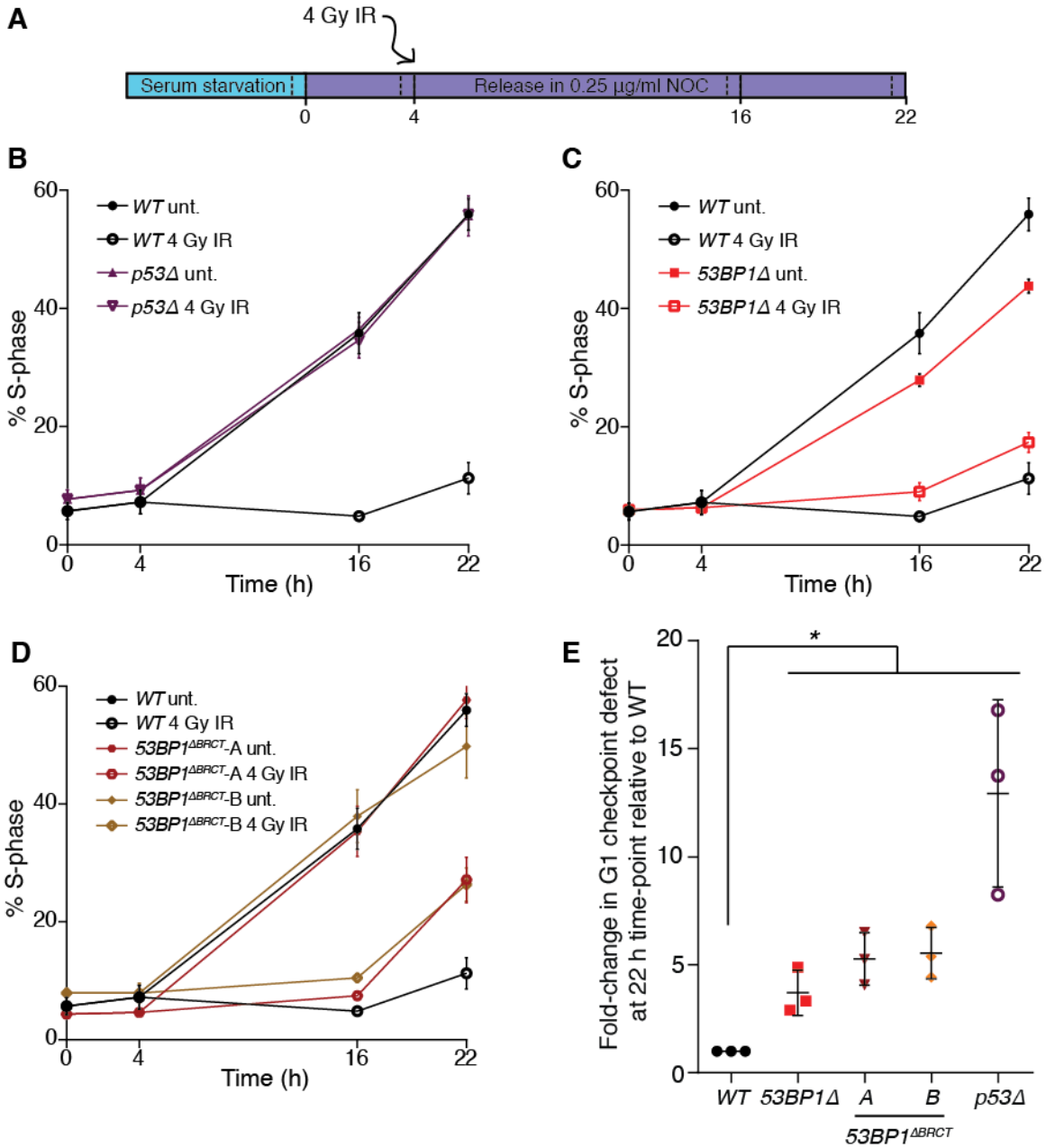


Figure 3.9. 53BP1 regulates IR-induced p53-dependent G1/S checkpoint arrest. (A) Schematic representation of the G1 checkpoint assay. Briefly, cells serum-free arrested in G1 for 24 h were released in serum-containing medium supplemented with 0.25 mg/ml nocodazole before irradiation (4 Gy) and collection at indicated time points for cell-cycle analysis. Solid bars indicate experimental time points. Dotted lines indicate BrdU addition. (B–D) S-phase cell indices for each indicated condition were obtained from flow cytometry in BrdU immunolabeled cells counterstained for DNA content (mean ± SD for n=3). *WT* results are plotted as a reference. (F) Significance of G1 checkpoint defects detected in (B-D) as a measurement of changes in S-phase indices in irradiated samples between 4 and 22 h time points. IR-treated sample values first corrected against the S phase index change in the corresponding untreated sample were then normalized against the WT value for each experiment. Values are plotted as fold change relative to WT. Mean ± SD; *p < 0.05 (unpaired, two-tailed Student's t test).

proficiency in *53BP1Δ* and *53BP1*$^{\Delta BRCT}$ lines when compared to the *WT* control. This effect was intermediate, closely correlating with the previously observed N3 and IR-related phenotypes. Furthermore, the contribution of the tandem BRCT domain pointed towards an essentiality of the 53BP1-p53 interplay in G1/S transition, and implied a divergent functional mechanism of 53BP1 checkpoint activities from yeast to human.

3.2.4 53BP1's tandem BRCT fosters dual p53-USP28 interactions required for modulation of p53 responses

While BRCTs are common domains involved in DDR, 53BP1's BRCT is not required for bulk NHEJ activities. Several 53BP1's BRCT interaction partners have been described, but their functional relevance has remained poorly defined. Here, 53BP1's BRCT acquires new relevance becoming the core domain coordinating p53 responses.

In order to specifically refine the contribution of 53BP1-p53 physical contacts, minimally impairing 53BP1's dynamics with other interaction partners, specific point mutants were designed. Prior structural data revealed two interaction surfaces, the inter-BRCT linker and the canonical phospholigand-binding pocket (Section 1.2.1.5). The inter-BRCT linker fosters the interactions with p53, using two key residues, N1845 and D1861, which form hydrogen bonds with p53 DBD residues. These residues were exchanged for both alanine and arginine aiming to create efficient disruption of 53BP1-p53 contacts (Fig. 3.10A, right panel). Mutations in the phospholigand-binding cage, R1811A and K1814M, were included as controls (Fig. 3.10A, right panel). *53BP1Δ* cells stably expressing the mutated proteins to equivalent levels (Fig. 3.10A, left panel) were

then analysed for its ability to support N3-mediated cell cycle arrest (Fig. 3.10B). Mutations in the phospholigand binding pocket resulted in different cellular response to the drug. As expected, 53BP1^{K1814M} was fully able to support N3-mediated arrest showing even higher sensitivity than the control cells

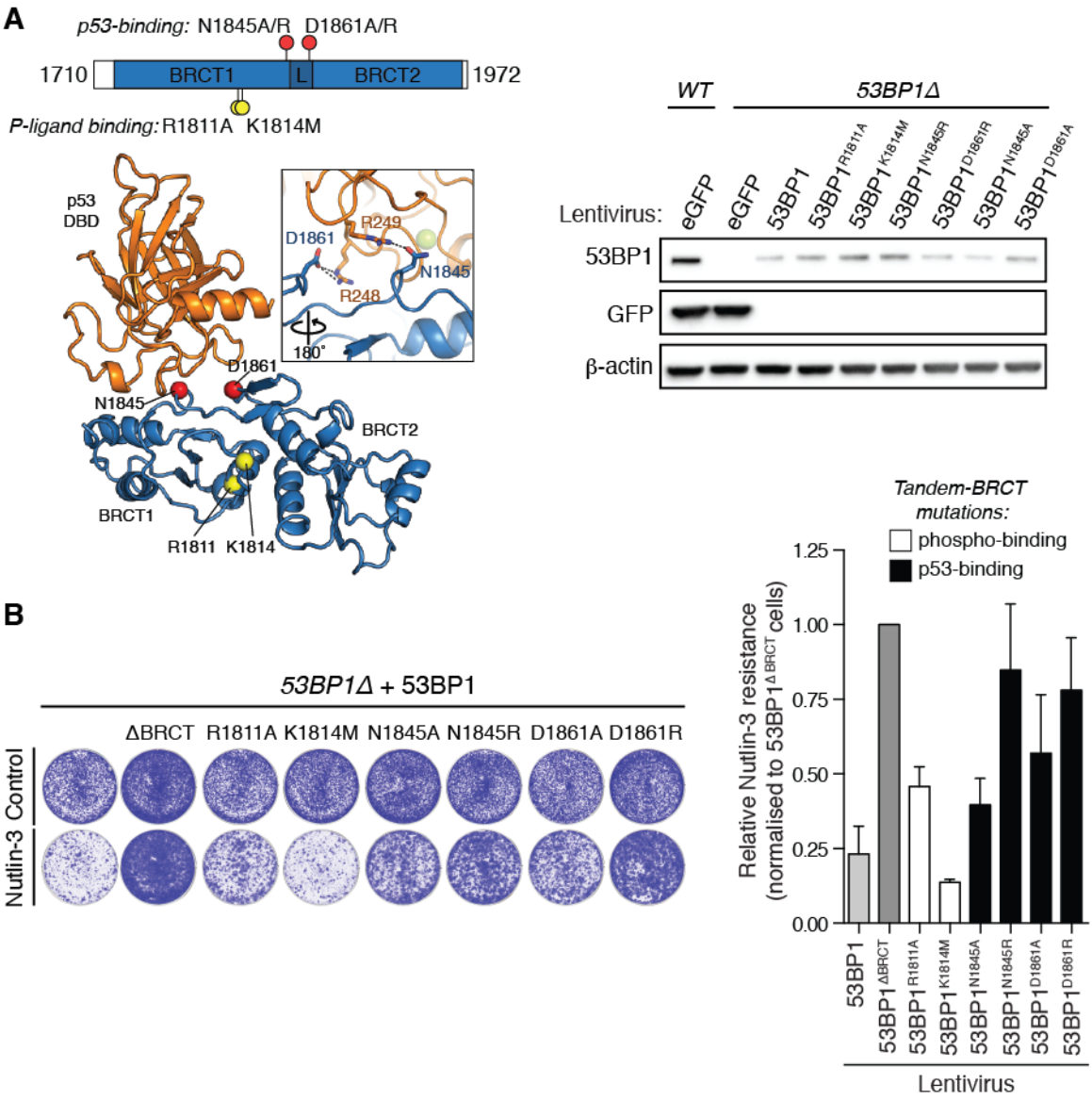


Figure 3.10. 53BP1^{R1811A} and p53-binding mutants fail to support efficient N3-mediated cellular arrest. (A) Schematic representation of 53BP1's tandem BRCT and corresponding structure bound to p53's DBD (PDB ID: 1KZY) with the position of the mutated residues highlighted. Immunoblot analysis of 53BP1 lines stably expressing the mutants depicted. (B) Visual representation and quantitative analysis of N3 resistance in *53BP1Δ* cells expressing the indicated 53BP1's BRCT point mutants. Absolute values were normalised against 53BP1$^{\Delta BRCT}$ cells. Mean ± SD (n=3, plated in triplicate).

complemented with 53BP1 (Fig. 3.9B). Conversely, 53BP1^{R1811A} was only able to support the arrest partially, in a phenotype closely resembling the one displayed by Tudor-mutated (53BP1^{D1521R}) cells (Fig. 3.9B). Considering the phosphobinding characteristics of the BRCT module (Section 1.2.1.5, Fig. 1.2B), this differential behaviour opened the possibility of a third interaction partner with unique binding dynamics and functional relevance in p53 responses. Mutation of p53-binding residues to alanine resulted in intermediate N3 resistance while substitution for the positively-charged amino acid arginine conferred cellular resistance to N3, reaching levels close to complete BRCT deletion (Fig. 3.10B). This phenotypical divergence could arise from differential binding dynamics. Substitution to alanine of a single residue in the interphase may not suffice for complete binding disruption, with the second residue still bridging efficient interactions. However, the presence of a bulky, positively charged arginine would interfere with the entire binding surface and hence the failure in supporting p53-dependent N3 cellular arrest.

To evaluate this hypothesis and additionally explore the relevance of the phosphobinding surface in p53 responses, immunoprecipitation of 53BP1-p53 complexes was performed. 53BP1 proteins mutated in the phosphobinding pocket residues efficiently interacted with p53 (Fig. 3.11A). Remarkably, 53BP1^{K1814M} showed enhanced affinity for p53, in agreement with the prominent rescue of N3 sensitivity, when compared to 53BP1-complemented cells (Fig. 3.11A). The inclusion of a methionine in this position may induce a conformational change in the opposite surface that would result in the stabilisation of the interaction. Alternatively, K1814M mutation may abrogate the interaction with a third partner masking p53's binding site, thus generating an

increase of 53BP1 protein available for interaction. p53 was undetectable in 53BP1^{N1845R} and 53BP1^{D1861R} immunocomplexes and 53BP1-p53 interactions were significantly destabilised upon alanine substitution (Fig. 3.11A). This biochemical analysis, joined to the functional characterisation previously described, established the specific requirement for 53BP1-p53 complex formation in supporting efficient p53-dependent responses.

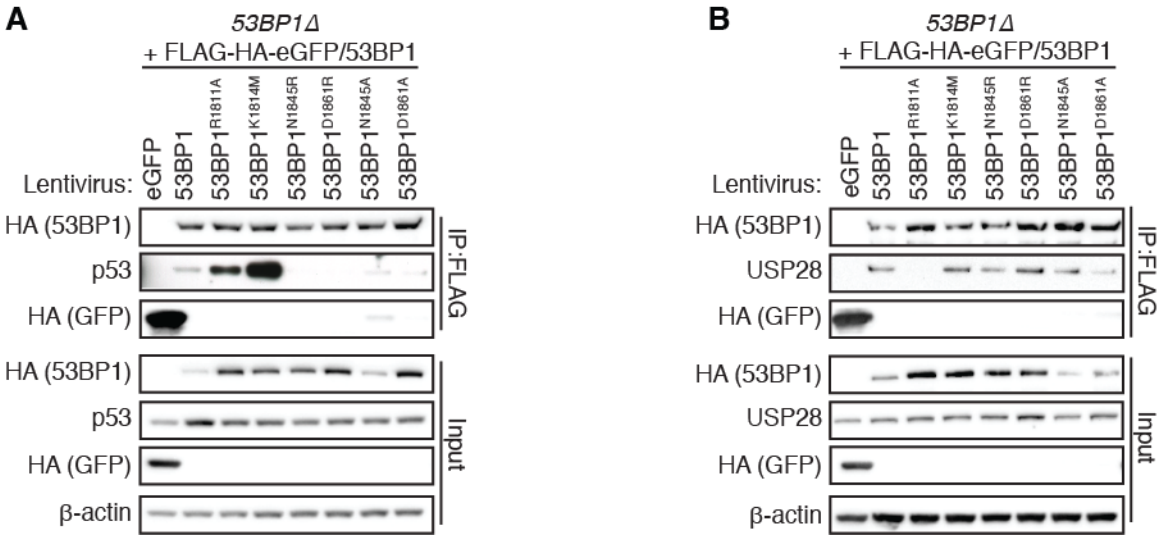


Figure 3.11. 53BP1's BRCT mediates p53 and USP28 interaction *via* different surfaces. (A) FLAG-HA-53BP1 protein complexes were immunoprecipitated from N3-treated (4 μM, 2 h) cell lysates and presence of p53 assessed by immunoblotting. (B) As in (A), evaluating the presence of USP28.

The relevance of residue R1811 could not be explained at the level of 53BP1-p53 interactions. I then proceeded to examine 53BP1 immunocomplexes for the presence of another reported BRCT-interacting protein, the ubiquitin specific protease USP28 [87]. USP28, whose role in 53BP1-driven NHEJ remains controversial, was identified as a low confidence hit in the shRNA screen looking for potential mediators of N3-induced cellular toxicity [86,87,240]. USP28 was co-immunoprecipitated with 53BP1 and the mutants tested with the sole exception of 53BP1^{R1811A} (Fig. 3.11B). USP28 thus fostered non-canonical interactions with a surface within 53BP1's BRCT phosphobinding pocket that

were required for modulation of p53-dependent N3 cellular arrest. Furthermore, USP28 and p53 had distinct surface requirements within 53BP1's tandem BRCT structure allowing bivalent interactions to occur simultaneously. Finally, these data identified a potential new role for USP28 as a novel component of the 53BP1-p53 regulatory node.

3.3 Concluding remarks

Soon after being discovered as a p53 binding protein, 53BP1 was functionally defined as a p53 cofactor involved in transcriptional activation [231,232]. Since, the scarce functional approaches have failed to define the impact of 53BP1 on p53 responses and the implications for cellular physiology.

In this chapter, I thoroughly demonstrated an important role for 53BP1 in enhancing p53 transcriptional activity. Far from being restricted to specific p53 target genes, 53BP1 promoted optimal genome-wide p53-dependent activation and repression events upon N3 and IR treatments. The magnitude of the molecular effect was phenotypically reflected in p53-dependent processes, as *53BP1Δ* cells failed to support efficient N3-mediated cellular toxicity and IR-induced G1/S checkpoint activation, in line with previous studies [240,250]. Interestingly, my data confirmed that 53BP1-mediated p53 modulation and 53BP1-driven NHEJ were distinct and separable activities integrated by 53BP1's architecture. Both functions shared common structural features: The requirement for oligomerisation and tandem Tudor domain implied the potential formation of protein macro-complexes and the involvement of methyl-interactions in 53BP1-dependent regulation p53 responses. Nonetheless, and consistent with the irrelevance of RNF8 and RNF168 in mediation of N3-induced cellular toxicity

[251], p53 functionality remained intact upon specific disruption of 53BP1 ubiquitin-dependent chromatin localisation, or block in the recruitment of downstream NHEJ effectors. Conversely, 53BP1's tandem BRCT, previously demonstrated as unrequired for 53BP1's NHEJ roles [59,63,252], constituted the central module in regulating p53 responses. The absence of a functional tandem BRCT mimicked 53BP1 loss-of-function in N3 resistance assays and p53-dependent p21 and MDM2 induction upon N3 and IR treatments. At a molecular level, the tandem BRCT fostered bulk p53 interactions, clearly outweighing the reported relevance of the Tudor domain in this context [236,241]. Indeed, 53BP1-p53 physical interactions were the bottom line in 53BP1's functionality in p53 responses. My refinement of the tandem BRCT domain revealed a perfect correlation between interaction and function. In fact, point mutations that strengthen 53BP1's BRCT-p53 interaction (K1814M) did not incur in competition with p53 binding to DNA, instead favouring more efficient p53-driven N3 cellular arrest. These results prompted me to propose that 53BP1 might act instead in priming p53 for downstream gene activation events.

As a scaffolding protein, 53BP1 is platform for the formation of multiprotein complexes with final effector roles [15]. To accomplish the modulation of p53 responses, 53BP1 not only recruited p53 itself, but also the deubiquitinating enzyme USP28. USP28, previously hinted as a mediator of N3 cellular toxicity [240], interacted with 53BP1's tandem BRCT via a different surface than p53, suggesting the formation of a ternary complex. Interestingly, the sequence requirements for USP28's interaction with 53BP1's BRCT were remarkably unusual. Mutations in the BRCT phospho-ligand binding pocket, that equally disrupted the interaction with γ-H2AX phosphopeptides [83,84], showed opposite

phenotypes in USP28 binding and, consequently, in N3 resistance assays. USP28's non-canonical BRCT binding opened an array of questions about the structural organisation of USP28-53BP1-p53 complexes. Furthermore, the functional connection between 53BP1 and USP28 reaffirmed the idea of a separation of function, '53BP1 drives NHEJ and p53 modulation activities through distinct structural elements and association with different interaction partners'.

Chapter 4

DEFINING A ROLE FOR USP28 IN p53-DEPENDENT RESPONSES

4.1 Introduction

Ubiquitination is a post-translational modification consisting in the conjugation of the 8.5-kDa protein ubiquitin to a target protein. The transfer of an ubiquitination molecule is catalysed in a step-wise process that ends with an E3 ubiquitin ligase covalently linking the ubiquitin moiety to a lysine residue in the destination protein. This reaction can be reversed by deubiquitinating enzymes, including USP28, maintaining an important equilibrium in many ubiquitin-regulated processes. Although ubiquitination has traditionally been associated with protein degradation, ubiquitination-dependent signalling acquires a prominent role in many cellular processes.

Throughout this thesis, I have already described the importance of ubiquitination events in regulating DNA damage signalling and 53BP1 recruitment to chromatin, and also in the regulation of p53 turnover. Here, I set out to test the possible contribution of USP28 in the 53BP1-dependent modulation of p53 responses, and determine the potential relevance of ubiquitination events in the functionality of this novel regulatory axis.

4.1.1 The USP28 protein

USP28 belongs to the ubiquitin specific protease (USP) superfamily that encompasses more than 50 DUBs that share similar catalytic domain

architecture. For USP28, two functional isoforms have been experimentally detected (Fig. 4.1) [253]. Despite being defined as the canonical sequence, isoform 1 is restricted to heart, skeletal muscle and brain, while isoform 2 possesses ubiquitous expression [253].

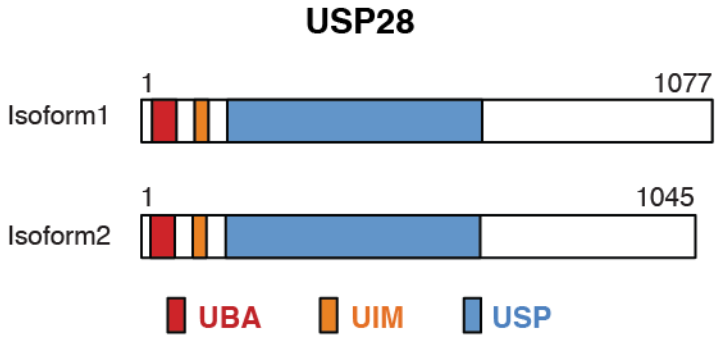


Figure 4.1. Schematic representation of USP28 isoforms. Isoform 2 differs from the canonical sequence in the absence of the amino acids 769-800 [253]. UBA, ubiquitin-associated domain; UIM, ubiquitin-interacting motif; USP, ubiquitin specific protease domain. Schematic representations are conveniently scaled and the positions of all features depicted accordingly.

The domain distribution is, nonetheless, identical and comprises an ubiquitin-binding region (UBR) with two ubiquitin binding modules in the N-terminal (UBA, UIM), a large, central catalytic domain (USP) and a highly structured C-terminal region of unknown function.

Structural nuclear magnetic resonance (NMR) of the UBR revealed a series of α-helices structured in two modules [254]. A three α-helix bundle spanning amino acids 22 to 60, forms a UBA domain sharing structural topology with previously described UBAs such as the present in mouse USP25 [254]. A flexible loop connects the UBA domain to a small turn-α-helix motif identified as a UIM (amino acids 88 to 116). Both modules can independently bind ubiquitin *in vitro*, and their deletion impairs USP28 catalytic activity in biochemical assays [254,255]. Additionally, K99 within the UIM can be subject to SUMO conjugation, in a process than negatively regulates USP28 activity [255]. Finally, the UBR's

flexibility confers USP28 high functional plasticity by recognising and efficiently processing K11-, K48- and K63-type ubiquitin chains [254,255].

The USP domain (amino acids 162 to 650) is the catalytic core of USP28. An N-terminal catalytic cysteine (C171) acts as a nucleophile and a C-terminal histidine (H600) as a proton acceptor to remove covalently bound ubiquitin residues. In addition to those two conserved residues, sequence alignment of USP28's USP with other USP domains revealed a high degree of sequence divergence, only sharing substantial amino acid identity with the close family member USP25 [253,256]. Interestingly, analysis of the crystal structures of USP domains available unravels a common architecture despite very low sequence identity. USP28 catalytic domain is thus likely to share the general topology, described as an open-hand divided in three subdomains, the thumb, the palm and the fingers (Fig. 3.2A).

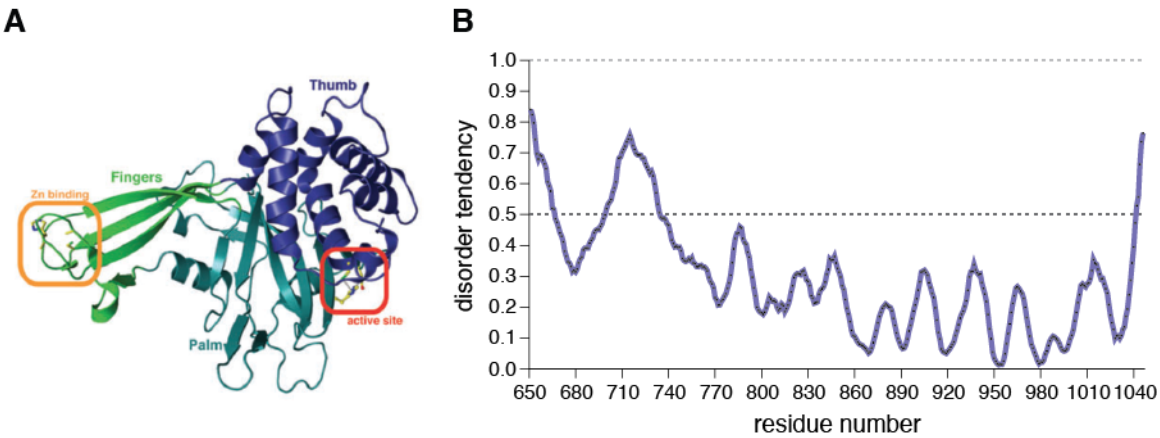


Figure 4.2. USP28 structural predictions. (A) Structure of USP7 catalytic domain. Structural organisation is shared amongst the USPs, and will likely resemble that of USP28. Image from [256]. (B) Prediction of disorder regions in USP28's C-terminal using meta protein disorder prediction system (metaPrDOS) [257]. Dotted line at disorder tendency value 0.5 represents the threshold for a false positive rate of 5%.

The catalytic domain ends in a C-terminal region that also shares remarkable sequence similarity with USP25. Structure prediction analysis

outlines the presence of a helix-based, highly structured module with minimal disorder regions (Fig. 3.2B). Interestingly, this module contains a reported ATM phosphorylation site (S714) within an SXXY consensus sequence that resembles a potential BRCT domain phospho-ligand [86].

4.1.2 USP28 functions

In 2006, mass spectrometry analysis identified USP28 as a 53BP1 interacting protein [86]. USP28 was attributed a role in regulating the stability of several DDR proteins, including 53BP1, Claspin, and MDC1, amongst others [86]. Additionally, loss of USP28, or catalytic inactivation, was found to directly impair Chk2 activation, p53 induction and subsequent *PUMA* transactivation [86]. However, a recent study mapped USP28-53BP1 interactions to 53BP1's BRCT domain [87]. Consistent with 53BP1's BRCT dispensability for NHEJ activities, genetic knockout of USP28 in cells and mouse models resulted in normal DSB responses and proficient NHEJ-driven DSB repair [87]. This striking contradiction leaves USP28-53BP1 structural and functional associations still to be revisited.

USP28 has been better studied in the regulation of the stability of the proto-oncogene MYC [258]. A genome-wide barcode shRNA screen highlighted USP28 as a requirement for correct MYC functions [258]. USP28 directly removes ubiquitin from MYC both in *in vitro* and *in vivo* assays, antagonizing the action of the E3-ubiquitin ligase F-box/WD repeat-containing protein 7 (Fbw7, Fbxw7) [258]. Later, USP28 was proposed to counteract Fbw7-dependent ubiquitination over many other targets such as cyclin E, Jun, and mammalian target of rapamycin (mTOR) [259]. Specifically, the activity of the USP28/Fbw7 duo acquires relevance in intestine homeostasis [260]. Conditional deletion of

Fbw7 in the intestinal tumour models harbouring mutation in APC ($APC^{min/+}$) results in offspring reduction, impaired gut differentiation, and enhanced tumourigenesis [260,261]. Codepletion of USP28 in this model ameliorates the defects caused by Fbw7 absence and largely resembles an $APC^{min/+}$ scenario [260]. These observations pinpoint the relevance of USP28 in gut differentiation and antitumorigenesis through its coordinate action with Fbw7.

4.1.3 Why USP28?

Several lines of evidence pointed to USP28 as a candidate partner in the 53BP1-p53 axis. Initially, the barcode shRNA screen that identified 53BP1 as a mediator of N3 toxicity, reported USP28 as a low confidence hit, implying its contribution to p53-mediated responses [240]. Simultaneously, USP28 was identified as a 53BP1 interactor [86]. This interaction was exclusive to USP28 within the USP family, not even mimicked by the closest family member and paralog, USP25 [86]. Additionally, USP28 physical association with 53BP1 relies on the tandem BRCT domain [87]. 53BP1's tandem BRCT is dispensable for NHEJ-directed repair, which explains the dubious role for USP28 in DSB repair [86,87]. This historical evidence, coupled with the functional relevance of 53BP1's tandem BRCT and its interaction with USP28 in p53 responses here described (Section 3.2.4), converge into the hypothesis of a functional connection between USP28 and the 53BP1-p53 regulatory node.

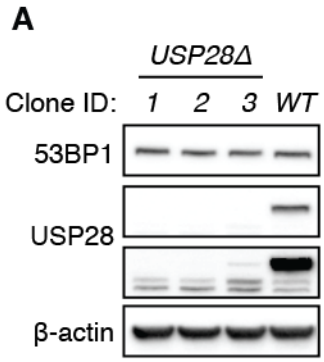
4.2 Results

4.2.1 USP28 modulates p53-dependent responses alongside 53BP1

In light of the results obtained from the mutagenesis analysis performed in 53BP1's BRCT, I set out to define USP28 contribution to p53-dependent responses. First, genetic knockouts of USP28 were generated in the model system, MCF-7 cells. CRISPR/Cas9 mediated genome editing was used (gRNAs yielding productive knockouts in Fig. 2.1) and individual clones isolated and screened by SDS-PAGE/WB. From the three clones selected in the screen, two (*USP28Δ-1* and *-2*) showed no detectable protein expression and 53BP1 levels comparable to *WT* cells (Fig. 4.3A). Further characterisation by locus-specific PCR and Sanger sequencing revealed biallelic frame-shift insertions at the Cas9 cutting point in exon 3 in *USP28Δ-1* resulting in the appearance of early stop codons (Fig. 4.3B). Analysis of *USP28Δ-2* showed a single editing event (-10 bp) at the exon 4 in the genomic locus (Fig. 4.3B), suggesting the presence of a single USP28 allele, equivalent biallelic editing, or the presence of large insertions or deletions impeding PCR amplification of the second allele.

Upon molecular characterisation of *USP28Δ* lines, cells were seeded in the presence of N3, including a *53BP1Δ* control for comparison purposes. Both *USP28Δ* lines presented an intermediate resistance to the drug, closely mimicking the phenotype of *53BP1Δ* cells (Fig. 4.3C). *USP28Δ* untreated control cells showed growth rates comparable to *WT*, not displaying the growth deficiency present in *53BP1Δ* cells (Fig. 4.3C, left panel).

In agreement with a suboptimal support of N3-induced arrest, N3-dependent induction of p21 and MDM2 proteins was diminished in *USP28Δ* lines compared to the *WT* controls (Fig. 4.4A). At 8 h, the reduction observed in both



B

Clone		Editing event	Protein product
USP28Δ	1	+1, +203	76 aa, 145 aa
	2	-10	160 aa

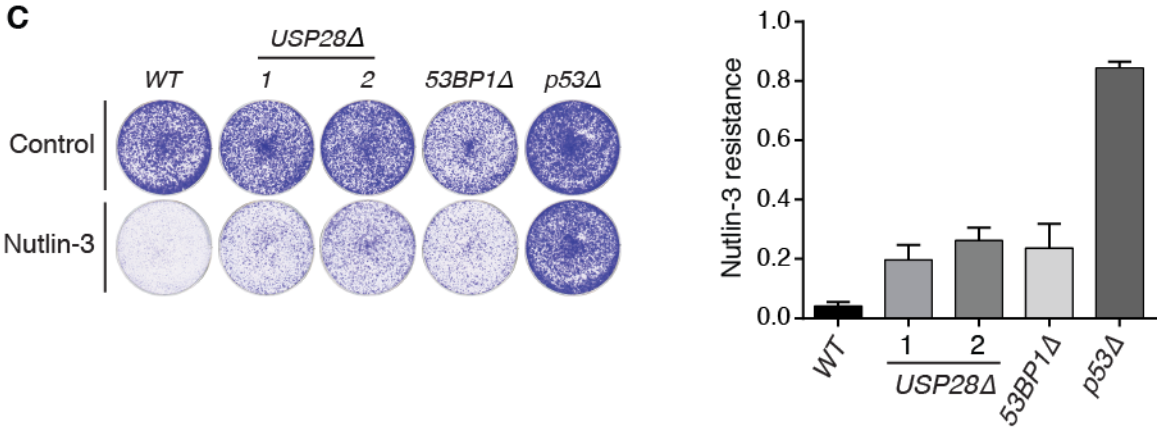


Figure 4.3. USP28 depletion confers resistance to Nutlin-3. (A) Immunoblot analysis of USP28 clones isolated upon CRISPR/Cas9 genome-editing. Short (top) and long (bottom) exposures are presented to ensure the absence of the protein of interest. (B) Single PCR products were amplified and individually sequenced. Insertions and deletions detected are depicted alongside the length of the expected protein products. (C) Visual and quantitative analysis of N3 resistance in *USP28Δ* cells as in Fig. 3.2. Mean ± SD (n=3, plated in triplicate). *USP28Δ* lines were generated by Helena Castillo-Ecija.

USP28Δ was more pronounced than the corresponding in *53BP1Δ* cells (Fig. 4.4A). However, this variation in phenotypic penetrance could be explained by the concomitant reduction in p53 protein levels at the late time-point analysed (Fig. 4.4A). These data revealed slight phenotypical variations between *USP28Δ* and *53BP1Δ* cells that may arise from direct or indirect mechanistical differences. Transcript analysis of *MDM2* supported the results obtained at a protein level. In the absence of USP28, consistent 2- to 3-fold reduction was observed in mRNA levels at mid- and late- time-points after N3 treatment (Fig. 4.4B). Similar trends

were observed in the analyses of representative apoptotic genes such as *TP53I3* and *BBC3* (*PUMA*) (Fig. 4.4B). The magnitude of mRNA induction deficiencies closely resembled that of *53BP1Δ* lines (Fig. 3.3-3.4), reflecting equivalent suboptimal p53-transactivation events in response to N3.

I then proceeded to examine p53-dependent cellular responses to ionising radiation. For this purpose, immunoblot analysis of irradiated cells was performed, and IR-induced G1/S arrest evaluated in *USP28Δ* cells. Similarly to N3, treatment with IR robustly stimulated MDM2 and p21 protein expression in *WT* MCF-7 cells, but had a reduced effect in cells lacking USP28 (Fig. 4.4C). While differences between *WT*, *USP28Δ* and *53BP1Δ* lines were detected in DNA-damaged induced phosphorylation of T68 in Chk2, the stabilisation of p53 remained equal across the three genotypes (Fig. 4.4C). Interestingly, no differences in Chk2 or 53BP1 stability were observed in absence of USP28, conflicting with previous reports in which USP28 was shown to regulate DDR protein turnover (Fig. 4.4C) [86].

USP28 involvement in G1/S transition was evaluated in checkpoint analysis using *USP28Δ-2* cell line (hereinafter *USP28Δ*) (Fig. 3.9A). Similar to *WT* cells, *USP28Δ* cells showed a noticeable initial arrest in response to IR (Fig. 4.4D, 16 h). Nonetheless, this arrest was fast overcome and *USP28Δ* cells re-entered the cell cycle more efficiently than the *WT* counterparts (Fig. 4.4D 22h, 4.4E). At 22 h, *USP28Δ* cells were able to evade the checkpoint, albeit less prominently than *53BP1Δ* cells (Fig. 4.4E).

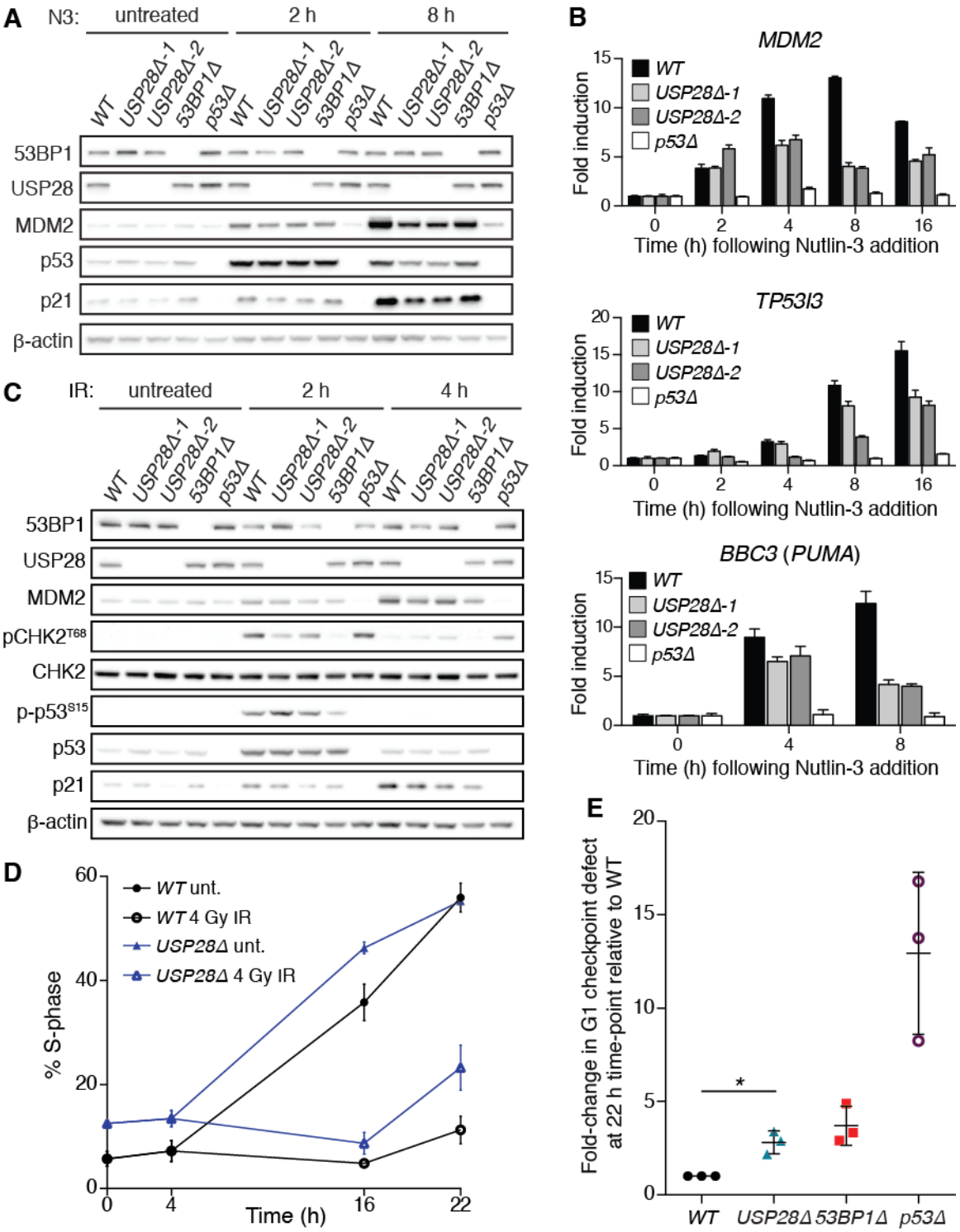


Figure 4.4. USP28-deficiency largely mimics 53BP1 deficiency in p53-dependent responses. (A) Immunoblot analysis of MCF-7 lines treated with 4 μM N3 for the indicated times. (B) MDM2, TP53I3 and PUMA transcript abundance in RNA extracts from cells treated with N3 as in (A) quantified by RT-qPCR. Data are representative of two independent experiments (mean ± SD). (C) Immunoblot analysis of MCF-7 lines treated with 5 Gy IR. (D) S-phase indices for each condition represented as in (Fig. 3.9B-D) (mean ± SD (n=3)). *WT* results are plotted as a reference. (E) Significance of G1 checkpoint defects in USP28 cells, calculated as in (Fig. 3.9F). Mean ± SD; *p < 0.05 (unpaired, two-tailed Student's t test).

These remarkable similarities between *53BP1Δ* and *USP28Δ* lines in the assays performed, and their physical interaction through 53BP1's BRCT strongly suggested a cooperative action for those two proteins in modulating p53 activity. To test this hypothesis, *53BP1Δ*/*USP28Δ* double knockout cells were generated using CRISPR/Cas9-mediated genome editing and a 53BP1-especific gRNA (gRNA 1, Fig. 2.1) in *USP28Δ* cells. Individual clones obtained were characterised by SDS-PAGE/WB. Clone *53BP1Δ/USP28Δ*-D (hereinafter *53BP1Δ*/*USP28Δ*) showed no detectable protein expression and was plated in N3 alongside single *USP28Δ* and *53BP1Δ* knockouts (Fig. 4.5A). *53BP1Δ*/*USP28Δ* cells had marked growth deficiencies in untreated conditions, evidencing that the combined loss of those two proteins generate an enhanced disadvantage over the individual deficiencies (Fig. 4.5B). Regardless, *53BP1Δ*/*USP28Δ* cells showed equivalent intermediate resistance to N3 as the individual knockout cells, confirming the epistatic relationship between those two genes in regulation of N3-mediated arrest (Fig. 4.5B).

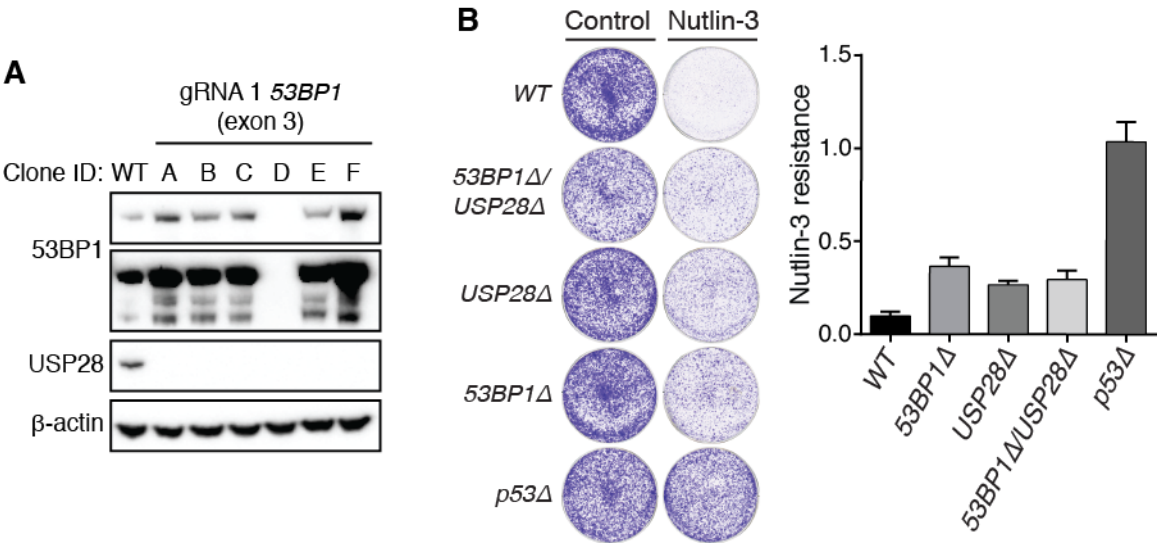


Figure 4.5. 53BP1 and USP28 act together in p53 modulation. (A) Immunoblot analysis of potential *53BP1Δ*/*USP28Δ* double knockout clones isolated. (B) Visual and quantitative analysis of N3 resistance in *53BP1Δ*/*USP28Δ* cells relative to single mutants as in Fig. 3.2. Mean ± SD (n=3, plated in triplicate).

4.2.2 USP28 catalytic activity is required for p53 modulation

Once the relevance of USP28 in p53-mediated responses had been defined, I set to explore the contribution of individual USP28's domains. Only three modules have been described in USP28: two ubiquitin-binding motifs (UBA and UIM) and an USP catalytic domain (Fig. 4.6A). Gene constructs carrying domain- and point- mutations directed to individually abolish the activity of these three domains were generated and expressed in *USP28Δ* cells (Fig. 4.6A, 4.7C). Their relevance to p53-dependent responses was subsequently evaluated using N3-dependent arrest as a readout. Expression of the ubiquitous isoform 2 of USP28 completely restored the sensitivity to N3, and equivalently did the expression of single deletion of the ubiquitin binding domains (Fig. 4.6B). However, disruption of the deubiquitinating activity by mutation of C171 resulted in inability to support N3-dependent cellular arrest, to levels comparable to the

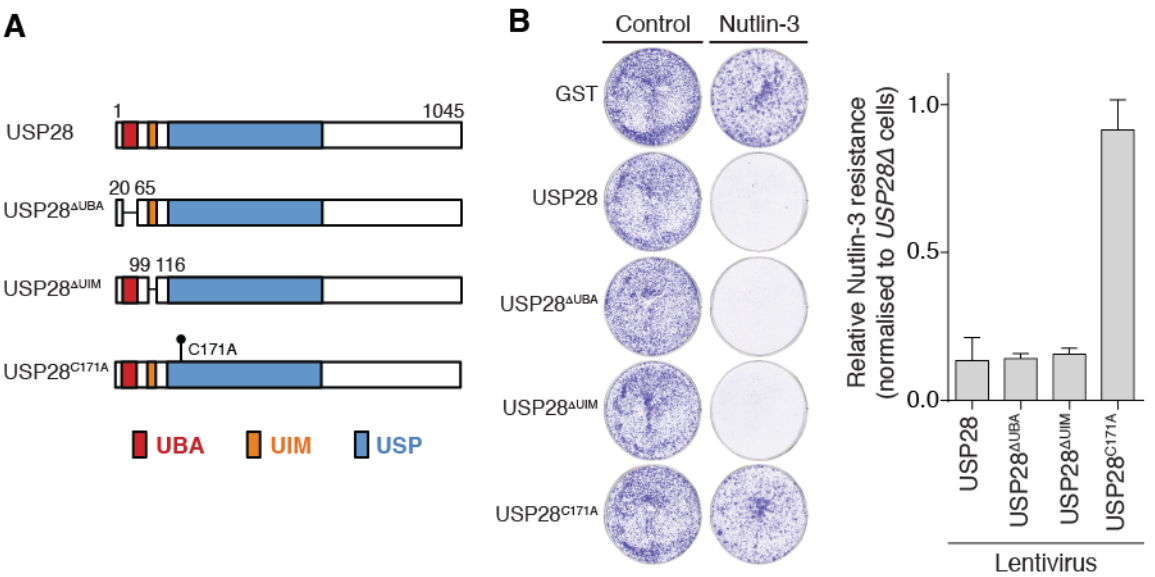


Figure 4.6. USP28 relies on the catalytic activity, but not the ubiquitin binding motifs, to regulate p53-dependent responses. (A) Schematic representation of the USP28 domain- and point-mutants. (B) Visual and quantitative analysis of N3 resistance in *USP28Δ* cells stably complemented with indicated USP28 gene constructs or GST as a control. Mean ± SD (n=3, plated in triplicate). USP28-complemented cell lines were generated by Prof J. R. Chapman.

knockout itself (Fig. 4.6B). The irrelevance of USP28's ubiquitin-binding motifs in p53-dependent responses suggested the presence of additional sequences in USP28 to foster the ubiquitin-independent interactions necessary for target specificity.

4.2.3 Sequences in USP28's catalytic domain and C-terminal are essential for its function in p53 responses

In addition to the USP28 catalytic activity, interactions between USP28 and 53BP1 were essential for p53 regulation, prompting me to consider the involvement of additional sequences in USP28 that might foster 53BP1 binding. The C-terminal region of USP28 is a highly ordered domain of unknown function. In order to determine whether this domain was required for optimal p53 functionality, C-terminal truncation mutants were generated. To minimise the effect of these mutants on the structural integrity of this domain, a disorder prediction analysis was carried out to determine potential truncation sites (Fig. 4.7A). Accordingly, three C-terminal truncation mutants were generated (Fig. 4.7B). Additionally, an N-terminal truncation, simultaneously removing UBA and UIM, was included to address the possibility of binding redundancy between those two modules (Fig. 4.7B). Gene constructs were stably expressed in *USP28Δ* cells and tested for their ability to support N3-dependent arrest (Fig. 4.7C). Individual domain- and point- mutants from Section 4.2.2 were included for comparison purposes (Fig. 4.7C). Deletion of the entire N-terminal was equivalent to individual deletions of UBA and UIM and completely restored N3-sensitivity in *USP28Δ* cells (Fig. 4.7D). These data confirmed the dispensability of the ubiquitin binding motifs and regulatory modifications occurring within that

region for USP28-dependent p53 modulation. Truncations of the C-terminal, however, influenced the response to N3. While expression of USP28$^{\Delta 1021+}$ largely

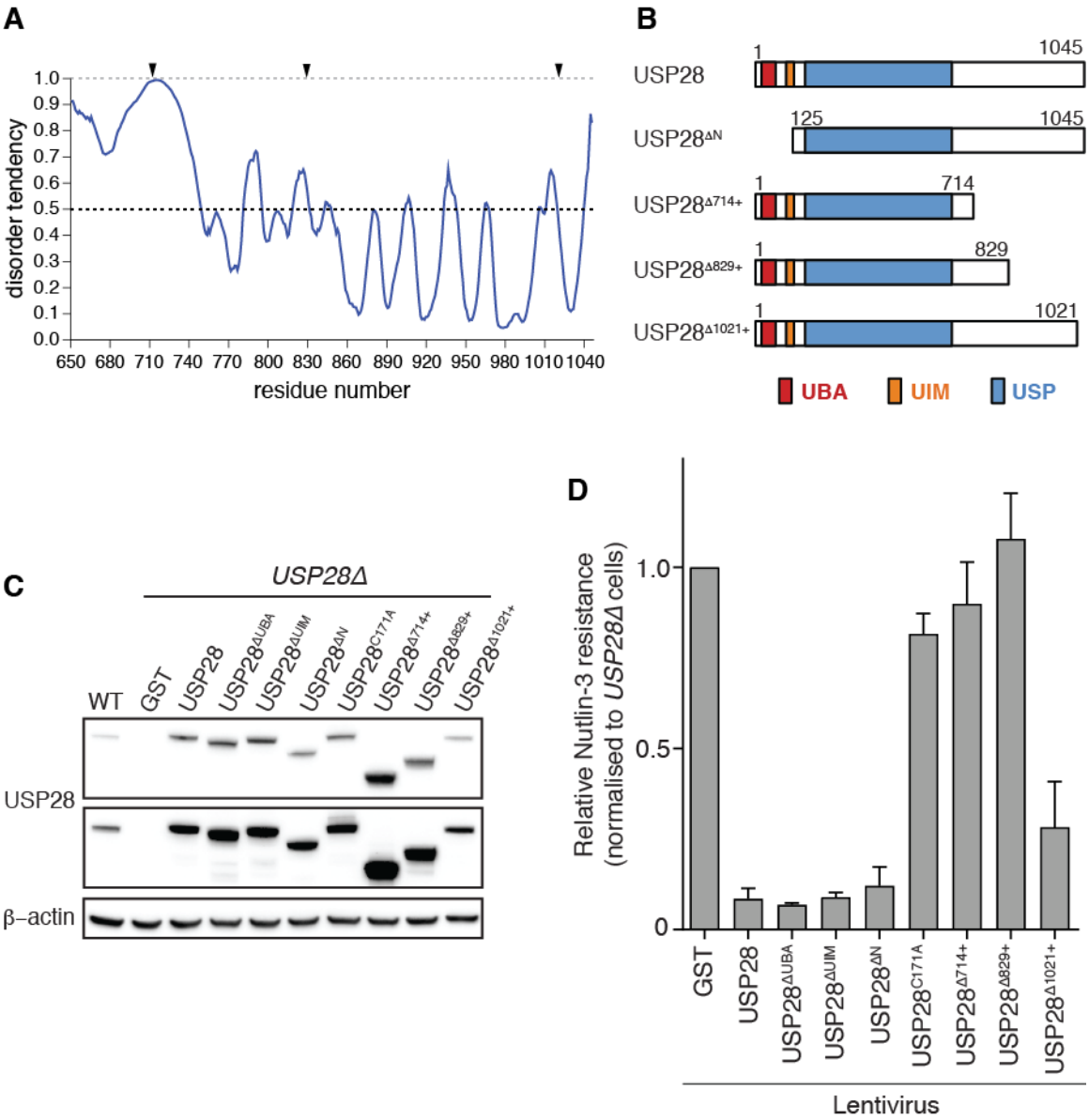


Figure 4.7. USP28 C-terminal region is required for USP28 functionality in p53 regulation. (A) Disorder prediction within the C-terminal region of USP28 using DISPROT (VSL2P) [262]. Dotted line at disorder tendency value 0.5 represents the threshold for a false positive rate of 5%. Arrowheads indicate cutting points for C-terminal truncation mutants displayed in (B). (B) Schematic representation of N- and C-terminal truncation mutants. Annotations are made taking USP28 isoform 2 as the reference. (C) Western blot displaying the protein levels of USP28 mutants in *USP28Δ* cells using the pLenti-PGK-PURO-DEST expression vector. *USP28Δ* expressing GST was used as a control. (D) Quantitative analysis of N3 resistance in *USP28Δ* cells in (C). Mean ± SD (n=2, plated in triplicate). USP28 truncation constructs were generated by Prof J. R. Chapman.

supported cellular arrest upon N3 treatment, USP28$^{\Delta 714+}$ and USP28$^{\Delta 829+}$ were completely dysfunctional in this context (Fig. 4.7D). Considering previous *in vitro* de-ubiquitination assays that showed USP28 carrying a large deletion in the C-terminal (USP28$^{\Delta 757+}$) to be as catalytic proficient as full length versions [255], it is unlikely that the resistance observed in the USP28$^{\Delta 829+}$ mutant will be explained by a catalytically inactive protein. Although the data will initially define the region between amino acids 829 and 1023 as relevant for p53 modulation, it remains possible that the large deletion may cause a domain disruption due to the heavily structured nature of the C-terminal region.

In light of these data, an alternative approach to achieve detailed structure-function analysis was established. USP28 shares more than 50% sequence identity with its paralog USP25, including a significant conservation in the C-terminal region [253]. However, USP25 does not establish interactions with 53BP1 [86]. Using a sequence alignment between the two proteins, chimeric proteins were designed. Substitution of USP28 sequences with the corresponding regions in its USP25 counterpart aimed to interfere with USP28's protein functionality while preserving the structural integrity. Sequential chimeras were designed based on regions of transition convergence/divergence within the alignment, targetting both the catalytic domain and the C-terminal region (Fig. 4.8B, left panel). *USP28Δ* cells stably expressing the constructs designed were characterised by immunoblotting with an USP28-specific antibody and an USP25 antibody that presented USP28 cross-reactivity (Fig. 4.8A-B). As previously observed, *USP28Δ* cells complemented with full-length USP28 restored full sensitivity to N3 (Fig. 4.8B). Surprisingly, expression of additional USP25 in those cells partially reverted N3 resistance, reaching levels of ~50% compared to

USP28Δ cells (Fig. 4.8B). USP25's unexpected behaviour implies certain functional redundancy between the two paralogs and may explain the reported differences in phenotypic penetrance between *53BP1Δ* and *USP28Δ* cells.

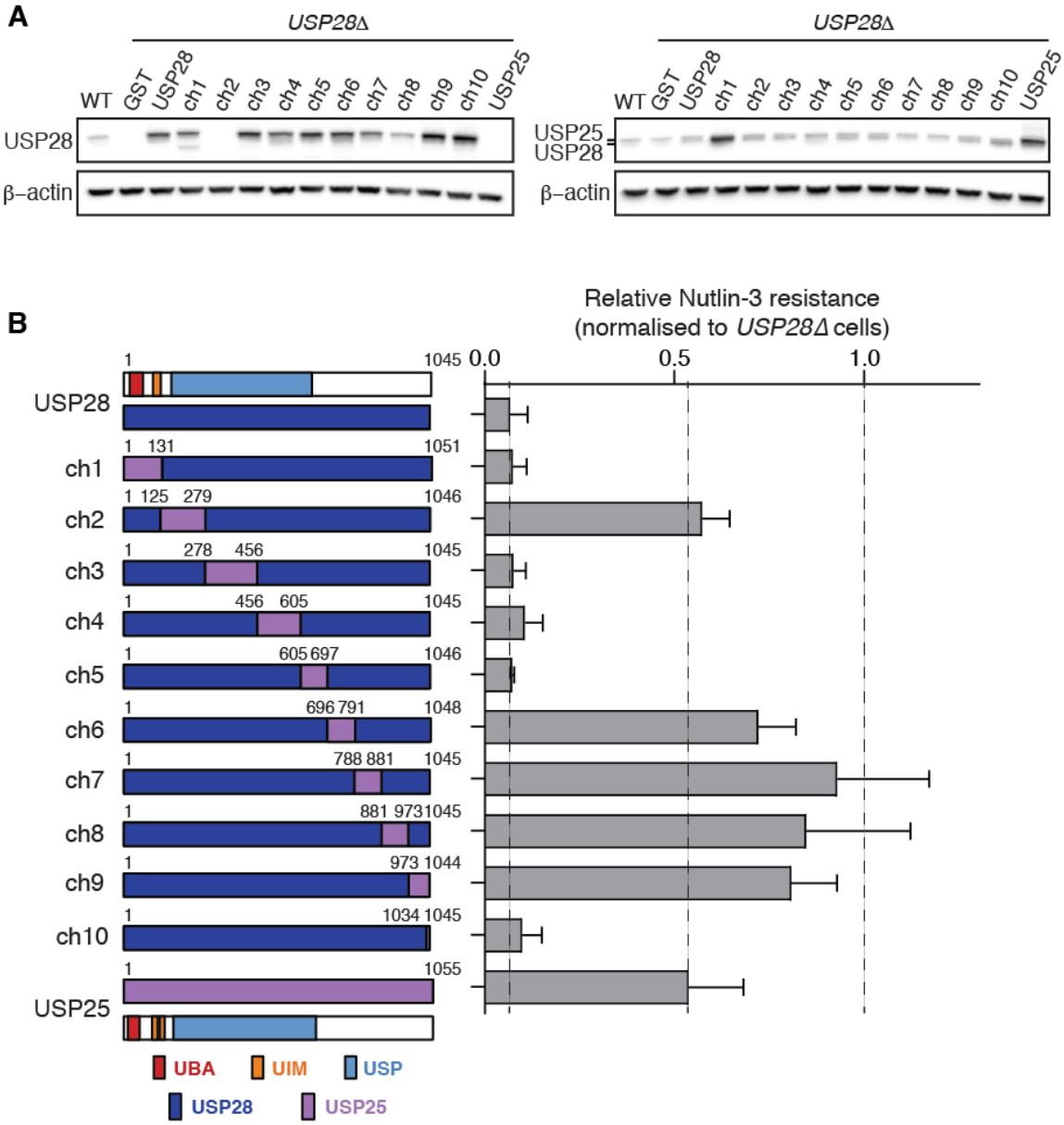


Figure 4.8. USP28 catalytic environment and C-terminal module are required for modulation of p53-dependent N3 toxicity. (A) Western blot analysis of USP28/25 chimeras in *USP28Δ* cells using the pLenti-PGK-PURO-DEST expression vector. *USP28Δ* expressing full length USP28 and USP25 were used as a control. USP25 antibody detected a specific band for USP25 (top) and another for USP28 (bottom). (B) Scaled schematic representation of USP28/25 chimeras used with corresponding quantitative analysis of N3 resistance (mean ± SD for n=2, plated in triplicate). Domain representation of USP28 and USP25 is included for reference. Dotted lines represent GST-, USP25- and USP28-complemented-like behaviour.

Similar to USP25-complemented cells, chimera 2 (ch2), where the environment surrounding the catalytic cysteine in USP28 was replaced by the corresponding USP25 region, partially rescued the sensitivity to N3, clearly outlining this region as the source of USP28 and USP25 differential behaviour (Fig. 4.8B, ch2). The remaining chimeric proteins harbouring substitutions in the N-terminal and the catalytic region (ch1, ch3-5) were fully proficient in mediating p53-dependent arrest in response to N3 (Fig. 4.8B, ch1, 3-5). Conversely, C-terminal chimeras displayed phenotypes close to *USP28Δ* cells reflecting a general inability to exert p53 regulatory functions (Fig. 4.8B, ch6-9). These results highlighted the structural relevance of the C-terminal module as a whole in USP28 functionality.

Collectively, these data defined the catalytic-cysteine environment and the C-terminal region as drivers of USP28's function in modulation of p53 responses. Although the functional specificity seemed to rely on the catalytic region, gaining structural knowledge on USP28 would allow to better tackle the relevance of self- and protein-protein interactions in the regulation of p53 responses.

4.3 Concluding remarks

The functional relevance of the USP28-53BP1 connection has remained controversial over the years. Initially, USP28 was granted a major role in controlling the stability of DDR proteins and IR-induced apoptosis through the Chk2-p53-PUMA pathway [86]. Later, USP28 interaction with 53BP1 was localised to the tandem BRCT domain, and *in vivo* studies supported the dispensability of USP28 in 53BP1-driven NHEJ [87].

Here, I defined the contribution of USP28 to the modulation of p53-dependent transcriptional programme. USP28 did enhance the induction of

PUMA as part of the p53-regulated transcriptome, but in a DNA-damage independent manner, as no DDR was activated upon N3 treatment in the cellular system here used (data not shown). These data provided an alternative mechanistic explanation to the prior described involvement of USP28 in apoptosis and partially resolved the controversy surrounding USP28's functionality [86]. Despite acting together with 53BP1 in p53 modulation, deficiencies in p53 transactivation events and G1/S checkpoint arrest were less pronounced in *USP28Δ* cells than in their *53BP1Δ* counterparts. Interestingly, my data suggested that the changes in phenotypic penetrance could be attributed to a certain degree of functional redundancy between USP28 and its paralog USP25. Alternatively, USP28 might regulate other cellular processes that ultimately interfere with p53 responses resulting in the variations described.

The catalytic activity of USP28 was central to its functionality in the USP28-53BP1-p53 axis. Remarkably, the ubiquitin-binding motifs within USP28's N-terminal region were completely dispensable for p53 modulation, hinting to alternative target recognition mechanisms. These observations suggested that 53BP1 could act as USP28's specificity factor, bringing the deubiquitinase in close proximity to its target(s) in this functional context.

The absence of structural information posed a challenge to structure-function analyses of the USP28 protein in p53 responses. Moreover, both catalytic and C-terminal regions are highly structured modules that largely impede truncation-based analyses. The generation of USP28/USP25 chimeric proteins provided an alternative to preserve structural integrity, and reveal regions that provide functional specificity to USP28. The system, however, presented a major caveat: Interchangeable sequences that define common USP

functional features (E. g. oligomerisation) would be undetected. The data obtained hinted to the presence of a unique structural organisation in USP28's C-terminal region. Any sequence substitution attempted within this module resulted in complete protein dysfunctionality, even in regions of major sequence similarity with its USP25 counterpart [253]. Nevertheless, this region seemed to hold relevance in both USP28 and USP25 proteins, likely encompassing common crucial features for the functionality of those paralogs. On the other hand, the catalytic environment was likely to be responsible for the functional diversification of USP28 and USP25 in p53 modulation. The sole substitution of the catalytic-cysteine environment in USP28 for the equivalent in USP25 sufficed to confer USP25-like behaviour in N3 resistance assays, despite presenting differential C-terminal regions. This region within USP28's catalytic domain was thus likely to hold enough sequence/structure divergence to encompass an exclusive motif that bridges interactions with 53BP1. In fact, a case of small sequence divergence causing functional specificity has been already described for USP25 and USP28: USP25's extreme C-terminal peptide (substituted in ch10) presents a tankyrase binding motif that is absent in USP28, and which provides USP25 with a role in regulation of Wnt/β-catenin signalling [263].

Although interaction profiles and structural analysis would further enlighten the fascinating interaction dynamics of the USP28-53BP1-p53 complex, this chapter succeeded to define the magnitude of USP28's role in p53 modulation and determine this to be dependent on the catalytic activity, and intact catalytic environment and C-terminal regions.

Chapter 5

MECHANISM OF USP28-53BP1-DEPENDENT p53 MODULATION

5.1 Introduction

Here, I have defined 53BP1 and USP28 as general p53 cofactors, whose activity is required for complete activation of p53-dependent responses. The structural data focalising USP28-53BP1-p53 interactions in 53BP1's tandem BRCT domain, and the requirement for USP28 catalytic activity strongly suggest a direct ubiquitin-dependent regulation of p53. 53BP1 and USP28 may act by priming p53 at one of the different regulation levels in the step-wise process from p53 induction to DNA binding and subsequent transcriptional activation.

Upon stress stimuli, p53 is released from the hold of MDM2 preventing further degradation-related ubiquitination events and thus leading to an increase in p53 protein levels. The ubiquitin-dependent regulation of p53 degradation can be counteracted by the action of deubiquitinases, USP28 being a promising candidate. Indeed, another DUB, USP7 (HAUSP) has been proposed to regulate the p53/MDM2 tandem by dual deubiquitination, and the action of USP10 specifically prevents p53 degradation upon genotoxic stress [264,265]. In addition, USP10-mediated p53 deubiquitination also interferes with p53 nuclear export, promoting p53 nuclear retention [265]. The ubiquitin-dependent regulation of p53 nuclear localisation also relies heavily on MDM2 [266]. p53 presents a nuclear localisation signal and a nuclear export signal (NES) within the loop connecting DBD and tetramerisation domain (amino acids 305-322), and the tetramerisation domain itself (amino acids 340-351), respectively [267-269]. MDM2-dependent mono-ubiquitination of p53 acts as an export signal, and

entirely depends on the presence of an intact NES [266,270]. A potential role for the USP28-53BP1 complexes in counteracting p53's export signal will favour a sustained p53 signalling and explain the phenotypes in *USP28Δ* and *53BP1Δ* cells. p53 nuclear export and tetramerisation share common sequence requirements and are often linked processes. In order to stably bind the DNA at the responsive elements of its target genes, p53 needs to acquire a tetrameric conformation (Section 1.3.1.3). In addition to the generation of a proficient DNA binding form, tetramerisation masks the NES preventing p53 to be shuttled back to the cytoplasm [268]. Upon tetramerisation, p53 binds its target genes at specific sequences. The involvement of ubiquitination events in regulation of p53-DNA binding has been largely undeciphered. A recent study showed that chromatin-bound p53 is largely monoubiquitinated and using structural prediction analysis suggested specific monoubiquination events in the DBD to enhance p53 transactivation [271]. However, since acetylation of specific lysines within the DBD (K120) is required for full p53 activation, it remains possible that ubiquitination may also play an inhibitory role in this context. The involvement of USP28-53BP1 complexes in positive regulation of p53 DNA binding activity is another mechanistic possibility to be examined.

5.2 Results

5.2.1 53BP1 and USP28 do not regulate p53 stability and localisation

The ubiquitin-dependent regulation of p53 turnover is one of the major mechanisms to keep p53's activity at bay. Although my initial characterisation studies did not show apparent changes in p53 stability in *53BP1Δ* and *USP28Δ*

cells, the reported ability of USP28 to deubiquitinate p53 *in vitro* prompted me to closely examine p53 half-life in presence and absence of 53BP1 and USP28.

First, steady-state p53 half-life was evaluated. *WT*, *53BP1Δ* and *USP28Δ* cells were treated with cycloheximide (CHX) to block *de novo* protein synthesis. Cells were then harvested at different time-points to follow the kinetics of p53 degradation. Involvement of USP28-53BP1 complexes in counteracting degradation-related p53 ubiquitination would be reflected in a quicker reduction of p53 protein levels upon CHX treatment in *53BP1Δ* and *USP28Δ* lines, due to a decrease in p53 protein stability. Basal p53 levels showed initial variations between genotypes (Fig. 5.1A, t=0 h); however, this observation was not consistent within the replicates performed and neither in equivalent controls in N3-induced p53 turnover experiments (Fig. 5.1B, columns 1-3). Despite the initial differences, p53 experienced equivalent or slightly reduced protein decay *53BP1Δ* and *USP28Δ* cells compared to *WT* controls across the time course, with an estimated half-life of 15-30 minutes (Fig. 5.1A). Accordingly, the E3 ubiquitin ligase responsible for p53 ubiquitination, MDM2, also displayed equal degradation kinetics across the genotypes examined (Fig. 5.1A). The same held true for the p53-regulated cell-cycle arrest protein p21 (Fig. 5.1A). Thus, the status of 53BP1 and USP28 did not interfere, directly or indirectly, with steady-state p53 half-life, excluding a role for USP28-53BP1 complexes in basal p53 degradation.

Remarkably, the role of 53BP1 and USP28 in p53-mediated responses became evident upon stress stimuli (Section 3.2.1, 4.2.1). It remained thus possible that USP28-53BP1 complexes acted over stressed-induced ubiquitination events, in order to maintain high p53 levels under stress conditions.

Considering this possibility, I performed the CHX-based half-life assay in *WT*, *53BP1Δ* and *USP28Δ* lines where p53 had been previously induced by treatment with 4 μM N3 for 2 h.

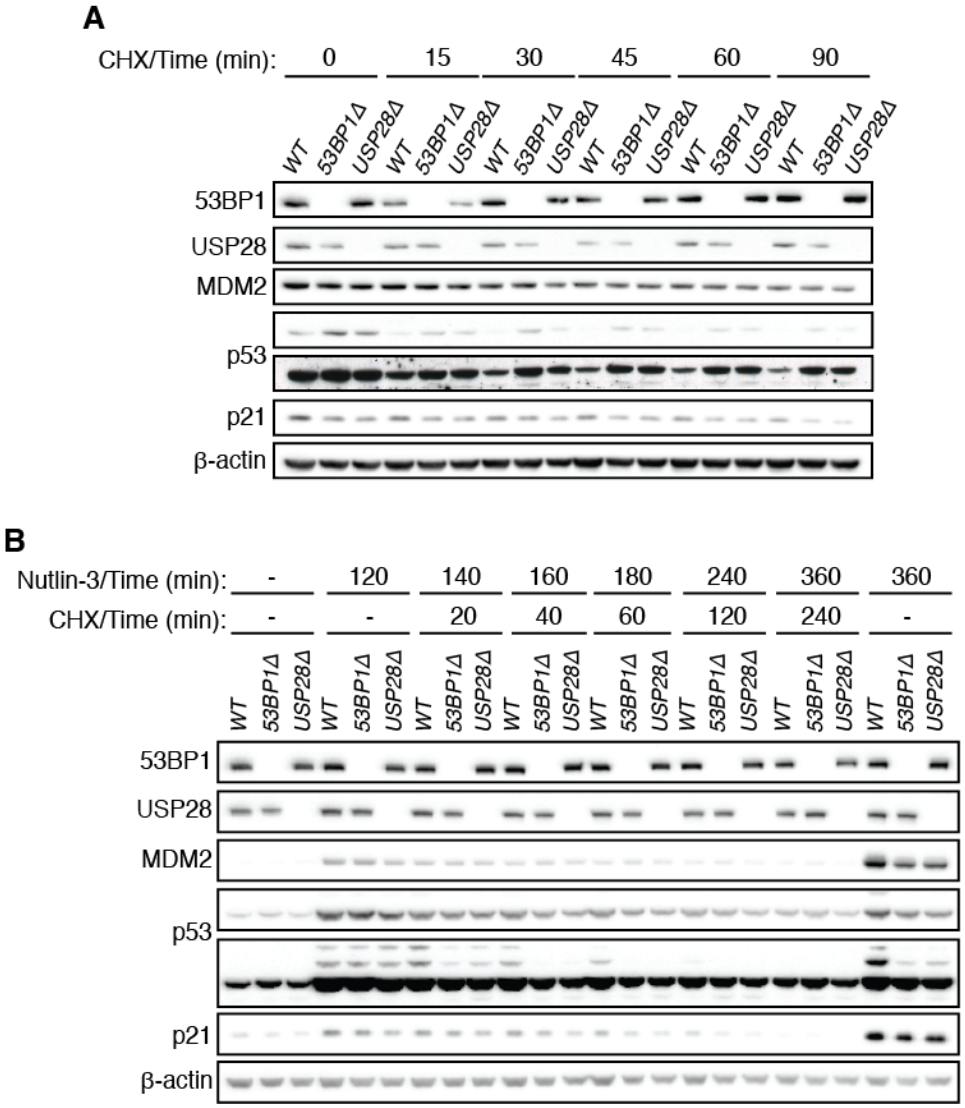


Figure 5.1. 53BP1 and USP28 do not regulate the turnover of basal and N3-induced p53 protein. (A) Steady-state p53 half-life evaluated by immunoblot analysis of MCF-7 cells treated with the protein-synthesis inhibitor cycloheximide (100 μg/ml) for the selected time points. (B) Assessment of N3-induced p53 half-life was performed as in (A) upon treatment with N3 (4 μM for 2 h).

As previously reported (Fig. 3.3A, B, 4.4A, C), p53 induction was robust and equivalent across the phenotypes, providing a solid starting point for the analysis (Fig. 5.1B, t(N3) =120 min). Interestingly, modified p53 forms, likely

encompassing mono- and di-ubiquitination events, seemed to persist longer in *WT* than in *53BP1Δ* and *USP28Δ* cells; however, no major differences were observed in bulk p53 degradation under those conditions (Fig. 5.1B).

The absence of changes in bulk p53 stability could not account for the ~50% reduction of p53 transactivation events; however, remarkable differences in modified p53 forms, likely corresponding with mono- and di-ubiquitination prompted me to evaluate alternative modes of p53 regulation affected by those changes. The nuclear localisation of p53 is regulated by ubiquitination events. Puzzlingly, MDM2-dependent p53 mono-ubiquitination, likely overrepresented in *WT* cells (Fig. 5.1B), acts as a nuclear export signal [266,270]. In order to clarify this apparent contradiction before investigating other mechanistic possibilities, subcellular localisation of p53 was examined. Cells were subject to immunofluorescence using a p53 specific antibody (clone DO-7), whose specificity was assessed by using *p53Δ* cells as a negative control. Counterstaining with cyclin A was performed to also identify potential cell cycle-associated deficiencies. In basal conditions, p53 was kept at low levels in the nuclear compartment, and no cytoplasmic p53 was detected (Fig. 5.2A). Equivalent, low levels of p53 were present in the genotypes evaluated, with complete absence in *p53Δ* cells (Fig. 5.2A). Upon treatment with N3 for 2 h, a prominent induction of p53 was observed regardless of genotype or cell cycle phase, with predominantly nuclear localisation (Fig. 5.2A). Although initially nuclear localisation of p53 appeared to be intact, I decided to monitor nuclear presence at later time-points to evaluate the possibility of differential nuclear export kinetics (Fig. 5.2B). p53 was barely detectable in the cytoplasmic compartment across the genotypes and time-points evaluated (Fig. 5.2B).

Notably, slightly enhanced levels of nuclear p53 were consistently detected in *WT* cell populations compared to *53BP1Δ* and *USP28Δ* cells (Fig. 5.2B). These differences could potentially account for the increased presence of modified p53 forms previously observed and be at the source of the phenotypical differences between *WT* and *53BP1Δ* and *USP28Δ* cells.

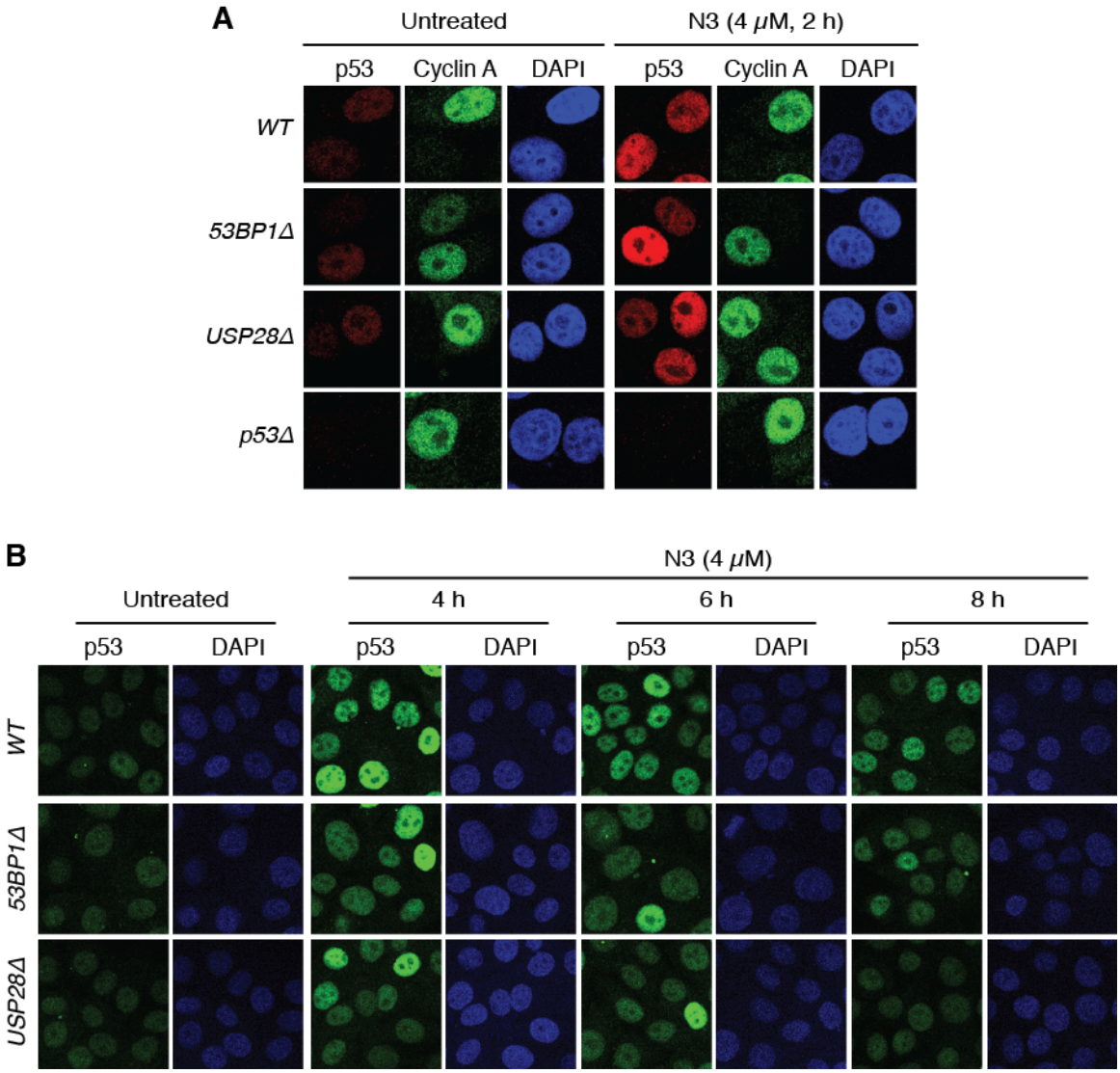


Figure 5.2. p53 localises to the nucleus independently of 53BP1 and USP28 status. (A) Immunofluorescence analysis of p53 in MCF-7 cells treated with N3 (4 μM for 2 h) or left untreated. Cells were counterstained with cyclin A for discrimination of G1 cells (cyclin A negative) and S/G2 cells (cyclin A positive). (B) Cells were treated as in (A) for the indicated durations. Staining of p53 was performed using the DO-1 antibody. Representative images of the behaviour of cell populations are depicted.

Taken together, the data demonstrated that p53 was able to retain *WT*-like half-life and nuclear localisation in the absence of 53BP1 and USP28. However, the differential behaviour of putative mono- and di-ubiquitinated forms suggested a role for 53BP1 and USP28 in the preservation of specific ubiquitination features that were likely to favour optimal p53-dependent responses.

5.2.2 Regulation of p53's DNA binding activity by 53BP1 and USP28

The function of p53 as a transcription factor relies on the ability to bind the REs at its target genes. The modulation of p53's DNA binding irrevocably results in differences in downstream transcription programmes. I then hypothesised that p53 could present an intrinsic inability to bind the responsive elements at the target genes in absence of 53BP1 and/or USP28, thus explaining the transcriptional deficiencies observed in RT-qPCR and RNA-seq analyses (Fig. 3.3, 3.4, 4.4). For this purpose, p53-bound DNA complexes were immunoprecipitated in *WT*, *53BP1Δ* and *USP28Δ* lines and site-specific primers used to quantify p53 binding by RT-qPCR. The *CDKN1A* (*p21*) locus was selected as a model due to the robust induction of transcription upon N3 treatment. Specific primer pairs placed at the 5' end, the two p53 responsive elements, the transcription start site and intronic and exonic regions were selected (Fig. 5.3A) [242]. ChIP analysis of p53 revealed the high specificity of p53 for the RE sequences, and marked the differences in binding affinity between the first (high) and second (low) binding sites (Fig. 5.3B). In steady-state conditions, low p53 binding was detected at the *CDKN1A* responsive elements of *WT* cells, correlating with the low basal abundance of p53 protein in cells (Fig. 5.3B, untreated). Treatment with N3 (4 μM, 6 h) triggered an increase of p53

binding to the REs up to ~7-fold in *WT* cells, as a direct result of p53 stabilisation (Fig. 5.2B, N3). Absence of 53BP1 or USP28 resulted in ~70% reductions in p53 occupancy on REs upon N3 treatment (Fig. 5.2B, N3). The phenotype was consistent across the two p53-REs in the *CDKN1A* promoter, reflecting the irrelevance of the RE intrinsic affinity in dictating p53 binding ability in this context (Fig.5.2B, N3). Binding of p53 to the responsible elements is coupled with the deposit of histone marks associated to transcriptional activation. In *WT* cells, treatment with N3 led to a pronounced enrichment of the acetylation of histone H4 (H4ac) at the promoter of the *CDKN1A* locus (Fig. 5.3C). Acetylation of lysine 9 on histone H3 (H3K9ac) was similarly enhanced across the promoter and transcription start site (TSS) regions after N3 treatment (Fig. 5.3D). However, consistent ~2-fold reductions in both H4ac and H3K9ac marks were detected in *53BP1Δ* and *USP28Δ* cells upon N3 treatment compared to the *WT* counterparts (Fig. 5.3C-D). In agreement with the reduction in p53 binding and transcriptional activation histone marks, the occupancy of the elongating RNA pol II (Pol pCTD^{S5}) was equivalently reduced across the gene body, to an extent that perfectly correlates with the deficiencies observed in p53-dependent transcription in RT-qPCR and RNA-seq analyses (Fig. 5.3E, N3). Even in basal conditions, slight deficiencies were observed, albeit to a markedly lesser extent that upon N3 treatment. These data explained the absence of detectable differences in mRNA levels in steady-state conditions, and how abnormalities became evident in *53BP1Δ* and *USP28Δ* cells after treatment with N3.

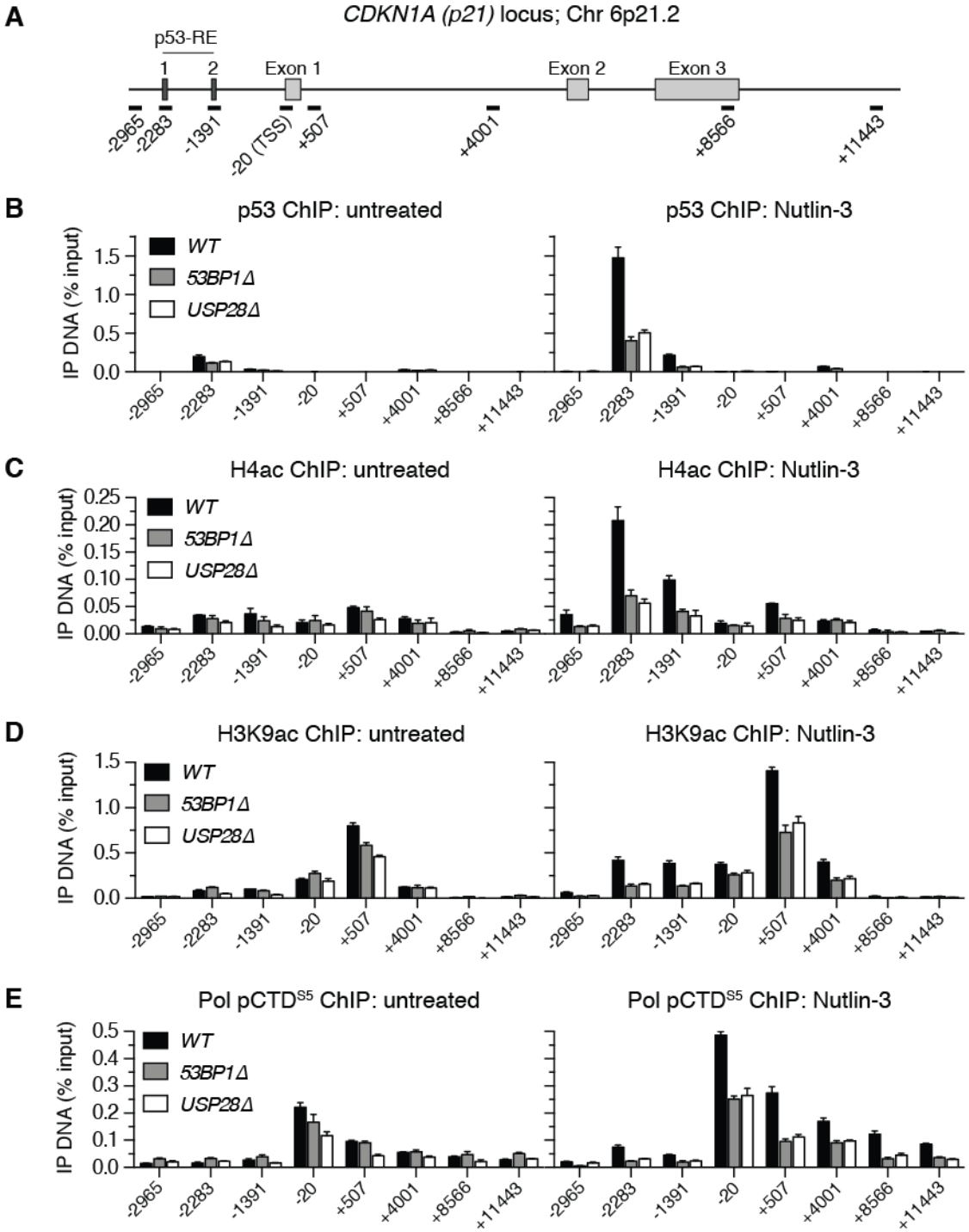


Figure 5.3. 53BP1 and USP28 stimulate p53 binding to the *CDKN1A* REs. (A) Schematic representation of the *CDKN1A* (p21) locus. Low and high affinity p53 binding sites (p53-RE 1 and 2) are represented within the gene structure. qPCR amplicons used to quantify ChIP- enriched DNA are indicated (bars) and named according to their relative distance to the TSS. (B-E) ChIP analysis of chromatin extracts from WT, 53BP1 and USP28 lines untreated or treated with N3 (4 μM, 6 h). DNA co-immunoprecipitated with (B) p53, (C) H4ac, (D) H3K9ac, (E) RNA pol II pCTD^{S5} was calculated as a percentage of total input DNA. Data are representative of two independent experiments (mean ± SD, RT-qPCR in triplicate). These experiments were performed and analysed by Prof J. R. Chapman.

These observations were consistent and reproducible at p53-REs in other target genes, such as *MDM2*, *GADD45A* and *FAS*, confirming the broad extent of p53 binding deficiencies, and drawing a perfect correlation with prior transcriptome-wide studies (Fig. 5.4). Binding of p53 displayed equivalent 2-3-fold reductions in N3-treated *53BP1Δ* and *USP28Δ* cells (Fig. 5.4A). Gene activation-related epigenetic marks, H4ac and H3K9ac, showed marked deficiencies in *GADD45A* p53-RE and *FAS* p53-RE, placed in the third intron and the promoter, respectively (Fig. 5.4B-C). Although the position of *MDM2* RE within the gene body impeded the detection of H4ac and H3K9ac inductions, the residency of the elongating RNA pol II was significantly diminished upon N3 treatment (Fig. 5.4C). Surprisingly, in *USP28Δ* cells, the gene *FAS* showed an intrinsic and prominent reduction of p53 binding and chromatin accessibility marks, potentially related to the loss of additional USP28-mediated roles (Fig. 5.4A-B).

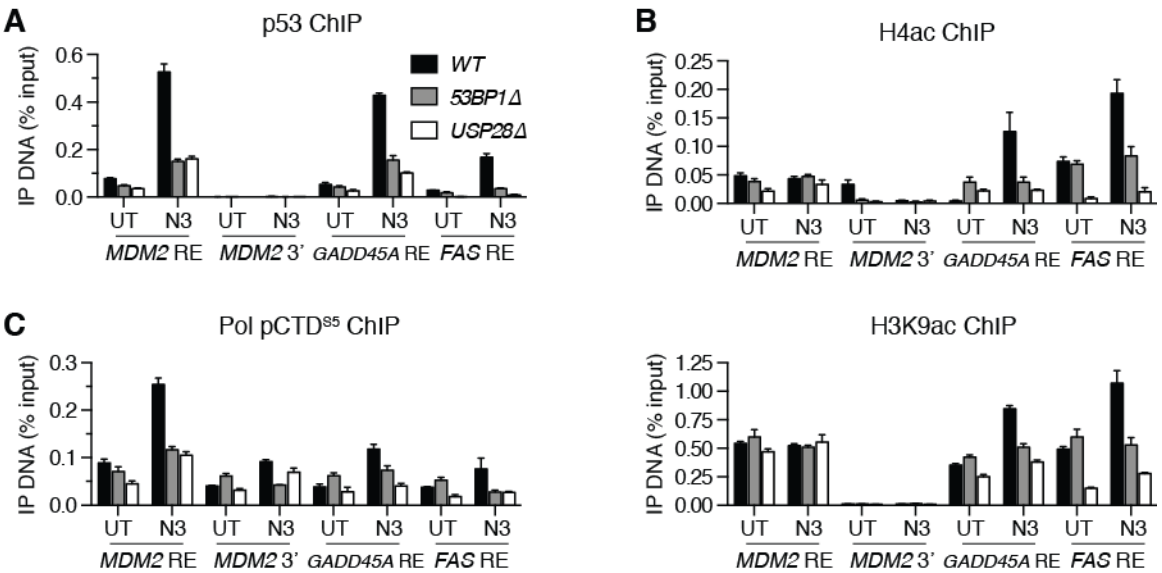


Figure 5.4. 53BP1 and USP28 enhance p53-RE interactions. (A-C) as in (Fig. 5.3B-E) using RT-qPCR amplicons in *MDM2*, *GADD45A* and *FAS* p53-REs. *MDM2* 3' amplicon placed in the last *MDM2* coding exon was used as a negative control. These experiments were performed and analysed by Prof J. R. Chapman.

Post-translational modifications in p53's DNA binding domain often translate into changes in p53 transcriptional activity [161]. While ubiquitination in the DNA binding domain has been reported in high-throughput proteomics studies, the functional relevance remains to be determined. The compact conformation of the DBD suggests that ubiquitination events are likely to constitute a physical impediment to efficient DNA binding within the tetrameric structure. Alternatively, site-specific ubiquitination events within this region have been recently suggested to positively regulate DNA binding [271]. Here, I have reported that 53BP1's tandem BRCT fosters interactions with USP28 and the DBD in p53, which are essential for the regulation of p53-dependent responses. I thus hypothesised that 53BP1 acted as a molecular bridge between those two proteins, to allow USP28's deubiquitinating action over p53, priming p53 for optimal DNA binding and subsequent transactivation events (Fig. 5.5A). If this action was direct and over an inhibitory ubiquitin mark, mutation in the USP28 target site(s) would impede the ubiquitination event and thus eliminate the requirement for the USP28-53BP1 de-repression mechanism. Experimentally, expression of a version of p53 carrying said mutation/s would be able to fully support N3-mediated cellular arrest independently of 53BP1 and/or USP28 status. In light of putative mono- and di-ubiquitination events persisting in *WT* cells in stability studies, I also considered the possibility of indirect priming to stabilise specific monoubiquitinated forms. If true, expression of a version of p53 carrying mutation/s preventing the deposit of the activation mark would be equally deficient to support N3-mediated arrest in both presence and absence of 53BP1 and/or USP28.

In order to generate an experimental system to test the hypotheses presented, reconstitution of p53 expression in *p53Δ* cells was attempted. Serial dilutions of viral supernatants were used and recovered cell populations screened by SDS-PAGE/WB against a *WT* MCF-7 control to select for *WT* levels of p53 expression (data not shown). The transcriptionally inactive, mutant p53 form, $p53^{R175H}$ was consistently expressed at higher levels than the *WT* form, reflecting the inability of those mutants to induce p53-dependent cell death programmes (Fig. 5.5B). *WT* MCF-7 cells and *p53Δ* cells stably expressing full-length p53 displayed indistinguishable p53 stabilisation kinetics and equivalent inductions of MDM2 and p21 upon N3 treatment (Fig. 5.5B). In striking contrast, $p53^{R175H}$ presented a delayed stabilisation compared to *WT* controls and, as previously reported, behaved as a knockout control regarding induction of MDM2 or p21 expression (Fig. 5.5B). Having successfully established a complementation system for p53, I then proceeded to knock out p53 in *USP28Δ* cells. Single clones were recovered from CRISPR/Cas9-edited cell populations and screened by SDS-PAGE/WB (Fig. 5.5C). Clone *p53Δ/USP28Δ-B* (hereinafter *p53Δ/USP28Δ*) showed no detectable p53 expression and was selected for further analyses (Fig. 5.5C). Subsequently, p53 was stably re-expressed by lentiviral transduction obtaining a cell population carrying physiological p53 levels equivalent to p53-complemented *p53Δ* cells (Fig. 5.5D). Evaluation of N3 resistance was then carried out to assess the validity of the experimental system generated. Consistent with the full restoration of target induction, exemplified by MDM2 and p21 (Fig. 5.5B), re-expressed p53 fully supported N3-dependent arrest in *p53Δ* cells (Fig. 5.5E-F). As expected, p53 expression did not suffice to restore full N3 sensitivity in absence of USP28, closely mimicking the

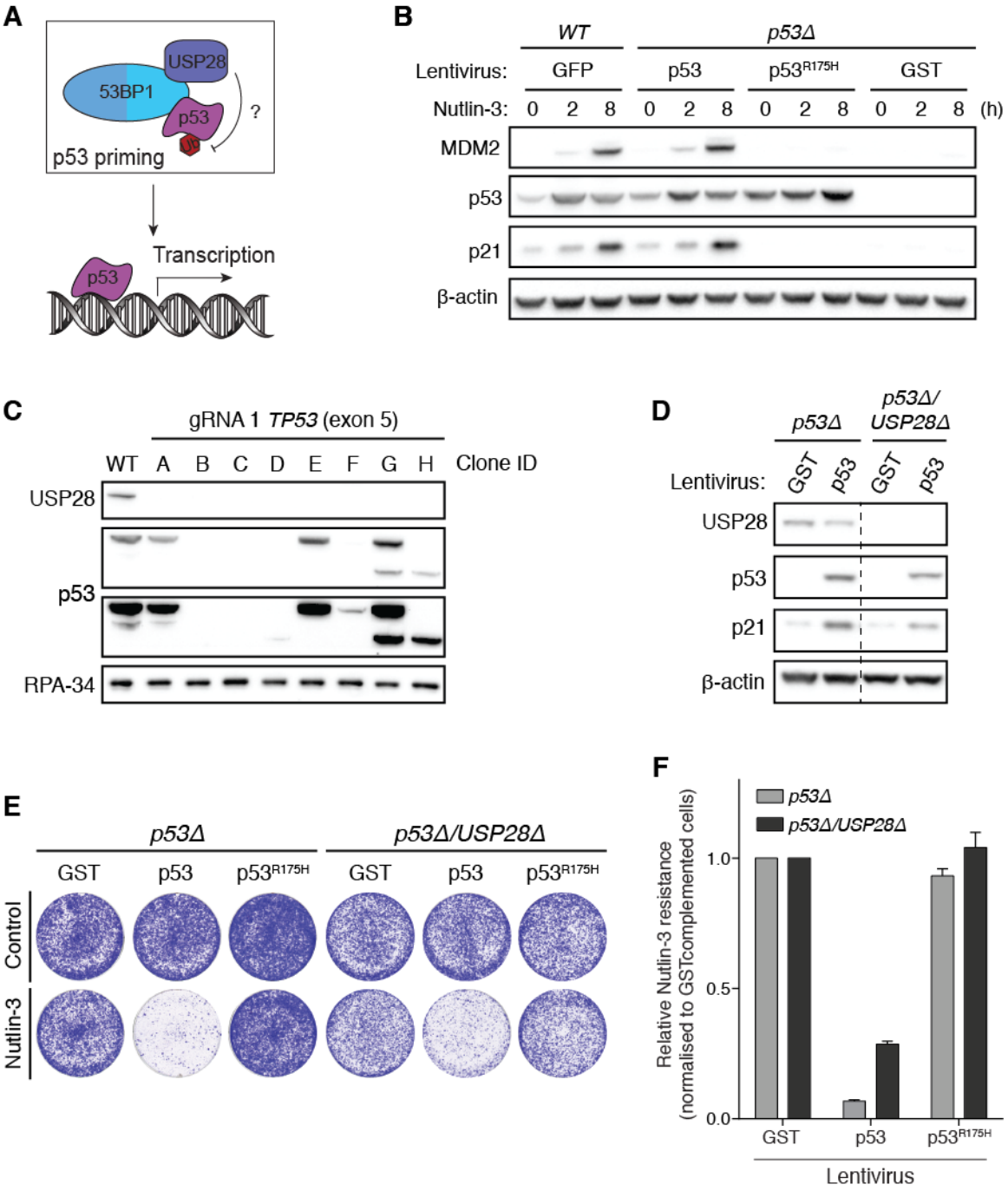


Figure 5.5. Reconstitution of p53 expression in *p53Δ* MCF-7 cells restores N3 sensitivity. (A) Proposed hypothesis for the molecular mechanism whereby 53BP1 and USP28 enhance p53 activity. (B) Immunoblot analysis of MCF-7 cells stably transduced with the indicated GFP/GST controls or p53 gene constructs in pLenti-PGK-PURO-DEST and subject to N3 treatment (4 μM). (C) Immunoblot analysis of potential *p53Δ/USP28Δ* clones. Long exposure for p53 immunoblot (bottom) is depicted to ensure protein absence. (D) Comparative immunoblot analysis of *p53Δ* and *p53Δ/USP28Δ* cells stably expressing full-length p53. Dashed line indicates discontinuous gel. (E) Visual analysis of N3 resistance in *p53Δ* and *p53Δ/USP28Δ* complemented lines. (F) Quantification of (E). Mean ± SD (n=2, plated in triplicate).

intermediate resistance displayed by *USP28Δ* lines (Fig. 5.5E-F). In both genetic backgrounds, transcriptional defective p53, $p53^{R175H}$, displayed a N3-resistant phenotype comparable to GST-complemented controls (Fig. 5.5E-F). These data confirmed the proficiency of this complementation system in restoring functional p53-dependent responses. In addition, the system evidenced the action of endogenous regulatory mechanisms over re-introduced p53 and further outlined its suitability to evaluate the effect of p53 mutations in presence and absence of USP28-mediated regulation.

The DNA binding domain in p53 possesses 7 lysines whose individual ubiquitination has been detected in high-throughput mass spectrometry assays. Five lysines (K101, K120, K132, K139, and K164) are visible in the crystal structure of the DBD bound to the DNA (Fig. 5.6A), while lysines 291 and 292 are placed at the α-helix in the DBD C-terminal end and the start of the long loop that connects to the tetramerisation domain (Fig. 5.6A). Aberrations in dynamic ubiquitination and de-ubiquitination events occurring within this region will potentially explain the deficiencies in DNA binding observed in ChIP assays (Fig. 5.3, 5.4). Individual lysine residues were thus mutated to arginine to preserve the positive charge while preventing the conjugation of ubiquitin. Mutant p53 forms were stably transduced in *p53Δ* and *p53Δ/USP28Δ* cells and the presence of physiological, *WT*-like p53 expression assessed by SDS-PAGE/WB (Fig. 5.6B). Subsequently, the ability of p53 mutants to support N3-mediated arrest was evaluated. Mutation to arginine preserved p53's ability to support N3-mediated cellular toxicity in 6 out of 7 mutants evaluated (Fig. 5.6C). Only mutation of K132 resulted in complete abrogation of p53 activity (Fig. 5.6C). This residue is placed in an antiparallel β-sheet structure within the DBD and its mutation might result in

conformational changes leading to the dysfunctionality presented. Perhaps surprisingly, mutation of K120, whose side chain is inserted in the DNA groove and is critical for DNA binding, largely retained p53 activity in the context examined (Fig. 5.6C). Ubiquitination in residue K292 was predicted to enhance p53-DNA binding properties in structure-based analysis [271]. Reconstitution of $p53^{K292R}$ in H1229 cells resulted in nearly complete depletion of DNA binding to *CDKN1A*, *MDM2* and *BAX* REs in luciferase reporter assays [271]. Here, I failed to observe the prominent N3 resistant phenotype that would be expected to result from the DNA binding disruption reported, with only a slight increase in resistance over p53-complemented cells, equivalent across *WT* and *USP28Δ* cells (Fig. 5.6C).

As mentioned above, ubiquitination has been detected in all the residues placed in the DNA binding domain. The structure of p53's DNA binding domain bound to the tandem BRCT of 53BP1 reveals the position of lysines in two different surfaces (Fig. 5.6D, in yellow and red), both of them potentially accessible by USP28. Nonetheless, the binding dynamics and structural position of USP28 respect to p53's DBD and 53BP1 tandem BRCT are unknown, as well as the structural changes that may occur in the complex upon ubiquitin conjugation in p53. Accordingly, it remains possible that USP28 surrounds the p53 unit and targets multiple residues in different surfaces. In order to test this hypothesis, surface-specific mutations were included (K101-64R and K120-39R) alongside a mutant encompassing the 4 lysines (quadruple mutant, QM). Consecutive lysine residues K291 and K292 were mutated in combination with the neighbouring lysine K305 placed in the loop connecting DBD and tetramerisation domain (K291-92-305R). K132R mutation, as proven to generate

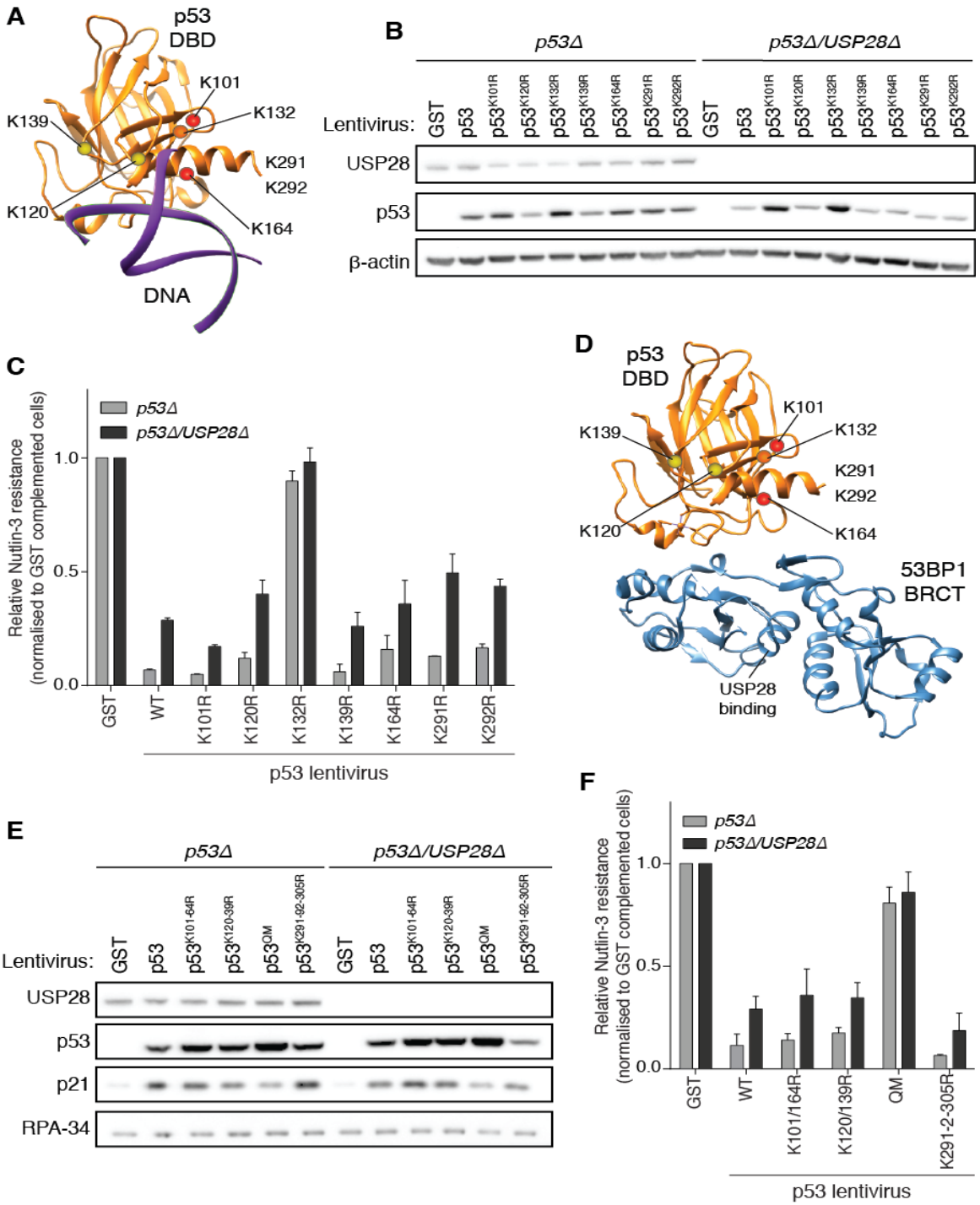


Figure 5.6. USP28 does not interfere with the functionality of p53's DBD. (A) Structure of p53's DBD bound to DNA (PDB ID: 1TUP). The position of lysine residues within this region is highlighted. (B) Immunoblot analysis of MCF-7 cells of the indicated genotypes stably transduced with p53 gene constructs or GST controls. (C) Quantitative analysis of N3 resistance in *p53Δ* and *p53Δ/USP28Δ* complemented lines. Mean ± SD (n=2, plated in triplicate). (D) Structure of p53 DBD bound to 53BP1's tandem BRCT (PDB ID: 1KZY). Positions of lysine residues placed in different interphases are depicted in different colours. (E) Immunoblot analysis of *p53Δ* and *p53Δ/USP28Δ* lines complemented with p53 mutants. (F) as in (C). Mean ± SD (n=3, plated in triplicate).

a dysfunctional protein, was not included in the analysis. Expression of mutated p53 versions was reconstituted in *p53Δ* and *p53Δ/USP28Δ* cells (Fig. 5.6E). In the protein analysis, $p53^{QM}$ evidenced deficiencies in transcriptional activity: Significantly higher levels of p53 protein were unable to restore basal p21 expression to *WT*-like levels (Fig. 5.6E). Consistently, $p53^{QM}$ failed to support N3-dependent arrest independently of USP28 status (Fig. 5.6F). Cells carrying $p53^{K101\text{-}64R}$, and $p53^{K120\text{-}39R}$ required higher p53 protein levels to achieve p21 induction equivalent to p53-complemented cells in both *p53Δ* and *p53Δ/USP28Δ* cells (Fig. 5.6E). The increase of p53 levels to compensate for a basal loss of binding affinity may respond to the cellular need to keep the homeostasis of downstream p53-mediated events. The response to N3 in $p53^{K101\text{-}64R}$, and $p53^{K120\text{-}39R}$-complemented lines was equivalent to their corresponding p53-complemented counterparts (Fig. 5.6F). Despite the ability of cells to regulate mutant p53 protein levels, they failed to compensate deficiencies associated to absence of USP28. Finally, $p53^{K291\text{-}92\text{-}305R}$-complemented cells showed p53 and p21 protein levels comparable to *WT* controls, indicating that combined mutation in residues K291, K292 and K305 did not interfere with basal p53 functionality. $p53^{K291\text{-}92\text{-}305R}$ efficiently rescued the sensitivity to N3 in *p53Δ* cells, even more prominently than reconstitution of non-mutated p53, and a proportionally intermediate phenotype in the *p53Δ/USP28Δ* background (Fig. 5.6F). Data strongly refuted the hypothesis of USP28-53BP1 complexes directly or indirectly targeting ubiquitination events in p53's DBD. However, the limitations of this experimental system impeded the collection of data for mutation of multiple ubiquitination sites or even single sites that caused a structural disruption and

complete protein dysfunctionality, and complicated the drawing of definitive conclusions.

The inability to efficiently bind DNA could also arise from an impaired assembly of p53 tetrameric structure. Examination of p53 tetramerisation was carried out by glutaraldehyde protein-protein crosslinking and input controls used to assess equal p53 protein levels across all the genotypes at each given time point. p53 tetramer assembly seemed to reach optimal levels at 2 h upon N3 treatment, but faltered at later time points in *53BP1Δ* and *USP28Δ* lines, reflecting an inability to sustain efficient tetramerisation (Fig. 5.2B). It was thus likely that the ubiquitination-dependent signalling driven by the USP28-53BP1 complex affected ultimate p53-DNA binding by impacting on p53's tetramerisation capacity.

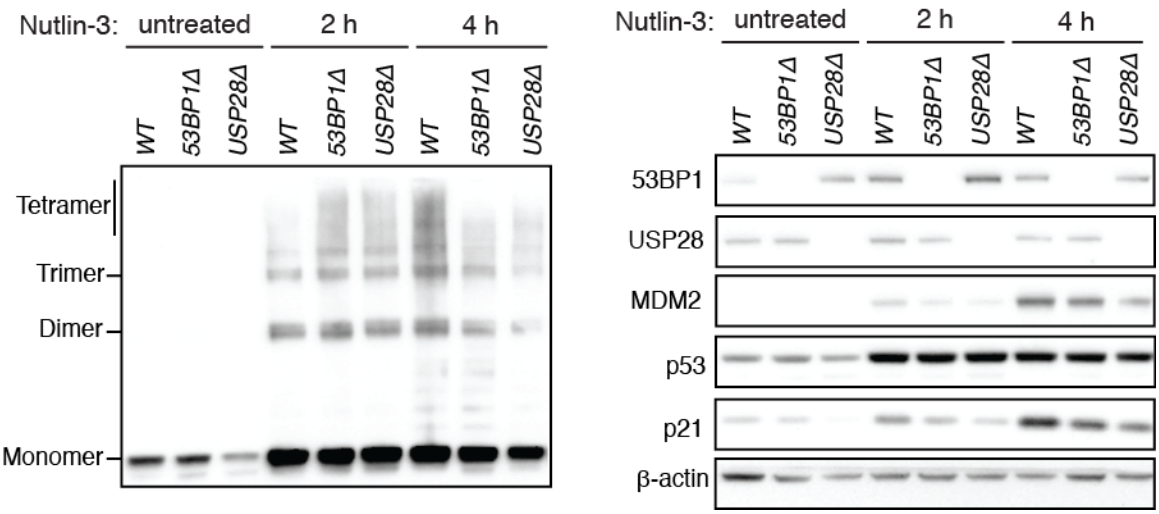


Figure 5.7. Absence of 53BP1 or USP28 affects p53 ability to sustain tetramerisation. Immunoblot analysis of p53 tetramerisation by glutaraldehyde crosslinking [0.01% (v/v) for 20 min] in cell extracts treated with N3 (4 μM) for the indicated times. Corresponding input controls for p53 stabilisation and downstream target activation are also depicted (right).

5.2.3 The role of 53BP1's Tudor in modulation of p53 responses is methylp53-interaction independent

The detailed structure-function analysis on 53BP1 highlighted the oligomerisation and tandem BRCT domains as core requirements to promote optimal p53 responses (Section 3.2.2). In addition, mutation on 53BP1's tandem Tudor resulted in an intermediate N3 resistant phenotype, also pinpointing a role for this domain in p53 modulation. Interestingly, 53BP1's tandem Tudor establishes physical interactions with dimethylation moieties in the C-terminal regulatory region of p53 (Section 1.4.2). Even if bulk 53BP1-p53 interactions were mediated via 53BP1's tandem BRCT (Fig. 3.7), I hypothesised that Tudor-p53me2 interactions could provide a second layer of regulation that relies on the deposit of the dimethyl mark. Using the p53 complementation system, re-expression of multiple lysine mutants in *p53Δ* and *p53Δ/USP28Δ* cells was achieved (Fig. 5.8A). p53 C-terminal region presents 6 lysines organised in two clusters i) K370, K372, K373 and ii) K380, K382, K386 that were independently mutated (3KR and 3KRII mutants respectively). Additionally, mutation of the 6 lysines (6KR) was included alongside a mutant of K380-K382 (2KR) to focus on specifically disrupting the high affinity 53BP1-p53K382me2 interaction [66,68]. Even considering the differences in the loading control, all the mutants analysed presented lower expression levels when reintroduced in *p53Δ/USP28Δ* cells compared to the equivalent *p53Δ* lines (Fig. 5.8A). None of the mutants analysed presented a differential behaviour from the corresponding controls in N3 resistance assays (Fig. 5.8B). However, the differences in protein expression prompted me to re-evaluate 53BP1 tandem Tudor mutations in order to reinforce the results obtained in the p53-complementation analysis. p53K370me2,

p53K372me2 and p53K382me2 bind 53BP1's tandem Tudor using a hydrophobic pocket in the first Tudor unit (Fig. 5.8C) [236]. The *in vitro* binding

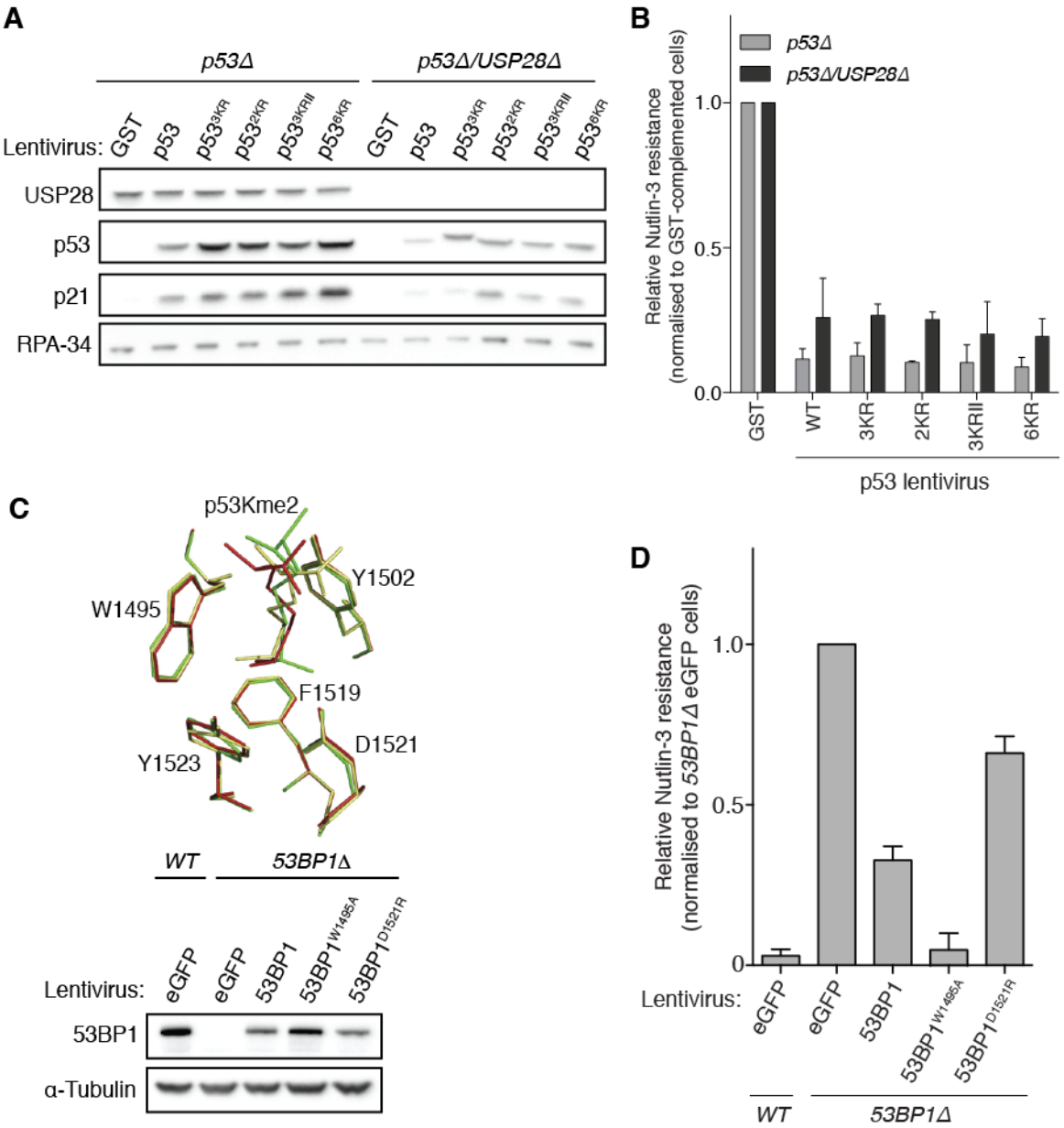


Figure 5.8. The role of 53BP1's Tandem Tudor domain in regulating p53 responses does not involve interactions with dimethylated p53 C-terminal residues. (A) Immunoblot analysis of *p53Δ* and *p53Δ/USP28Δ* lines complemented with p53 harbouring combination mutation in C-terminal lysines. (B) Quantitative analysis of N3 resistance in *p53Δ* and *p53Δ/USP28Δ* complemented lines. Mean ± SD (n=2, plated in triplicate). (C) Superimposed 53BP1's Tudor hydrophobic cage bound to the three p53Kme2 residues. Red, p53K382me2/53BP1; green, p53K370me2/53BP1; yellow, p53K372me2/53BP1. Image from [236]. Immunoblot analysis of *53BP1Δ* cells complemented with 53BP1 Tudor mutants or eGFP controls. (D) N3 resistance in 53BP1-complemented cells. eGFP-complemented *53BP1Δ* cells were used for reference. Mean ± SD (n=2, plated in triplicate).

affinity of p53K382me2 is significantly diminished upon mutation of D1521, but even more when a mutation is introduced in residue W1495 [235,272]. In order to test whether 53BP1^{W1495A} recapitulated the intermediate N3 phenotype observed in 53BP1^{D1521R}-complemented *53BP1Δ* cells, a stably expressing cell line was efficiently generated and N3 resistance evaluated (Fig. 5.8C). As previously observed, 53BP1^{D1521R}-complemented cells presented an intermediate N3 resistant phenotype, between eGFP -*WT* and -*53BP1Δ* controls. Surprisingly, 53BP1^{W1495A} supported N3-dependent cellular arrest to a higher extent than full-length 53BP1, closely resembling the previously observed behaviour of 53BP1^{L1619A} and 53BP1^{20AQ} classical NHEJ-dead mutants (Fig. 5.8D). This puzzling phenotypic divergence suggested for amino acid D1521 a role in p53 responses separate from canonical Tudor-methyl peptide interactions. Moreover, it supported the dispensability of physical contacts between 53BP1's tandem Tudor and methy-p53 peptides for 53BP1-dependent regulation of p53 responses.

Intriguingly, the Tudor mutants evaluated (W1495A, D1521R) shared the unusual phenotypic divergence with the mutants in 53BP1's BRCT phosphobinding pocket (R1811A, K1814M) that challenges all previous studies about Tudor and BRCT binding dynamics [23,83,84,235,236]. This curious parallelism prompted me to re-evaluate prior analysis of 53BP1^{D1521R} immunocomplexes for presence of USP28. Consistent with observations by us and others [87], USP28 was unable to interact with 53BP1 lacking the tandem BRCT domain or functional oligomerisation domain (Fig. 5.9). Surprisingly, mutation in D1521 also sufficed to block USP28 binding (Fig. 5.9). Thus, individual mutation of residues D1521, and the previously reported R1811 (Fig.

3.11), generated a significant disruption of USP28 interaction and the subsequent deficiency in supporting p53-mediated N3 arrest. The data clarified the role of 53BP1's tandem Tudor domain in p53 responses, but added further mystery to the already unusual structural association USP28-53BP1.

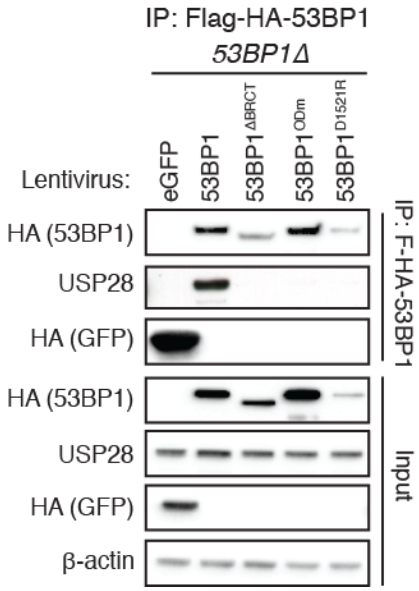


Figure 5.9. Mutation in residue D1521 within 53BP1's tandem Tudor domain blocks the interaction with USP28. Experiment performed in Fig. 3.7A assessing FLAG-HA-53BP1 protein complexes for presence of USP28.

5.3 Concluding remarks

The impact of the USP28-53BP1 regulatory node on p53 responses has been thoroughly addressed in previous chapters. The structural and functional properties of the USP28-53BP1-p53 axis suggested the involvement of direct ubiquitin-dependent regulatory activities that primed p53 for optimal downstream transactivation activities. In this chapter, I evaluated the effect of 53BP1 and USP28 in different p53 processes subject to ubiquitin-dependent regulation.

The stability of bulk p53 protein levels remained unaffected by USP28 or 53BP1 status. Remarkably, modified p53 forms generated upon N3 treatment were stabilised in presence of 53BP1 and USP28. Although specific p53

immunoprecipitation and subsequent immunoblot with PTM-specific antibodies would definitely reveal the nature of those p53 forms, the pattern closely resembled that of stress-induced ubiquitination. Considering the requirement of USP28's catalytic activity in the regulation of p53-dependent responses, it remains possible that USP28-53BP1 complexes could directly counteract the removal of poly-ubiquitination and thus favour the stability of these forms or, alternatively, regulate the activity of the E3-E4 ubiquitin ligases responsible for its deposit.

In fact, a differential presence of mono and di-ubiquitinated p53 could potentially explain the transcriptional differences in light of recent studies defining mono/di-ubiquitinated p53 as chromatin-bound and transcriptionally active [271]. Regardless of the nature of the ubiquitination event, activation or inhibition, mutation of the target site(s) should eliminate the requirement for the USP28-53BP1 complex-dependent p53 regulation and render the response to N3 independent of the 53BP1 and/or USP28 status. Mutations in lysines within p53's DBD failed to support this hypothesis. Furthermore, specific substitution of K292, reported to carry an activating ubiquitination mark, largely preserved p53 functionality, contradicting the described impediment of p53-mediated transactivation in H1299 cells [271].

Additionally, p53 DNA binding activity can be indirectly affected by upstream regulatory events. The data reported a reduced ability to sustain efficient p53 tetramer formation in absence of 53BP1 or USP28. These results suggested a role for the USP28-53BP1 complex in assisting the formation of p53 tetramers and consequently, downstream p53-DNA binding activities. Understanding how the accumulation of putative mono- and di-ubiquitinated

forms correlates with efficient tetramerisation and DNA binding and ties together with the action of USP28-53BP1 complexes will be the next step to enlighten the details of this p53 regulatory mechanism.

Beyond the ubiquitin-dependent regulation, 53BP1's structure-function analyses hinted to the tandem Tudor and methyl-dependent interactions as an additional requirement for p53 modulation. Several lines of evidence here presented disproved the reported 53BP1's tandem Tudor-p53me2 interaction as possible mechanistic explanation underlying the N3 resistant phenotype [241]. Despite being described as a 53BP1's BRCT interactor [87], my data pointed to a non-canonical, dual binding of USP28 to 53BP1 Tudor and BRCT domains. Additionally, both components were required for the interaction, and individual loss sufficed to disturb the entire binding dynamics. Aside from the structural interest, these data also provided insightful functional information: Although the involvement of additional proteins in this regulatory axis could not be excluded, every 53BP1 mutant altering N3 responses presented associated variations in p53 and/or USP28 interaction status.

Chapter 6

53BP1 INTEGRATES NHEJ AND p53 MODULATION ACTIVITIES

6.1 Introduction

In vivo studies have thoroughly characterised the physiological and pathological relevance of 53BP1-driven NHEJ. *53bp1*$^{-/-}$ mice display immunodeficiency due to loss of NHEJ-driven repair, and present a predisposition to the development of blood malignancies that is exacerbated by concomitant loss of p53 [96,97,109,237,238]. Here 53BP1 is presented as an enhancer of p53 responses. Until now, no phenotype described for *53bp1*$^{-/-}$ mice correlates with a loss of p53 functionality, evidencing the need to contextualise the findings here described in an *in vivo* setting to fully understand the physiological and pathological contributions of the USP28-53BP1-p53 regulatory axis.

The phenotypes observed in MCF-7 cells suggested a remarkable impact of 53BP1 and USP28 in p53 responses. However, I failed to observe N3 resistance in *53BP1Δ* and/or *USP28Δ* cancer cell lines (HCT116, A549) or immortalised normal cells (RPE-1) (Fig. 6.1 and data not shown). The overreliance in the USP28-53BP1 regulatory node shown by MCF-7 cells may arise from alterations in complementary pathways or pathway components (E3-ubiquitin ligases) and is potentially shared with other cell types. Indeed, 53BP1 knockdown was shown to confer resistance to N3-induced apoptosis in CH12F3-2 cells, and, more recently, the N3 resistant phenotype and p21 induction deficiencies here reported have been reproduced in *USP28Δ* human BJ fibroblasts [251,273].

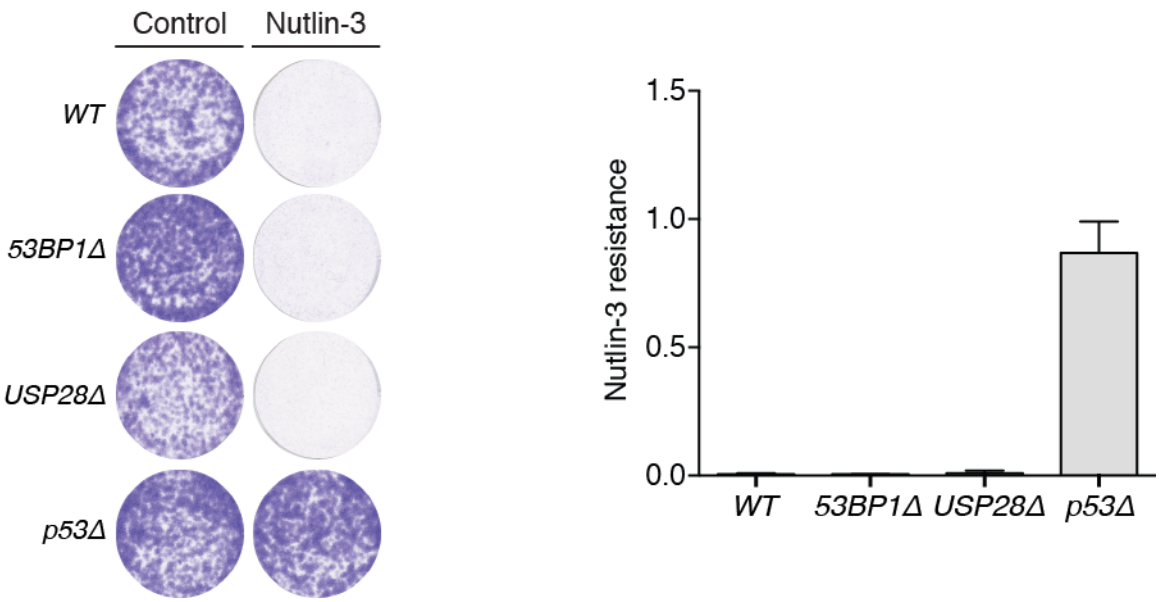


Figure 6.1. 53BP1 and USP28 deficiency does not confer N3 resistance to RPE-1 cells. Visual and quantitative analysis of N3 resistance (4 μM, 7 days) in *53BP1Δ*, *USP28Δ* and *p53Δ* RPE-1 cells. Mean ± SD (n=2, plated in triplicate). RPE-1 knockout cell lines were generated and characterised by Peter Yeow.

Interestingly, the USP28-53BP1-p53 regulatory axis has been rediscovered in the field of centrosome biology. Specifically, three parallel CRISPR/Cas9-based screens revealed 53BP1 and USP28 as essential mediators of cell cycle arrest in response to centrosome abnormalities in RPE-1 cells [274-276]. RPE-1 cells where PLK4 kinase had been inhibited exhibited a progressive loss of centrosomes throughout successive cell divisions, which resulted in prolonged mitotic duration, aberrant chromosomal segregations and p53-dependent senescence [274-276]. Absence of 53BP1 or USP28 abrogated the p53-dependent cell cycle arrest triggered by centrosome loss and resulted in intermediate resistance to the PLK4 inhibitor centrinone (Fig. 6.2). Together, these studies contributed to contextualise the relevance of the USP28-53BP1-p53 regulatory node in normal cells, where it acted as a surveillance mechanism to detect abnormal mitotic delays and activate p53 to prevent the proliferation of cells with potential chromosome misegregations.

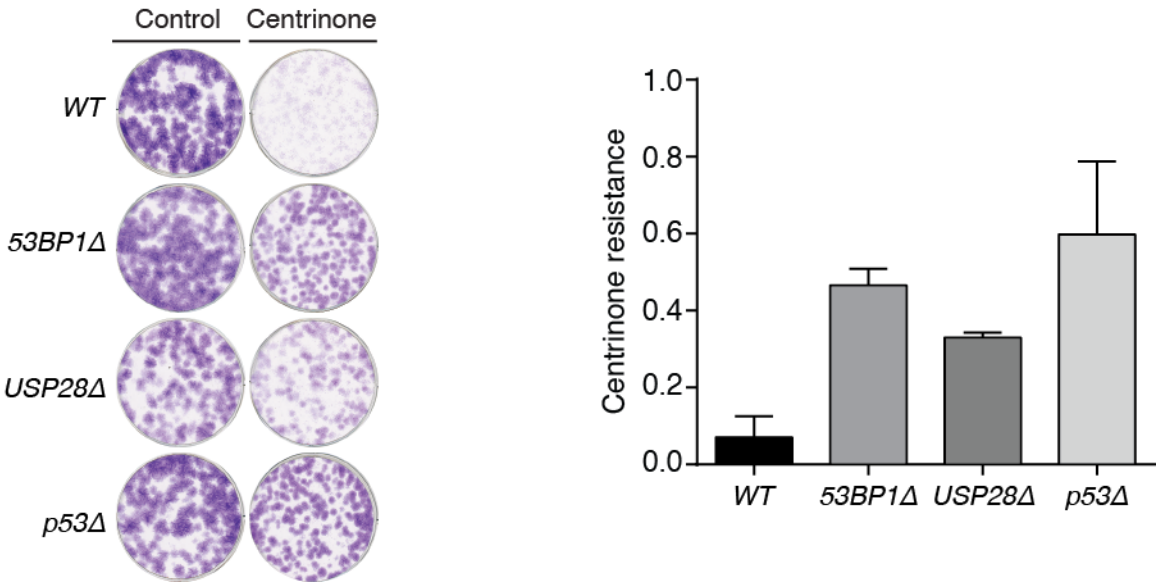


Figure 6.2. RPE-1 cells lacking 53BP1 or USP28 override centrinone-induced cell cycle arrest. Visual and quantitative analysis of centrinone resistance (125 nM, 11 days) in *53BP1Δ*, *USP28Δ* and *p53Δ* RPE-1 cells. Mean ± SD (n=2, plated in triplicate). This experiment was performed by Peter Yeow.

In light of these studies, 53BP1 acquires an extraordinary relevance as a p53 cofactor with potential physiological implications in protection against chromosomal misegregations in normal cells. The association with USP28 finally finds functional significance and further evidences how 53BP1 exerts its molecular roles by fostering differential protein interactions. The detailed structure-function analysis performed strongly suggests a separation of function between NHEJ DSB repair and p53 modulation within the 53BP1 architecture. While these two distinct functions share a common dependence in self-oligomerisation and Tudor domain-directed interactions, they present additional unique sequence requirements. On one side, the BRCT domain, completely dispensable for NHEJ activities, emerges as the scaffolding unit bridging USP28 and p53 interactions, essential for optimal p53 responses. On the other side, UDR-driven chromatin binding is central to 53BP1 recruitment to sites of DNA damage while no UDR-dependent activities are involved in p53-dependent N3-

induced cellular arrest in MCF-7 cells. Consequently, point mutations at the level of BRCT and UDR domains will allow the separation of these distinct functions and generate an exceptional system to tease apart their individual contribution in both *in vitro* and *in vivo* scenarios.

6.2 Results

6.2.1 *In vitro* separation of function: UDR *vs* BRCT mutant in IR responses

The cellular response to ionising radiation involves two processes tightly interconnected, DNA repair and checkpoint activation. Their coordinate action ensures the stability of the genome and correct life-death decisions. The individual loss of the repair capacity leads to sensitivity to ionising radiation thanks to proficient p53-dependent checkpoint responses triggering death programmes in damaged cells. Accordingly, simultaneous loss of checkpoint activities (loss of p53) allows cell cycle progression in the presence of high levels of genomic instability.

53BP1Δ cells only present mild sensitivity to ionising radiation [49]. Considering the dual role for 53BP1 described in this study, I hypothesised that, in *53BP1Δ* cells, the loss of optimal p53-checkpoint responses would allow cell cycle progression even in absence of NHEJ-driven repair activities. To test this 'double-loss' hypothesis and add further proof to the separation of function concept here presented, the survival to ionising radiation was evaluated in cells carrying different 53BP1 mutations. First, the radiosensitivity of *WT*, *p53Δ*, *53BP1Δ* and *53BP1*$^{\Delta BRCT}$ cells, where the tandem BRCT domain was removed by specific deletion at the endogenous locus, was examined (Section 3.2.3). Consistent with previous reports in other cell types, *53BP1Δ* MCF-7 lines

presented mild radiosensitivity compared to their *WT* counterparts (Fig. 6.3A). On the other hand, loss of p53 conferred an enhanced resistance to ionising radiation (Fig. 6.3A). Similarly, both MCF-7 *53BP1*$^{\Delta BRCT}$ lines were more radioresistant than *WT* cells, closely mimicking p53 loss-of-function (Fig. 6.3A). These data confirmed the repair proficiency of *53BP1*$^{\Delta BRCT}$ mutants and reinforced the relevance of 53BP1 in regulation of p53-dependent exit responses. Additionally, *53BP1Δ* cells complemented with the UDR-mutant, 53BP1^{L1619A}, showed a radiosensitive phenotype more pronounced than a GFP-complemented knockout control further supporting the hypothesis of the 'double-loss' of function in *53BP1Δ* cells (Fig. 6.3B). Finally, 53BP1 mutated in the phosphobinding pocket within the tandem BRCT, 53BP1^{K1814M}, reported to disrupt γH2AX binding and impede heterochromatin repair, behaved as a full-length WT 53BP1 in response to IR (Fig. 6.3B) [83]. This behaviour further proved the dispensability of 53BP1's tandem BRCT domain in the 53BP1-dependent DSB repair.

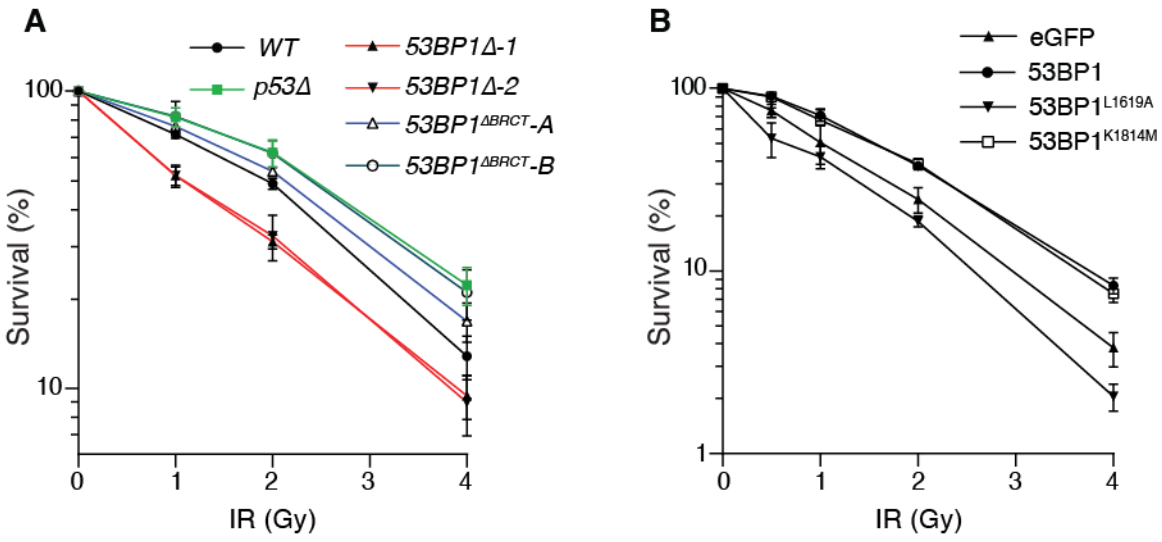


Figure 6.3. 53BP1 independently regulates NHEJ-driven repair and p53-driven cell death in response to IR. (A) The survival of MCF-7 lines upon X-ray irradiation treatment was assessed by colony survival assay. Mean ± SD (n = 3, plated in triplicate). (B) Evaluation of survival to X-ray radiation as in (A) in *53BP1Δ* cells where expression of the depicted mutants has been reconstituted by lentiviral transduction. Mean ± SD (n = 3, plated in duplicate). These experiments were performed and analysed by Dr C. Oliveira.

6.2.2 *In vivo* separation of function: NHEJ-driven repair *vs* mitotic surveillance

MCF-7 cells, unlike other cell types, strongly depend on the USP28-53BP1 regulatory node to fully activate p53 responses. While this cell line constitutes the perfect *in vitro* system for mechanistic studies, it fails to provide information about the context-specificity of the USP28-53BP1-p53 axis in a physiological scenario. The generation of mouse models harbouring separation of function mutations in 53BP1 overcomes this caveat and allows the independent study and contextualisation of 53BP1-driven NHEJ and p53 regulation.

The UDR mutant, 53BP1^{L1619A}, has been previously characterised *in vitro* as NHEJ repair-dead, and here shown its proficiency supporting p53-dependent responses [24]. Throughout this study, I have also accomplished a deep *in vitro* characterisation of the repair-proficient 53BP1$^{\Delta BRCT}$ mutant [63] as deficient to support optimal p53-dependent responses. Full deletion of 53BP1's tandem BRCT unavoidably involves the loss of interaction with additional partners, such as EXPAND1 or γH2AX potentially disrupting their functionality. In order to minimise undesired loss of interactions, which could influence the final phenotype and mislead my conclusions, point mutations within the tandem BRCT structure were designed. Prior analyses revealed that individual point mutations in the p53 binding surface in 53BP1 (N1845R and D1861R) conferred resistance to N3 albeit to a slightly lower extent than full deletion of the tandem BRCT itself (Fig. 3.10B). Full length 53BP1 carrying the double arginine substitution (hereinafter named 53BP1^{NDRR}) was then generated and its ability to bind p53 and promote N3-dependent arrest evaluated (Fig. 6.4A). p53 immunocomplexes showed complete absence of 53BP1 protein when the NDRR mutation was present (Fig. 6.4B). According to its inability to foster physical interactions with p53,

53BP1^{NDRR} failed to restore N3 sensitivity, conferring a resistant phenotype even more pronounced than the deletion of the whole BRCT domain (Fig. 6.4C). This mechanistic information pinpointed the suitability of this mutant for separation of function studies, and was selected for the generation of a mouse model.

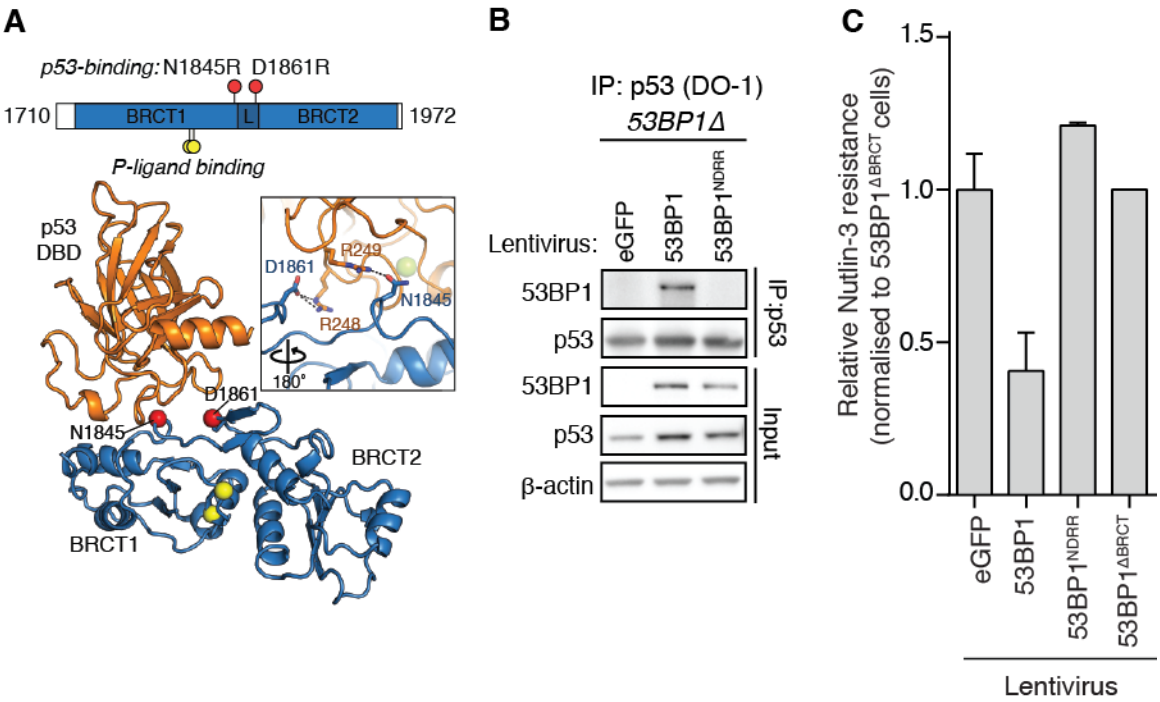


Figure 6.4. 53BP1 simultaneously mutated in N1845 and D1861 fails to bind p53 and promote N3-induced cellular arrest. (A) Schematic representation of 53BP1's tandem BRCT and corresponding structure bound to p53's DBD (PDB ID: 1KZY) depicting the double mutation used in these assays. (B) *53BP1Δ* cells were stably complemented using pLENTI-PGK-DEST vectors carrying 53BP1 gene constructs or an eGFP control. Cells were treated with N3 (4 μM, 2 h) and p53 immunocomplexes purified and analysed by western blot. (C) Cell lines were treated with N3 (4 μM) for 11 days or left untreated for 7 days. Relative N3 resistance was calculated by taking 53BP1$^{\Delta BRCT}$ as a reference for normalisation. Mean ± SD (n=2, plated in triplicate).

Equivalent UDR (L1616A) and tandem BRCT (N1845R, D1861R) point mutations were thus introduced into the mouse genome using homology-based CRISPR/Cas9-mediated editing. The integration of the mutation within the mouse genome was assessed by amplification of the specific gene locus and restriction digestion (Section 2.2.3). Heterozygous individuals in the first generation were crossed to obtain the homozygous mice used throughout this study (hereinafter

referred as *L1616A* and *NDRR* mice) and corresponding *wt* littermates were used as controls. *53bp1*$^{-/-}$ mice from established homozygous breedings were included as loss-of-function controls. Using this unique *in vivo* system, we then proceeded to re-examine the role of 53BP1 in the immune system, readout of 53BP1-dependent NHEJ activities.

The process of B- and T-cell maturation is intrinsically linked to the success of V(D)J recombination. Unsuccessful recombination events result in the apoptotic elimination of lymphocytes at the control points impeding their progression through the maturation stages. Therefore, analysis of cell populations in every maturation stage, thanks to specific cell surface markers, allowed to draw a development outline that grants an indirect readout for V(D)J recombination proficiency. Recent studies reported a decrease in B lymphocytes undergoing the maturation process (B220+) in bone marrow and spleen in *53bp1*$^{-/-}$ mice, result of deficiencies in B-cell development [97]. Using this phenotype as a reference, we proceeded to monitor B-lymphocyte numbers and development in the bone marrow of *wt*, *NDRR*, *L1616A* and *53bp1*$^{-/-}$ mice using the Hardy fraction analysis [247]. B220+ lymphocytes were significantly depleted in *L1616A* mice in bone marrow to a comparable extent than in *53bp1*$^{-/-}$ mice (Fig. 6.5A, left panel). A similar trend was hinted in the quantification of B220+ lymphocytes in spleen (Fig. 6.5B, right panel). *NDRR* mice displayed variable percentages of B220+ lymphocytes in both bone marrow and spleen, ranging between *wt* and *53bp1*$^{-/-}$ mice (Fig. 6.5A). Although experimental fluctuations could account for those differences, and the number of mice subject to the analysis should be increased to reach definitive conclusions, the involvement of intact 53BP1-dependent p53 regulation for successful B-cell maturation could not be excluded.

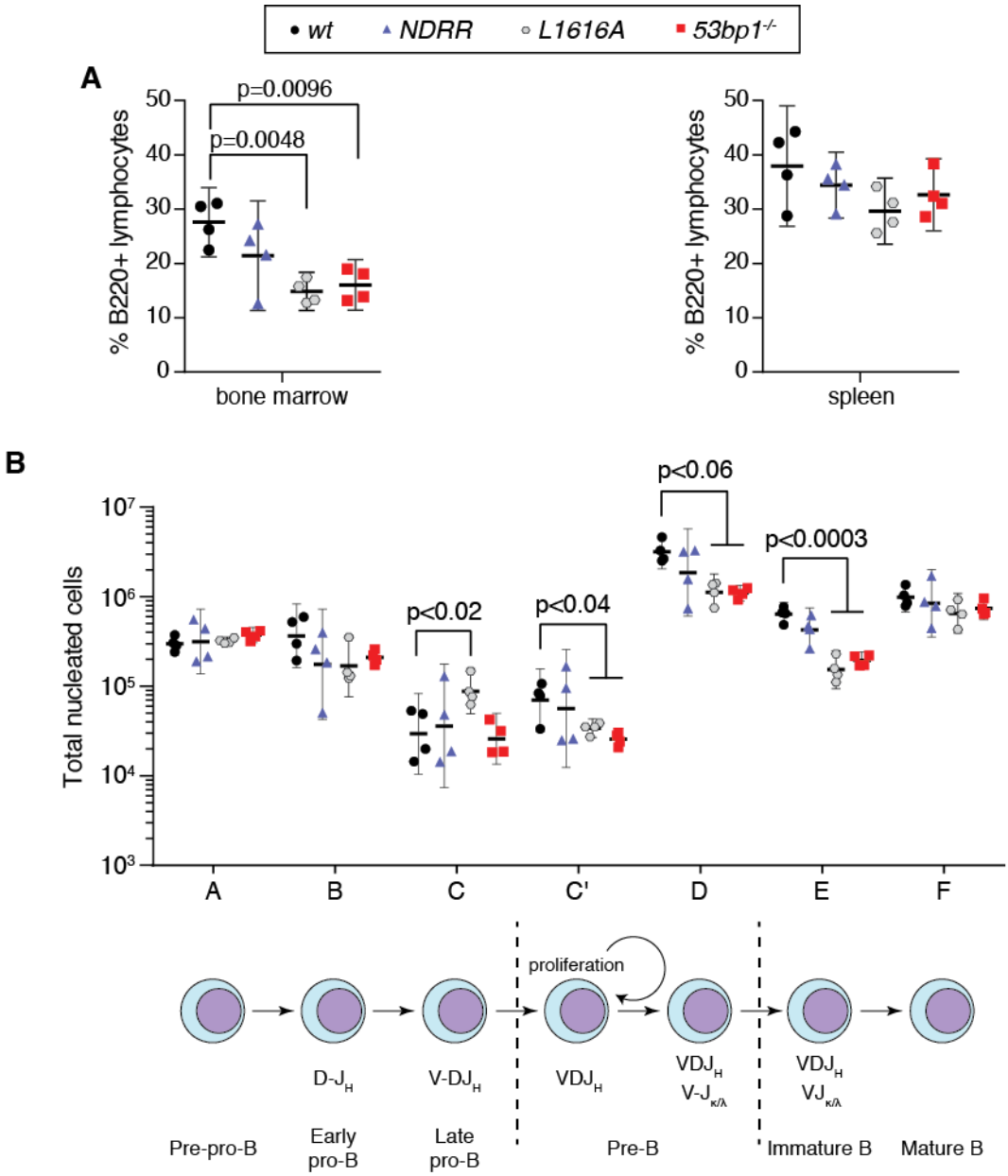


Figure 6.5. B-cell development requires intact 53BP1-driven NHEJ activities. (A) Quantification of B220+ B cells as a proportion of total lymphocytes in the bone marrow (1 femur and 1 tibia) and spleen obtained from *wt* (n=4), *L1616A* (n=4), *NDRR* (n=4) and *53bp1*$^{-/-}$ (n=4) mice (mean ±SD). P-values were calculated using unpaired Student's t-test. (B) Hardy fraction analysis of bone marrow lymphocytes. Total nucleated cells were calculated for each B-cell lineage stage, gated as in [247] (mean ±SD). P-values were calculated as in (A). Schematic representation of the B-cell maturation process and corresponding rearrangements occurring in each stage are also depicted and adjusted to corresponding Hardy fractions. Dashed lines represent the two control points that evaluate productive rearrangements. These experiments were performed and analysed by Dr C. Oliveira with assistance from Dr K. Bilham.

Consistent with previous reports, deficiencies in V(D)J recombination in absence of 53BP1 were reflected in abnormal percentages in the different B-cell lineage stages determined by Hardy fraction analysis (Fig. 6.5B) [97]. Steady 3-fold reductions in total nucleated cells were observed after the pre-B cell receptor checkpoint control (Fig. 6.5B, first dashed line), consistent with unproductive rearrangement of the heavy chain (VDJ_H), and extended during the subsequent pre-B and immature B-cell stages where arrangement of the light chains (kappa and lambda, $VJ_{\kappa/\lambda}$) takes place (Fig. 6.5B, fractions C', D and E). 53BP1's ability to bind ubiquitinated nucleosomes is essential for B-cell maturation: *L1616A* mice displayed equivalent depletion of pre-B and immature B-cell populations (Fig. 6.5B C', D and E). Interestingly, *L1616A* mice also presented a reproducible and significant 3-fold increase in the late pro-B population (Fig. 6.5B, fraction C), likely indicative of a block in the pre-B cell receptor checkpoint. The differential behaviour between *L1616A* and *53bp1*$^{-/-}$ B lymphocytes in the C-C' transition hinted to a potential interplay with p53 cell cycle arrest and apoptotic activities. However, the impact of the sole loss of 53BP1-dependent p53 regulation was difficult to determine with the mice cohort evaluated, as *NDRR* mice presented a phenotypic variability that yielded no significant differences with their *wt* or *53bp1*$^{-/-}$ counterparts (Fig. 6.5B).

In order to obtain a full picture of 53BP1's separation of function in V(D)J recombination processes, T-cell maturation within the thymus was evaluated. Similar to the Hardy fraction analysis in B-cell development, the four main T-cell compartments were discriminated by specific staining of the cell surface receptors CD4 and CD8. Thymuses from *L1616A* and *53bp1*$^{-/-}$ mice showed reduced populations of mature T helper (Th) lymphocytes compared to *wt*

controls, compensated with a higher proportion of immature CD4-CD8- (DN, double negative) T cells (Fig. 6.6A). *NDRR* mice presented consistent *wt* behaviour in this context (Fig. 6.6A). A closer look at the CD4-/CD8- and CD4+/CD8+ (DP, double positive) populations allowed the monitoring of T-cell maturation stages. *L1616A* and *53bp1*$^{-/-}$ lymphocytes experienced an accumulation of DN3 lymphocytes and a concomitant reduction of DN4, suggesting the presence of a maturation block coinciding with the first point of control for productive rearrangement of the β chain in the T-cell receptor (Fig. 6.6B, left panel). However, these deficiencies in DN4 lymphocytes did not result in a reduction of downstream DP cell populations (Fig. 6.6A). Despite the equivalent overall DP numbers between genotypes, a 2-3-fold reduction in DP cells carrying high levels of complete TCR receptor (TCRhi, CD3^{high}+) was present in cells lacking functional NHEJ activities (Fig. 6.6B, right panel). Reductions in TCRhi cells could explain the depletion in Th cells previously observed (Fig. 6.6A-B). The close parallelism between *L1616A* and *53bp1*$^{-/-}$ behaviours in both bone marrow and thymus analyses further suggested an exclusive dependence on 53BP1 NHEJ activities to successfully accomplish lymphocyte maturation. In addition, mice lacking 53BP1-dependent p53 regulation abilities perfectly clustered with their *wt* counterparts in all T-cell maturation stages (Fig. 6.6).

Together, these data largely excluded a role for 53BP1-dependent p53 modulation in BCR/TCR checkpoints control and apoptotic induction during lymphocyte development and intimately linked successful development to proficient 53BP1-driven NHEJ in V(D)J recombination processes.

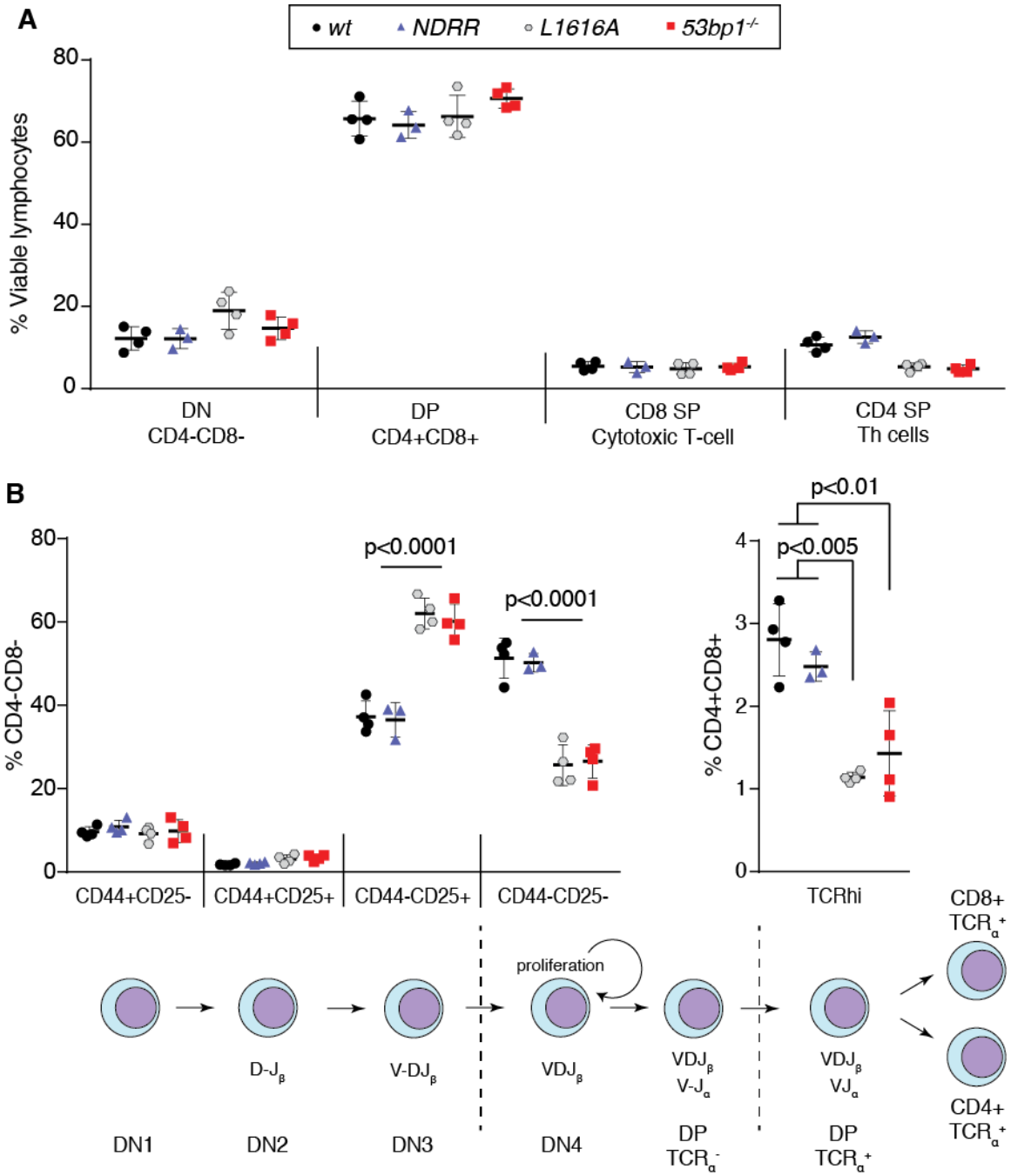


Figure 6.6. 53BP1 action in T cell maturation depends exclusively on its ability to support NHEJ. (A) Distribution of thymic cells according to CD4/CD8 presence represented as percentage of total viable lymphocytes obtained from *wt* (n = 4), *L1616A* (n = 4), *NDRR* (n = 3) and *53bp1*$^{-/-}$ (n = 4) mice (mean ± SD). DN, double negative; DP, double positive; SP, single positive. (B) Analysis of specific T-cell maturation stages within DP and DN cell populations. DN cells were gated based on CD44/CD25 staining and DP positive cells selected for presence of TCR receptor. Two-way and one-way ANOVA, respectively, mean ± SD (n = 4 mice/genotype). Schematic representation of the T-cell maturation process and corresponding rearrangements occurring in each stage are depicted under the corresponding data. Dashed lines represent the two control points that evaluate productive rearrangements. These experiments were performed and analysed by Dr C. Oliveira with assistance from Dr K. Bilham.

Once the V, D and J fragments are successfully assembled, mature B lymphocytes rearrange the constant region fragments in the *IgH* locus to generate the array of immunoglobulin isotypes. This rearrangement, named class-switch recombination (CSR), requires proficient 53BP1-directed NHEJ [104,105]. CSR events were induced *ex vivo* by culturing splenic primary B cells from *wt*, *NDRR*, *L1616A* and *53bp1*$^{-/-}$ mice in presence of different cytokine cocktails, and CSR efficiency was examined. *NDRR* mice displayed efficient CSR to all the isotypes examined, consistent with the previously reported dispensability of 53BP1's BRCT in CSR (Fig. 6.7A) [63]. As expected, NHEJ-dead, *L1616A* B cells were unable to support CSR, presenting only residual activity comparable to *53bp1*$^{-/-}$ B cells (Fig. 6.7A). Experimental differences were not attributed to proliferation-dependent depletion of CSR, as equivalent proliferation was observed across the four genotypes tested (data not shown). These data further confirmed the complete dispensability of 53BP1-dependent p53 modulation in 53BP1's most prominent physiological functions in the immune system, which entirely relied on its role in NHEJ.

Next, we examined the sensitivity to ionising radiation in splenocytes. Ionising radiation activates the DNA damage response, combining DNA repair *per se* and the activation of p53-dependent transcriptional programmes. More specifically, lymphocytes induce robust p53-dependent apoptosis upon IR treatment [39]. Evaluation of the survival to IR was thus assessed using the apoptotic detection staining with fluorophore-conjugated annexin V and propidium iodide. *53bp1*$^{-/-}$ splenocytes presented mild radiosensitivity compared to *wt* controls (Fig. 6.7B). Remarkably, the response to IR in *NDRR* and *L1616A* splenocytes overlapped with *wt* and *53bp1*$^{-/-}$, respectively (Fig. 6.7B). The *wt*-like

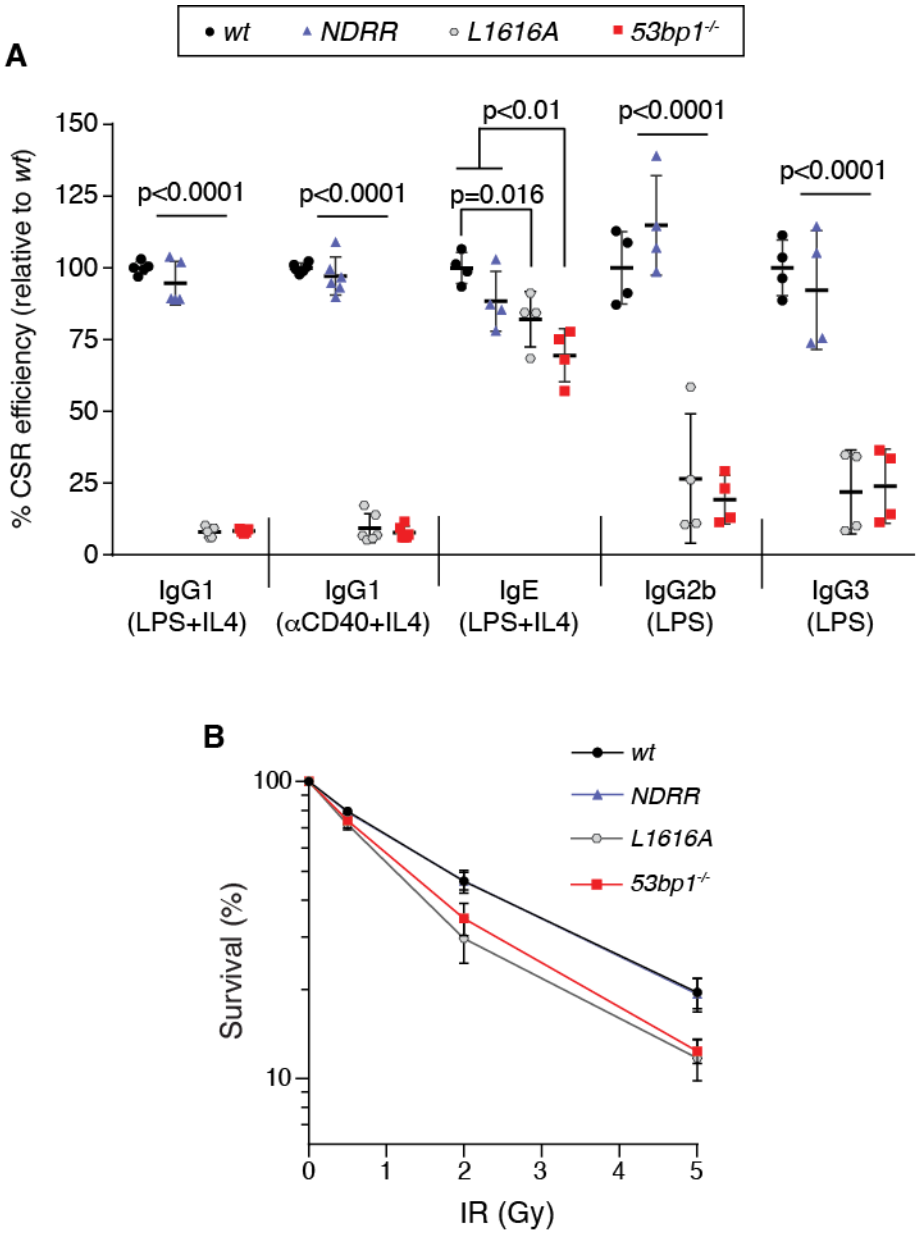


Figure 6.7. 53BP1 requires its NHEJ activity but not p53 regulatory functions to promote efficient CSR and survival to IR. (A) Quantitative analysis of CSR efficiency in splenic B cells stimulated with the specified cytokines for 96 h. Two-way ANOVA, mean ± SD (n = 4 mice/genotype). (B) Survival to IR of annexin V-FITC/PI-stained splenocytes was evaluated by flow cytometry. Double negative cell populations were selected and relative survival calculated against corresponding untreated controls. Mean ± SD (n = 4 mice/genotype). Dr C. Oliveira performed and analysed the CSR experiments and provided assistance in IR-induced apoptotic assays.

response in *NDRR* splenocytes largely excludes the possibility of an extensive role for 53BP1-dependent p53 modulation in IR-induced apoptosis control. Additionally, these data failed to support the hypothesis of 'double-loss' of

function in *53bp1*$^{-/-}$ cells (Section 6.2.1) and left the mild radiosensitivity phenotype, caused by 53BP1 absence, unexplained in this context.

Having defined the context(s) where *L1616A* perfectly mimics 53BP1 loss-of function, and excluded a role for 53BP1 in p53 regulation of IR-induced apoptosis in splenocytes, I aimed to contextualise the *in vivo* contribution of the 53BP1-p53 interaction. The studies in the non-transformed cell line RPE-1 highlighted the relevance of the USP28-53BP1-p53 axis in mitotic surveillance, preventing possible misegregations and subsequent aneuploidy [274-276]. Inhibition of PLK4 using centrinone generated progressive centrosome loss and extended mitotic duration, the activation stimulus for the USP28-53BP1-p53 axis [274-276]. Accordingly, *53BP1Δ* and *USP28Δ* RPE-1 cells survived in the presence of centrinone, presumably allowing aberrant chromosomal segregation and cell cycle progression (Fig. 6.2).

In order to define the *in vivo* relevance of the USP28-53BP1-p53 axis and the effect of specific UDR and BRCT mutations, the response to centrinone in primary mouse embryonic fibroblasts was explored. MEFs were obtained from *wt*, *L1616A*, *NDRR* and *53bp1*$^{-/-}$ embryos, genotyped and two independent cell lines selected for analysis. *L1616A* and *NDRR* MEFs expressed 53BP1 at levels comparable to *wt* cells (Fig. 6.8A). As expected, 53BP1 was recruited to IR-induced foci in both *wt* and *NDRR* lines while *L1616A* lines presented pan-nuclear 53BP1 staining (Fig. 6.8A). MEFs were then seeded in the presence of centrinone to induce centrosomal abnormalities. At the dose tested, *wt* cells showed a survival of ~40% compared to the corresponding untreated controls (Fig. 6.8C). Loss of 53BP1 enhanced cellular progression in centrinone, with *53bp1*$^{-/-}$ cells presenting survivals ranging from 65 to 80% (Fig. 6.8C).

Remarkably, *NDRR* lines displayed even more pronounced centrinone survival than *53bp1*$^{-/-}$ lines (~90%) (Fig. 6.8C). *NDRR* cells lack the intrinsic genomic instability present in *53bp1*$^{-/-}$ cells, which not only causes proliferation defects but may also synergise with centrinone in cell death induction attenuating the resistance phenotype. The response to centrosome loss relied on the 53BP1-p53 connection but was independent of 53BP1-driven NHEJ: Both *L1616A* lines reproduced the same level of resistance as *wt* cells (Fig. 6.8C).

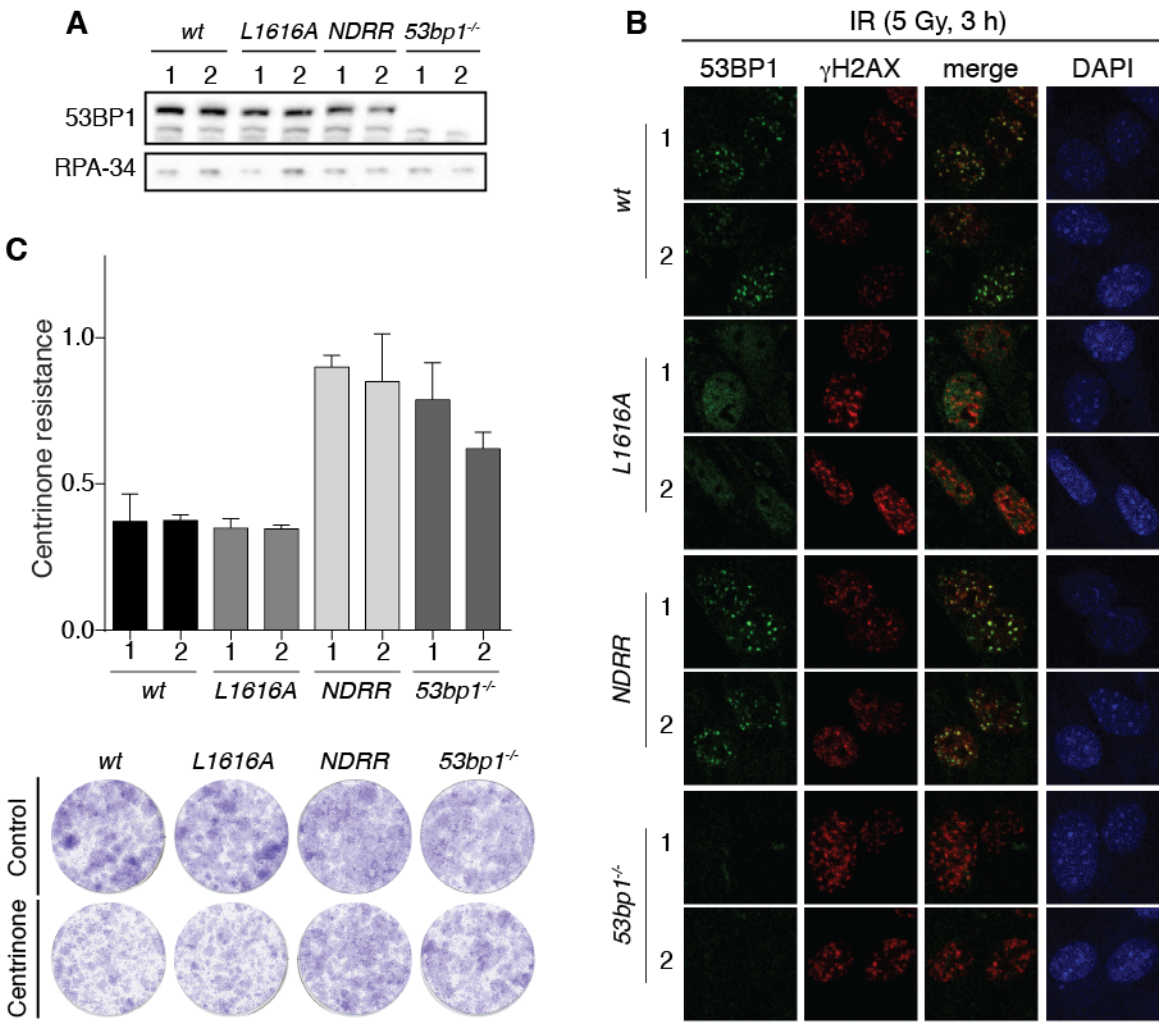


Figure 6.8. Cellular response to centrosome loss depends on 53BP1-p53 physical interactions. (A) Immunoblot analysis of 53BP1 protein expression in primary MEFs. (B) Evaluation of 53BP1 foci formation by indirect immunofluorescence. (C) Quantitative analysis of centrinone resistance (250 nM, 11 days) in MEFs of the indicated genotypes. Due to low plating efficiency, initial cell numbers were doubled for *53bp1*$^{-/-}$ cells (See Section 2.6.1). Mean ± SD (n=2, plated in triplicate). A representative image is also depicted. Primary MEF cell cultures were established with assistance from Dr K. Bilham.

Resistance to the drug centrinone implied cell division upon centrosome loss that might generate daughter cells carrying aberrant chromosome numbers. Slow division rates and spontaneous increase in ploidy in culture made MEFs cells unsuitable for the assessment of this phenotype. Splenocytes were selected as a model system thanks to their genomic stability in culture and a high cell division capacity that enabled centrinone to act within a short period of time. In addition, this could provide a scenario where lymphocytes rely on 53BP1-dependent p53 modulation, separated from their well-described requirements of 53BP1-driven NHEJ activities.

To this end, I mock-treated or treated LPS-stimulated splenocytes with centrinone for 72 h prior to metaphase preparation and chromosome counting. Untreated splenocytes presented similar distributions of chromosome numbers independent of the genotype (Fig. 6.9A). The equivalent distributions suggested low frequency of stochastic misegregations events, with the small chromosome gains and losses depicted rather attributed to technical difficulties of metaphase sample preparation and chromosome counting. Treatment with centrinone generated a genotype-independent bias towards chromosome gains and increases in ploidy (Fig. 6.9B). Notably, the proportion of cells presenting centrinone-induced chromosome gains was diminished in *wt* and *L1616A* cells compared to their *NDRR* and *53bp1*$^{-/-}$ counterparts (Fig. 6.9B). *NDRR* and *53bp1*$^{-/-}$ splenocytes presented an enhanced tolerance to chromosomal abnormalities, with a small proportion of cells even carrying ~6n and ~8n chromosomal content (Fig. 6.9B). These results further confirmed the *in vivo* role in prevention of chromosomal abnormalities undertaken by 53BP1-dependent p53 regulation and highlighted its independence from 53BP1-driven NHEJ.

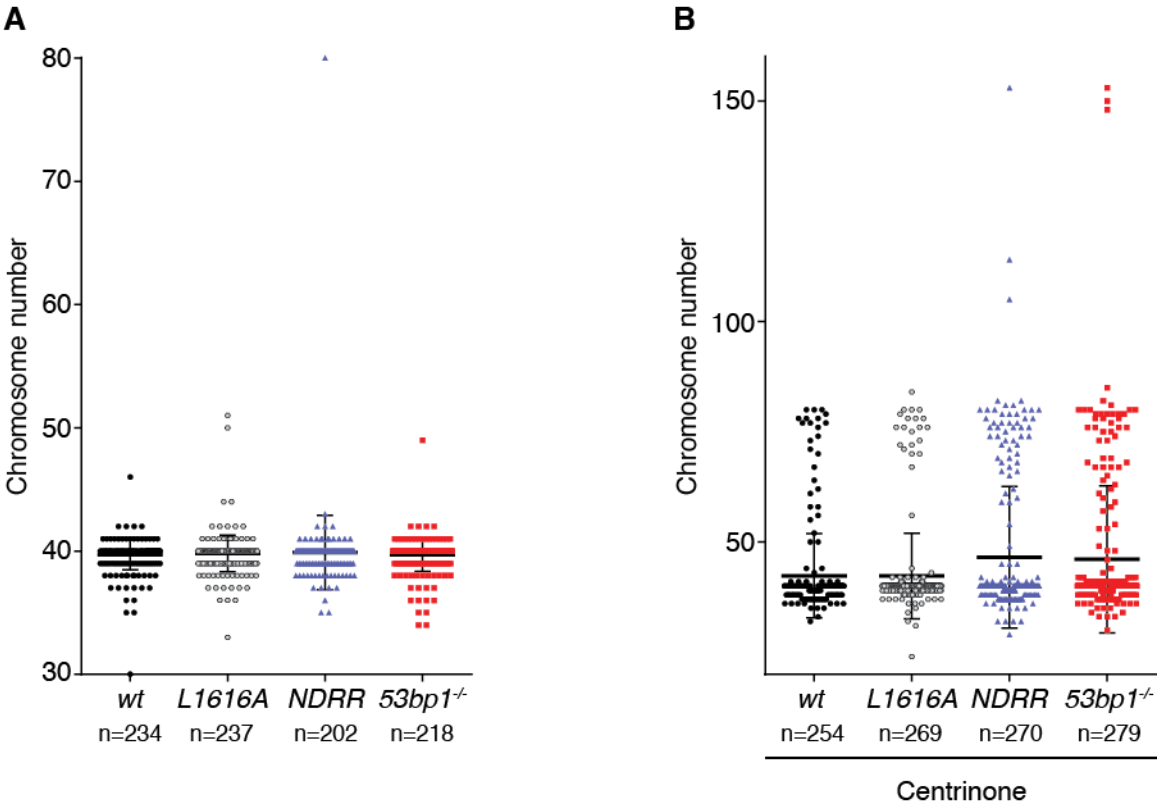


Figure 6.9. Loss of 53BP1-dependent p53 modulation results in enhanced chromosomal gains in splenocytes. (A) Metaphase analysis of untreated splenocytes cultured for three days in LPS to induce proliferation. A minimum of 30 metaphases per mice was counted from a total of 6 mice per genotype. Total number of cells evaluated per genotype is depicted (mean ± SD). (B) Metaphase analysis of LPS-stimulated splenocytes treated with 1 μM centrinone for 72 h carried out as in (A).

6.3 Concluding remarks

The functionality of 53BP1 is founded in the interactions fostered by its multidomain architecture. In 53BP1-driven NHEJ, the tandem Tudor-UDR provides chromatin anchorage to oligomerised 53BP1, while a heavily phosphorylated N-terminal region constitutes a recruitment platform for downstream effectors. Here, I describe oligomerised 53BP1 to drive modulation of p53 *via* interactions primarily focalised in the tandem BRCT domain. Data from Sections 3.2.2-4 converged with the IR-induced survival analyses to endorse the separation of function idea: 53BP1-driven NHEJ and p53 modulation are distinct

functions that can be separated at the level of point mutations within the 53BP1 protein.

MCF-7s constituted a powerful system for mechanistic studies, but failed to provide information about the relevance of the USP28-53BP1-p53 axis in normal cell physiology. Though seemly shared with other cell types like CH12F3-2 or BJ fibroblasts [251,273], such a prominent reliance on this regulatory node for p53 priming was unlikely to extrapolate to an *in vivo* context. Therefore, to perform *in vivo* separation of function analyses, I combined the molecular dissection of 53BP1 with existing knowledge on 53BP1-driven NHEJ activities in the immune system, and the reported relevance of the USP28-53BP1-p53 axis in mitotic surveillance [15,274-276]. Consistent with previous studies [95,97,104], 53BP1 absence resulted in immunological deficiencies associated to diminished V(D)J recombination and CSR. Here, we have shown these effects to correspond in its entirety with loss of NHEJ functions and confirmed the dispensability of 53BP1's tandem BRCT, and consequently, 53BP1-dependent p53 modulation, in these physiological scenarios [63,252]. The tables turned in the evaluation of tolerance to PLK4 inhibition and subsequent centrosome loss and extended mitotic duration. Disruption of 53BP1-p53 physical contacts enhanced cellular resistance to centrosome loss and increased tolerance to chromosomal aberrations in primary cells, mimicking complete 53BP1 loss of function. Although perhaps expected, it was encouraging that separation of function mutations generated using N3-based assays in MCF-7 cells translated into defective mitotic surveillance *in vivo*, outlining the ultimate mechanistic similarities. Chemical PLK4 inhibition generated a cellular stress resolved by 53BP1-dependent p53 modulation; however, massive centrosome loss is not a common occurrence,

suggesting that the USP28-53BP1-p53 axis is likely to acquire specific physiological relevance in a context yet to be discovered.

Collectively, my data suggested for 53BP1 a dual impact on the preservation of genome integrity *in vivo* by driving i) NHEJ DSB repair and ii) p53-dependent protection against chromosomal misegregations.

Chapter 7

DISCUSSION

Discovered in 1994 as a p53 binding protein, the initial characterisation of 53BP1 revealed two remarkable observations: i) 53BP1 was a coactivator of p53-dependent transcription of p21, and ii) 53BP1 presented a nuclear dotted distribution in response to DNA damage [41,230]. Soon attracting the interest of the DNA repair field, 53BP1 has since been attributed major roles in NHEJ-driven DSB repair [15]. In fact, the study of 53BP1's protein architecture, interacting partners and mechanism of action has been complemented with the definition of 53BP1's impact on the physiology of the immune system and the pathology of BRCA1-deficient cancers. Conversely, the interest for 53BP1's relevance in p53 responses decayed, leaving largely unexplored a whole level of 53BP1's functionality. This piece of research directs the focus back to p53, and proposes a change in the actual conception of 53BP1 as a repair protein. Under this new light, 53BP1 will be better defined as an integral node of genome instability control, through both NHEJ-driven DSB repair and modulation of p53-mediated responses.

7.1 53BP1 in p53 responses: the tandem BRCT and the structural implications

Initial reports and crystal structure analysis pointed to 53BP1 as one of the rare interactors of p53 DNA binding domain [41,78,229,233]. 53BP1, *a priori* a competition for the p53-DNA interaction, is here proven to enhance p53

transcriptional activity (Fig. 3.3). Accordingly, the magnitude of 53BP1 impact extends further beyond the previously reported inductions of *CDKN1A* (*p21)*, *MDM2* or *BBC3* (*PUMA)*, over the whole p53 transcriptome (Fig. 3.4) [230,241]. This role of 53BP1 inherently influences optimal p53-mediated cell cycle arrest, apoptosis and senescent responses, and provides a mechanistic explanation for the resistance to N3 and the diminished IR-induced G1/S checkpoint arrest in 53BP1-deficient cells (Fig. 3.2, 3.9) [240,250].

The tandem BRCT domain is central to 53BP1-dependent p53 regulation. 53BP1's orthologues, *S. cerevisiae* Rad9 and *S. pombe* Crb2, rely on the tandem BRCT domain for dimerisation and nucleosome binding to exert checkpoint control [44]. In 53BP1, however, the requirement for the tandem BRCT domain has been eliminated by functional evolution of the oligomerisation domain and the Tudor-UDR module for nucleosome recognition at damage sites. Fascinatingly, in the striking functional evolution of 53BP1, the tandem BRCT has acquired a novel mode of checkpoint control through p53 interactions, ultimately retaining the functionality of its yeast counterparts.

Mechanistically, 53BP1's tandem BRCT orchestrates the regulation of p53 responses by fostering dual binding with p53 and the deubiquitinating enzyme USP28 (Fig. 3.11, 7.1). After many years of highlighting the dispensability of 53BP1's tandem BRCT in NHEJ [59,63,252], this study contextualises the relevance of this domain on p53 regulation, and first provides functional significance to BRCT-mediated 53BP1-p53 and USP28-53BP1 interactions. Both interactions are indeed essential, as individual disruption results in functional failure of the axis, and require different surfaces within 53BP1's tandem BRCT (Fig. 3.11). While the structural details of 53BP1's BRCT-p53 interaction have

been previously described [78,233], the USP28-53BP1 module challenges the existent knowledge about BRCT interaction dynamics (Fig. 7.1). Traditionally, BRCTs have been characterised as modules for protein-protein interactions with specific ability to bind phosphoproteins [75,277]. In fact, 53BP1's tandem BRCT itself has been co-crystallised with the γH2AX peptide in a perfectly canonical BRCT-phosphoprotein interaction [83,84]: A lysine residue in 53BP1 (K1814) hydrogen bonds with the phosphorylated serine in γH2AX and an arginine (R1811) contacts with the amino moiety of the aromatic residue in position +3 (Fig. 7.1). Conversely, the constitutive interaction with USP28 requires the presence of an intact arginine (R1811) but not the lysine (K1814) residue within

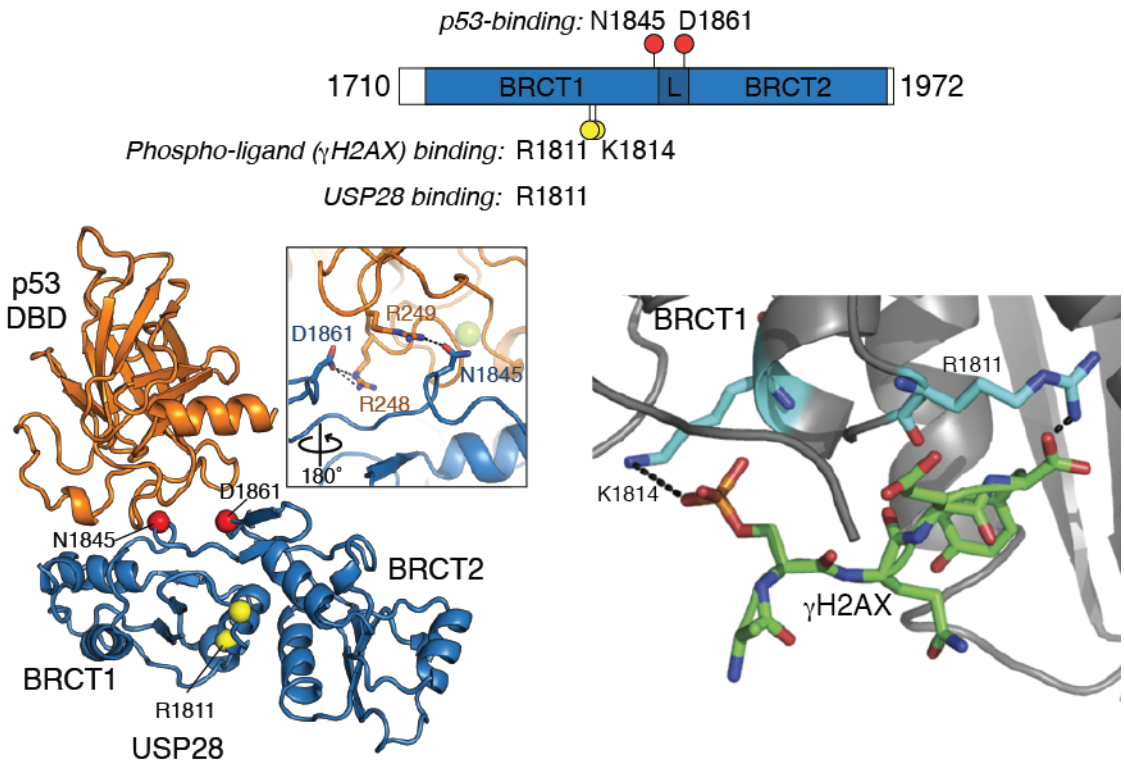


Figure 7.1. 53BP1's tandem BRCT fosters non-canonical interactions with USP28 using residue R1811 within the phosphobinding pocket. Schematic representation of 53BP1's tandem BRCT with residues required for p53 (red) and γH2AX and USP28 (yellow) highlighted (top). USP28 does not interfere with p53 binding and fosters interactions with residue R1811 within 53BP1's BRCT phosphobinding pocket (right). The non-requirement of residue K1814M suggests a phospho-independent interaction whose dynamics are likely to diverge significantly from the reported canonical γH2AX interaction (left).

53BP1's tandem BRCT (Fig. 3.11, 7.1) [87]. Furthermore, USP28 functionality in p53-dependent responses is unaffected by mutation of the ATM-phosphorylated, potential BRCT docking site in USP28, pS714 (data not shown) [86]. These particularities about the 53BP1's BRCT-USP28 interaction raise structural implications towards new modes of protein-protein interactions for BRCT modules.

The contribution of 53BP1's tandem Tudor domain to p53 responses further adds to the peculiar structural conformation of USP28-53BP1 complexes. In 53BP1-driven NHEJ, the tandem Tudor-UDR acts together in nucleosome recognition at damaged chromatin [74]. In p53-dependent responses, the dispensability of the UDR motif contrasts with the atypical involvement of the tandem Tudor domain (Fig. 3.6). Specific point mutations in the methyl-binding pocket within the Tudor domain, W1495(A), and D1521(A), equally disrupt binding to H4K20me2 peptides *in vitro* and p53K382me2 in co-immunoprecipitation assays [23,235]. Shockingly, while Tudor mutant $53BP1^{D1521R}$ is unable to support p53-dependent cellular arrest, $53BP1^{W1495A}$ essentially displays a *WT*-like behaviour (Fig. 5.8). The deficiency caused by D1521R mutation is not attributed to abrogation of 53BP1-p53 binding as previously suggested (Fig. 3.7) [241], but rather to impairment in USP28-53BP1 connections (Fig. 5.9). The novel mode of bivalent binding to USP28 by 53BP1's Tudor-BRCT module, somehow reminiscent of Crb2's Tudor-BRCT-mediated nucleosome recognition [278,279], highlights the structural plasticity of 53BP1 to accommodate its distinct cellular functionalities.

Finally, protein oligomerisation statuses add another layer of structural complexity to the USP28-53BP1-p53 complex. 53BP1 self-association appeared

crucial for the modulation of p53 responses (Fig. 3.6), a shared requirement with 53BP1-driven NHEJ activities [59,60]. In fact, specific mutations disrupting 53BP1's oligomerisation negatively impact on both p53 and USP28 binding (Fig. 3.7, 5.9). The incompatibility of 53BP1-p53 and p53-DNA complexes, and the impossibility to detect 53BP1 associated to p53's RE (ChIP analysis, data not shown) imply a dynamic nature and nucleoplasmic localisation for the complex. Hence, 53BP1 self-interaction is not limited to DNA-damage induced chromatin associations, likely constituting dynamic multimeric structures in the nucleoplasm in steady-state cellular conditions.

Collectively, my data reveal a 53BP1 multiunit complex that presents a particular requirement for Tudor and BRCT domains to foster dual interactions with USP28 and p53, and further provide a solid base for future structural approaches.

7.2 USP28 and the ubiquitin-dependent regulation of p53 responses

The definition of the functional relevance of USP28 in p53 responses shed some light in the controversy surrounding USP28-53BP1 association [86,87]. USP28 acts alongside 53BP1 in regulation of p53-dependent transcription (Fig. 4.4, 4.5), a process independent of DNA damage and 53BP1's NHEJ activities. This new role for USP28 explains the functional relationship between USP28 and p53, and the absence of NHEJ-related phenotypes in *Usp28*$^{-/-}$ mice [86,87]. USP28's catalytic activity is an absolute requirement for p53 modulation, functionally defining the USP28-53BP1 complex as a regulatory node of ubiquitin-dependent events (Fig. 4.6). 53BP1 and USP28 both possess ubiquitin-binding motifs but curiously, all of them remain dispensable for the complex

activity (Fig. 3.6, 4.6). Structure-function analyses in USP28 to determine additional sequences involved in p53 responses has proven extremely challenging. Nonetheless, using the divergence between paralogs, USP28 and USP25 [86,253], as a tool, I have defined the environment surrounding the catalytic cysteine as the region that generates USP28's functional uniqueness in p53 responses (Fig. 4.8). Remarkably, the functional diversification is not complete, and USP25 retains residual activity in enhancing p53-dependent responses, presumably caused by a reduction, but not complete loss, of the interaction with 53BP1.

Mechanistically, USP28 has been reported to deubiquitinate p53 *in vitro* and ectopic expression of USP28 to affect p53 stability *via* 53BP1 [275]. However, stability of bulk p53 protein and additionally, p53 subcellular localisation, remains largely unaffected by USP28 and 53BP1 status in the cellular system used (Fig. 5.1, 5.2). Intriguingly, I observed increased stability of modified p53 forms in presence of USP28 and 53BP1 (Fig. 5.1). These forms are likely to encompass mono and di-ubiquitination events, and having considered p53 as the main potential target of the USP28-53BP1 module, one could hypothesise that mono and di-ubiquitination are activating marks on p53, and the USP28-53BP1 complex interferes directly and specifically with the stability of those ubiquitinated forms. Overexpression of ubiquitin mutants with inability to form poly-ubiquitin chains in our cellular model could potentially interfere with the ability of USP28-53BP1 complexes to specifically counteract p53 polyubiquitination and shed light into the mechanism behind the action of this regulatory node.

The concept of mono-ubiquitination in facilitating p53 function has been recently suggested [271]. Deposit of ubiquitin moieties in lysines in p53's DBD

(K292, K164) potentially enhances DNA binding [271]. In fact, the USP28-53BP1 module does enhance p53 binding to the responsive elements in the target genes (Fig. 5.4). However, charge-conserving mutations in p53's DBD lysines directed to prevent ubiquitination fail to provide mechanistic evidence of activating ubiquitination events (Fig. 5.6). Instead, diminished p53 binding to DNA correlates with inability to sustain efficient p53 tetramerisation (Fig. 5.7). MDM2-dependent mono-ubiquitination in p53's tetramerisation domain impedes tetramer formation and concomitantly creates a mark for nuclear export [266,270]. Since no major alterations in nuclear export were detected, it remains possible that ubiquitination and de-ubiquitination events outside the tetramerisation domain impact on tetramer integrity and subsequent DNA binding. Despite the thorough study of the p53 protein, substantial knowledge is still missing regarding the physiological relevance of site-specific post-translational modifications. Structural insight on the relative position of USP28 catalytic domain to 53BP1 and p53 will help to define the targeted residues and disentangle the mechanism behind USP28-53BP1 action on p53 tetramerisation and DNA binding.

Our study focuses on the effector end of the USP28-53BP1 module; however, the activation of the complex constitutes a second raising incognita. In MCF-7 cells, the action of the USP28-53BP1 complex over p53 acquires extreme importance. The robust reliance on the USP28-53BP1-p53 axis to drive N3-mediated cellular toxicity is common to other cellular systems, as CH12F3-2 B cells and BJ fibroblasts [251,273], but absolutely absent in others like HCT116, A549, and RPE-1 cell lines (Fig. 6.1 and data not shown). Alterations in complementary pathways, e.g. aberrant activity of the putative E3-E4 ubiquitin ligases, can lead to the constitutive activation of the USP28-53BP1 module in

order to counteract a prominent inhibitory signal to p53 functionality. RPE-1 cells, that are capable of promoting N3-mediated arrest independently of USP28 and 53BP1, require nonetheless the USP28-53BP1-p53 axis to induce cellular arrest in response to mitotic stresses (Fig. 6.2) [274-276]. Primary MEFs and B cells show similar dependence on 53BP1-dependent p53 modulation to exert surveillance of mitotic defects (Fig. 6.8, 6.9), suggesting this specific contextualisation to be extensive to an *in vivo* setting. Molecularly, one could hypothesise that 53BP1's interaction with the spindle assembly checkpoint components (APC/C) [58], and its ability to localise to the kinetochore in mitosis [57,280] could be at the source of aneuploidy detection and trigger the action of the USP28-53BP1-p53 axis. However, the action of the USP28-53BP1-p53 axis is independent of mitotic events like the SAC or mitosis-induced 53BP1's UDR phosphorylation [275,281]. Instead, the complex drives cellular arrest in the G1 phase of the subsequent cell cycle following aberrant mitosis [274-276]. The ultimate cellular response holds similarities with N3 and IR-induced cellular arrest in MCF-7 cells suggesting equivalent effector mechanisms. Furthermore, the constitutive 53BP1-p53 and USP28-53BP1 interactions [87] open the door to a substrate specific regulation downstream of an alternative sensing mechanism: The complex members establish constant dynamic contacts, but cleavage only occurs when the target mark is present.

Collectively, compelling evidence presents the USP28-53BP1 regulatory node as an ultimate effector mechanism driving optimal p53 life-death cell fate decisions. Future studies examining MCF-7 cells' overreliance in this pathway along the connection between the sensing of chromosomal abnormalities and

this effector response in RPE-1 cells could provide a full picture of the regulatory network and enlighten novel mechanistic implications for the p53 biology field.

7.3 The 'separation of function' and the physiological relevance of the USP28-53BP1-p53 axis

In addition to the repair of DNA lesions, the DDR pathways are tightly connected to cellular processes including checkpoint control, replication, transcription, or the regulation of chromatin dynamics. Several proteins from the DDR machinery have been reported to integrate multiple, distinct functionalities; for instance, HR-driven DSB repair and replication fork protection are independent functions integrated in the BRCA2 protein [282], and similarly occurs with REV7's coordination of intercrosslink repair and NHEJ-directed DSB repair [97]. Here, I describe 53BP1 as a 'dual-function' protein by defining its novel role in p53 modulation and proving this to be distinct and separable of its well-described NHEJ activities.

While the study of 53BP1-driven NHEJ and its relevance to the biology of the immune system has experienced advances over the last two decades, we are only now starting to fathom the potential of 53BP1-mediated p53 regulation. Prior analyses of the 53BP1-p53 connection unravelled a synergistic relationship in tumour suppression: Absence of p53-dependent checkpoint controls allows cellular progression in the presence of high levels of genomic instability generated by loss of 53BP1-driven NHEJ [237,238]. In addition to this synergistic relationship, I provide evidence for cooperation between 53BP1 and p53 in the downstream control of genome integrity. Particularly, 53BP1 and USP28 promote efficient p53-mediated G1 cellular arrest upon detection of chromosomal

misegregations, constituting a surveillance mechanism for mitotic defects (Fig. 6.8, 6.9) [274-276]. Aberrancies in chromosomal segregation generated by centriole dysfunction result in two prominent phenotypical manifestations: microcephaly, and deficient male gametogenesis [283]. In both cases, p53-dependent apoptotic events aiming to eliminate genomically aberrant cells in such sensitive contexts, brain and gametes, are at the source of massive cellular loss and the subsequent developmental problems; accordingly, concomitant p53 loss is able to restore normal brain size [283]. In line with these observations, *p53*$^{-/-}$ mice present higher percentage of abnormal sperm cells, directly reflecting a loss in the quality control mechanism [284]. Considering the remarkable relevance of USP28-53BP1 complexes in regulating p53-dependent mitotic surveillance upon induction of centrosomal abnormalities [274-276], *53bp1*$^{-/-}$ and *Usp28*$^{-/-}$ deficient mice could potentially present elevated levels of sperm cells harbouring aberrant chromosome numbers. In fact, 53BP1 deficiency does not result in male sterility, but homozygous *53bp1*$^{-/-}$ crosses produce reduced litters compared to their *wt* counterparts [96]. Therefore, the analysis of testes development and sperm quality in the separation of function mice constitutes an ideal first step in the physiological contextualisation of 53BP1's contribution in p53 responses.

Additionally, in light of this newly described dual functionality, 53BP1's tumour suppressor role should be revisited in order to define the individual contribution of NHEJ-driven repair and modulation of p53 responses. *53bp1*$^{-/-}$ mice develop late onset tumours at low frequency [96,237]. This phenotypic manifestation contrasted dramatically with the reported enhanced basal aneuploidy in *53bp1*$^{-/-}$ splenocytes (~40%), that would initially suggest a marked

tendency to tumour development [237]. Conversely, I report comparable chromosomal dosage in unstressed *wt*, *53bp1*$^{-/-}$ and *L1616A* and *NDRR* splenic cell populations (Fig. 6.9A). However, inhibition of PLK4 evidences the deficiencies in mitotic surveillance in absence of 53BP1-dependent p53 regulation, reflected in pronounced ploidy increases (Fig. 6.9). Thus, the loss of 53BP1-p53 connections, while not being a driver of malignancies, may act as an ultimate enabling factor for the progression of premalignant conditions. In this line, MCF-7 cells present an overreliance on 53BP1 activity to achieve optimal p53 functionality that is shared in CH12-F3 cells and BJ fibroblasts, suggesting the presence of a common genetic occurrence likely to be extensive to other cell types. It remains thus possible that specific tissues are particularly sensitive to succumb to premalignant conditions, such as oncogene-driven tumourigenesis (RAS), due loss of 53BP1-dependent p53 regulation.

The mechanistic characterisation of 53BP1's impact on p53 responses reveals a consistent 2-fold reduction in the induction of p53-transactivation events in *53BP1Δ* cells upon N3 and IR treatments compared to the *WT* counterparts (Fig. 3.4). In light of these data, loss of 53BP1 could potentially mimic a loss of p53 dosage, or haploinsufficiency, with the consequent implications in cellular physiology. Particularly interesting towards 53BP1 separation of function studies is the effect of p53 haploinsufficiency in *Brca1*$^{\Delta 11/\Delta 11}$ mice. Deletion of the exon 11 of the *BRCA1* gene results in embryonic lethality in mice, and specific deletion in the mammary gland causes ductal development and late onset tumour formation [285,286]. Monoallelic loss of p53 in this context rescues both embryonic development and normal ductal gland development, but results in premature aging and mammary tumourigenesis

[286,287]. *Brca1*$^{\Delta 11/\Delta 11}$ combined with biallelic loss of 53BP1, however, presents complete *wt* behaviour, presumably by restoration of homologous recombination [113,287]. Exploring whether the *NDRR* and *L1616A* separation of function mutants here characterised can recapitulate p53 haploinsufficiency and 53BP1 loss, respectively, will provide further insight into the biology of 53BP1 functionalities and its relevance in different cellular contexts.

Collectively, I set here the basis for the determination of the physiological and pathological implications of 53BP1-dependent p53 quality control that will converge with the established 53BP1-driven NHEJ activities to ultimately define 53BP1 as an integral node in the preservation of genomic stability.

7.4 Conclusions and proposed model

- 53BP1 and USP28 cooperate to enhance p53-dependent transcriptional programmes in response to different stress stimuli.
- Oligomerised 53BP1 relies on its tandem BRCT domain to establish dual interactions with p53 and USP28 that are essential for ultimate p53 modulation.
- Structurally, USP28-53BP1 interaction requires 53BP1's tandem Tudor-tandem BRCT modules and presents remarkable non-canonical binding dynamics.
- Mechanistically, 53BP1 and USP28 regulate ubiquitin-dependent events that ultimately result in optimal p53 binding to the responsive elements in the target genes.

- 53BP1 requires distinct domains and interaction partners to undertake NHEJ and p53 modulation, and these activities can be separated at the level of point mutations within 53BP1 architecture.
- 53BP1's role in the immune system relies exclusively on its NHEJ activities, while 53BP1-dependent p53 modulation appears essential in the control of chromosomal misegregations upon centrosomal abnormalities.

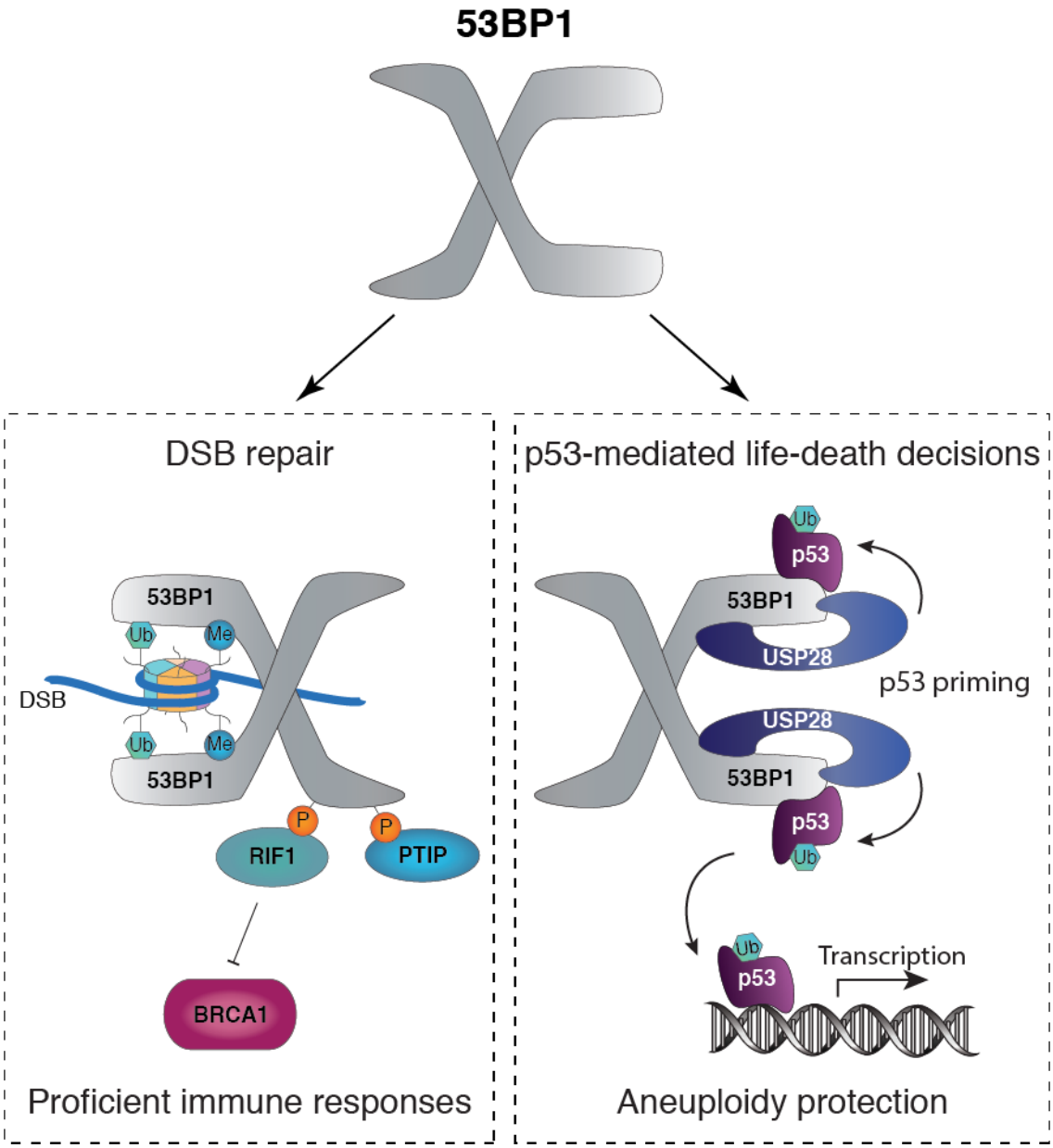


Figure 7.2. Proposed model of 53BP1 functionality as a hub of genome stability control. 53BP1 drives DSB repair *via* NHEJ, whose intact action is crucial for proficient immune responses. Additionally, 53BP1 and USP28 cooperate to modulate p53 transactivation events and ultimately regulate p53-dependent life-death cell fate decisions. The physiological relevance of this pathway is reflected in the protection against chromosomal misegregations upon centrosomal abnormalities.

Chapter 8

REFERENCES

1. Cuella-Martin R, Oliveira C, Lockstone HE, Snellenberg S, Grolmusova N, Chapman JR. 53BP1 Integrates DNA Repair and p53-Dependent Cell Fate Decisions via Distinct Mechanisms. Mol Cell 2016;64:51–64.

2. Khanna KK, Jackson SP. DNA double-strand breaks: signaling, repair and the cancer connection. Nat Genet 2001;27:247–54.

3. Jackson SP, Bartek J. The DNA-damage response in human biology and disease. Nature 2009;461:1071–8.

4. McKinnon PJ. DNA repair deficiency and neurological disease. Nat Rev Neurosci 2009;10:100–12.

5. Pannunzio NR, Watanabe G, Lieber MR. Nonhomologous DNA End Joining for Repair of DNA Double-Strand Breaks. J Biol Chem 2017;:jbc.TM117.000374.

6. Jasin M, Rothstein R. Repair of strand breaks by homologous recombination. Cold Spring Harb Perspect Med 2013;5:a012740–0.

7. Lee J-H, Paull TT. ATM activation by DNA double-strand breaks through the Mre11-Rad50-Nbs1 complex. Science 2005;308:551–4.

8. Williams RS, Williams JS, Tainer JA. Mre11–Rad50–Nbs1 is a keystone complex connecting DNA repair machinery, double-strand break signaling, and the chromatin template. Biochem Cell Biol 2007;85:509–20.

9. Maréchal A, Zou L. DNA damage sensing by the ATM and ATR kinases. Cold Spring Harb Perspect Med 2013;5:a012716–6.

10. Rogakou EP, Pilch DR, Orr AH, Ivanova VS, Bonner WM. DNA Double-stranded Breaks Induce Histone H2AX Phosphorylation on Serine 139. J Biol Chem 1998;273:5858–68.

11. Meier A, Fiegler H, Muñoz P, Ellis P, Rigler D, Langford C, et al. Spreading of mammalian DNA-damage response factors studied by ChIP-chip at damaged telomeres. EMBO J 2007;26:2707–18.

12. Stucki M, Clapperton JA, Mohammad D, Yaffe MB, Smerdon SJ, Jackson SP. MDC1 Directly Binds Phosphorylated Histone H2AX to Regulate Cellular Responses to DNA Double-Strand Breaks. Cell 2005;123:1213–26.

13. Chapman JR, Jackson SP. Phospho-dependent interactions between

NBS1 and MDC1 mediate chromatin retention of the MRN complex at sites of DNA damage. EMBO Rep 2008;9:795–801.

14. Savic V, Yin B, Maas NL, Bredemeyer AL, Carpenter AC, Helmink BA, et al. Formation of Dynamic γ-H2AX Domains along Broken DNA Strands Is Distinctly Regulated by ATM and MDC1 and Dependent upon H2AX Densities in Chromatin. Mol Cell 2009;34:298–310.

15. Panier S, Boulton SJ. Double-strand break repair: 53BP1 comes into focus. Nat Rev Mol Cell Biol 2013;15:7–18.

16. Kolas NK, Chapman JR, Nakada S, Ylanko J, Chahwan R, Sweeney FD, et al. Orchestration of the DNA-Damage Response by the RNF8 Ubiquitin Ligase. Science 2007;318:1637–40.

17. Mailand N, Bekker-Jensen S, Faustrup H, Melander F, Bartek J, Lukas C, et al. RNF8 Ubiquitylates Histones at DNA Double-Strand Breaks and Promotes Assembly of Repair Proteins. Cell 2007;131:887–900.

18. Huen MSY, Grant R, Manke I, Minn K, Yu X, Yaffe MB, et al. RNF8 Transduces the DNA-Damage Signal via Histone Ubiquitylation and Checkpoint Protein Assembly. Cell 2007;131:901–14.

19. Thorslund T, Ripplinger A, Hoffmann S, Wild T, Uckelmann M, Villumsen B, et al. Histone H1 couples initiation and amplification of ubiquitin signalling after DNA damage. Nature 2015;527:389–93.

20. Mattiroli F, Vissers JHA, van Dijk WJ, Ikpa P, Citterio E, Vermeulen W, et al. RNF168 Ubiquitinates K13-15 on H2A/H2AX to Drive DNA Damage Signaling. Cell 2012;150:1182–95.

21. Doil C, Mailand N, Bekker-Jensen S, Menard P, Larsen DH, Pepperkok R, et al. RNF168 Binds and Amplifies Ubiquitin Conjugates on Damaged Chromosomes to Allow Accumulation of Repair Proteins. Cell 2009;136:435–46.

22. Stewart GS, Panier S, Townsend K, Al-Hakim AK, Kolas NK, Miller ES, et al. The RIDDLE Syndrome Protein Mediates a Ubiquitin-Dependent Signaling Cascade at Sites of DNA Damage. Cell 2009;136:420–34.

23. Botuyan MV, Lee J, Ward IM, Kim J-E, Thompson JR, Chen J, et al. Structural Basis for the Methylation State-Specific Recognition of Histone H4-K20 by 53BP1 and Crb2 in DNA Repair. Cell 2006;127:1361–73.

24. Fradet-Turcotte A, Canny MD, Escribano-Díaz C, Orthwein A, Leung CCY, Huang H, et al. 53BP1 is a reader of the DNA-damage-induced H2A Lys 15 ubiquitin mark. Nature 2013;499:50–4.

25. Wang B, Matsuoka S, Ballif BA, Zhang D, Smogorzewska A, Gygi SP, et al. Abraxas and RAP80 Form a BRCA1 Protein Complex Required for the DNA Damage Response. Science 2007;316:1194–8.

26. Sobhian B, Shao G, Lilli DR, Culhane AC, Moreau LA, Xia B, et al. RAP80 targets BRCA1 to specific ubiquitin structures at DNA damage sites. Science 2007;316:1198–202.

27. Kim H, Chen J, Yu X. Ubiquitin-binding protein RAP80 mediates BRCA1-dependent DNA damage response. Science 2007;316:1202–5.

28. Hu Y, Scully R, Sobhian B, Xie A, Shestakova E, Livingston DM. RAP80-directed tuning of BRCA1 homologous recombination function at ionizing radiation-induced nuclear foci. Genes Dev 2011;25:685–700.

29. Chapman JR, Sossick AJ, Boulton SJ, Jackson SP. BRCA1-associated exclusion of 53BP1 from DNA damage sites underlies temporal control of DNA repair. J Cell Sci 2012;125:3529–34.

30. Chapman JR, Taylor MRG, Boulton SJ. Playing the End Game: DNA Double-Strand Break Repair Pathway Choice. Mol Cell 2012;47:497–510.

31. Anand R, Ranjha L, Cannavo E, Cejka P. Phosphorylated CtIP Functions as a Co-factor of the MRE11-RAD50-NBS1 Endonuclease in DNA End Resection. Mol Cell 2016;64:940–50.

32. Harper JW, Adami GR, Wei N, Keyomarsi K, Elledge SJ. The p21 Cdk-interacting protein Cip1 is a potent inhibitor of G1 cyclin-dependent kinases. Cell 1993;75:805–16.

33. Xiong Y, Hannon GJ, Zhang H, Casso D, Kobayashi R, Beach D. p21 is a universal inhibitor of cyclin kinases. Nature 1993;366:701–4.

34. Waga S, Hannon GJ, Beach D, Stillman B. The p21 inhibitor of cyclin-dependent kinases controls DNA replication by interaction with PCNA. Nature 1994;369:574–8.

35. Li R, Waga S, Hannon GJ, Beach D, Stillman B. Differential effects by the p21 CDK inhibitor on PCNA-dependent DNA replication and repair. Nature 1994;371:534–7.

36. Fridman JS, Lowe SW. Control of apoptosis by p53. Oncogene 2003;22:9030–40.

37. Gudkov AV, Komarova EA. The role of p53 in determining sensitivity to radiotherapy. Nat Rev Cancer 2003;3:117–29.

38. Meek DW. The p53 response to DNA damage. DNA Repair (Amst) 2004;3:1049–56.

39. Lowe SW, Schmitt EM, Smith SW, Osborne BA, Jacks T. p53 is required for radiation-induced apoptosis in mouse thymocytes. Nature 1993;362:847–9.

40. Hanahan D, Weinberg RA. Hallmarks of Cancer: The Next Generation. Cell 2011;144:646–74.

41. Iwabuchi K, Bartel PL, Li B, Marraccino R, Fields S. Two cellular proteins that bind to wild-type but not mutant p53. Proc Natl Acad Sci U S A 1994;91:6098–102.

42. Schultz LB, Chehab NH, Malikzay A, Halazonetis TD. p53 binding protein 1 (53BP1) is an early participant in the cellular response to DNA double-strand breaks. J Cell Biol 2000;151:1381–90.

43. Adams MM, Carpenter PB. Tying the loose ends together in DNA double strand break repair with 53BP1. Cell Div 2006;1:19–13.

44. Harrison JC, Haber JE. Surviving the Breakup: The DNA Damage Checkpoint. Annu Rev Genet 2006;40:209–35.

45. Jowsey P, Morrice NA, Hastie CJ, McLauchlan H, Toth R, Rouse J. Characterisation of the sites of DNA damage-induced 53BP1 phosphorylation catalysed by ATM and ATR. DNA Repair (Amst) 2007;6:1536–44.

46. Matsuoka S, Ballif BA, Smogorzewska A, McDonald ER, Hurov KE, Luo J, et al. ATM and ATR substrate analysis reveals extensive protein networks responsive to DNA damage. Science 2007;316:1160–6.

47. Munoz IM, Jowsey PA, Toth R, Rouse J. Phospho-epitope binding by the BRCT domains of hPTIP controls multiple aspects of the cellular response to DNA damage. Nucleic Acids Res 2007;35:5312–22.

48. Callen E, Di Virgilio M, Kruhlak MJ, Nieto-Soler M, Wong N, Chen H-T, et al. 53BP1 mediates productive and mutagenic DNA repair through distinct phosphoprotein interactions. Cell 2013;153:1266–80.

49. Chapman JR, Barral P, Vannier J-B, Borel V, Steger M, Tomas-Loba A, et al. RIF1 Is Essential for 53BP1-Dependent Nonhomologous End Joining and Suppression of DNA Double-Strand Break Resection. Mol Cell 2013;49:858–71.

50. Zimmermann M, Lottersberger F, Buonomo SB, Sfeir A, de Lange T. 53BP1 regulates DSB repair using Rif1 to control 5' end resection. Science 2013;339:700–4.

51. Di Virgilio M, Callen E, Yamane A, Zhang W, Jankovic M, Gitlin AD, et al. Rif1 prevents resection of DNA breaks and promotes immunoglobulin class switching. Science 2013;339:711–5.

52. Boersma V, Moatti N, Segura-Bayona S, Peuscher MH, van der Torre J, Wevers BA, et al. MAD2L2 controls DNA repair at telomeres and DNA breaks by inhibiting 5' end resection. Nature 2015;521:537–40.

53. Xu G, Chapman JR, Brandsma I, Yuan J, Mistrik M, Bouwman P, et al. REV7 counteracts DNA double-strand break resection and affects PARP inhibition. Nature 2015;521:541–4.

54. Linding R, Jensen LJ, Ostheimer GJ, van Vugt MATM, Jørgensen C, Miron IM, et al. Systematic Discovery of In Vivo Phosphorylation Networks. Cell 2007;129:1415–26.

55. Dephoure N, Zhou C, Villén J, Beausoleil SA, Bakalarski CE, Elledge SJ, et al. A quantitative atlas of mitotic phosphorylation. Proc Natl Acad Sci U S A 2008;105:10762–7.

56. van Vugt MATM, Gardino AK, Linding R, Ostheimer GJ, Reinhardt HC, Ong S-E, et al. A mitotic phosphorylation feedback network connects Cdk1, Plk1, 53BP1, and Chk2 to inactivate the G(2)/M DNA damage checkpoint. PLoS Biol 2010;8:e1000287.

57. Benada J, Burdova K, Lidak T, Morgen von P, Macurek L. Polo-like kinase 1 inhibits DNA damage response during mitosis. Cell Cycle 2015;14:219–31.

58. Kucharski TJ, Minshall PE, Moustafa-Kamal M, Turnell AS, Teodoro JG. Reciprocal Regulation between 53BP1 and the Anaphase-Promoting Complex/Cyclosome Is Required for Genomic Stability during Mitotic Stress. Cell Rep 2017;18:1982–95.

59. Lottersberger F, Bothmer A, Robbiani DF, Nussenzweig MC, de Lange T. Role of 53BP1 oligomerization in regulating double-strand break repair. Proc Natl Acad Sci U S A 2013;110:2146–51.

60. Becker JR, Cuella-Martin R, Barazas M, Oliveira C, Liu R, Oliver AW, et al. DYNLL1 promotes non-homologous end joining by enforcing 53BP1 oligomerization. 2018;unpublished.

61. Adams MM, Wang B, Xia Z, Morales JC, Lu X, Donehower LA, et al. 53BP1 oligomerization is independent of its methylation by PRMT1. Cell Cycle 2005;4:1854–61.

62. Zgheib O, Pataky K, Brugger J, Halazonetis TD. An Oligomerized 53BP1 Tudor Domain Suffices for Recognition of DNA Double-Strand Breaks. Mol Cell Biol 2009;29:1050–8.

63. Bothmer A, Robbiani DF, Di Virgilio M, Bunting SF, Klein IA, Feldhahn N, et al. Regulation of DNA End Joining, Resection, and Immunoglobulin Class Switch Recombination by 53BP1. Mol Cell 2011;42:319–29.

64. Charier G, Couprie J, Alpha-Bazin B, Meyer V, Quéméneur E, Guérois R, et al. The Tudor Tandem of 53BP1. Structure 2004;12:1551–62.

65. Huyen Y, Zgheib O, Ditullio RA, Gorgoulis VG, Zacharatos P, Petty TJ, et al. Methylated lysine 79 of histone H3 targets 53BP1 to DNA double-strand breaks. Nature 2004;432:406–11.

66. Shi X, Kachirskaia I, Yamaguchi H, West LE, Wen H, Wang EW, et al. Modulation of p53 Function by SET8-Mediated Methylation at Lysine 382. Mol Cell 2007;27:636–46.

67. Carr SM, Munro S, Zalmas LP, Fedorov O, Johansson C, Krojer T, et al. Lysine methylation-dependent binding of 53BP1 to the pRb tumor suppressor. Proc Natl Acad Sci U S A 2014;111:11341–6.

68. Tong Q, Cui G, Botuyan MV, Rothbart SB, Hayashi R, Musselman CA, et al. Structural plasticity of methyllysine recognition by the tandem tudor domain of 53BP1. Structure 2015;23:312–21.

69. Drané P, Brault M-E, Cui G, Meghani K, Chaubey S, Detappe A, et al. TIRR regulates 53BP1 by masking its histone methyl-lysine binding function. Nature 2017;543:211–6.

70. Beck DB, Oda H, Shen SS, Reinberg D. PR-Set7 and H4K20me1: at the crossroads of genome integrity, cell cycle, chromosome condensation, and transcription. Genes Dev 2012;26:325–37.

71. Schotta G, Sengupta R, Kubicek S, Malin S, Kauer M, Callen E, et al. A chromatin-wide transition to H4K20 monomethylation impairs genome integrity and programmed DNA rearrangements in the mouse. Genes Dev 2008;22:2048–61.

72. Pellegrino S, Michelena J, Teloni F, Imhof R, Altmeyer M. Replication-Coupled Dilution of H4K20me2 Guides 53BP1 to Pre-replicative Chromatin. Cell Rep 2017;19:1819–31.

73. Carr SM, Munro S, Kessler B, Oppermann U, La Thangue NB. Interplay between lysine methylation and Cdk phosphorylation in growth control by the retinoblastoma protein. EMBO J 2010;30:317–27.

74. Wilson MD, Benlekbir S, Fradet-Turcotte A, Sherker A, Julien J-P, McEwan A, et al. The structural basis of modified nucleosome recognition by 53BP1. Nature 2016;536:100–3.

75. Manke IA. BRCT Repeats As Phosphopeptide-Binding Modules Involved in Protein Targeting. Science 2003;302:636–9.

76. Leung CCY, Glover JNM. BRCT domains. Cell Cycle 2014;10:2461–70.

77. Zhang X, Moréra S, Bates PA, Whitehead PC, Coffer AI, Hainbucher K, et al. Structure of an XRCC1 BRCT domain: a new protein-protein interaction module. EMBO J 1998;17:6404–11.

78. Joo WS, Jeffrey PD, Cantor SB, Finnin MS, Livingston DM, Pavletich NP. Structure of the 53BP1 BRCT region bound to p53 and its comparison to the Brca1 BRCT structure. Genes Dev 2002;16:583–93.

79. Gerloff DL, Woods NT, Farago AA, Monteiro ANA. BRCT domains: A little more than kin, and less than kind. FEBS Lett 2012;586:2711–6.

80. Morales JC, Xia Z, Lu T, Aldrich MB, Wang B, Rosales C, et al. Role for the BRCA1 C-terminal repeats (BRCT) protein 53BP1 in maintaining genomic stability. J Biol Chem 2003;278:14971–7.

81. Nakamura TM, Du LL, Redon C, Russell P. Histone H2A Phosphorylation Controls Crb2 Recruitment at DNA Breaks, Maintains Checkpoint Arrest, and Influences DNA Repair in Fission Yeast. Mol Cell Biol 2004;24:6215–30.

82. Hammet A, Magill C, Heierhorst J, Jackson SP. Rad9 BRCT domain interaction with phosphorylated H2AX regulates the G1 checkpoint in budding yeast. EMBO Rep 2007;8:851–7.

83. Baldock RA, Day M, Wilkinson OJ, Cloney R, Jeggo PA, Oliver AW, et al. ATM Localization and Heterochromatin Repair Depend on Direct Interaction of the 53BP1-BRCT2 Domain with γH2AX. Cell Rep 2015;13:2081–9.

84. Kleiner RE, Verma P, Molloy KR, Chait BT, Kapoor TM. Chemical proteomics reveals a γH2AX-53BP1 interaction in the DNA damage response. Nat Chem Biol 2015;11:807–14.

85. Huen MSY, Huang J, Leung JWC, Sy SMH, Leung KM, Ching Y-P, et al. Regulation of Chromatin Architecture by the PWWP Domain-Containing DNA Damage-Responsive Factor EXPAND1/MUM1. Mol Cell 2010;37:854–64.

86. Zhang D, Zaugg K, Mak TW, Elledge SJ. A Role for the Deubiquitinating Enzyme USP28 in Control of the DNA-Damage Response. Cell 2006;126:529–42.

87. Knobel PA, Belotserkovskaya R, Galanty Y, Schmidt CK, Jackson SP, Stracker TH. USP28 Is Recruited to Sites of DNA Damage by the Tandem BRCT Domains of 53BP1 but Plays a Minor Role in Double-Strand Break Metabolism. Mol Cell Biol 2014;34:2062–74.

88. Bassing CH, Swat W, Alt FW. The mechanism and regulation of chromosomal V(D)J recombination. Cell 2002;109 Suppl:S45–55.

89. Oettinger M, Schatz D, Gorka C, Baltimore D. RAG-1 and RAG-2, adjacent genes that synergistically activate V(D)J recombination. Science 1990;248:1517–23.

90. Hardy RR, Hayakawa K. B Cell Development Pathways. Annu Rev Immunol 2001;19:595–621.

91. Mårtensson I-L, Almqvist N, Grimsholm O, Bernardi AI. The pre-B cell receptor checkpoint. FEBS Lett 2010;584:2572–9.

92. Boehmer von H, Melchers F. Checkpoints in lymphocyte development and autoimmune disease. Nat Immunol 2010;11:14–20.

93. Schatz DG, Ji Y. Recombination centres and the orchestration of V(D)J recombination. Nat Rev Immunol 2011;11:251–63.

94. Ma Y, Pannicke U, Schwarz K, Lieber MR. Hairpin Opening and

Overhang Processing by an Artemis/DNA-Dependent Protein Kinase Complex in Nonhomologous End Joining and V(D)J Recombination. Cell 2002;108:781–94.

95. Difilippantonio S, Gapud E, Wong N, Huang C-Y, Mahowald G, Chen H-T, et al. 53BP1 facilitates long-range DNA end-joining during V(D)J recombination. Nature 2008;456:529–33.

96. Ward IM, Minn K, van Deursen J, Chen J. p53 Binding Protein 53BP1 Is Required for DNA Damage Responses and Tumor Suppression in Mice. Mol Cell Biol 2003;23:2556–63.

97. Ghezraoui H, Oliveira C, Becker JR, Bilham K, Moralli D, Anzilotti C, et al. 53BP1 cooperation with the Rev7-Shieldin complex underpins DNA structure-specific NHEJ. Nature 2018; in press.

98. Dimitrova N, Chen Y-CM, Spector DL, de Lange T. 53BP1 promotes non-homologous end joining of telomeres by increasing chromatin mobility. Nature 2008;456:524–8.

99. Lottersberger F, Karssemeijer RA, Dimitrova N, de Lange T. 53BP1 and the LINC Complex Promote Microtubule-Dependent DSB Mobility and DNA Repair. Cell 2015;163:880–93.

100. Stavnezer J, Guikema JEJ, Schrader CE. Mechanism and Regulation of Class Switch Recombination. Annu Rev Immunol 2008;26:261–92.

101. Soulas-Sprauel P, Rivera-Munoz P, Malivert L, Le Guyader G, Abramowski V, Revy P, et al. V(D)J and immunoglobulin class switch recombinations: a paradigm to study the regulation of DNA end-joining. Oncogene 2007;26:7780–91.

102. Chaudhuri J, Tian M, Khuong C, Chua K, Pinaud E, Alt FW. Transcription-targeted DNA deamination by the AID antibody diversification enzyme. Nature 2003;422:726–30.

103. Bregenhorn S, Kallenberger L, Artola-Borán M, Peña-Diaz J, Jiricny J. Non-canonical uracil processing in DNA gives rise to double-strand breaks and deletions: relevance to class switch recombination. Nucleic Acids Res 2016;44:2691–705.

104. Ward IM, Reina-San-Martin B, Olaru A, Minn K, Tamada K, Lau JS, et al. 53BP1 is required for class switch recombination. J Cell Biol 2004;165:459–64.

105. Manis JP, Morales JC, Xia Z, Kutok JL, Alt FW, Carpenter PB. 53BP1 links DNA damage-response pathways to immunoglobulin heavy chain class-switch recombination. Nat Immunol 2004;5:481–7.

106. Yan CT, Boboila C, Souza EK, Franco S, Hickernell TR, Murphy M, et al. IgH class switching and translocations use a robust non-classical end-joining pathway. Nature 2007;449:478–82.

107. Boboila C, Yan C, Wesemann DR, Jankovic M, Wang JH, Manis J, et al. Alternative end-joining catalyzes class switch recombination in the absence of both Ku70 and DNA ligase 4. J Exp Med 2010;207:417–27.

108. Boboila C, Jankovic M, Yan CT, Wang JH, Wesemann DR, Zhang T, et al. Alternative end-joining catalyzes robust IgH locus deletions and translocations in the combined absence of ligase 4 and Ku70. Proc Natl Acad Sci U S A 2010;107:3034–9.

109. Reina-San-Martin B, Chen J, Nussenzweig A, Nussenzweig MC. Enhanced intra-switch region recombination during immunoglobulin class switch recombination in 53BP1–/– B cells. Eur J Immunol 2007;37:235–9.

110. Gupta R, Somyajit K, Narita T, Maskey E, Stanlie A, Kremer M, et al. DNA Repair Network Analysis Reveals Shieldin as a Key Regulator of NHEJ and PARP Inhibitor Sensitivity. Cell 2018;173:972–988.e23.

111. Scully R, Livingston DM. In search of the tumour-suppressor functions of BRCA1 and BRCA2. Nature 2000;408:429–32.

112. Cavanagh H, Rogers KMA. The role of BRCA1 and BRCA2 mutations in prostate, pancreatic and stomach cancers. Hered Cancer Clin Pract 2015;13:16.

113. Bunting SF, Callen E, Wong N, Chen H-T, Polato F, Gunn A, et al. 53BP1 inhibits homologous recombination in Brca1-deficient cells by blocking resection of DNA breaks. Cell 2010;141:243–54.

114. Bouwman P, Aly A, Escandell JM, Pieterse M, Bartkova J, van der Gulden H, et al. 53BP1 loss rescues BRCA1 deficiency and is associated with triple-negative and BRCA-mutated breast cancers. Nat Struct Mol Biol 2010;17:688–95.

115. Farmer H, McCabe N, Lord CJ, Tutt ANJ, Johnson DA, Richardson TB, et al. Targeting the DNA repair defect in BRCA mutant cells as a therapeutic strategy. Nature 2005;434:917–21.

116. Kress M, May E, Cassingena R, May P. Simian virus 40-transformed cells express new species of proteins precipitable by anti-simian virus 40 tumor serum. J Virol 1979;31:472–83.

117. Linzer DIH, Levine AJ. Characterization of a 54K Dalton cellular SV40 tumor antigen present in SV40-transformed cells and uninfected embryonal carcinoma cells. Cell 1979;17:43–52.

118. DeLeo AB, Jay G, Appella E, Dubois GC, Law LW, Old LJ. Detection of a transformation-related antigen in chemically induced sarcomas and other transformed cells of the mouse. Proc Natl Acad Sci U S A 1979;76:2420–4.

119. Lane DP. p53, guardian of the genome. Nature 1992;358:15–6.

120. Joerger AC, Fersht AR. Structural biology of the tumor suppressor p53. Annu Rev Biochem 2008;77:557–82.

121. Candau R, Scolnick DM, Darpino P, Ying CY, Halazonetis TD, Berger SL. Two tandem and independent sub-activation domains in the amino terminus of p53 require the adaptor complex for activity. Oncogene 1997;15:807–16.

122. Walker KK, Levine AJ. Identification of a novel p53 functional domain that is necessary for efficient growth suppression. Proc Natl Acad Sci U S A 1996;93:15335–40.

123. Momand J, Zambetti GP, Olson DC, George D, Levine AJ. The mdm-2 oncogene product forms a complex with the p53 protein and inhibits p53-mediated transactivation. Cell 1992;69:1237–45.

124. Shvarts A, Steegenga WT, Riteco N, van Laar T, Dekker P, Bazuine M, et al. MDMX: a novel p53-binding protein with some functional properties of MDM2. EMBO J 1996;15:5349–57.

125. Gu W, Shi X-L, Roeder RG. Synergistic activation of transcription by CBP and p53. Nature 1997;387:819–23.

126. Di Lello P, Jenkins LMM, Jones TN, Nguyen BD, Hara T, Yamaguchi H, et al. Structure of the Tfb1/p53 Complex: Insights into the Interaction between the p62/Tfb1 Subunit of TFIIH and the Activation Domain of p53. Mol Cell 2006;22:731–40.

127. Kubbutat MH, Jones SN, Vousden KH. Regulation of p53 stability by Mdm2. Nature 1997;387:299–303.

128. Haupt Y, Maya R, Kazaz A, Oren M. Mdm2 promotes the rapid degradation of p53. Nature 1997;387:296–9.

129. Jackson MW, Berberich SJ. MdmX protects p53 from Mdm2-mediated degradation. Mol Cell Biol 2000;20:1001–7.

130. Banin S. Enhanced Phosphorylation of p53 by ATM in Response to DNA Damage. Science 1998;281:1674–7.

131. Chehab NH, Malikzay A, Stavridi ES, Halazonetis TD. Phosphorylation of Ser-20 mediates stabilization of human p53 in response to DNA damage. Proc Natl Acad Sci U S A 1999;96:13777–82.

132. Shieh S-Y, Ikeda M, Taya Y, Prives C. DNA Damage-Induced Phosphorylation of p53 Alleviates Inhibition by MDM2. Cell 1997;91:325–34.

133. Lambert PF, Kashanchi F, Radonovich MF, Shiekhattar R, Brady JN. Phosphorylation of p53 Serine 15 Increases Interaction with CBP. J Biol Chem 1998;273:33048–53.

134. Dornan D, Hupp TR. Inhibition of p53‐dependent transcription by BOX‐I phospho‐peptide mimetics that bind to p300. EMBO Rep 2001;2:139–44.

135. Feng H, Jenkins LMM, Durell SR, Hayashi R, Mazur SJ, Cherry S, et al. Structural Basis for p300 Taz2-p53 TAD1 Binding and Modulation by Phosphorylation. Structure 2009;17:202–10.

136. Miller Jenkins LM, Feng H, Durell SR, Tagad HD, Mazur SJ, Tropea JE, et al. Characterization of the p300 Taz2–p53 TAD2 Complex and Comparison with the p300 Taz2–p53 TAD1 Complex. Biochemistry 2015;54:2001–10.

137. Jin Q, Yu L-R, Wang L, Zhang Z, Kasper LH, Lee J-E, et al. Distinct roles of GCN5/PCAF-mediated H3K9ac and CBP/p300-mediated H3K18/27ac in nuclear receptor transactivation. EMBO J 2011;30:249–62.

138. Cho Y, Gorina S, Jeffrey PD, Pavletich NP. Crystal structure of a p53 tumor suppressor-DNA complex: understanding tumorigenic mutations. Science 1994;265:346–55.

139. Bullock AN, Henckel J, Fersht AR. Quantitative analysis of residual folding and DNA binding in mutant p53 core domain: definition of mutant states for rescue in cancer therapy. Oncogene 2000;19:1245–56.

140. El-Deiry WS, Kern SE, Pietenpol JA, Kinzler KW, Vogelstein B. Definition of a consensus binding site for p53. Nat Genet 1992;1:45–9.

141. Kitayner M, Rozenberg H, Kessler N, Rabinovich D, Shaulov L, Haran TE, et al. Structural Basis of DNA Recognition by p53 Tetramers. Mol Cell 2006;22:741–53.

142. Sykes SM, Mellert HS, Holbert MA, Li K, Marmorstein R, Lane WS, et al. Acetylation of the p53 DNA-binding domain regulates apoptosis induction. Mol Cell 2006;24:841–51.

143. Tang Y, Luo J, Zhang W, Gu W. Tip60-dependent acetylation of p53 modulates the decision between cell-cycle arrest and apoptosis. Mol Cell 2006;24:827–39.

144. Tang Y, Zhao W, Chen Y, Zhao Y, Gu W. Acetylation Is Indispensable for p53 Activation. Cell 2008;133:612–26.

145. Li T, Kon N, Jiang L, Tan M, Ludwig T, Zhao Y, et al. Tumor suppression in the absence of p53-mediated cell-cycle arrest, apoptosis, and senescence. Cell 2012;149:1269–83.

146. Jiang L, Kon N, Li T, Wang S-J, Su T, Hibshoosh H, et al. Ferroptosis as a p53-mediated activity during tumour suppression. Nature 2015;520:57–62.

147. Bouaoun L, Sonkin D, Ardin M, Hollstein M, Byrnes G, Zavadil J, et al.

TP53Variations in Human Cancers: New Lessons from the IARC TP53 Database and Genomics Data. Hum Mutat 2016;37:865–76.

148. Tidow H, Melero R, Mylonas E, Freund SMV, Grossmann JG, Carazo JM, et al. Quaternary structures of tumor suppressor p53 and a specific p53 DNA complex. Proc Natl Acad Sci U S A 2007;104:12324–9.

149. Samuels-Lev Y, O'Connor DJ, Bergamaschi D, Trigiante G, Hsieh JK, Zhong S, et al. ASPP proteins specifically stimulate the apoptotic function of p53. Mol Cell 2001;8:781–94.

150. Kraiss S, Quaiser A, Oren M, Montenarh M. Oligomerization of oncoprotein p53. J Virol 1988;62:4737–44.

151. Stenger JE, Mayr GA, Mann K, Tegtmeyer P. Formation of stable p53 homotetramers and multiples of tetramers. Mol Carcinog 1992;5:102–6.

152. Friedman PN, Chen X, Bargonetti J, Prives C. The p53 protein is an unusually shaped tetramer that binds directly to DNA. Proc Natl Acad Sci U S A 1993;90:3319–23.

153. Pavletich NP, Chambers KA, Pabo CO. The DNA-binding domain of p53 contains the four conserved regions and the major mutation hot spots. Genes Dev 1993;7:2556–64.

154. Jeffrey PD, Gorina S, Pavletich NP. Crystal structure of the tetramerization domain of the p53 tumor suppressor at 1.7 angstroms. Science 1995;267:1498–502.

155. Weinberg RL, Veprintsev DB, Fersht AR. Cooperative binding of tetrameric p53 to DNA. J Mol Biol 2004;341:1145–59.

156. Weinberg RL, Freund SMV, Veprintsev DB, Bycroft M, Fersht AR. Regulation of DNA binding of p53 by its C-terminal domain. J Mol Biol 2004;342:801–11.

157. Meek DW, Anderson CW. Posttranslational modification of p53: cooperative integrators of function. Cold Spring Harb Perspect Biol 2009;1:a000950–0.

158. Krummel KA, Lee CJ, Toledo F, Wahl GM. The C-terminal lysines fine-tune P53 stress responses in a mouse model but are not required for stability control or transactivation. Proc Natl Acad Sci U S A 2005;102:10188–93.

159. Feng L, Lin T, Uranishi H, Gu W, Xu Y. Functional analysis of the roles of posttranslational modifications at the p53 C terminus in regulating p53 stability and activity. Mol Cell Biol 2005;25:5389–95.

160. Wang YV, Leblanc M, Fox N, Mao J-H, Tinkum KL, Krummel K, et al. Fine-tuning p53 activity through C-terminal modification significantly contributes to HSC homeostasis and mouse radiosensitivity. Genes Dev

2011;25:1426–38.

161. Kruse J-P, Gu W. Modes of p53 Regulation. Cell 2009;137:609–22.

162. Honda R, Tanaka H, Yasuda H. Oncoprotein MDM2 is a ubiquitin ligase E3 for tumor suppressor p53. FEBS Lett 1997;420:25–7.

163. Shloush J, Vlassov JE, Engson I, Duan S, Saridakis V, Dhe-Paganon S, et al. Structural and functional comparison of the RING domains of two p53 E3 ligases, Mdm2 and Pirh2. J Biol Chem 2011;286:4796–808.

164. Tanimura S, Ohtsuka S, Mitsui K, Shirouzu K, Yoshimura A, Ohtsubo M. MDM2 interacts with MDMX through their RING finger domains. FEBS Lett 1999;447:5–9.

165. Barak Y, Juven T, Haffner R, Oren M. mdm2 expression is induced by wild type p53 activity. EMBO J 1993;12:461–8.

166. Pant V, Lozano G. Dissecting the p53-Mdm2 feedback loop in vivo: uncoupling the role in p53 stability and activity. Oncotarget 2014;5:1149–56.

167. de Oca Luna RM, Wagner DS, Lozano G. Rescue of early embryonic lethality in mdm2-deficient mice by deletion of p53. Nature 1995;378:203–6.

168. Jones SN, Roe AE, Donehower LA, Bradley A. Rescue of embryonic lethality in Mdm2-deficient mice by absence of p53. Nature 1995;378:206–8.

169. Tollini LA, Jin A, Park J, Zhang Y. Regulation of p53 by Mdm2 E3 ligase function is dispensable in embryogenesis and development, but essential in response to DNA damage. Cancer Cell 2014;26:235–47.

170. Nomura K, Klejnot M, Kowalczyk D, Hock AK, Sibbet GJ, Vousden KH, et al. Structural analysis of MDM2 RING separates degradation from regulation of p53 transcription activity. Nat Struct Mol Biol 2017;24:578–87.

171. Leng RP, Lin Y, Ma W, Wu H, Lemmers B, Chung S, et al. Pirh2, a p53-induced ubiquitin-protein ligase, promotes p53 degradation. Cell 2003;112:779–91.

172. Dornan D, Wertz I, Shimizu H, Arnott D, Frantz GD, Dowd P, et al. The ubiquitin ligase COP1 is a critical negative regulator of p53. Nature 2004;429:86–92.

173. Chen D, Kon N, Li M, Zhang W, Qin J, Gu W. ARF-BP1/Mule is a critical mediator of the ARF tumor suppressor. Cell 2005;121:1071–83.

174. Parant J, Chavez-Reyes A, Little NA, Yan W, Reinke V, Jochemsen AG, et al. Rescue of embryonic lethality in Mdm4-null mice by loss of Trp53

suggests a nonoverlapping pathway with MDM2 to regulate p53. Nat Genet 2001;29:92–5.

175. Migliorini D, Lazzerini Denchi E, Danovi D, Jochemsen A, Capillo M, Gobbi A, et al. Mdm4 (Mdmx) regulates p53-induced growth arrest and neuronal cell death during early embryonic mouse development. Mol Cell Biol 2002;22:5527–38.

176. Finch RA, Donoviel DB, Potter D, Shi M, Fan A, Freed DD, et al. mdmx is a negative regulator of p53 activity in vivo. Cancer Res 2002;62:3221–5.

177. Arva NC, Gopen TR, Talbott KE, Campbell LE, Chicas A, White DE, et al. A chromatin-associated and transcriptionally inactive p53-Mdm2 complex occurs in mdm2 SNP309 homozygous cells. J Biol Chem 2005;280:26776–87.

178. Minsky N, Oren M. The RING domain of Mdm2 mediates histone ubiquitylation and transcriptional repression. Mol Cell 2004;16:631–9.

179. Ohkubo S, Tanaka T, Taya Y, Kitazato K, Prives C. Excess HDM2 impacts cell cycle and apoptosis and has a selective effect on p53-dependent transcription. J Biol Chem 2006;281:16943–50.

180. White DE, Talbott KE, Arva NC, Bargonetti J. Mouse double minute 2 associates with chromatin in the presence of p53 and is released to facilitate activation of transcription. Cancer Res 2006;66:3463–70.

181. Weinberg RL, Veprintsev DB, Bycroft M, Fersht AR. Comparative Binding of p53 to its Promoter and DNA Recognition Elements. J Mol Biol 2005;348:589–96.

182. Zhao R, Gish K, Murphy M, Yin Y, Notterman D, Hoffman WH, et al. Analysis of p53-regulated gene expression patterns using oligonucleotide arrays. Genes Dev 2000;14:981–93.

183. Bieging KT, Mello SS, Attardi LD. Unravelling mechanisms of p53-mediated tumour suppression. Nat Rev Cancer 2014;14:359–70.

184. Hartwell LH, Weinert TA. Checkpoints: controls that ensure the order of cell cycle events. Science 1989;246:629–34.

185. Kastan MB, Zhan Q, el-Deiry WS, Carrier F, Jacks T, Walsh WV, et al. A mammalian cell cycle checkpoint pathway utilizing p53 and GADD45 is defective in ataxia-telangiectasia. Cell 1992;71:587–97.

186. Deng C, Zhang P, Wade Harper J, Elledge SJ, Leder P. Mice Lacking p21CIP1/WAF1 undergo normal development, but are defective in G1 checkpoint control. Cell 1995;82:675–84.

187. Brugarolas J, Chandrasekaran C, Gordon JI, Beach D, Jacks T, Hannon GJ. Radiation-induced cell cycle arrest compromised by p21 deficiency. Nature 1995;377:552–7.

188. Taylor WR, Stark GR. Regulation of the G2/M transition by p53. Oncogene 2001;20:1803–15.

189. Mailand N, Falck J, Lukas C, Syljuâsen RG, Welcker M, Bartek J, et al. Rapid destruction of human Cdc25A in response to DNA damage. Science 2000;288:1425–9.

190. Zhan Q, Antinore MJ, Wang XW, Carrier F, Smith ML, Harris CC, et al. Association with Cdc2 and inhibition of Cdc2/Cyclin B1 kinase activity by the p53-regulated protein Gadd45. Oncogene 1999;18:2892–900.

191. Wang XW, Zhan Q, Coursen JD, Khan MA, Kontny HU, Yu L, et al. GADD45 induction of a G2/M cell cycle checkpoint. Proc Natl Acad Sci U S A 1999;96:3706–11.

192. Peng CY, Graves PR, Thoma RS, Wu Z, Shaw AS, Piwnica-Worms H. Mitotic and G2 checkpoint control: regulation of 14-3-3 protein binding by phosphorylation of Cdc25C on serine-216. Science 1997;277:1501–5.

193. Krenning L, Feringa FM, Shaltiel IA, van den Berg J, Medema RH. Transient activation of p53 in G2 phase is sufficient to induce senescence. Mol Cell 2014;55:59–72.

194. Lindqvist A, de Bruijn M, Macurek L, Brás A, Mensinga A, Bruinsma W, et al. Wip1 confers G2 checkpoint recovery competence by counteracting p53-dependent transcriptional repression. EMBO J 2009;28:3196–206.

195. Cross SM, Sanchez CA, Morgan CA, Schimke MK, Ramel S, Idzerda RL, et al. A p53-dependent mouse spindle checkpoint. Science 1995;267:1353–6.

196. Andreassen PR, Lohez OD, Lacroix FB, Margolis RL. Tetraploid state induces p53-dependent arrest of nontransformed mammalian cells in G1. Mol Biol Cell 2001;12:1315–28.

197. Vogel C, Kienitz A, Hofmann I, Müller R, Bastians H. Crosstalk of the mitotic spindle assembly checkpoint with p53 to prevent polyploidy. Oncogene 2004;23:6845–53.

198. Kuilman T, Michaloglou C, Mooi WJ, Peeper DS. The essence of senescence. Genes Dev 2010;24:2463–79.

199. Rufini A, Tucci P, Celardo I, Melino G. Senescence and aging: the critical roles of p53. Oncogene 2013;32:5129–43.

200. Brown JP, Wei W, Sedivy JM. Bypass of senescence after disruption of p21CIP1/WAF1 gene in normal diploid human fibroblasts. Science 1997;277:831–4.

201. Beauséjour CM, Krtolica A, Galimi F, Narita M, Lowe SW, Yaswen P, et al. Reversal of human cellular senescence: roles of the p53 and p16 pathways. EMBO J 2003;22:4212–22.

202. Serrano M, Lin AW, McCurrach ME, Beach D, Lowe SW. Oncogenic ras Provokes Premature Cell Senescence Associated with Accumulation of p53 and p16INK4a. Cell 1997;88:593–602.

203. Elmore S. Apoptosis: a review of programmed cell death. Toxicol Pathol 2007;35:495–516.

204. Chipuk JE. Direct Activation of Bax by p53 Mediates Mitochondrial Membrane Permeabilization and Apoptosis. Science 2004;303:1010–4.

205. Michalak EM, Villunger A, Adams JM, Strasser A. In several cell types tumour suppressor p53 induces apoptosis largely via Puma but Noxa can contribute. Cell Death Differ. 2008;15:1019–29.

206. Green DR, Kroemer G. Cytoplasmic functions of the tumour suppressor p53. Nature 2009;458:1127–30.

207. Speidel D. Transcription-independent p53 apoptosis: an alternative route to death. Trends Cell Biol 2010;20:14–24.

208. Mihara M, Erster S, Zaika A, Petrenko O, Chittenden T, Pancoska P, et al. p53 Has a Direct Apoptogenic Role at the Mitochondria. Mol Cell 2003;11:577–90.

209. Tasdemir E, Maiuri MC, Galluzzi L, Vitale I, Djavaheri-Mergny M, D'Amelio M, et al. Regulation of autophagy by cytoplasmic p53. Nat Cell Biol 2008;10:676–87.

210. Freed-Pastor WA, Prives C. Mutant p53: one name, many proteins. Genes Dev 2012;26:1268–86.

211. Donehower LA, Harvey M, Slagle BL, McArthur MJ, Montgomery CA, Butel JS, et al. Mice deficient for p53 are developmentally normal but susceptible to spontaneous tumours. Nature 1992;356:215–21.

212. Levine AJ, Oren M. The first 30 years of p53: growing ever more complex. Nat Rev Cancer 2009;9:749–58.

213. Milner J, Medcalf EA, Cook AC. Tumor suppressor p53: analysis of wild-type and mutant p53 complexes. Mol Cell Biol 1991;11:12–9.

214. Kim E, Deppert W. Interactions of mutant p53 with DNA: guilt by association. Oncogene 2007;26:2185–90.

215. Baker SJ, Preisinger AC, Jessup JM, Paraskeva C, Markowitz S, Willson JKV, et al. p53 Gene Mutations Occur in Combination with 17p Allelic Deletions as Late Events in Colorectal Tumorigenesis. Cancer Res 1990;50:7717–22.

216. Jacks T, Remington L, Williams BO, Schmitt EM, Halachmi S, Bronson RT, et al. Tumor spectrum analysis in p53-mutant mice. Curr Biol 1994;4:1–7.

217. Liu G, Parant JM, Lang G, Chau P, Chavez-Reyes A, El-Naggar AK, et al. Chromosome stability, in the absence of apoptosis, is critical for suppression of tumorigenesis in *Trp53* mutant mice. Nat Genet 2004;36:63–8.

218. Timofeev O, Schlereth K, Wanzel M, Braun A, Nieswandt B, Pagenstecher A, et al. p53 DNA Binding Cooperativity Is Essential for Apoptosis and Tumor Suppression In Vivo. Cell Rep 2013;3:1512–25.

219. Barboza JA, Liu G, Ju Z, El-Naggar AK, Lozano G. p21 delays tumor onset by preservation of chromosomal stability. Proc Natl Acad Sci U S A 2006;103:19842–7.

220. Harris AW, Pinkert CA, Crawford M, Langdon WY, Brinster RL, Adams JM. The E mu-myc transgenic mouse. A model for high-incidence spontaneous lymphoma and leukemia of early B cells. J Exp Med 1988;167:353–71.

221. Eischen CM, Weber JD, Roussel MF, Sherr CJ, Cleveland JL. Disruption of the ARF-Mdm2-p53 tumor suppressor pathway in Myc-induced lymphomagenesis. Genes Dev 1999;13:2658–69.

222. Eischen CM, Roussel MF, Korsmeyer SJ, Cleveland JL. Bax loss impairs Myc-induced apoptosis and circumvents the selection of p53 mutations during Myc-mediated lymphomagenesis. Mol Cell Biol 2001;21:7653–62.

223. Michalak EM, Jansen ES, Happo L, Cragg MS, Tai L, Smyth GK, et al. Puma and to a lesser extent Noxa are suppressors of Myc-induced lymphomagenesis. Cell Death Differ. 2009;16:684–96.

224. Post SM, Quintás-Cardama A, Terzian T, Smith C, Eischen CM, Lozano G. p53-dependent senescence delays Eμ-myc-induced B-cell lymphomagenesis. Oncogene 2009;29:1260–9.

225. Di Micco R, Fumagalli M, Cicalese A, Piccinin S, Gasparini P, Luise C, et al. Oncogene-induced senescence is a DNA damage response triggered by DNA hyper-replication. Nature 2006;444:638–42.

226. Bartkova J, Rezaei N, Liontos M, Karakaidos P, Kletsas D, Issaeva N, et al. Oncogene-induced senescence is part of the tumorigenesis barrier imposed by DNA damage checkpoints. Nature 2006;444:633–7.

227. Xue W, Zender L, Miething C, Dickins RA, Hernando E, Krizhanovsky V, et al. Senescence and tumour clearance is triggered by p53 restoration in murine liver carcinomas. Nature 2007;445:656–60.

228. Sarkisian CJ, Keister BA, Stairs DB, Boxer RB, Moody SE, Chodosh LA. Dose-dependent oncogene-induced senescence in vivo and its evasion during mammary tumorigenesis. Nat Cell Biol 2007;9:493–505.

229. Thukral SK, Blain GC, Chang KK, Fields S. Distinct residues of human p53 implicated in binding to DNA, simian virus 40 large T antigen, 53BP1,

and 53BP2. Mol Cell Biol 1994;14:8315–21.

230. Iwabuchi K, Li B, Massa HF, Trask BJ, Date T, Fields S. Stimulation of p53-mediated transcriptional activation by the p53-binding proteins, 53BP1 and 53BP2. J Biol Chem 1998;273:26061–8.

231. Koonin EV, Altschul SF, Bork P. …Functional motifs…. Nat Genet 1996;13:266–8.

232. Callebaut I, Mornon JP. From BRCA1 to RAP1: a widespread BRCT module closely associated with DNA repair. FEBS Lett 1997;400:25–30.

233. Derbyshire DJ, Basu BP, Serpell LC, Joo WS, Date T, Iwabuchi K, et al. Crystal structure of human 53BP1 BRCT domains bound to p53 tumour suppressor. EMBO J 2002;21:3863–72.

234. Sibanda BL, Critchlow SE, Begun J, Pei XY, Jackson SP, Blundell TL, et al. Crystal structure of an Xrcc4-DNA ligase IV complex. Nat Struct Biol 2001;8:1015–9.

235. Kachirskaia I, Shi X, Yamaguchi H, Tanoue K, Wen H, Wang EW, et al. Role for 53BP1 Tudor Domain Recognition of p53 Dimethylated at Lysine 382 in DNA Damage Signaling. J Biol Chem 2008;283:34660–6.

236. Roy S, Musselman CA, Kachirskaia I, Hayashi R, Glass KC, Nix JC, et al. Structural insight into p53 recognition by the 53BP1 tandem Tudor domain. J Mol Biol 2010;398:489–96.

237. Ward IM, Difilippantonio S, Minn K, Mueller MD, Molina JR, Yu X, et al. 53BP1 cooperates with p53 and functions as a haploinsufficient tumor suppressor in mice. Mol Cell Biol 2005;25:10079–86.

238. Morales JC, Franco S, Murphy MM, Bassing CH, Mills KD, Adams MM, et al. 53BP1 and p53 synergize to suppress genomic instability and lymphomagenesis. Proc Natl Acad Sci U S A 2006;103:3310–5.

239. Vassilev LT. In Vivo Activation of the p53 Pathway by Small-Molecule Antagonists of MDM2. Science 2004;303:844–8.

240. Brummelkamp TR, Fabius AWM, Mullenders J, Madiredjo M, Velds A, Kerkhoven RM, et al. An shRNA barcode screen provides insight into cancer cell vulnerability to MDM2 inhibitors. Nat Chem Biol 2006;2:202–6.

241. Huang J, Sengupta R, Espejo AB, Lee MG, Dorsey JA, Richter M, et al. p53 is regulated by the lysine demethylase LSD1. Nature 2007;449:105–8.

242. Donner AJ, Szostek S, Hoover JM, Espinosa JM. CDK8 is a stimulus-specific positive coregulator of p53 target genes. Mol Cell 2007;27:121–33.

243. Lefever S, Vandesompele J, Speleman F, Pattyn F. RTPrimerDB: the

portal for real-time PCR primers and probes. Nucleic Acids Res 2009;37:D942–5.

244. Lamble S, Batty E, Attar M, Buck D, Bowden R, Lunter G, et al. Improved workflows for high throughput library preparation using the transposome-based Nextera system. BMC Biotechnol 2013;13:104.

245. Kim D, Pertea G, Trapnell C, Pimentel H, Kelley R, Salzberg SL. TopHat2: accurate alignment of transcriptomes in the presence of insertions, deletions and gene fusions. Genome Biol 2013;14:R36.

246. Robinson MD, McCarthy DJ, Smyth GK. edgeR: a Bioconductor package for differential expression analysis of digital gene expression data. Bioinformatics 2010;26:139–40.

247. Hardy RR. Resolution and characterization of pro-B and pre-pro-B cell stages in normal mouse bone marrow. J Exp Med 1991;173:1213–25.

248. Schindelin J, Arganda-Carreras I, Frise E, Kaynig V, Longair M, Pietzsch T, et al. Fiji: an open-source platform for biological-image analysis. Nat. Methods 2012;9:676–82.

249. Brinkman EK, Chen T, Amendola M, van Steensel B. Easy quantitative assessment of genome editing by sequence trace decomposition. Nucleic Acids Res 2014;42:e168–8.

250. Cescutti R, Negrini S, Kohzaki M, Halazonetis TD. TopBP1 functions with 53BP1 in the G1 DNA damage checkpoint. EMBO J 2010;29:3723–32.

251. Ramachandran S, Chahwan R, Nepal RM, Frieder D, Panier S, Roa S, et al. The RNF8/RNF168 ubiquitin ligase cascade facilitates class switch recombination. Proc Natl Acad Sci U S A 2010;107:809–14.

252. Ward I, Kim J-E, Minn K, Chini CC, Mer G, Chen J. The tandem BRCT domain of 53BP1 is not required for its repair function. J Biol Chem 2006;281:38472–7.

253. Valero R, Bayés M, Francisca Sánchez-Font M, González-Angulo O, Gonzàlez-Duarte R, Marfany G. Characterization of alternatively spliced products and tissue-specific isoforms of USP28 and USP25. Genome Biol 2001;2:RESEARCH0043.

254. Wen Y, Shi L, Ding Y, Cui R, He W-T, Hu H-Y, et al. The N-terminal ubiquitin-binding region of ubiquitin-specific protease 28 modulates its deubiquitination function: NMR structural and mechanistic insights. Biochem J 2015;471:155–65.

255. Zhen Y, Knobel PA, Stracker TH, Reverter D. Regulation of USP28 deubiquitinating activity by SUMO conjugation. J Biol Chem 2014;289:34838–50.

256. Ye Y, Scheel H, Hofmann K, Komander D. Dissection of USP catalytic

domains reveals five common insertion points. Molecular BioSystems 2009;5:1797–808.

257. Ishida T, Kinoshita K. Prediction of disordered regions in proteins based on the meta approach. Bioinformatics 2008;24:1344–8.

258. Popov N, Wanzel M, Madiredjo M, Zhang D, Beijersbergen R, Bernards R, et al. The ubiquitin-specific protease USP28 is required for MYC stability. Nat Cell Biol 2007;9:765–74.

259. Schülein-Völk C, Wolf E, Zhu J, Xu W, Taranets L, Hellmann A, et al. Dual regulation of Fbw7 function and oncogenic transformation by Usp28. Cell Rep 2014;9:1099–109.

260. Diefenbacher ME, Chakraborty A, Blake SM, Mitter R, Popov N, Eilers M, et al. Usp28 counteracts Fbw7 in intestinal homeostasis and cancer. Cancer Res 2015;75:1181–6.

261. Moser AR, Luongo C, Gould KA, McNeley MK, Shoemaker AR, Dove WF. ApcMin: a mouse model for intestinal and mammary tumorigenesis. Eur J Cancer 1995;31A:1061–4.

262. Peng K, Radivojac P, Vucetic S, Dunker AK, Obradovic Z. Length-dependent prediction of protein intrinsic disorder. BMC Bioinformatics 2006;7:208.

263. Xu D, Liu J, Fu T, Shan B, Qian L, Pan L, et al. USP25 regulates Wnt signaling by controlling the stability of tankyrases. Genes Dev 2017;31:1024–35.

264. Brooks CL, Gu W. p53 regulation by ubiquitin. FEBS Lett 2011;585:2803–9.

265. Yuan J, Luo K, Zhang L, Cheville JC, Lou Z. USP10 regulates p53 localization and stability by deubiquitinating p53. Cell 2010;140:384–96.

266. Boyd SD, Tsai KY, Jacks T. An intact HDM2 RING-finger domain is required for nuclear exclusion of p53. Nat Cell Biol 2000;2:563–8.

267. Shaulsky G, Goldfinger N, Ben-Ze'ev A, Rotter V. Nuclear accumulation of p53 protein is mediated by several nuclear localization signals and plays a role in tumorigenesis. Mol Cell Biol 1990;10:6565–77.

268. Stommel JM, Marchenko ND, Jimenez GS, Moll UM, Hope TJ, Wahl GM. A leucine-rich nuclear export signal in the p53 tetramerization domain: regulation of subcellular localization and p53 activity by NES masking. EMBO J 1999;18:1660–72.

269. Liang SH, Clarke MF. A bipartite nuclear localization signal is required for p53 nuclear import regulated by a carboxyl-terminal domain. J Biol Chem 1999;274:32699–703.

270. Li M. Mono- Versus Polyubiquitination: Differential Control of p53 Fate by Mdm2. Science 2003;302:1972–5.

271. Landré V, Revi B, Mir MG, Verma C, Hupp TR, Gilbert N, et al. Regulation of transcriptional activators by DNA-binding domain ubiquitination. Cell Death Differ. 2017;24:903–16.

272. Tong Q, Mazur SJ, Rincon-Arano H, Rothbart SB, Kuznetsov DM, Cui G, et al. An acetyl-methyl switch drives a conformational change in p53. Structure 2015;23:322–31.

273. Mazzucco AE, Smogorzewska A, Kang C, Luo J, Schlabach MR, Xu Q, et al. Genetic interrogation of replicative senescence uncovers a dual role for USP28 in coordinating the p53 and GATA4 branches of the senescence program. Genes Dev 2017;31:1933–8.

274. Meitinger F, Anzola JV, Kaulich M, Richardson A, Stender JD, Benner C, et al. 53BP1 and USP28 mediate p53 activation and G1 arrest after centrosome loss or extended mitotic duration. J Cell Biol 2016;214:155–66.

275. Fong CS, Mazo G, Das T, Goodman J, Kim M, O'Rourke BP, et al. 53BP1 and USP28 mediate p53-dependent cell cycle arrest in response to centrosome loss and prolonged mitosis. eLife 2016;5:E1491.

276. Lambrus BG, Daggubati V, Uetake Y, Scott PM, Clutario KM, Sluder G, et al. A USP28-53BP1-p53-p21 signaling axis arrests growth after centrosome loss or prolonged mitosis. J Cell Biol 2016;214:143–53.

277. Yu X, Chini CCS, He M, Mer G, Chen J. The BRCT domain is a phospho-protein binding domain. Science 2003;302:639–42.

278. Sanders SL, Portoso M, Mata J, Bähler J, Allshire RC, Kouzarides T. Methylation of Histone H4 Lysine 20 Controls Recruitment of Crb2 to Sites of DNA Damage. Cell 2004;119:603–14.

279. Kilkenny ML, Doré AS, Roe SM, Nestoras K, Ho JCY, Watts FZ, et al. Structural and functional analysis of the Crb2-BRCT2 domain reveals distinct roles in checkpoint signaling and DNA damage repair. Genes Dev 2008;22:2034–47.

280. Jullien D, Vagnarelli P, Earnshaw WC, Adachi Y. Kinetochore localisation of the DNA damage response component 53BP1 during mitosis. J Cell Sci 2002;115:71–9.

281. Orthwein A, Fradet-Turcotte A, Noordermeer SM, Canny MD, Brun CM, Strecker J, et al. Mitosis inhibits DNA double-strand break repair to guard against telomere fusions. Science 2014;344:189–93.

282. Schlacher K, Christ N, Siaud N, Egashira A, Wu H, Jasin M. Double-strand break repair-independent role for BRCA2 in blocking stalled replication fork degradation by MRE11. Cell 2011;145:529–42.

283. Marjanović M, Sánchez-Huertas C, Terré B, Gómez R, Scheel JF, Pacheco S, et al. CEP63 deficiency promotes p53-dependent microcephaly and reveals a role for the centrosome in meiotic recombination. Nat Commun 2015;6:7676.

284. Yin Y, Stahl BC, DeWolf WC, Morgentaler A. p53-mediated germ cell quality control in spermatogenesis. Dev Biol 1998;204:165–71.

285. Xu X, Wagner K-U, Larson D, Weaver Z, Li C, Ried T, et al. Conditional mutation of Brca1 in mammary epithelial cells resultsin blunted ductal morphogenesis and tumour formation. Nat Genet 1999;22:37–43.

286. Xu X, Qiao W, Linke SP, Cao L, Li W-M, Furth PA, et al. Genetic interactions between tumor suppressors Brca1 and p53 in apoptosis, cell cycle and tumorigenesis. Nat Genet 2001;28:266–71.

287. Cao L, Xu X, Bunting SF, Liu J, Wang R-H, Cao LL, et al. A Selective Requirement for 53BP1 in the Biological Response to Genomic Instability Induced by Brca1 Deficiency. Mol Cell 2009;35:534–41.